

**ROLE OF DIETARY ETHIOLOGICAL FACTORS IN THE MOLECULAR  
PATHOGENESIS OF LIVER CANCER**

**A THESIS SUBMITTED TO  
THE DEPARTMENT OF MOLECULAR BIOLOGY AND GENETICS  
AND THE INSTITUTE OF ENGINEERING AND SCIENCE OF  
BILKENT UNIVERSITY  
IN PARTIAL FULFILLMENT OF THE REQUIREMENTS  
FOR THE DEGREE OF DOCTOR OF PHILOSOPHY**

**BY  
ŞEHRİBAN ÖZGE GÜRİSOY YÜZÜGÜLLÜ  
FEBRUARY, 2011**

I certify that I have read this thesis and that in my opinion it is fully adequate, in scope, and in quality, as a thesis for the degree of Doctor of Philosophy.

\_\_\_\_\_  
Prof. Dr. Mehmet Öztürk

I certify that I have read this thesis and that in my opinion it is fully adequate, in scope, and in quality, as a thesis for the degree of Doctor of Philosophy.

\_\_\_\_\_  
Assoc. Dr. Rengül Çetin Atalay

I certify that I have read this thesis and that in my opinion it is fully adequate, in scope, and in quality, as a thesis for the degree of Doctor of Philosophy.

\_\_\_\_\_  
Assist. Dr. Uygur Tazebay

I certify that I have read this thesis and that in my opinion it is fully adequate, in scope, and in quality, as a thesis for the degree of Doctor of Philosophy.

\_\_\_\_\_  
Prof. Dr. Belma Giray

I certify that I have read this thesis and that in my opinion it is fully adequate, in scope, and in quality, as a thesis for the degree of Doctor of Philosophy.

\_\_\_\_\_  
Prof. Dr. Meral Özgüç

Approved for the Institute of Engineering and Science

\_\_\_\_\_  
Prof. Dr. Levent Onural

Director of the Institute of Engineering and  
Science

**TO MY FAMILY**

## ABSTRACT

### **Role of dietary etiological factors involved in the molecular pathogenesis of liver cancer**

Şehriban Özge Gürsoy Yüzügüllü  
Ph.D. in Molecular Biology and Genetics  
Supervisor: Prof. Dr. Mehmet Öztürk  
February, 2011, 183 Pages

Hepatocellular carcinoma is ranked third foremost cause of cancer deaths. Dietary factors play a crucial role in the molecular pathogenesis of liver cancer. Oxidative stress is usually coupled with the malignancy and progression of HCC since it is considered as a common factor during inflammation after chronic viral infection. Chemical stress caused by aflatoxin exposure, metabolic stress produced by alcohol abuse and selenium deficiency as a risk factor for HCC are associated with oxidative stress. It should be eliminated with an intact antioxidant defense mechanism. It is a major cause of genotoxicity endogenously through metabolic stress and exogenously produced by chemical and physical carcinogens. Even though the contribution of dietary factors in HCC progression has been established, the underlying molecular mechanism has not been fully understood.

Cancer cells may respond to genotoxic stress with a cryptic development of survival advantage mechanisms. Therefore we wanted to investigate this idea with dietary factors involved in liver cancer. In this work, we studied the implication of Se-deficiency in tumorigenesis of hepatocytes and the mechanism underlying the selective selection of aflatoxins for p53-249 mutation in HCC. Aflatoxins are the most potent naturally occurring carcinogens and may play a causative role in 5-28% of hepatocellular carcinomas, worldwide. Aflatoxins are activated in liver cells and induce principally G->T mutations, including a codon 249 (G->T) hotspot mutation of TP53 gene that is specifically associated with aflatoxin-related hepatocellular carcinoma.

However, our comparative analysis showed that R249S does not provide survival advantage at heterozygous state. Thus, the selection could be at the mutation induction

stage. The lack of p53 activation in Aflatoxin B1 exposed HCC cells led us to test DNA damage response after aflatoxin exposure. Unexpectedly, DNA damage checkpoint response to aflatoxins has not been studied thoroughly before. Although, DNA damage checkpoint response acts as an anti-tumor mechanism by protecting genome integrity against genotoxic agents, this highly critical aspect of aflatoxin carcinogenicity is poorly known.

Our findings provide evidence for the contribution of ERK, p38MAPK and PI3K/Akt survival pathways under selenium supplementation in some HCC cell lines. Apart from the effect of selenium deficiency, our results enlighten the aflatoxin carcinogenicity *in vitro*. Our study pointed out for a negligent G1 and G2/M checkpoint response to aflatoxin B1-induced DNA damage. This defective response may account mostly for mutagenic and carcinogenic influences of aflatoxins. It may also associate with the frequent induction of TP53 hotspot mutation in aflatoxin-related human HCC.

## ÖZET

### **Karaciğer kanserinin moleküler patogenezinde diyet etiyolojik faktörlerin rolü**

Şehriban Özge Gürsoy Yüzügüllü  
Moleküler Biyoloji ve Genetik Doktorası  
Tez Yöneticisi: Prof. Dr. Mehmet Öztürk  
Şubat, 2011, 183 sayfa

Hepatoselüler karsinoma, kansere bağlı ölüm oranlarında üçüncü sırada yer almaktadır. Diyete bağlı faktörler karaciğer kanserinin moleküler patogenezinde önemli rol oynamaktadır. Oksidatif stres kronik viral enfeksiyonuna bağlı enflamasyon sırasında HCC ilerleyişi ile beraber devam eden yaygın bir durumdur. Aflatoksin maruz kalmaya bağlı kimyasal stres, alkol alımıyla oluşan metabolik stres ve HCC için bir risk faktörü olan selenyum eksikliği oksidatif stres ile ilişkilidir. Oksidatif stresin fonksiyonel bir antioksidan savunma mekanizması ile uzaklaştırılması gerekmektedir. Oksidatif stres metabolik stres yoluyla oluşan endojen ve kimyasal ya da fiziksel karsinojenlerin oluşturduğu egzogen genotoksitenin major nedenidir. Diyet faktörlerin HCC ilerleyişindeki katkısı yerleşmiş olduğu halde, bu katkının altında yatan moleküler mekanizma tam anlamıyla anlaşılmamıştır.

Kanser hücreleri genotoksik strese karşı şifreli bir sağkalım avantajı gelişimi ile yanıt verebilir. Bu nedenle, bu fikri karaciğer kanserinde rol alan diyet faktörleri ile araştırmak istedik. Bu çalışmada, Se-eksikliğinin hepatositlerin tümörigenezindeki etkisi ve HCC p53-249 mutasyonu için aflatoksinin seçici seçiminin altında yatan mekanizma araştırıldı. Aflatoksinler en doğal yollarla oluşan, dünya çapında hepatosellüler karsinomların % 5-28 olarak katkıda bulunabilen kanserojenlerdir. Aflatoksin karaciğer hücrelerinde aktive edilir ve TP53 genindeki özellikle aflatoksin ile ilgili hepatosellüler kanser ile ilişkili 249 kodonu da dahil olmak üzere esas olarak G-> T mutasyonlarını tetikler.

Ancak, bizim karşılaştırmalı sonuçlarımız R249S mutasyonunun heterozigot koşullar altında sağkalım avantajı sağlamadığını gösterdi. Böylece, bu seçicilik mutasyon indüksiyon aşamasında olabilir. Aflatoksin maruz kalan HCC hücrelerinde p53 aktivasyon eksikliği, bizi aflatoksin maruz kalımdan sonra DNA hasarına verilen cevabı

test etmeye yöneltti. Aflatoksine karşı DNA hasarı kontrol noktası yanıtlarının en ince ayrıntısına kadar çalışılmamış olmasını beklemiyorduk. DNA hasarı kontrol noktası yanıtlarının genotoksik ajanlara karşı genom bütünlüğünü koruyarak anti-tümör mekanizması oluşturduğu halde, aflatoksin karsinogenezindeki bu kritik yön az bilinmektedir.

Bulgularımız, bazı HCC hücre hatlarında selenyum desteğinin altında ERK, p38MAPK ve PI3K/Akt sağkalım yollarının katkısını ortaya koymuştur. Selenyum eksikliğinin etkisi dışında, sonuçlarımız *in vitro* koşullar altında aflatoksin kanserojenitesini aydınlattı. Bizim çalışmamız, aflatoksin B1 ile oluşan DNA hasarına verilen cevabın ihmalkar bir G1 ve G2 / M kontrol noktası yanıtı olduğunu gösterdi. Bu yetersiz yanıt aflatoksinin çoğunlukla mutajen ve kanserojen olan etkileri için sorumlu tutulabilir. Aynı zamanda bu durum aflatoksin ile ilişkilendirilen HCC'de sık rastlanan spesifik TP53 mutasyonu ile bağdaştırılabilir.

## ACKNOWLEDGMENTS

Thank you ...

...Prof. Dr. Mehmet Öztürk, my supervisor, for all that I have learnt from you. Without your unconditional support, guidance, and patience, none of this would be possible. He was a lot more than a supervisor for me.

...Assoc. Dr. Rengül Çetin-Atalay, for the knowledge and experience you have shared, the patience and support you gave.

...Dr. Stefan Dimitrov for the experience you have shared and for your career advises.

...Dr. Ralph Meuwissen for the experience you have shared, for your advices and for your friendship.

...TUBITAK for funding this project

...EMBO for supporting me as a short-term fellow

...All the members of Equipe 2, Equipe 5 and Equipe 12 for the friendship and the experience you have shared, especially Dr. Jean Luc Coll for their reagents and technical helps in Institut Albert Bonniot.

...All the current and former members of Atalay lab for the friendship and the friendly environment,

...All the current and former members of Ozturk lab for the great friendly environment and support you have given, especially to Çiğdem, Dilek, Ayşegül, Bilge.

...All MBG family.

...Gülşah, I am very lucky to have such a generous roommate.

...Esra, for your understanding and endless support, through the duration of my studies.

...My family for their unconditional support at each turn of the road...

...Haluyum, my husband, my dearly loved for always being my pillar, my joy and my guiding light. Life blessed me with the opportunity to give him into my years, after all everything got a meaning.



## TABLE OF CONTENTS

SIGNATURE PAGE.....	I
ABSTRACT.....	III
ÖZET.....	V
ACKNOWLEDGEMENTS .....	VII
TABLE OF CONTENTS.....	VIII
LIST OF TABLES .....	XIII
LIST OF FIGURES .....	XIV
ABBREVIATIONS.....	XVII

## CHAPTER 1. INTRODUCTION..... 1

1.1	Hepatocellular malignancy.....	1
1.2	Pathogenesis of hepatocellular carcinoma.....	2
1.2.1	Viral factors.....	2
1.2.2	Genetic alterations.....	4
1.2.2.1	Allelic imbalance and microsatellite instability.....	4
1.2.2.2	Cell cycle regulation.....	5
1.2.2.3	Alterations of the TGF- $\beta$ and PI3Kinase pathway.....	6
1.2.3	TP53.....	8
1.2.3.1	p53 and HCC.....	11
1.2.4	Epigenetic Regulations.....	12
1.2.4.1	DNA methylation.....	12
1.2.4.2	Histone modifications.....	13
1.2.4.3	Histone methylation and cancer.....	13
1.2.5	Dietary Factors.....	14
1.2.5.1	Alcohol abuse.....	14
1.2.5.2	Obesity.....	14
1.2.5.3	Selenium deficiency and liver diseases.....	15
1.2.5.3.1	Selenium and its deficiency.....	15
1.2.5.3.2	Selenium and oxidative stress.....	17
1.2.5.3.3	Selenium and cancer.....	18

1.2.5.3.3.1	Selenium and liver cancer.....	19
1.2.5.3.3.2	Signaling pathways and selenium.....	21
1.2.5.4	Hepatotoxic Chemicals.....	23
1.2.5.4.1	Aflatoxins.....	23
1.2.5.4.2	Aflatoxin exposure in humans.....	23
1.2.5.4.3	AFB1-induced DNA damage and HCC.....	24
1.2.5.4.3.1	Aflatoxin and HCC.....	24
1.2.5.4.3.2	Aflatoxin metabolism and DNA damage..	24
1.2.5.4.3.3	Correlation between aflatoxin exposure and p53.....	25
1.2.5.4.3.3.1	Functional characteristics of R249S p53.....	26
1.2.5.4.4	Response to AFB1-induced DNA damage.....	27
<b>CHAPTER 2. OBJECTIVES AND RATIONALE.....</b>		<b>30</b>
<b>CHAPTER 3. MATERIALS AND METHODS.....</b>		<b>32</b>
3.1	MATERIALS.....	32
3.1.1	General reagents.....	32
3.1.2	Enzymes.....	32
3.1.3	Nucleic Acids.....	32
3.1.4	Oligonucleotides.....	32
3.1.5	Electrophoresis and photography and spectrophotometer .....	32
3.1.6	Tissue culture reagents and cell lines .....	33
3.1.7	Western immunoblotting, antibodies and chemiluminescence.....	33
3.2	SOLUTIONS AND MEDIA.....	34
3.2.1	General Solutions.....	34
3.2.2	Tissue culture solutions.....	34
3.2.3	Immunoblotting solutions.....	36
3.2.4	RNA Study solutions.....	36
3.2.5	Immunofluorescence and immunoperoxidase solutions.....	36

3.2.6	Single cell gel electrophoresis (COMET ASSAY) solutions.....	37
3.3	METHODS.....	38
3.3.1	Tissue culture techniques.....	38
3.3.1.1	Cell Lines and stable clones.....	38
3.3.1.2	Thawing cell lines .....	38
3.3.1.3	Transient transfection and stable clone formation.....	38
3.3.1.4	Cell culture treatments .....	39
3.3.1.4.1	Treatment of cell lines with Se-adequate vs. Se-deficient medium and Wortmannin.....	39
3.3.1.4.2	Treatment of cell lines with TGF-beta and Adriamycin .....	39
3.3.1.4.3	Treatment of cell lines with AflatoxinB1 .....	39
3.3.1.5	Cryopreservation of cell lines.....	39
3.3.1.6	Colony-forming ability assay.....	40
3.3.2	Analysis of nucleic acids.....	40
3.3.2.1	Purification of plasmid DNA using Qiagen miniprep kit.....	40
3.3.2.2	Quantification and qualification of nucleic acids.....	40
3.3.2.3	Extraction of total RNA from tissue culture.....	40
3.3.2.4	First strand cDNA synthesis.....	41
3.3.2.5	Primer design for expression analysis by semi-quantitative PCR	41
3.3.2.6	Selection of R249S expressing clones with PCR followed by restriction enzyme digestion.....	41
3.3.2.7	Gel electrophoresis of nucleic acids.....	42
3.3.3	Computer analyses.....	42
3.3.4	Quantification of Proteins using Bradford Assay.....	42
3.3.5	Western Blotting.....	42
3.3.6	Senescence-associated beta-galactosidase (SABG) assay.....	43
3.3.7	Immunoperoxidase Staining .....	43
3.3.8	Immunoperoxidase detection of AFB1-DNA adducts and 8-OHdG .....	43
3.3.9	Indirect immunofluorescence .....	44

3.3.10	Costaining with immunofluorescence .....	44
3.3.11	Cell cycle analysis and bromodeoxyuridine (BrdU) incorporation assay	45
3.3.12	Single-cell gel electrophoresis (comet) assay .....	45
<b>CHAPTER 4. RESULTS.....</b>		<b>48</b>
4.1	Tolerance to selenium-deficient conditions.....	48
4.1.1	Analysis of Survival Pathways .....	49
4.1.2	AKT; as a Key for Survival under Selenium deficient conditions .....	53
4.1.3	Inhibition of AKT reverts HepG2-2.2.15 phenotype under Se-deficient conditions.....	56
4.1.4	Inhibition of constitutively active Akt did not recapitulate apoptosis in Mahlavu and Snu475.....	56
4.2	Exploration of oncogenicity of R249S p53 mutation in HCC.....	58
4.2.1	Formation and validation of R249S p53 expressing HepG2 clones.....	58
4.2.2	Subcloning of the selected R249S p53 expressing HepG2 clones.....	61
4.2.3	Survival advantage of R249S p53.....	63
4.2.4	Global histone methylation marker status check.....	70
4.2.4.1	Histone methylation marker status in R249S p53 bearing clones.....	70
4.2.4.2	Histone methylation marker status check in HCC upon Adriamycin and AFB1 treatment.....	76
4.3	Effects of AflatoxinB1-induced genotoxicity in HCC.....	80
4.3.1	AFB1 induced DNA adducts and 8-OHdG lesions in hepatocyte-like cells .....	80
4.3.2	AFB1 exposure induces single and double strand breaks.....	82

4.3.3	AFB1-induced genotoxicity did not affect cell growth and colony survival	84
4.4	AFB1-induced DNA damage response in HCC	92
4.4.1	Increased DNA damage checkpoint foci in aflatoxin B1-exposed cells	92
4.5	Recapitulating the effects of AFB1 in isogenic wild-type and p53 <sup>-/-</sup> HCT116 cells	99
4.5.1	Dose-dependent and differential response of HCT116 and HCT116-p53 <sup>-/-</sup> cells to adriamycin treatment	104
4.5.2	Absence of p53 accumulation and lack of cell cycle arrest in response to AFB1-induced DNA damage	106
4.5.3	DNA damage checkpoint response to AFB1 was incomplete	107
4.6	Mechanism of p53 activation bypass after AFB1 induced DNA damage	111
<b>CHAPTER 5. DISCUSSION and FUTURE PERSPECTIVES</b>		114
5.1	AKT activation is required for selenium deficiency induced resistance	114
5.2	R249S p53 status did not lead to significant growth advantage	116
5.3	After AFB1 exposure DNA damage checkpoint response was incomplete without a p53 activation response	118
<b>REFERENCES</b>		121
<b>ARTICLES PUBLISHED</b>		137
<b>COPYRIGHT PERMISSIONS</b>		176

## LIST OF TABLES

<b>Table 1.2.4.1:</b> DNA methylation alterations observed in some human cancer types.....	12
<b>Table 1.2.5.1:</b> Mammalian selenoproteins and their biological functions.....	15
<b>Table 1.2.5.2:</b> Examples of selenoproteins and corresponding human diseases and cellular functions.....	16
<b>Table 1.2.5.3:</b> Selenium Levels in serum, plasma, whole blood, tissue and erythrocytes in healthy control and patients with different pathology.....	21
<b>Table 3.3.1:</b> Primer Sequences used in this study.....	41
<b>Table 3.3.2:</b> Antibodies used for immunoblotting, immunoflorescence and immunoperoxidase assays.....	45

## LIST OF FIGURES "\*\*\*\*\*"

<b>Figure 1.1.1:</b> Multistages and contributing factors of hepatocellular carcinoma.....	2
<b>Figure 1.2.1:</b> Distribution of HCC incidences, aflatoxin exposure, Hepatitis B virus infection rate and occurrence of R249S mutation according to geographical area.....	3
<b>Figure 1.2.2:</b> Structural depiction of TP53.....	8
<b>Figure 1.2.3:</b> TP53 activation and its functional involvement in cellular process.....	9
<b>Figure 1.2.4:</b> High prevalence of missense mutations involved in p53 compared to other tumor suppressors.....	10
<b>Figure 1.2.5:</b> p53: a two-faced cancer gene.....	11
<b>Figure 1.2.6:</b> Anti-ROS Internal Protection Mechanisms.....	18
<b>Figure 1.2.7:</b> A model of selenium and its association with cell metabolism.....	19
<b>Figure 1.2.8:</b> ROS signaling targets in various biological signaling pathways.....	22
<b>Figure 1.2.9:</b> Aflatoxin Metabolism In Liver and Aflatoxin-induced DNA damage.....	25
<b>Figure 1.2.10:</b> DNA damage checkpoint mechanism and its key regulators in humans..	28
<b>Figure 4.1.1:</b> Analysis of MAPK/ERK signaling pathway under selenium-deficiency..	50
<b>Figure 4.1.2:</b> Analysis of SAPK/JNK signaling pathway under selenium-deficiency.....	51
<b>Figure 4.1.3:</b> Analysis of p38MAPK stress signaling pathway under selenium-deficiency.....	52
<b>Figure 4.1.4:</b> Analysis of p38MAPK stress signaling pathway downstream apoptosis targets .....	53
<b>Figure 4.1.5:</b> Akt survival pathway is induced under selenium deficient conditions.....	54
<b>Figure 4.1.6:</b> Analysis of downstream signals in Akt induced survival under selenium deficient conditions.....	55
<b>Figure 4.1.7:</b> Inhibition of PI3K/Akt induced apoptosis under selenium deficient conditions.....	57
<b>Figure 4.1.8:</b> Inhibition of PI3K/Akt did not induce apoptosis under selenium deficient conditions in Mahlavu and Snu475.....	58
<b>Figure 4.2.1:</b> Validation of transcription of R249S p53 mutation in stable clones.....	60
<b>Figure 4.2.2:</b> Expression of p53 target p21 <sup>cip1</sup> after treatment with Adriamycin in stable clones.....	60

<b>Figure 4.2.3:</b> Validation of transcription of R249S p53 mutation and expression of p21 <sup>cip1</sup> after Adriamycin treatment in subclones .....	63
<b>Figure 4.2.4:</b> Long-term colony formation assay.....	64
<b>Figure 4.2.5:</b> Long-term colony formation assay after DNA damage induction.....	65
<b>Figure 4.2.6:</b> Difference between senescence response induced by low-dose Adriamycin and TGF- $\beta$ 1.....	67
<b>Figure 4.2.7:</b> Aflatoxin induced AFB <sub>1</sub> -DNA adduct detection.....	68
<b>Figure 4.2.8:</b> Comparison of response after AFB <sub>1</sub> and ADR treatment in R249S p53 and wt p53 subclones.....	69
<b>Figure 4.2.9:</b> Global histone methylation marker status check.....	75
<b>Figure 4.2.10:</b> Global histone methylation marker status check upon DNA damage induction.....	78
<b>Figure 4.3.1:</b> Induction of DNA adducts and 8-hydroxy-deoxyguanosine lesions following aflatoxin B1 exposure.....	81
<b>Figure 4.3.2:</b> Induction of persistent single and double strand DNA breaks after AFB1 treatment.....	83
<b>Figure 4.3.3:</b> Aflatoxin treatment does not induce senescence or apoptosis.....	85
<b>Figure 4.3.4:</b> Lack of permanent cell cycle arrest in response to AFB1-induced DNA damage.....	86
<b>Figure 4.3.5:</b> Cell cycle analysis of HepG2 cells after Aflatoxin and Adriamycin treatment.....	87
<b>Figure 4.3.6:</b> Cell cycle analysis of Huh7 cells after Aflatoxin and Adriamycin treatment .....	88
<b>Figure 4.3.7:</b> Cell cycle analysis of Hep3B cells after Aflatoxin treatment.....	88
<b>Figure 4.3.8:</b> Cell cycle checkpoint key players localize into nucleus.....	90
<b>Figure 4.3.9:</b> The effects of AFB1 or ADR treatment of HepG2 cells for 4 hours or 24 hours on cell survival-colony forming ability.....	91
<b>Figure 4.4.1:</b> Induction of 53BP1 and phospho-H2AX foci following aflatoxin B1 exposure.....	93
<b>Figure 4.4.2:</b> Time-dependent increase in 53BP1 foci-positive cells under aflatoxin B1 exposure .....	94



<b>Figure 4.4.3:</b> The duration of 53BP1 foci after 24 hours of exposure to AFB1.....	95
<b>Figure 4.4.4:</b> Activation of ATM, but not ATR after aflatoxin B1 exposure.....	96
<b>Figure 4.4.5:</b> Nuclear phospho-Chk1 expression was not affected after exposure AFB1 or ADR.....	96
<b>Figure 4.4.6:</b> Incomplete DNA damage checkpoint response of HepG2 cells to AFB1..	98
<b>Figure 4.4.7:</b> Incomplete DNA damage checkpoint response of Huh7 cells to AFB1.....	99
<b>Figure 4.5.1:</b> Induction of 8-hydroxy-deoxyguanosine lesions and double strand breaks following aflatoxin B1 exposure.....	101
<b>Figure 4.5.2:</b> Increased DNA damage foci detection after exposure of HCT116 isogenic clones to aflatoxin B1.....	103
<b>Figure 4.5.3:</b> p53-dependent and p53-independent cell cycle arrest after adriamycin treatment.....	105
<b>Figure 4.5.4:</b> Lack of cell cycle arrest in response to AFB1-induced DNA damage.....	107
<b>Figure 4.5.5:</b> Incomplete DNA damage checkpoint response to AFB1.....	110
<b>Figure 4.5.6:</b> Demonstration of the lack of phospho-p53ser15 accumulation in phospho-ATMser1981-positive nuclei after aflatoxin B1 exposure.....	111
<b>Figure 4.6.1:</b> Comparative analysis of wild-type p53 response of HCT116 cells to AFB1 and Adriamycin treatment indicates that AFB1 cannot induce effective p53 activation.....	113
<b>Figure 5.1.1:</b> Activated signaling pathways and cell fate upon oxidative stress.....	115
<b>Figure 5.3.1:</b> Schematic representation of proposed mechanism of response after Adriamycin and AFB1 exposure.....	120

## ABBREVIATIONS

8-OHdG	8-hydroxydeoxyguanosine
ADR	Adriamycin
AFB1	AflatoxinB1
AFB1-N7-Gua	8,9-dihydro-8-(N7-guanyl)-9-hydroxy AFB1
AFB1-FAPY	AFB1-formamidopyrimidine
AI	Allelic imbalance
APC	Adenomatous polyposis coli
BSA	Bovine serum albumin
BrdU	Bromodeoxyuridine
CGH	Comparative genomic hybridization
DAB	Diaminobenzidine
DBD	DNA binding domain
DDR	DNA damage response
DEPC	Diethylpyrocarbonate
DMEM	Dulbecco's Modified Eagle's Medium
DNA	Deoxyribonucleic acid
ECL	Enhanced ChemiLuminescence
EDTA	Ethylenediaminetetraacetic acid
ERK	Extracellular signal-regulated kinase
FBS	Fetal bovine serum
FDA	Food and Drug Administration
g	Gram
GAPDH	Glyceraldehyde-3-phosphate dehydrogenase
Gpx	Glutathione peroxidase
GSK3 $\beta$	Glycogen synthase kinase 3 beta

HBV	Hepatitis B Virus
HbX	Hepatitis B virus X protein
HBXAg	Hepatitis B virus X antigen
HCC	Hepatocellular Carcinoma
HCV	Hepatitis C Virus
HIV	Human immunodeficiency virus
hMSH2	Human Mut S homolog-2
HRP	Horse radish peroxidase
hTERT	Human Telomerase Reverse Transcriptase
HU	Hydroxyurea
IGF2	Insulin-like growth factor 2
IGF2R1	IGF2 Receptor
JNK	Jun Kinase
KO	Knock out
LOH	Loss of heterozygosity
MAPK	Mitogen Activated Protein Kinase
MDM2	Mouse Double Minute 2
mg	Milligram
$\mu$ M	Micromolar
ml	Milliliter
$\mu$ l	Microliter
NaCl	Sodium Chloride
NaOH	Sodium Hydroxide
NADP hydrate	$\beta$ -Nicotinamide adenine dinucleotide phosphate sodium salt
NAD(P)H	Nicotinamide adenine dinucleotide phosphate
NAFLD	Non alcoholic fatty liver disease
NER	Nucleotide excision repair
NS3	Nonstructural Protein 3
NS5A	Nonstructural Protein 5A
O/N	Over night

PBS	Phosphate Buffered Saline
PBS-T	Phosphate Buffered Saline with Tween-20
PCR	Polymearase chain reaction
PDGFR- $\beta$	Platelet-derived-growth-factor receptor- $\beta$
PI-3 kinase	Phosphatidylinositol 3-kinase
PKR	Double-stranded RNA protein kinase
pRb	Retinoblastoma protein
RNA	Ribonucleic acid
ROS	Reactive oxygen species
RTK	Receptor tyrosine kinases
SABG	Senescence associated beta galactosidase
SAPK	Stress-activated protein kinase
Se	Selenium
SOD	Superoxide dismutase
TAE	Tris-acetic acid-EDTA
TBS	Tris Buffered Saline
TBS-T	Tris Buffered Saline with Tween-20
TGF- $\alpha$	Transforming growth factor alpha
TGF- $\beta$	Transforming growth factor beta
TLS	Translesion bypass synthesis
TNF	Tumor necrosis factor
Tris	Tris (hydroxymethyl)-methylamine
TRxR	Thioredoxin reductase
UV	Ultraviolet

# CHAPTER 1. INTRODUCTION

## 1.1 Hepatocellular malignancy

Hepatocellular carcinoma (HCC) is considered as one of the most widespread malignancies worldwide. It is ranked as the fifth most common cancer [1]. Due to its resistance to therapy and the limitations of the existing chemotherapeutic drugs and lack of biomarkers for early detection and resection, the five year survival of HCC patients is less than 3% [2][1]. HCC frequency fluctuates depending on the geographical area. Eastern and southeastern Asia, some part of Western Pacific Islands, and most parts of South Africa are the areas with high occurrence, [3], [4], its incidence in Europe and USA is low, but increasing [5], [6].

More than 90 % HCC tumor development takes place in chronic hepatitis or a cirrhosis background [7]. Although under normal cellular conditions, adult hepatocytes do not divide, as a response to chronic exposure to Hepatitis B Virus (HBV), Hepatitis C Virus (HCV), alcohol, Aflatoxins [8] and cellular factors such as iron, copper and reactive oxygen species (ROS) accumulation in liver [9] (Figure 1.1.1), many hepatocytes are killed, [10], [3] and in order to compensate the liver necrosis hepatocyte proliferation increases. Rounds of destructive and regenerative proliferation process lead not only to chronic liver disease which ends up with liver cirrhosis but also this turnover causes the accumulation of irreversible genetic alterations [11]. Cirrhosis is a stage caused by excessive collagen deposition induced by fibrotic scarring of the liver. Cirrhosis is followed by hyperplastic nodules and subsequently with dysplastic nodules. The last stage of 10-30 years of this slow process is HCC [12], which is classified as well differentiated, moderately differentiated and poorly differentiated [13].

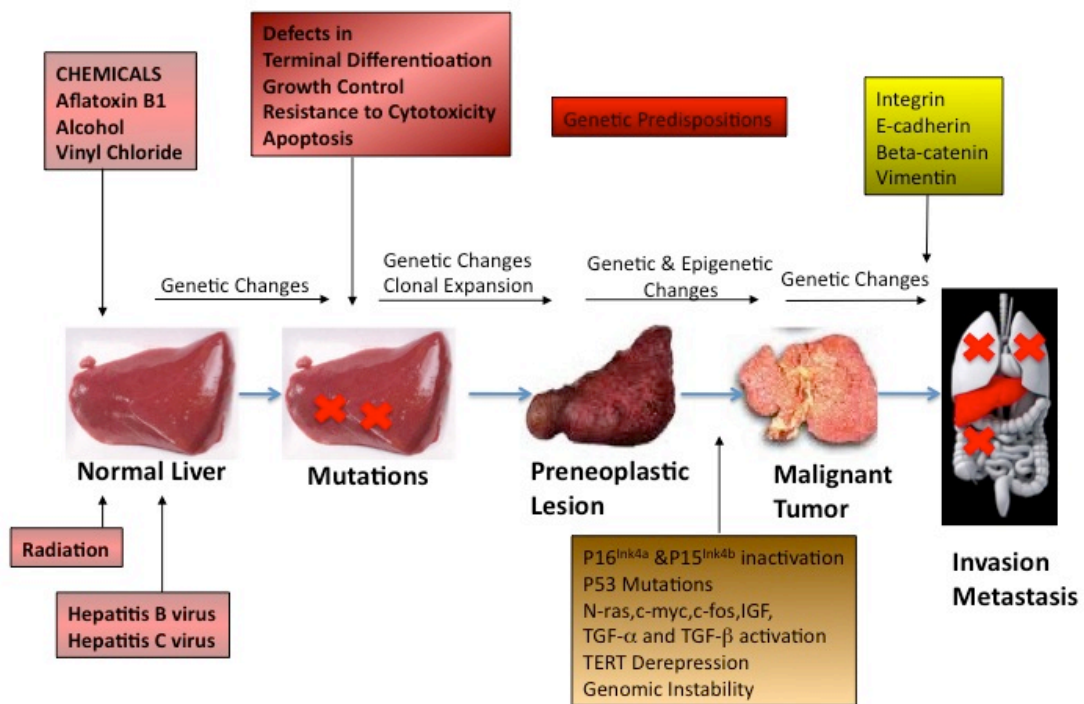


Figure 1.1.1 Multistages and contributing factors of hepatocellular carcinoma. Modified from [14].

## 1.2 Pathogenesis of hepatocellular carcinoma

### 1.2.1 Viral factors

Two billions and 170 million people are infected by HBV and HCV respectively worldwide [15]. Nearly, 30-50 % of the HBV-related deaths are due to HCC. HCV on the other hand contributes to 20% of liver cirrhosis and 2.5% of HCC [16], [17]. (Figure 1.2.1)

HBV can lead to carcinogenesis by mainly 3 different ways. First, the viral DNA can be integrated into the host genome and cause chromosome instability [18]. Second, while integrating into the host genome, insertional mutations can be induced associated with activation of certain genes such as retinoic acid  $\beta$ -receptor [19], cyclin A [20], platelet-derived-growth-factor receptor- $\beta$  (PDGFR $\beta$ ), mitogen activated protein kinase 1 (MAPK1) and human telomerase reverse transcriptase (hTERT) [21] in which site specific HBV integrations were observed in independent tumors[22], [23], [24]. Third mechanism is based on HBV encoded X antigen (HBxAg), one of

the viral proteins expressed by HBV. Even though, the function of HBxAg is still not fully understood, it has been reported to be a modulator of cell proliferation and viability [25],[26, 27]. Along with HBxAg, PreS2 structural protein, encoded by viral S gene can serve as transactivator proteins [28] and activate AP-1 and NFκB transcription factors that, in turn, lead to the activation of signaling pathways. The most important function of HBx in terms of tumorigenesis consists in its ability to bind the tumor suppressor p53 in vitro. Thus, while inactivating p53 activities, it contributes to cell survival and proliferation [29, 30].

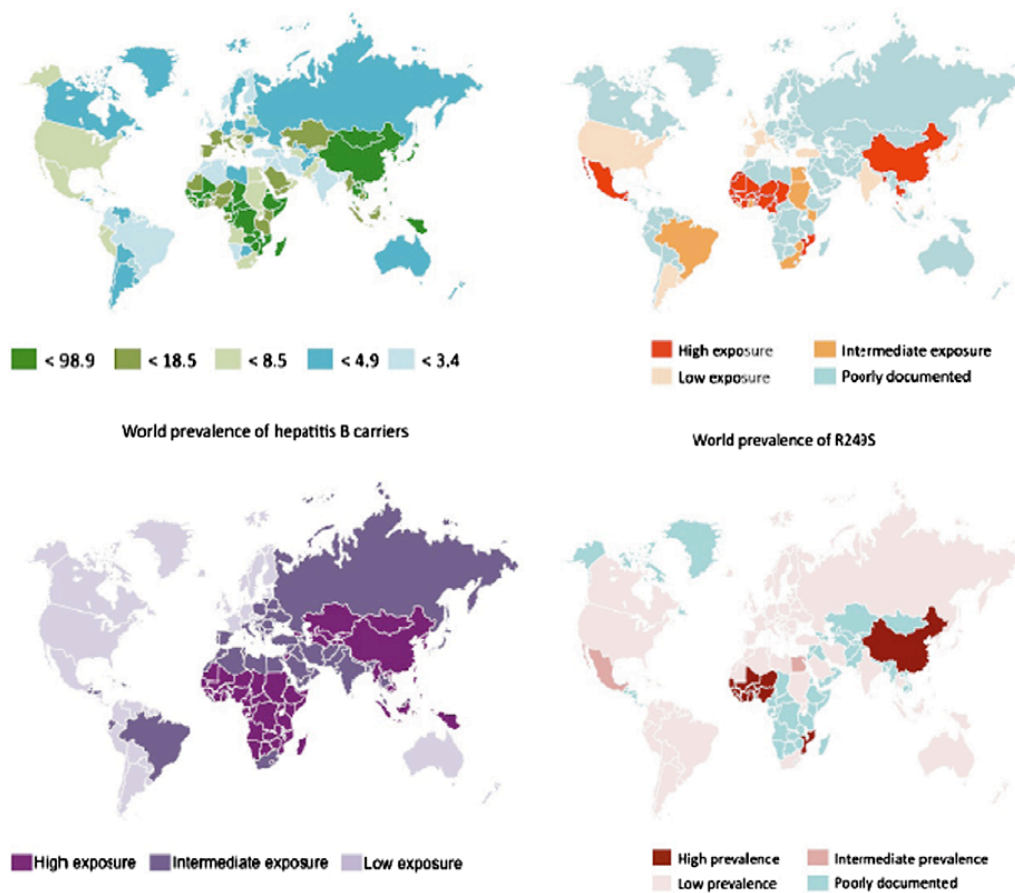


Figure 1.2.1 Distribution of HCC incidences, aflatoxin exposure, Hepatitis B virus infection rate and occurrence of R249S mutation according to geographical area [31].

HCV, opposite of HBV is an RNA virus, and can not integrate into the host genome [32]. The molecular mechanisms of HCV-induced persistent infection in hepatocytes

are not fully known. Recent studies indicated that viral proteins interact with a variety of important cellular proteins, such as apolipoprotein AII, 14-3-3 protein, tumor necrosis factor (TNF) receptor, DEAD domain of RNA helicase, lymphotoxin- $\beta$  receptor, double-stranded RNA protein kinase (PKR), nuclear ribonucleoprotein, p53, SNARE-like protein [33-35]. It causes the down-regulation of p21<sup>cip1</sup> expression [36], the activation of Ras/Raf signaling pathway and has an anti-apoptotic activity [37]. The 5' region of the HCV genome encoding the nonstructural protein 3 (NS5A) has an oncogenic potential and NS5A was shown to interact with p53 *in vivo* [38]. HCV core protein and NS3 or NS5A inactivate p53 by transcriptional repression [39, 40], or directly binding to p53 [41, 42], respectively.

In addition to the functions of virus proteins in HCC, chronic infection by HBV and HCV contribute to HCC by activating cytokines and growth factors including insulin-like growth factor-2 (IGF2) and transforming growth factor- $\alpha$  (TGF- $\alpha$ ) in preneoplastic hepatocytes, leading to the enhancement of proliferation and accumulation of genomic alterations [10, 43].

## 1.2.2 Genetic alterations

### 1.2.2.1 Allelic imbalance and microsatellite instability

Many chromosomal aberrations and genetic mutations in HCC have been detected by genome-wide allelotyping studies. These conventional cytogenetic methods performed with hepatocellular cell lines and liver tumor tissues demonstrated that most HCCs are aneuploid and harbor multiple allelic imbalances (AI) on 1p, 1q, 4q, 6q, 8p, 8q, 9p, 10q, 13q, 16p, 16q and 17p chromosomal arms [44-51].

Further studies with comparative genomic hybridization (CGH) revealed that AI was associated with gene dose decrease on 1p, 4q, 6q, 8p, 9p, 10q, 13q, 16q and 17p and gene dose increase on 1q and 8q [52-59]. However, due to the technical limitations of the conventional methods, the frequency of AI with gene dose increase was underestimated and recent studies indicated additional gene dose increases on 6p, 17q, 20q, 1q and 8q [51].



Alterations on chromosomes 3p, 5q and 6q can be related to the activation of  $\beta$ -catenin (CTNNB1) that is reported to be associated with 19% of HCC [60], the adenomatous polyposis coli (APC) gene that is involved in the Wnt signaling pathway and is responsible for the initiation of  $\beta$ -catenin degradation, and the loss of mannose 6-phosphate/insulin-like growth factor II receptor (M6P/IGF2R) that contributes to the dysplastic nodules and HCC [61]. Loss of heterozygosity occurs in 50-80% of dysplastic nodules [10]. Although the microsatellite instability is associated with the failure of DNA mismatch repair genes *MSH2* and *MLH1* on chromosomes 2 and 3 [62], in HCC those chromosomal locations are not commonly disturbed by allelic deletions. However, about 30% of HCCs were reported to be linked to mutations in another DNA mismatch repair gene called Human Mut S homolog-2 [63].

Aberrations on chromosome 9p are associated with two-tumor suppressor proteins p16<sup>ink4A</sup> and p14ARF. p16<sup>ink4A</sup> inactivation was detected in 48% of HCC due to the hypermethylation of its promoter [64-66], while p14ARF inactivation was found in 15 % of HCC cases, caused by deletion or promoter methylation [67]. An allelic loss of 10q resulting in the loss of somatic phosphatase and tensin homolog (PTEN) gene, a negative regulator of the phosphoinositide 3-kinase/AKT signaling pathway [68, 69], was observed in 27 % of HCC cases. The amplification and overexpression of cyclin D1 on 11q has been stated [70]. The loss of 13q region attributes to the loss of Rb tumor suppressor gene in 16% of HCC [71] and BRCA2 in 3 out of 60 HCCs, [72]. Alterations in Axin1 gene, which is crucial for the degradation of cytoplasmic  $\beta$ -catenin on 16p, was reported to be involved in 5 % of HCC without  $\beta$ -catenin mutation [73]. TP53 tumor suppressor gene located on 17p.13.1 was indicated to contain mutations in 32% of HCC.

#### 1.2.2.2 Cell cycle regulation

Signaling pathways, connecting growth and metabolic signals to the control of the cell cycle checkpoints in hepatocytes, have drawn attention since their key players are frequently disrupted in HCC.

The period between the late G1 and S phases is one of the most important phases of the cell cycle. During this period, G1 checkpoint barriers decide whether to proceed

with the S phase or to rest at G1. At this point the most important pathways are the cyclin D1-Rb-CDK4/6 pathway or the p53-p14ARF pathway [74, 75].

Basically, during the G1/S transition, cyclin D1/cyclin dependent kinase 4 or 6 and cyclin E/cyclin dependent kinase 2 dimers sequentially phosphorylate the retinoblastoma (Rb) protein to allow the dissolution of the repressive complex thereby allowing the transcription of E2F target genes. Consequently, cells can enter the S phase for proliferation [76-78]. Several evidences have been provided indicating the link between HCC and cyclin D1-Rb-CDK4/6 pathway. *In vivo* studies revealed that in early stages of carcinogenesis, hepatocyte proliferation is associated with E2F-1 overexpression [79, 80]. Cyclin D1 overexpression in the liver is sufficient to induce hepatocyte replication [81] and research on transgenic models using chemical inhibitors revealed the importance of cyclinD1 for the signaling of hepatocytes progression through the G1/S barrier [81-85]. The increased expression of the cyclin D1 in HCCs is considered to be due to gene amplification or chromosomal rearrangements, thus is probably a late event in HCC that causes tumor growth rather than tumor initiation [70].

INK4a ARF locus on 9q21 encodes two proteins with different functions; p16 (INK4a) which acts as an inhibitor of CDK4 and cyclin D association, thereby contributing to the maintenance of Rb protein in its anti-proliferative-active state [75] and the p14<sup>ARF</sup> tumor suppressor is a key regulator of p53 stabilization [86] by antagonizing the activity of MDM2, a negative regulator of p53 stability. It initiates a p53-dependent transcriptional response such as growth arrest or apoptosis in normal and cancer cells. As it is discussed in previous section, INK4a-ARF locus is disturbed in HCC; 50% of HCC presents *de novo* methylation and 20 % of HCC shows LOH in the same locus [11, 87].

### 1.2.2.3 Alterations of the TGF- $\beta$ and PI3K pathway

Transforming growth factor- $\beta$  (TGF- $\beta$ ) mediates growth arrest through the transcriptional activation of p15<sup>ink4B</sup> and p21<sup>cip1</sup>; the CDK inhibitors. TGF- $\beta$  allows also the transcriptional suppression of c-myc, CDK4 and cdc25A expression in epithelial and other cell types[88]. TGF- $\beta$  is considered as a double-edged sword,

because of the fact that it can act as an early tumor suppressor, but later contributes to tumor progression by its action on the tumor cells and their microenvironment inducing invasion and metastasis.

Regarding to the role of TGF- $\beta$  in hepatocarcinogenesis, current data is conflicting. While in normal cultured hepatocytes, the addition of TGF- $\beta$  inhibits hepatocyte proliferation; studies in multiplicity of cell types that express TGF- $\beta$  and its receptors in the liver indicated the role of TGF- $\beta$  in the regulation of proliferation, apoptosis, angiogenesis, tumor invasiveness and immune surveillance in liver carcinogenesis. In clinical samples, TGF- $\beta$  and TGF- $\beta$ RII receptors have been found to be downregulated in early HCC compared to surrounding liver, while the expression of TGF- $\beta$  receptors were inversely correlated with tumor size and proliferative index [89-92]. Recent studies performed by our group indicated that TGF- $\beta$  induces p21<sup>Cip1</sup> and p15<sup>Ink4b</sup> and ROS-dependent senescence in well-differentiated HCC cells, along with a strong anti-tumor response *in vivo*, yet poorly differentiated HCC cells found to be resistant to TGF- $\beta$  induced senescence [93]. All these findings are consistent with the concept of the function of TGF- $\beta$  as a tumor suppressor in early stages, yet, in late tumors; this cytokine may contribute to tumor progression by activating pathways involved in tumor invasion and angiogenesis.

The activation of phosphatidylinositol 3-kinase (PI3K)/Akt/mTOR signaling cascade has been identified in many cancer cells [94]. The function of PI3K is controlled by PTEN in a negative direction. Mutations [95] and the functional loss of PTEN [96] have been reported in about 0-11% and >55% of HCC cases respectively. Upon activation of PI3K cascade, various survival genes are transcribed [97]. An important survival target of PI3K is a serine/threonine kinase AKT. When activated, it inactivates many pro-apoptotic proteins as well as its important downstream effector mTOR by phosphorylating them [97]. Activation of this pathway is associated with poor prognosis in HCC [98].

Inhibition of the PI3K/AKT/mTOR pathway as a chemotherapeutic treatment is possible at various levels. Research in HCC animal models and HCC cell lines demonstrated limited efficiency of PI3K inhibitors such as wortmannin, LY294002 [99] and FTY720 [100]. The most promising inhibitors of PI3K pathway are mTOR and have been tested in pre-clinical and clinical studies of HCC [101-103]. The major

concern for the use of kinase inhibitors as chemotherapeutic drugs in HCC is the potential limitations due to the cross-talk between different signal-transducing pathways as well as the complexity of HCC [104].

### 1.2.3 TP53

The TP53 gene, located on chromosome 17p13.1 is regarded as an important tumor suppressor protein and “the guardian of genome” and possesses a fundamental role as the major controller of cellular activities concerning the genomic integrity, transcription, cell cycle, development process and the control of apoptosis, senescence and DNA repair [105, 106]. It encodes a 53kD DNA-binding transcription factor and it is a haploinsufficient tumor suppressor [107, 108]. Accordingly, malfunction in the p53 pathway is a hallmark of human cancers [109]. Wild-type p53 protein functions as a tumor suppressor *in vitro* and *in vivo*. Around 50% of all human cancers contain p53 mutations [110]. Beside the incidence of such frequent somatic mutations in human cancers, there are germline mutations in the p53 gene in some cancer-prone families with Li-Fraumeni syndrome as well [111].

p53 protein is structurally organized with several domains consisting of transactivation domain in its N-terminal region, a proline rich regulatory domain, a central DNA binding domain (DBD) and a C-terminal regulatory area including nuclear localization and oligimerization domains [112] (Figure 1.2.2).

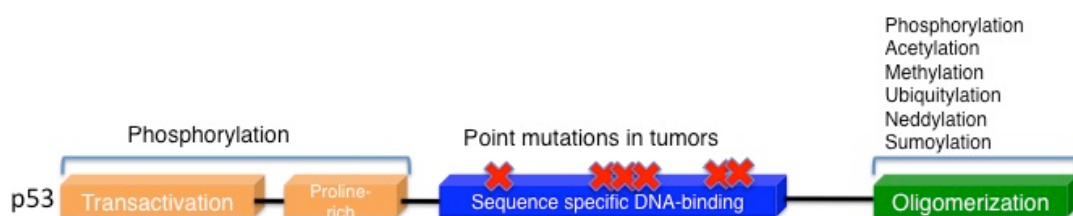


Figure 1.2.2 Structural depiction of TP53. Each cube represents p53 functional domains. Modified from [109].

Control of regulation and activation of p53 is a crucial event for the cells. Under normal unstressed conditions, p53 is kept inactive with the activity of negative regulator MDM2. MDM2 can either directly bind to the N-terminal transactivation domain of p53 [113, 114]) or ubiquitylate the protein and lead to the export of p53 to the cytoplasm [114]. Under high levels of stress conditions, the interaction between MDM2 and p53 are disrupted by post transcriptional modifications allowing the active p53 to function as a transcription factor; depending on the response to be given, inducing or suppressing the target genes involved in apoptosis, senescence, cell cycle arrest, DNA repair, angiogenesis[115] (Figure 1.2.3).

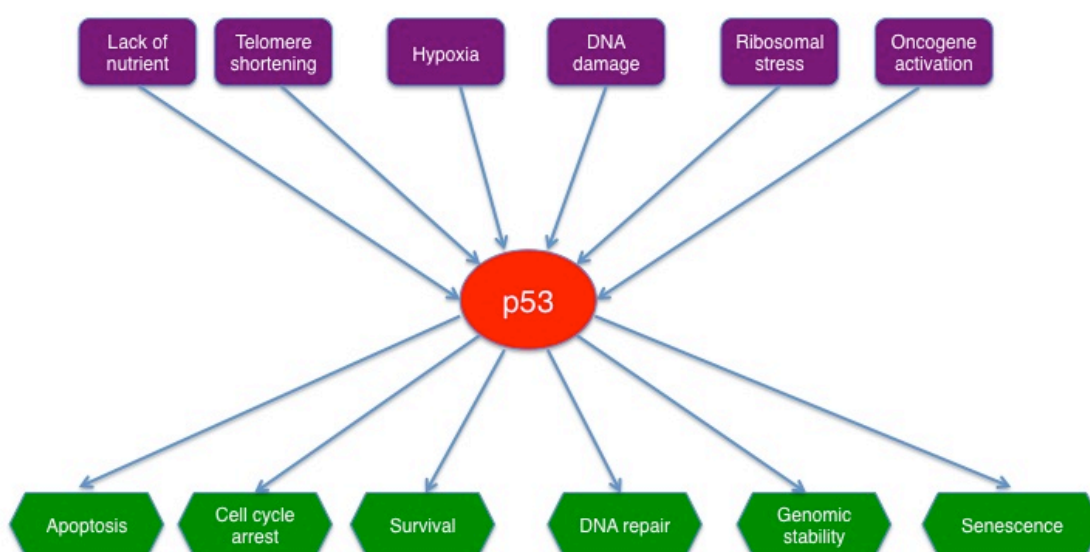


Figure 1.2.3 TP53 activation and its functional involvement in cellular process. Purple boxes and green boxes represent the various types of stress and cellular events, respectively. (Modified from [116]).

TP53 is unique with an incidence of 74% of missense mutations (Figure 1.2.4), occurring in the DBD of p53, yet resulting in full-length, slightly altered, albeit stable proteins with varying residual activities [117, 118]. Such elevated occurrence of mutations proposes a powerful selective pressure for disturbance of normal p53 function in the development of tumorigenesis [119]. Interestingly, mutant p53 proteins have very unique features in terms of structure, biochemical and biological aspects. Mutations in DBD are classified into two groups based on their thermodynamic stability and DNA binding properties; contact mutations that affect

directly DNA binding such as Arg-248 and Arg-273 and structural mutations that affect structural integrity of DNA binding site such as Arg-175, Gly-245, Arg-249 and Arg-282 [120].

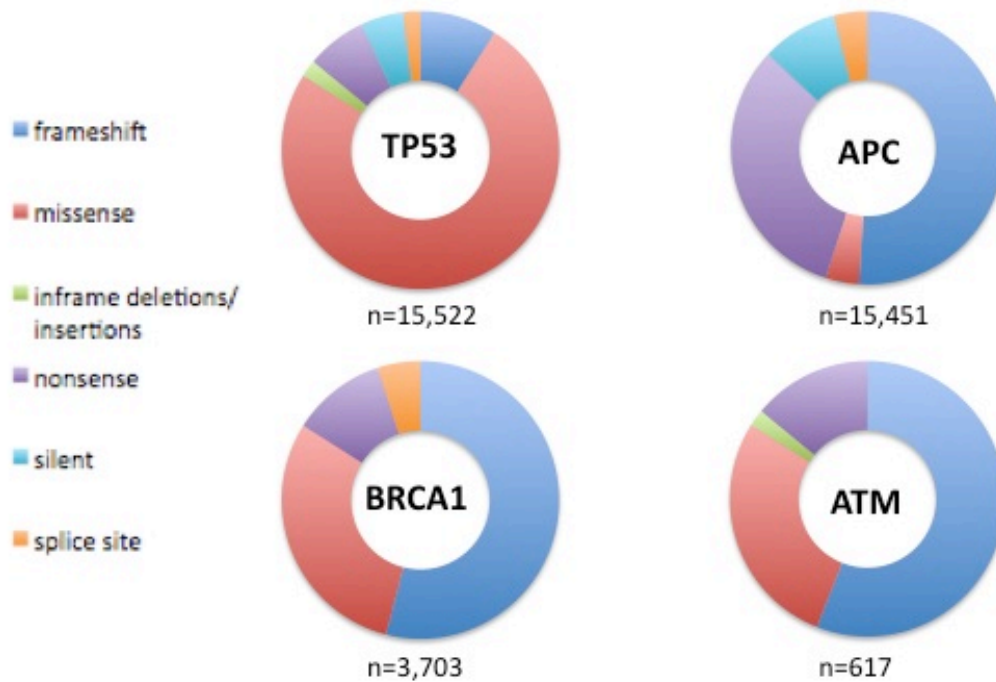


Figure 1.2.4 High prevalence of missense mutations involved in p53 compared to other tumor suppressors. (Modified from Weinberg RA. Biology of Cancer, Chapter 9:311-314, Garland Pub, 2006)

Mutant p53 proteins are considered to have oncogenic activities in tumor cells (Figure 1.2.5) [121]. In addition, observed amounts of mutant p53 protein in tumor cells are elevated when compared to both wild-type p53 and mutant p53 amounts in normal cells [122-124]. However, how this selectivity is established and sustained is not fully evidenced yet.

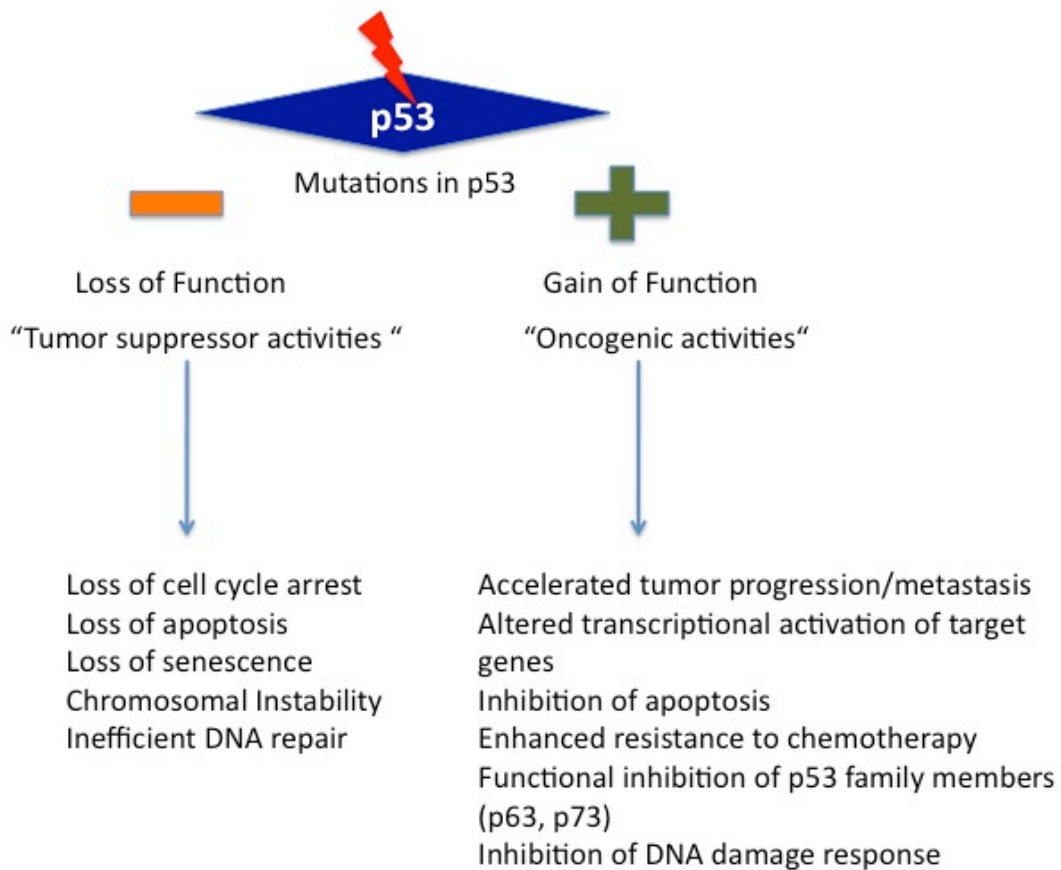


Figure 1.2.5 p53: a two-faced cancer gene. Modified from [125].

### 1.2.3.1 p53 and HCC

p53 alterations are generally linked to poorly differentiated tumors and low survival rate [126]. After the restoration of p53 expression in murine liver tumors, senescence is triggered and tumor development is diminished [127]. Functional inactivation of p53 by HBx has been described in HCC and discussed in detail in section 1.2.1. The loss of p53 almost certainly plays an important role in HCC progression by contributing to proliferation under cirrhotic conditions in which oxidative stress; regeneration and genomic instability are provoked. Recent *in vivo* data indicated that, defect in a DNA repair gene Ku70 accelerates liver carcinogenesis under the setting of loss of p53 through proteosomal degradation [128]. Heterozygosity in p53 in the course of germ line mutations may also facilitate HCC progression *in vivo* with telomere shortening, thereby chromosome instability [129-131].

The alterations in p53 are concentrated between exon 4 and 9 of DBD. The most important alteration among these mutations is the transversion in codon 249 (G→T), which causes an arginine to serine (R→S) substitution and exists in 50% of HCCs. This mutation will be discussed in detail in following sections.

## 1.2.4 Epigenetic regulations

### 1.2.4.1 DNA methylation

Cancer is closely associated with global hypomethylation and CpG island hypermethylation [132]. The shift in DNA methylation pattern commonly results in improper silencing of genes especially the tumor suppressors through hypermethylation or protooncogene activation including c-JUN, c-MYC, and c-Ha-Ras; and generates genomic instability through global DNA demethylation. Table 1.2.4.1 depicts the DNA methylation alterations observed in different human cancer types.

Table 1.2.4.1 DNA methylation alterations observed in some human cancer types. (Modified from [133]).

Cancer Type	Epigenetic Alteration
<b>Colon cancer</b>	CpG-island hypermethylation (MLH1, p16, p14, RARB2, SFRP1, WRN), global genomic hypomethylation, hypermethylation of miRNAs, loss of imprinting of IGF2, mutations of histone modifiers, decrease monoacetylated and trimethylated forms of H4
<b>Breast cancer</b>	CpG-island hypermethylation (BRCA1, E-cadherin, TMS1, ER), global genomic hypomethylation
<b>Lung cancer</b>	CpG-island hypermethylation (p16, DAPK, RASSF1A), global genomic hypomethylation, genomic deletions of CBP and BRG1
<b>Glioma</b>	CpG-island hypermethylation (MGMT, EMP3, THBS1)
<b>Leukemia</b>	CpG-island hypermethylation (p15, EXT1, ID4), translocations of histone modifiers
<b>Lymphoma</b>	CpG-island hypermethylation (p16, p73, MGMT), decrease monoacetylated and trimethylated forms of H4
<b>Bladder cancer</b>	CpG-island hypermethylation (p16, TPEF/HPP1), hypermethylation of miRNAs, global genomic hypomethylation
<b>Kidney cancer</b>	CpG-island hypermethylation (VHL), loss of imprinting of IGF2, global genomic hypomethylation
<b>Prostate cancer</b>	CpG-island hypermethylation (GSTP1), gene amplification of EZH2, aberrant modification pattern of H3 and H4
<b>Esophageal cancer</b>	CpG-island hypermethylation (p16, p14), gene amplification of JMJD2C/GASC1
<b>Stomach cancer</b>	CpG-island hypermethylation (MLH1, p14)
<b>Liver cancer</b>	CpG-island hypermethylation (SOCS1, GSTP1), global genomic hypomethylation
<b>Ovarian cancer</b>	CpG-island hypermethylation (BRCA1)



#### 1.2.4.2 Histone modifications

Nucleosomes are the basic units of DNA packaging. They are made up of 147 base pairs of DNA wrapped around a histone protein core. The core histones (H3, H4, H2A and H2B) undergo posttranslational modifications including methylation, acetylation, phosphorylation, ubiquitination. Combinations of these modifications constitute a “histone code” which is important for the biological activities such as gene expression regulation and DNA repair.

However, the modifications that occur on histones are extremely complex and diverse due to the fact that lysines or arginines can be methylated with one of three different forms: mono-, di-, or trimethyl and mono- or di- (asymmetric or symmetric) respectively [134].

Lysine methylation takes part in gene regulation depending on which residue is modified. While methylation of histone H3 lysine 4 (H3K4) and histone H3 lysine 36 (H3K36) is related with transcription, methylations of H3 lysine 9 (H3K9), H3 lysine 27 (H3K27), and H4 lysine 20 (H4K20) are usually associated with deactivation. Lysine acetylation, is almost always linked to chromatin accessibility and transcriptional activity.

#### 1.2.4.3 Histone methylation and cancer

Novel technologies provide global assays for the exploration of key epigenetic marks including histone modifications. Accumulating data suggested the relationship between cell or context-specific histone modification patterns and cell or context-specific gene expression, and these modulations have been associated with many cancers. Recent research demonstrated the association with H3K27 trimethylation patterns with prostate, lung, and breast cancers; and H3K9 and H3K79 modification patterns with leukemia [135-142]. Association of H4K20 with cancer is demonstrated in a study, which reports the selective loss of the trimethylation of H4K20 in tumor cells, thereby contributing to the sensitization of mice to tumorigenesis [143].

The major clue, which demonstrates the direct link between histone methylation, marks and HCC comes from a study that was conducted in a methyl deficient rat

model. During hepatocarcinogenesis, in rats fed with a methyl-deficient diet, H4K20 trimethylation levels were diminished along with an ongoing reduction in the expression of Suv4-20h2 histone methyltransferase and a major rise in H3K9 trimethylation in preneoplastic nodules and liver tumors [144].

Even though, all these current studies provide experimental evidence on the inevitable role of histone methylation in the course of tumor onset and/or progression in various cancer types including HCC, ongoing research will enlighten this relationship better.

### 1.2.5 Dietary factors involved in HCC

#### 1.2.5.1 Alcohol abuse

Alcohol consumption is related to an augmented risk of liver cancer in the absence of chronic hepatitis and is considered not to be safe at any level of consumption [145, 146]. Alcohol intake contributes to liver cancer by facilitating the onset of liver cirrhosis [147]. During alcohol metabolism, the generation of acetaldehyde and free radicals is enhanced [148] and these reactive species can immediately bind to DNA and proteins [149-151] and decrease the DNA repair capacity and antioxidant defense mechanisms [150, 152]. Thus, consequences of alcohol metabolism on genomic integrity and DNA repair processes are expected to participate considerably to the development of transformation. Alcohol also affects hepatic metabolism and hepatocyte signal transduction pathways involved in the regulation of normal hepatocyte function and proliferation as well [153].

#### 1.2.5.2 Obesity

Obesity has been established to be an important risk factor for the progression of various malignancies, including liver cancer by contributing to the onset of NAFLD (non alcoholic fatty liver disease)[154];[155]. Obesity and hepatic steatosis also play role in the development of HCC in other liver diseases such as chronic HCV [155]. Death from liver cancer among obese males demonstrated the highest relative risk of

all the cancers. In a population-based cohort study, only men had significantly increased risks for cancers of the small intestine, liver, and pancreas, and for Hodgkin's disease [156, 157]. The higher risks observed for liver and pancreas cancers among men were correlated with higher plasma insulin concentrations and alcohol abuse [157].

### 1.2.5.3 Selenium deficiency and liver diseases

#### 1.2.5.3.1 Selenium and its deficiency

Selenium (Se) is an essential trace element, which is a major component of selenoproteins with essential biological functions (Table 1.2.5.1).

Table 1.2.5.1 Mammalian selenoproteins and their biological functions ([158] see copyright permissions).

Selenoproteins	Biological Functions
Glutathione peroxidases [GPx1 (in erythrocytes or cystolic), GPx2(gastro intestinal), GPx3 (in plasma or extracellular) and GPx4 (phospholipid hidroperoxide or intracellular)]	Antioxidant enzymes that protect against the oxidative stress by scavenging of hydrogen peroxide and lipid and phospholipidic hydroperoxides. Finally, H <sub>2</sub> O <sub>2</sub> and a wide range of organic hydroperoxides are transformed to water and corresponding alcohols, respectively.
Iodothyronine deiodinases (three isoforms: type I in liver, kidney and thyroid gland; type II in encephalon; and type III inactivant)	Synthesis and metabolic regulation of thyroid sulphated hormones (T <sub>3</sub> , T <sub>4</sub> and T <sub>2</sub> ).
Thioredoxin reductases (also three isoforms)	Reduction of intracellular substrates like dehydroascorbic being related with anticancer effects. Specifically it participates in the reduction of nucleotides in the DNA synthesis as well as in the regulation of gene expression by redox control of binding of transcription factors to DNA.
Selenoprotein P	Extracellular antioxidant associated to the vascular endothelium that protects endothelial cells against damage from peroxynitrite.
Selenoprotein W	Although it is necessary for muscle function its biological function is still unknown.
Selenophosphate syntetase (two isoforms)	Necessary for the biosynthesis of selenophosphate and, consequently, for that of S-Cys necessary for the selenoprotein synthesis.
Mitochondrial capsule selenoprotein	GPx4 form that shields developing sperm cells from oxidative damage.
Prostate epithelial selenoprotein	It is a 15 kDa selenoprotein that seems to have redox function that resembles that of GPx4 in the epithelial cells of ventral prostate.
DNA-bound spermatid selenoprotein	It is a 34 kDa selenoprotein with a biological activity like the GPx.
18 kDa selenoprotein	Essential selenoprotein preserved in selenium deficiency.

Selenium's antioxidant effects stem from its necessity for many enzyme families such as glutathione peroxidases (Gpxs) and thioredoxin reductases that function to protect cellular macromolecules from the oxidative stress damage.

Se-deficiency is associated with diseases such as Keshan disease, heart diseases, liver necrosis, and some cancer types (Table 1.2.5.2).

Table 1.2.5.2 Examples of selenoproteins and corresponding human diseases and cellular functions

Disorder	Cause	Selenoprotein or cofactor	Function
Keshan Disease	Selenium deficiency/ coxsackie B virus	Various, GPX?	??
Kashin-Beck disease	Selenium/iodine deficiency	DIO	Thyroid hormone production
Epilepsy	Selenium deficiency?	GPX?	Oxidative stress
Multiminicore disease	Mutations	SeIN	Calcium signaling
Thyroid dysfunction	Mutations	SBP2	Selenoprotein synthesis
Inflammation responses	Polymorphisms	SeIS	Removal of misfolded proteins
Neurodegeneration	??	SeIP, SeIM, ??	Oxidative stress
Cancer	Polymorphisms/ Expression	GPX1, GPX2 and GPX4, SeIS, SeIP, Sep15, TRXR	Various
HIV	Virus	TRXR1, GPX?	Viral gene expression, oxidative stress

([159] see copyright permissions).

Low Se intake from agricultural products leads to serious health consequences that result from the induction of oxidative stress, especially in low Se areas of China and Eastern Siberia. In the Keshan region of China, Se deficiency causes endemic Keshan disease with the pathology of juvenile cardiomyopathy with myocardial insufficiency that affects mostly children aged from 2 to 10 years old [160].

Furthermore, several studies indicated that Se contributes to the defense of animals against the toxicity of high exposure and/or intake of heavy metals like mercury, lead, cadmium and silver [161-165]. Previous studies also correlated Se-deficiency with the pathology and virulence of viral infections [166-168]. Additionally, Se supplementation inhibits TNF $\alpha$  (tumour necrosis factor  $\alpha$ )-induced HIV replication [169].

#### 1.2.5.3.2 Selenium and oxidative stress

Reactive oxygen species (ROS) are formed by sequential reduction of one electron from oxygen. They are very reactive due to the presence of the unpaired valence shell electrons. ROS are generated as natural byproducts during the normal oxygen metabolism by NAD(P)H oxidases, xanthine oxidase, myeloperoxidase, cyclooxygenase and lipoxygenase [170]. However, when the biological system is exposed to environmental stress, ROS levels can raise significantly resulting in a condition called oxidative stress accompanied with considerable damage to cell structures such as DNA, lipids and proteins. In this condition, cells cannot cope with the produced ROS and repair the resulting damage [171].

Cells possess a defense mechanism for the detoxification of ROS and the repair of deleterious oxidative damage. Among these mechanisms antioxidant enzymes such as superoxide dismutases (SOD), catalase and glutathione peroxidases (GPx) are the most important in humans. All these GPx isoenzymes and thioredoxin reductases (TrxRs) share a catalytic selenoprotein in their active center, consisting of selenocysteine [172-174].

GPx isoenzymes reduce hydrogen peroxide, organic hydroperoxides, and phospholipid hydroperoxides [175]. In addition to glutathione peroxidases, TrxRs degrade hydroperoxides including hydrogen peroxide and lipid hydroperoxides, as well (Figure 1.2.6) [176].

Apart from the degradation of hydroperoxides, TrxRs reduce thioredoxin which is an intracellular protein located in the cytoplasm and mitochondria and serve as an electron and hydrogen donor when reduced, thereby restoring the activities of antioxidant enzymes [177-179].

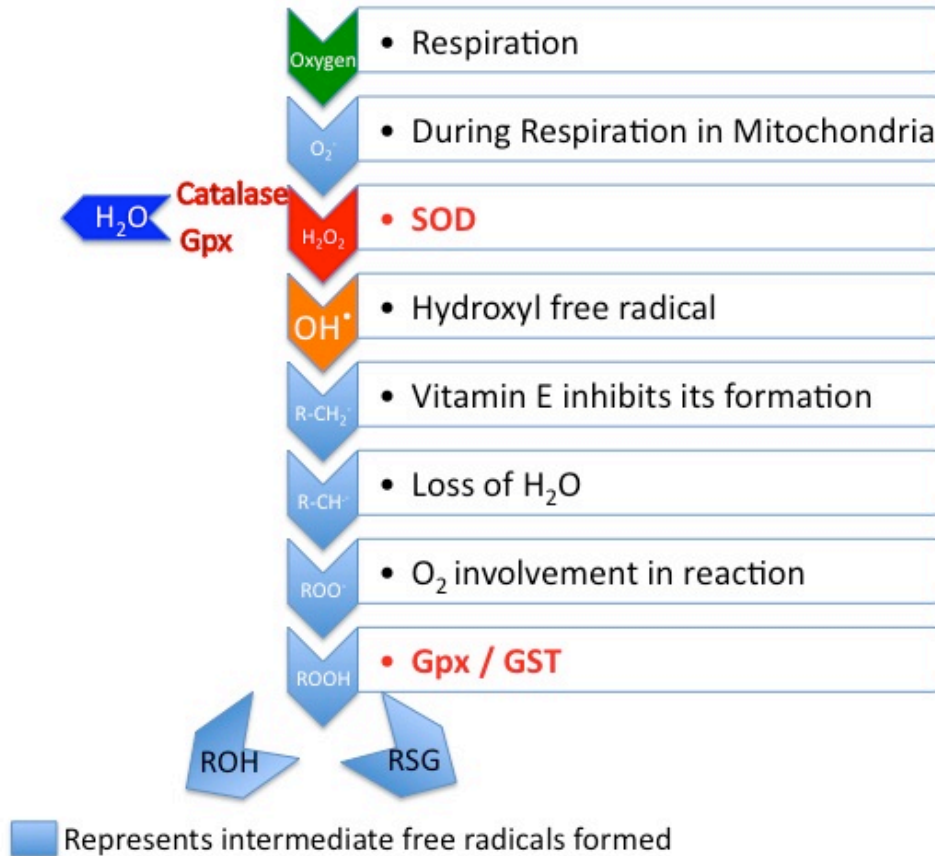


Figure 1.2.6 Anti-ROS Internal Protection Mechanisms. SOD is implicated in the removal of  $\cdot\text{O}_2^-$ . Gpx and CAT are implicated in the removal of  $\text{H}_2\text{O}_2$ , and Gpx and GST are implicated in the removal of lipid peroxides (ROOH) evading a chain reaction (Halliwell and Gutteridge, 1999, J.M.C., Free Radicals in Biology and Medicine, 3<sup>rd</sup> edition). Vitamin E inhibits lipid peroxidation by scavenging  $\text{OH}\cdot$  [180]. (Modified from Irmak MB, thesis subject: Acquired Tolerance of Hepatocellular Carcinoma Cells to Selenium-Deficiency: A Selective Survival Mechanism, 2003)

### 1.2.5.3.3 Selenium and cancer

The relationship between selenium and cancer has been well documented. Se is considered as an anticarcinogenic as suggested by several animal studies [181] and previous studies indicated that Se could decrease the risk of different cancer types [182]. Figure 1.2.7 depicts the proposed link between Se and cell metabolism.

Many selenoprotein gene alterations that are responsible for the inhibition of oxidative stress have been associated to the risk of cancer. These gene polymorphisms

including GPX1, GPX2, GPX4 and Sep15 are implicated in breast, prostate, lung, head, neck and colorectal cancer [183-188]. Additionally, changes in the expression of GPX1, GPX2, Sep15, SelP and TRXR1 have been documented in different forms of cancer [189].

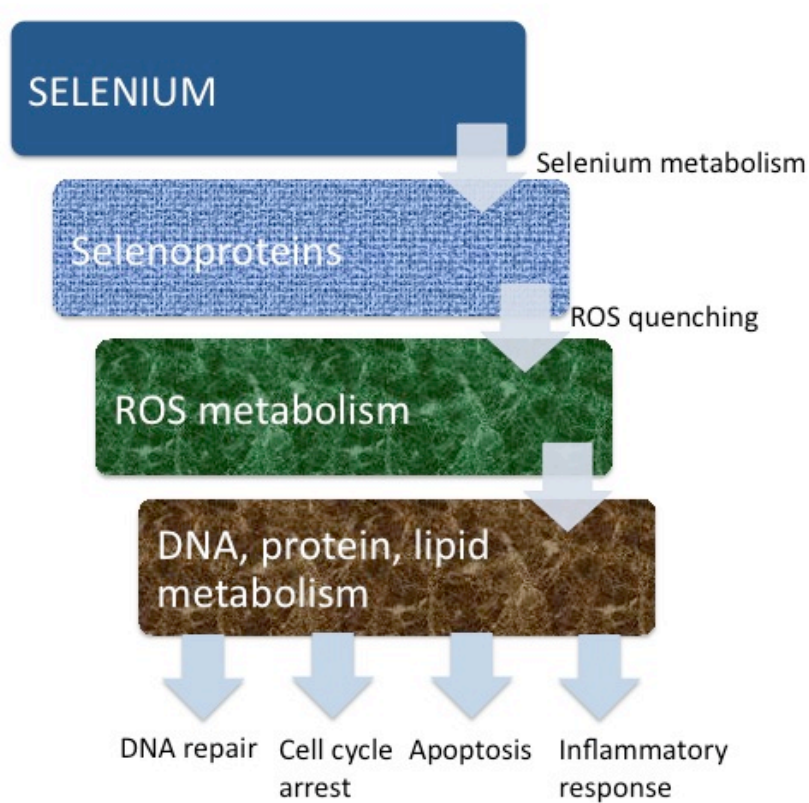


Figure 1.2.7 A model of selenium and its association with cell metabolism.

#### 1.2.5.3.3.1 Selenium and liver cancer

Analogous to chronic alcohol exposure, Se-deficiency has also been associated with hepatocyte damage and necrosis[158]. As previously discussed in section 1.2.4.1, pathological mechanism of liver injury associated with alcohol abuse lies beneath the production of ROS [148].

Aside from the capability of ROS to attack proteins, polysaccharides, nucleic acids and polyunsaturated fatty acids, these species also have the ability to activate the cytokine release from immune cells to trigger inflammatory pathways and induce the expression of adhesion molecules, leading to the accumulation of granulocytes in organs and further increase the generation of ROS thus augmenting the inflammatory response and tissue injury [190]. Knowing the fact that, continuous tissue injury and inflammation are the major driving force for the onset of cirrhosis and HCC, oxidative stress scavengers are essential for liver function.

Since, GPxs, the most effective defense mechanism proteins that cope with ROS and oxidative stress require Se to be incorporated in their catalytic center to function [191], chronic Se deficiency is a major risk factor in liver cirrhosis.

Several case studies conducted in individuals with different liver pathologies indicated that serum or plasma Se levels of these individuals were considerably less than those in healthy control group (Table 1.2.5.3) [158, 192]. In correlation with this, chronic alcoholics suffer from the limited food intake and malnourishment since too much alcohol consumption disturb their diet, preventing the Se supply from food [158].



Table 1.2.5.3 Selenium levels in serum, plasma, whole blood, tissue and erythrocytes in healthy control and patients with different pathology.

Pathology and/or status	Group (n)	Mean Se ( $\mu\text{g/l}$ )	Se range ( $\mu\text{g/l}$ )	Sample type	Area (country)	Reference	
Hepatopathies	Cirrhosis group	12	41.0 $\pm$ 12.4	17.7–61.5	Serum	Spain	Navarro-Alarcon et al. (2002)
	Hepatitis group	38	52.4 $\pm$ 15.6	15.8–80.5	Serum		
	Control group	130	74.9 $\pm$ 27.3	30.2–175.0	Serum		
Chronic liver diseases	Chronic hepatitis C or C virus infection group	59	48.6 $\pm$ 11.8	-	Plasma	Poland	Czuczajko et al. (2003)
	Alcoholic, autoimmune or cryptogenic chronic liver disease group	64	66.4 $\pm$ 14.1	-	Whole Blood		
	Healthy controls	50	43.0 $\pm$ 13.3	-	Plasma		
			58.4 $\pm$ 16.6	-	Whole Blood		
			67.4 $\pm$ 11.7	-	Plasma		
Chronic hepatitis C	Hepatitis group	33	89.5 $\pm$ 15.6	-	Whole Blood	China	Ko et al. (2005)
	Control group	31	159.1 $\pm$ 5.3	-	Plasma		
			55.1 $\pm$ 3.8	-	Erythrocyte		
			216.7 $\pm$ 7.4	-	Plasma		
Alcoholic liver disease Hepatopathies	Cirrhosis group	24	46.1	31.9–60.6	Serum	United Kingdom	Pemberton et al. (2005)
	Control group	49	100.6	92.3–105.45	Serum		
	Non-alcoholic fatty liver disease group	17	114.5 $\pm$ 15.81	-	Plasma	France	Bonnefont-Rousselot et al. (2006)
	Viral hepatitis group	47	90.8 $\pm$ 7.1	-	Plasma		
Viral hepatic diseases	Hepatitis B virus carriers group	50	124.3 $\pm$ 22.6	-	Serum	Taiwan (China)	Lin et al. (2006)
	Chronic hepatitis B group	40	123.5 $\pm$ 20.4	-	Serum		
	Hepatic cirrhosis group	20	117.5 $\pm$ 25.3	-	Serum		
	Hepatocellular carcinoma group	18	108.5 $\pm$ 21.8	-	Serum		
	Control group	50	129.0 $\pm$ 21.5	-	Serum		
Hepatopathies	Cirrhosis group	15	0.023 $\pm$ 0.008	-	Liver tissue	Poland	Czeczot et al. (2006)
	Hepatocellular carcinoma group	15	0.023 $\pm$ 0.008	-	Liver tissue		
	Adjacent healthy liver group	15	0.031 $\pm$ 0.015	-	Liver tissue		

([193] see copyright permissions).

Selenium supplementation has a protective role against hepatitis B and C virus (HBV, HCV) infection [194]. Although the exact underlying mechanism is not determined, selenium has been shown to maintain the growth of some HCC cell lines, Hep3B, HepG2, Hep40 and Huh-7 under serum-free conditions [195-197]. A recent study performed by our group indicated that ten out of thirteen HCC cell lines are resistant to Se-deficiency, while in a couple of them oxidative stress and apoptosis are induced [197].

#### 1.2.5.3.3.2 Signaling pathways and selenium

The role of Se in the activation of specific signaling cascades that contributes to carcinogenesis is not fully characterized. However, growing evidence from clinical trials suggest that Se supplementation and certain Se metabolites effectively diminish

the incidence of cancers such as lung, colorectal, prostate and liver cancer [194, 198, 199].

Several studies reported that selenium functions directly in the regulation of many important survival and apoptosis signaling pathways. Figure 1.2.8 demonstrates the major response pathways after ROS formation and their key targets.

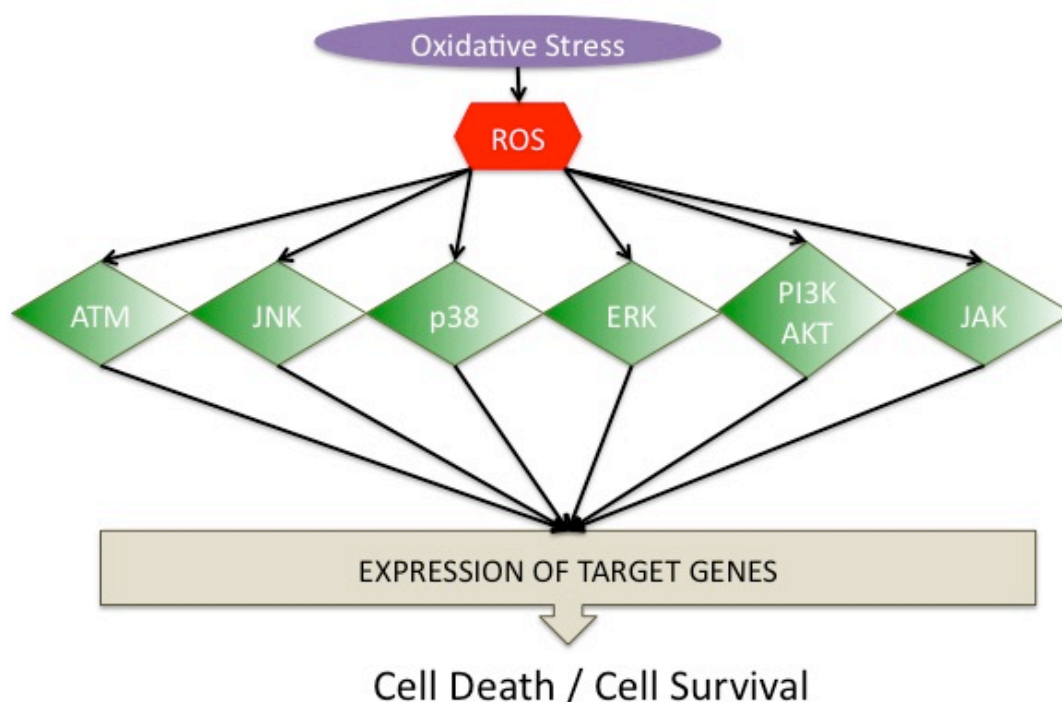


Figure 1.2.8 ROS signaling targets in various biological signaling pathways (Modified from [200]).

The activities of NF- $\kappa$ B, AP-1 [201], JNK1 [202], and caspase-3 [203] are inhibited through the redox regulation of their reactive cysteine residues. In those studies selenite is indicated as a suppressor of the JNK, stress-activated protein kinase (SAPK) and the p38 mitogen-activated protein kinase (p38MAPK) pathway, which are extremely fundamental cascades upon ROS induced oxidative stress response [202]. Apoptotic response is a common response after strong oxidative damage, one of its key elements; caspase-3 activity is also inhibited by selenium in embryonic kidney cells [203]. Another study indicated the anti-apoptotic role of selenite after hydrogen peroxide treatment through the inhibition of the ASK1/JNK pathway and

the induction of the PI3K/Akt survival pathway [204], complementary with a follow-up study performed on Huh-7 HCC cell line [205], demonstrating the involvement of selenium supplementation for the inhibition of apoptosis and the activation of the PI3K/Akt kinase pathway.

#### 1.2.5.4 Hepatotoxic chemicals

Multiple chemical components such as benzo(a)pyrene, 4-aminobiphenyl, vinyl chloride [206, 207] constituents of tobacco, inorganic arsenic [208] and aflatoxins [209] are hepatic carcinogens in animals. Along with the data provided for the genotoxic effects of benzo(a)pyrene and vinyl chloride on *p53* gene in human and animal [210, 211], many epidemiological studies strengthen the notion of cigarette smoking as a hepatic carcinogen in humans. The consumption of aflatoxin contaminated food and inorganic arsenic contamination in drinking water supplies have been allied with HCCs [208, 212-214].

##### 1.2.5.4.1 Aflatoxins

Aflatoxins are mycotoxins produced by some *Aspergillus flavus*, *A. parasiticus* and *A. nomius* strains and production of aflatoxins B1, B2, G1, G2, and M1 contaminates several agricultural products [215]. These mold species are common and widespread in nature and they can contaminate grain prior to harvest and during improper drying, storage and processing by infection and colonization of the fungus. Cereals, oilseeds, spices and nuts are commonly affected with the aflatoxin contamination. Aflatoxin can also be present in the milk of animals, which are fed with contaminated crops [216].

##### 1.2.5.4.2 Aflatoxin exposure in humans

The US Food and Drug Administration (FDA) regards aflatoxins as unavoidable food contaminants, thus in order to minimize the level of contamination, implementing strict regulations is a necessary precaution to be taken. The FDA's goal has been to minimize contamination; this goal was realized by implementing regulations that

required special attention to the management of the problem. In developed countries, aflatoxin contamination is diminished by the regulations in imported food and industrial food processing techniques. However, in developing countries due to the characteristics of the food systems and the technological infrastructure, these methods remain to be limited and no control is applicable, hence people in these countries remain at high risk of exposure to aflatoxins.

Though rare, acute exposure to high levels of aflatoxins ( $>20 \mu\text{g}/\text{kg}/\text{day}$ ) leads to a lethal syndrome called aflatoxicosis associated with the symptoms of hemorrhagic necrosis of the liver and bile duct proliferation [217]. However, more than 90 % of people at high risk for aflatoxin-caused HCC are chronically exposed to low doses of aflatoxin ( $0.01\text{-}0.3 \mu\text{g}/\text{kg}/\text{day}$ ) [217, 218]. Chronic exposure to low or moderate doses of aflatoxin may lead to the development of HCC [217].

#### 1.2.5.4.3 AFB1-induced DNA damage and HCC

##### 1.2.5.4.3.1 Aflatoxin and HCC

Dietary exposure to aflatoxins and infections with hepatitis B virus (discussed in section 1.2.1) are the major risk factors for HCC in Southeast Asia, sub-Saharan Africa and China [219] where populations suffer from both high hepatitis B virus prevalence and largely uncontrolled aflatoxin exposure in food. A recently published risk assessment study indicated that about 5-28 % of all global HCC cases might be caused by aflatoxin exposure [218].

##### 1.2.5.4.3.2 Aflatoxin metabolism and DNA damage

Aflatoxin B1 (AFB1) is the most prevalent and carcinogenic of aflatoxins. After the intake of AFB1, it is oxidized into AFB1-8,9-*exo*-epoxide and 8,9-*endo*-epoxide by mainly cytochrome P450-mediated enzyme metabolism in liver (Figure 1.2.9). The *exo*-epoxide form of AFB1 binds to DNA to form the predominant 8,9-dihydro-8-(N7-guanyl)-9-hydroxy AFB1 (AFB1-N7-Gua) adduct with an extremely short half-life, so it immediately undergoes processing reactions to form a more stable imidazole ring-opened AFB1-formamidopyrimidine (AFB1-FAPY) [220] DNA adducts which

can accumulate for several days and remain detectable for several weeks [221, 222] (Figure 1.2.9). In addition to AFB<sub>1</sub>-DNA adduct formation, AFB<sub>1</sub> exposure has been reported to cause DNA damage through oxidative stress leading to the formation of 8-hydroxydeoxyguanosine (8-OHdG) lesions in rat and duck liver [223, 224]. Mismatching of AFB<sub>1</sub>-DNA adducts induce mainly G:C to T:A transversions [225]. Earlier studies showed the prevalence of G:C to T:A transversions in *E. coli* and plasmid based experimental settings [210, 226, 227].

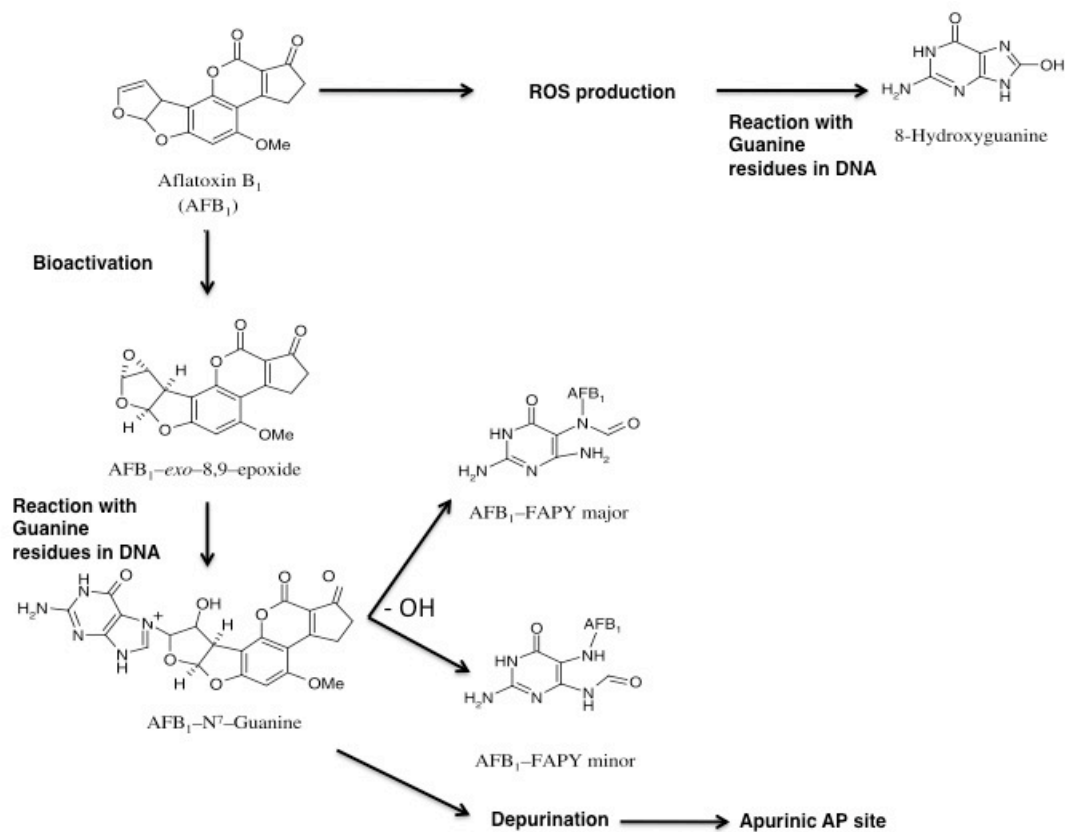


Figure 1.2.9 Aflatoxin metabolism in liver and Aflatoxin-induced DNA damage (Modified from [228]).

#### 1.2.5.4.3.3 Correlation between aflatoxin exposure and p53

Experimental data that have been conducted for almost two decades defined aflatoxin as a causative factor for p53 mutations. These studies have led to the identification of

a HCC specific G->T mutation at codon 249 of *TP53* gene (encoding the mutant p53ser249 protein) in HCC tissues of patients exposed to aflatoxins [212, 213, 229]. Later, this hot spot mutation was indicated to be detectable in non-tumor liver samples [230] as well as in the plasma of 6 % healthy individuals and 15% of cirrhotic patients, and 40% of HCC patients living in aflatoxin-contaminated area [231]. Therefore, AFB1-specific G->T mutation of *TP53* is commonly present in people exposed to aflatoxins, regardless of any clinically detectable liver tumor. Overall, all these findings present strong support for the mutagenicity of low level AFB1 in people chronically exposed to this hepatocarcinogenic agent. However, HCC patients carrying R249S p53 mutation drops to around 2-5% in regions where aflatoxin exposure is low or moderate [31].

#### 1.2.5.4.3.3.1 Functional characteristics of R249S p53

R249S mutation in p53 is a structural mutation which destabilizes the core domain of p53 and disrupts its DNA-binding capacity [232]. Like many other common p53 mutants in cancer, R249S mutant lacks the wild-type p53-dependent tumor suppressor functions. Other than the loss of tumor suppression activity, an abundance of data suggests that mutant p53 proteins including R249S gain additional functions that enhance genetic instability, tumorigenesis and drug resistance [233-236].

Interestingly, HCCs in areas not exposed to AFB1 do not harbor R249S mutation, which is extremely specific to AFB1 exposure [14]. Presently, the nature of this selective pressure to induce and maintain the expression of this hot spot R249S mutation of p53 is not fully known. After the initial description of increased mitotic activity associated with p53-249ser expression in human HCC cells [237], mouse equivalent of this mutation (p53-246ser) was shown enhance hepatocarcinogenesis induced by other factors [238], but it was not sufficient for hepatocyte immortalization by itself [239]. P53-249ser was reported to stimulate G0 to G1 and/or M to G1 transition in hepatocytes [240]. Recently, p53-249ser was shown to protect HCC cells from cytotoxic effects [241] of PRIMA-1, which restores sequence-specific DNA binding and the active conformation to mutant p53 proteins [242]. However, *in vivo* studies failed to recapitulate the R246S (mouse equivalent of R249S) after AFB1 treatment even in the Hupki mice, which carry the human p53

locus in germ line, indicating the yet-undiscovered mechanisms [238, 243, 244]. Moreover, a very recent study indicated that, p53-246ser has dominant negative activity over wild-type p53 both in differentiated and undifferentiated embryonic stem cells [245]. Despite all the efforts, a common and well-accepted mechanism for selection of p53-249ser in HCC has not emerged yet. The underlying mechanism of its contribution to hepatocarcinogenesis is not fully-known.

#### 1.2.5.4.4 Response to AFB1-induced DNA damage

In order to protect the genomic stability, eukaryotic cells, from yeast to human have a sophisticated and powerful DNA damage response system. Upon DNA damage, several cellular responses are induced to enable the cell either to repair the damage or to activate senescence and apoptosis processes. DNA damage checkpoint proteins play a central role in the coordination of repair and cell cycle progression to prevent mutations. In response to DNA damage, cell cycle checkpoint proteins at G1/S, S or G2/M barriers are induced. Damage is recognized by sensors, kinases including ATM and ATR and mediated by adaptor proteins such as 53BP1 and  $\gamma$ -H2AX to the transducers; Chk1 and Chk2. The final induction of the effectors like p53 and cdc25 arrest the cells at either of these checkpoints and inhibit cell cycle transition depending on the amount of damage (Figure 1.2.10). DNA damage response also triggers a DNA repair process. DNA repair mechanisms are classified as direct repair, base excision repair, nucleotide excision repair (NER), double-strand break repair, and cross-link repair[246] [247].

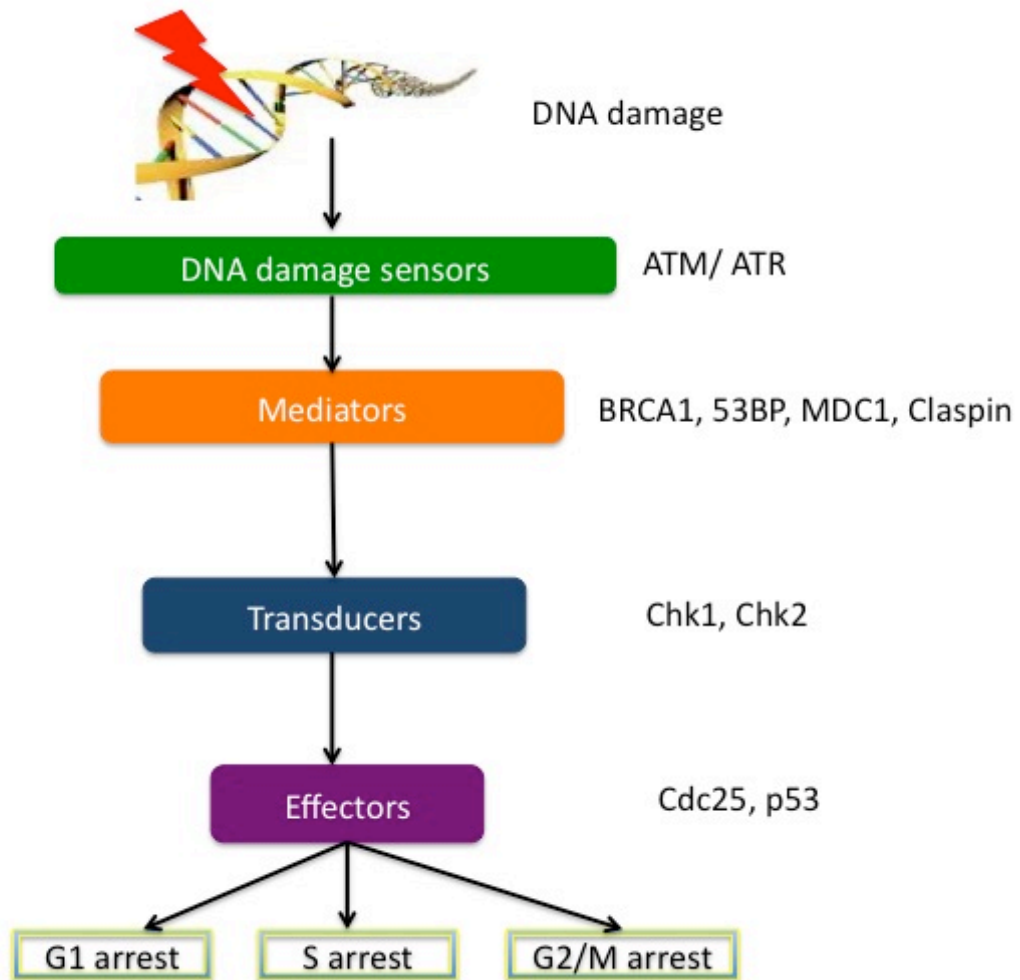


Figure 1.2.10 DNA damage checkpoint mechanism and its key regulators in humans. (Modified from [246]).

AFB1-DNA adducts are believed to be repaired primarily by NER in prokaryotes and eukaryotes [248, 249] [250, 251] [252]. As a consequence of the attempted repair of AFB1-DNA adducts by NER DNA double-strand breaks (DSB) and single-strand breaks may form. It is also believed that replication forks collapse while AFB1-DNA adducts are encountered. Accordingly, in yeast, lack of NER and recombinational repair is proposed to contribute to mutagenesis proceeding *via* the error prone translesion bypass synthesis (TLS) pathway [249, 250] that is evolved to allow replication bypassing the damage to minimize cell death from replication blockage [253]. In mammals, further understanding of damage recognition by DNA repair enzymes in response to AFB1-DNA adducts is required. In mouse liver, after AFB1 treatment, NER induction was observed but the exact mechanism is ill-known [254].



Apurinic sites induced by AFB1 instead are believed to be repaired by base excision repair [255]. The susceptibility to AFB-induced carcinogenesis also shows differences between species, which correlates with the difference in DNA repair activity [254]. All in all, in order to fully understand the mechanism of DNA damage recognition and repair mechanism after AFB1 exposure, more mechanistic studies and considering the contributions of other repair pathways are required.

## **CHAPTER 2: OBJECTIVES and RATIONALE**

Dietary factors play a crucial role in the molecular pathogenesis of liver cancer. In this study we aimed to decipher the role of dietary factors in the pathogenesis of liver cancer.

Oxidative stress is associated with the malignancy and progression of HCC. It is considered as a common factor during inflammation as a result of chronic viral infection, chemical stress caused by aflatoxin exposure, metabolic stress produced by alcohol abuse and selenium deficiency. Oxidative stress causes genotoxicity when the antioxidant defense mechanism of the organism is malfunctioning. It is a major cause of endogenous mutation source through metabolic stress and implicated in many tumors as a cause of exogenous mutation source produced by chemical and physical carcinogens.

Our first specific aim was to clarify the implication of Se-deficiency in the tumorigenesis of hepatocytes. A recent study performed in our group showed the selective survival advantage of some HCC cell lines under Se-deficiency while a couple of them go through apoptosis under oxidative stress induced by Se-deficiency. In order to understand the mechanism and the key regulators beneath this selective survival under oxidative stress, we selected two isogenic HCC cell lines one of which was reported to be resistant to oxidative stress whereas the other was sensitive to Se-deficiency induced oxidative stress. In this experimental model, the only difference between the isogenic clones is the presence of HBV in the apoptosis tolerant HepG2-2.2.15 cells. Using this isogenic model we tried to provide evidence for the selective survival capacity by performing a comparative study of the main stress activated and survival signaling pathways.

Cancer cells may respond to genotoxic stress with a cryptic survival advantage development. Therefore we wanted to further investigate this idea with other dietary factors involved in liver carcinogenesis. Hence, in the second part of our study we tried to identify the mechanisms underlying the selective selection of AFB1 for p53-249 mutation in HCC. Aflatoxins are the most potent naturally occurring carcinogens and may play a causative role in 5- 28% of liver cancers. Aflatoxins are activated in liver cells and induce G->T mutations, specifically codon 249 (G->T) hotspot

mutation of the TP53 gene associated with aflatoxin-related HCC. For this purpose we first performed a comparative study using HepG2 p53<sup>wt</sup> and p53 R249S transfected clones of this cell line in order to check the acquired survival advantage of R249S mutation. We showed that R249S does not provide survival advantage at heterozygous state. Thus, the selection could be at the mutation induction stage. The lack of p53 activation in AFB1 exposed HCC cells led us to test the following hypothesis: DNA damage response (DDR) to AFB1 may be deficient in hepatic cells allowing mutation accumulation. Surprisingly, DNA damage checkpoint response to aflatoxins has not been studied previously. DNA damage checkpoint response acts as an anti-tumor mechanism by protecting genome integrity against genotoxic agents. However, this highly critical aspect of aflatoxin carcinogenicity is poorly known. Therefore, in the last part of our work, we have studied the DNA damage checkpoint response in human cells after exposure to AFB1, the most common and mutagenic form of aflatoxins. Hepatocyte-like HepG2 and HCT116 cells have been used as our working model for the convenience of p53 and p53 knock out studies. Treatment of those cells with mutation-inducing doses (3-5  $\mu\text{mol/L}$ ) of AFB1 induced DNA adducts, 8-hydroxyguanine lesions, as well as single and double strand DNA breaks that lasted several days. Persistent DNA damage in aflatoxin B1-treated cells, did not affect not only effect cell growth but also in wild-type p53 and p53-deficient HCT116 cells exhibited an incomplete checkpoint response. AFB1-exposed failed to activate Chk1, Chk2 and p53. Consequently, AFB1-exposed cells did not show sustained p53-dependent G1 arrest, or a p53-independent G2/M arrest. In conclusion, a fully functional DNA damage response was inapplicable to AFB1 exposed cells in contrast with the Adriamycin treated ones. Thus, genotoxic doses of AFB1 induce an incomplete and inefficient checkpoint response in human cells.

## **CHAPTER 3: MATERIALS and METHODS**

### **3.1 MATERIALS**

#### **3.1.1 General Reagents**

All laboratory chemicals were analytical grade from either Sigma (St. Louis, MO, U.S.A), Carlo Erba (Milano, Italy), Merck (Schuchardf, Germany), VWR company, (International S.A.S.. Le Périgares, France).

#### **3.1.2 Enzymes**

Restriction endonucleases used for restriction digestion confirmation experiments were purchased from either MBI Fermentas GmbH (Germany) or from Gibco Invitrogen SARL –France.

#### **3.1.3 Nucleic Acids**

DNA molecular weight standard and ultrapure deoxyribonucleotides were from MBI Fermentas GmbH (Germany).

PCMV-p53 R249S vector is gift from Bert Vogelstein.

#### **3.1.4 Oligonucleotides**

p53-primers for mutation confirmation polymerase chain reactions (PCR) were synthesized by either İONTEK (Istanbul, Turkey) or Eurofins MWG Operon (Roissy CDG, France).

#### **3.1.5 Electrophoresis, photography and spectrophotometer**

Electrophoresis grade agarose was obtained from Sigma Biosciences Chemical Company Ltd. (St. Louis, MO, USA) and from Agarose D5 DNA grade from

Euromedex (Souffelweyersheim-France). Horizontal electrophoresis apparatuses were from Stratagene (Heidelberg, Germany) and Bio Rad Laboratories (CA, USA). The power supply Power-PAC300 and Power-PAC200 was from Bio Rad Laboratories (CA, USA). GeneFlash SYNGENE Bioimaging is used to visualize DNA. The Molecular Analyst software used in agarose gel profile visualizing was from BioRad Laboratories (CA, USA). The spectrophotometer was from Beckman Coulter (CA, USA).

### **3.1.6 Tissue Culture Reagents**

Dulbecco's Modified Eagle's Medium (DMEM), HAM's medium (with 10  $\mu$ M Copper and 3mM Zinc), McCoy's medium, nonessential amino acids, penicillin/streptomycin, trypsin /EDTA, calcium, magnesium-free phosphate buffered saline (PBS), HBBS Hanks balanced salt solution and transfection reagent Lipofectamine were purchased from Gibco Invitrogen company (Invitrogen SARL – France) and fetal bovine serum (FBS) was purchased from PAA, France. Tissue culture petri dishes, flasks, 15 and 50 ml polycarbonate centrifuge tubes with lids, 6-well, 24-well plates and cryotubes were from Costar Corp. VWR company International S.A.S.. Le Périgares, France).

Geneticin-G418 sulfate was purchased GIBCO Invitrogen company (Invitrogen SARL –France). AFB1 (aflatoxin B1), ADR (adriamycin), Hydroxyurea (HU), sodium selenite, isocitric acid and  $\beta$ -Nicotinamide adenine dinucleotide phosphate sodium salt hydrate (NADP) were purchased from Sigma (St. Louis, MO, USA).. Sprague-Dawley rat liver and Wortmannin were purchased from Xenotech (Kansas, USA) and Calbiochem (NJ, USA) respectively.

### **3.1.7 Western immunoblotting, antibodies and chemiluminescence**

10% or 4-12% Bis-Tris NuPAGE Novex Mini gel systems and 7% or 3-8% Tris-Acetate NuPAGE Novex Mini gel systems were purchased from Invitrogen, SARL – France. The antibodies used in immunoblotting, immunoperoxidase and immunoflorescence experiments were obtained from different sources, and are given in Table 3.3.2. Enhanced ChemiLuminescence (ECL) plus detection kit was from

Amersham-Pharmacia, Buckinghamshire, England. Nitrocellulose membrane was from Roche, Mannheim, Germany and Immobilon-P PVDF membrane were from Millipore, USA. Negative X-ray film was from Blue Devil, France.

## **3.2 SOLUTIONS AND MEDIA**

### **3.2.1 General Solutions**

50X Tris-acetic acid-EDTA (TAE): 2 M Tris-acetate, 50 mM EDTA pH 8.5  
Diluted to 1X for working solution  
purchased from Euromedex.

Ethidium bromide: Uptime Interchim company  
10 mg/ml in water (stock solution),  
30 ng/ml (working solution)

4X Gel loading buffer: Purchased from Invitrogen (SARL–  
France).

Bradford Stock Solution Purchased ready-use solution from Sigma  
company with catalog number B6916

### **3.2.2 Tissue culture solutions**

Standard working medium 10% FBS, 1% penicillin/streptomycin,  
1% Non-Essential Amino Acid were  
added and stored at 4°C.

McCoy's working medium 10% FBS, 1% penicillin/streptomycin,  
were added and stored at 4°C.

Selenium adequate medium	Standard medium with 0.01% FBS and 0.1 $\mu\text{M}$ $\text{Na}_2\text{SeO}_3$ .
Selenium deficient medium	Standard medium with 0.01% FBS.
10X Phosphate-buffered saline (PBS)	Purchased from Invitrogen Company Invitrogen SARL –France
Freeze medium	70% DMEM control medium, 20% FBS, and 10% DMSO in 1 ml per cell line.
Wortmannin	500mM stock solution in DMSO was prepared, aliquots were stored at $-20^\circ\text{C}$ . Working solutions of 500nM were used.
Aflatoxin B1	20mM stock solution in DMSO was prepared aliquots were stored at $-20^\circ\text{C}$ . Working solutions were prepared and used freshly.
Adriamycin (ADR)	6.66mg/ml stock solution in sterile double-distilled water. Working solutions were prepared and used freshly.
S9-activation solution	0.20 g/L S9 fraction, 10.5 mM isocitric acid in ddH <sub>2</sub> O, 1.8 mM $\beta$ -Nicotinamide adenine dinucleotide phosphate sodium salt hydrate (NADP) in H <sub>2</sub> O. It was filtered and used at 1:10 dilution in the cell culture medium.

Geneticin-(G418 Sulfate) 500 mg/ml solution in double-distilled water. Sterilized by filtration and stored at -20°C (stock solution). 1500 µg/ml (working solution for stable cell line selection), and 750 µg/ml (working solution for maintenance of stable cell lines) were used.

### 3.2.3 Immunoblotting solutions

10X Tris-buffer saline (TBS) *Per liter:* 100 mM Tris-base, 1.5 M NaCl, pH 7.6 in double distilled water.

TBS-Tween (TBS-T) 0.1-0.5% Tween-20 solution in TBS. (Prepared freshly)

Blocking solution 5% (w/v) non-fat milk or BSA, 0.1% Tween-20 in TBS.

### 3.2.4 RNA Study Solutions

DEPC-treated water 0.1% Diethylpyrocarbonate (DEPC) (v/v) in double-distilled water was autoclaved and stored at room temperature.

### 3.2.5 Immunofluorescence and Immunoperoxidase solutions

H33258 fluorochrome dye 1 mg/ml solution in double-distilled water and stored at -20 °C. Working solution was 1 µg/ml.



DAPI (4', 6-diamidino-2-phenylindole)	0.1-1 µg/ml (working solution in PBS).
4% paraformaldehyde	4 g paraformaldehyde, 5 mM NaOH in 100 ml. PBS, pH 7.4. Stable at 4°C for a week.
PBS-TritonX-100 (PBS-T)	0.1 TritonX-100 in PBS.
Permeabilization Solution	0.5% Saponine (w/v) and 0.3% Triton-X-100 in PBS
Blocking Solution	10% FBS, 0.3% Triton-X-100 in PBS
Antibody Dilution and Wash Solution	2%FBS, 0.3% Triton-X-100 in PBS

### 3.2.6 Single cell gel electrophoresis (COMET ASSAY) solutions

Membrane Lysis Solution (pH 10.0)	2.5 M NaCl, 0.1M Na <sub>2</sub> EDTA, 0.01M Tris, 0.25M NaOH and 0.77% Na-Lauroylsarcosinate were dissolved and working solution was prepared by adding 1:10 DMSO and 1% Triton-X
Alkaline Electrophoresis Solution (pH 12.8)	0.555 gr Na <sub>2</sub> EDTA, 10 gr NaOH were dissolved in 1500 ml double distilled H <sub>2</sub> O.
Neutral Electrophoresis Solution (5X)	54g Tris Base, 27.5g Boric Acid, 20 mL of 0.5 M EDTA (pH 8.0) in 1 liter double distilled H <sub>2</sub> O.

Neutralization Buffer (pH 7.5)                      48.44g Trisma Base in 1 liter double distilled H<sub>2</sub>O.

### **3.3 METHODS**

#### **3.3.1 Tissue culture techniques**

##### **3.3.1.1 Cell Lines and stable clones**

Huh7, Hep3B, PLC/PRF/5, HepG2, HepG2-2.2.15 HCC cell lines and HCT116, HCT116 p53KO colon cancer cell lines used in this study, were cultured as described previously [256, 257].

##### **3.3.1.2 Thawing cell lines**

Frozen cell line vial taken from the liquid nitrogen tank was instantly put onto ice. The vial was placed into 37°C water bath until the external part of the cell solution was thawed. The cells were resuspended gently with 10 ml of standard medium and centrifuged at 1500 rpm at 4°C for 5 minutes. Supernatant was discarded and the pellet was resuspended in 10 ml 37°C culture medium and plated into T25 or T75 flask depending on the amount of cell pellet.

##### **3.3.1.3 Transient transfection and stable clone formation**

Transfection was performed with Lipofectamine 2000 reagent with the manufacturer's protocols. p53-R249S PCMV and empty vector transfected HepG2 cells were selected for 15 days with 1500 µg/ml Geneticin until the non-transfected control cells were all dead. Selected colonies were trypsinized and passaged into 24-well plates and tested for p53-R249S expression after they reach to a certain number of cells.

### **3.3.1.4 Cell Culture treatments**

#### **3.3.1.4.1 Treatment of cell lines with Se-adequate vs. Se-deficient medium and Wortmannin**

HepG2 and HepG2-2.2.15 cell lines were cultured in either Se-adequate standard medium supplemented with 0.01% FBS and 0.1  $\mu\text{M}$   $\text{Na}_2\text{SeO}_3$  for 24h, 48h or 72h or Se-deficient medium. Cells were treated with 500nM Wortmannin or its vehicle control DMSO (<10<sup>-3</sup> v/v dilution) in Se-adequate/Se-deficient medium.

#### **3.3.1.4.2 Treatment of cell lines with TGF-beta and Adriamycin**

Purified recombinant human TGF- $\beta$ 1 (R&D Systems, Minneapolis, USA) was reconstituted in sterile 4 mM HCl containing 1 mg/ml bovine serum albumin (BSA, Sigma, St. Louis, MO, USA) and cells were treated with 5ng/ml TGF- $\beta$ 1 for 72h. Adriamycin treatments were done in standard medium with a changing dose of 0.1-1 $\mu\text{M}$ .

#### **3.3.1.4.3 Treatment of cell lines with Aflatoxin B1**

Aflatoxin B1 treatment was performed in the presence of S9-activation system for all HCT116, HCT116-p53<sup>-/-</sup> and some HepG2 experiments for enzymatic activation into AFB1-8,9-exo-epoxide form. S9 activation system was prepared as described previously [258, 259].

#### **3.3.1.5 Cryopreservation of cell lines**

Exponentially growing cells with 60-70% confluency were trypsinized and collected with growth medium. The cells were centrifuged at 1500 rpm for 5 min. The precipitated cell pellet was resuspended in a freezing solution (10% DMSO, 20% FCS and 70% DMEM at a concentration of 3-4x10<sup>6</sup>cells/ml. 1 ml of this solution was placed into 1 ml screw capped-cryotubes. The tubes were left at -80°C overnight in a isopropanol containing shuttle container. The next day, the tubes were transferred into the liquid nitrogen storage tank.

### **3.3.1.6 Colony-forming ability assay**

Cell survival was determined by assessing cell growth in 100 mm dishes after exposure to AFB1 (0-50 $\mu$ M) in the presence of S9-activation system for 4 hours and 24 hours. Control cells were exposed to ADR (0-5 $\mu$ M) in parallel. Following exposure, 10<sup>4</sup> cells were seeded into 100 mm dishes and cultured for 10 days. After fixation of colonies in cold methanol, they were stained with Crystal Violet (Sigma), and counted in triplicates. Cell survival was calculated as the % ratio of cell numbers in treated versus untreated cells. Survival parameters were determined by plotting in excel data sheets.

### **3.3.2 Analysis of nucleic acids**

#### **3.3.2.1 Purification of plasmid DNA using Qiagen miniprep kit**

This method was employed for the isolation of p53 plasmids in order to use in transfection protocol. 5 ml of saturated culture medium was used for the isolation of plasmid DNA by using “QI Prep spin miniprep plasmid DNA purification kit” (Qiagen- Courtaboeuf, France) according to the manufacture’s instructions.

#### **3.3.2.2 Quantification and qualification of nucleic acids**

RNA, Plasmid and genomic DNA concentrations and purity were determined using the Nanodrop from ThermoScientific Company.

#### **3.3.2.3 Extraction of total RNA from tissue culture cells and tissue samples**

Total RNAs were isolated from cultured cells using the NucleoSpin RNA II Kit (MN Macherey-Nagel, Duren, Germany) according to the manufacturer’s instructions.

### 3.3.2.4 First strand cDNA synthesis

First strand cDNA synthesis from total RNA was performed using RevertAid First Strand cDNA synthesis kit (MBI Fermentas, Germany). The first strand reactions were performed according to the instructions for priming with oligo(dT) primer and RT- controls were also synthesized to make sure that there is no DNA contamination. 1.5 to 3 µg total RNA was used to synthesize the first stand cDNA.

### 3.3.2.5 Primer design for expression analysis by semi-quantitative PCR

The primer pairs that have been used for the selection of p53-R249S expressing colonies were designed carefully. Forward and reverse primer were positioned between exon4, exon6 and exon8 of the TP53 respectively, so that the primer pair was including the R249S codon and not able to amplify from the covered genomic DNA region during PCR. Primers used for the selection have been designed strictly considering these criteria, and listed in Table 3.3.1.

Table 3.3.1 Primer Sequences used in this study

Target Gene	Primer Sequence
TP53	F 5' AAA ACC TAC CAG GGC A 3' R 5' CTC GTG GTG AGG CTC 3'
TP53	F 5' TAT TTG GAT GAC AGA 3' R 5' CTC GTG GTG AGG CTC 3'
GAPDH	F 5' GGC TGA GAA CGG GAA GCT TGT CAT 3' R 5' CAG CCT TCT CCA TGG TGG TGA AGA 3'

### 3.3.2.6 Selection of R249S expressing clones with PCR followed by restriction enzyme digestion.

10x Invitrogen PCR supermix was used to perform PCR according to manufacturer's instructions.

Restriction enzyme digestions were routinely performed in 20 µl total reaction volumes with 2-5 µg PCR product. Reactions were carried out with the appropriate

reaction buffers for BsuRI and HinfI enzymes separately under conditions according to the manufacturer's recommendations.

### **3.3.2.7 Gel electrophoresis of nucleic acids**

DNA fragments were fractionated by horizontal electrophoresis by using standard buffers and solutions. DNA fragments less than 1 kb were generally separated on 1.0% or 2 % agarose gel prepared with 1X TAE buffer and 30 µg/ml ethidium bromide and the gel was run in 1XTAE at various time and voltage depending on the size of fragments.

### **3.3.3 Computer analyses**

Primers were designed by using web software provided by Steve Rozen and Whitehead Institute for Biomedical Research at [http://frodo.wi.mit.edu/cgi-bin/primer3/primer3\\_www.cgi](http://frodo.wi.mit.edu/cgi-bin/primer3/primer3_www.cgi). Alignments of nucleic acids or protein sequence were performed by using web page; <http://www.ncbi.nlm.nih.gov/BLAST/>.

Analysis of COMET assay results were performed by CASP (Comet Assay Software Project) which measures tail moment, using DNA content in the tail and head along with the distance between the means of the head and tail distributions (<http://casplab.com>).

### **3.3.4 Quantification of Proteins using Bradford Assay**

The conventional Bradford protein assay was employed to quantify protein concentration in the total cell lysates. After protein quantification, protein lysate aliquots were stored at -80°C.

### **3.3.5 Western blotting**

RIPA extracted proteins were subjected to electrophoresis using 10% or 4-12% Bis-Tris NuPAGE Novex or 3-8% Tris-Acetate Nupage mini gel systems (Invitrogen), according to the manufacturer's instructions. For the detection of phosphorylated proteins, cell lysates were prepared according to the protocol provided by the supplier

using the following lysis buffer: 20mmol/L Tris (pH 7.5), 150 mmol/L NaCl, 1 mmol/L EDTA, 1 mmol/L EGTA, 1% Triton X-100, 1 mmol/L Na<sub>3</sub>VO<sub>4</sub>, 1µg/ml leupeptin, 1 mmol/L phenylmethylsulfonyl fluoride. Following electrophoresis, proteins were transferred on to Immobilon-P PVDF membrane (Millipore, USA), and analyzed, using antibodies against target proteins listed in Table 3.3.2.

### **3.3.6 Senescence-associated beta-galactosidase (SABG) assay**

SABG activity was detected as described previously [260], using senescent cell staining kit (Sigma).

### **3.3.7 Immunoperoxidase Staining**

Cells were fixed with 4% formaldehyde, and permeabilized with permeabilization solution. After blocking for one hour, cells were incubated overnight at 4°C with primary antibodies and washed three times with washing solution. The signals were detected by the Dako EnVision + Dual method, according to the manufacturer's instructions. The specimens were counterstained with hematoxylin.

### **3.3.8 Immunoperoxidase detection of AFB1-DNA adducts and 8-OHdG**

AFB1-DNA adducts and 8-OHdG lesions were detected by immunoperoxidase assays, as described previously [224], with minor changes. Briefly, cells were treated with AFB1 or DMSO on coverslips, washed with PBS, and then fixed in ice-cold methanol. AFB1-DNA adducts were detected using a monoclonal antibody 6A10 (Santa Cruz, Trevigen, France) against imidazol ring-opened persistent form of the major N7-guanine adduct of AFB1 [261]. Prior to immunoperoxidase assay of AFB1 adducts, cells were treated with a buffer containing 15mmol/L Na<sub>2</sub>CO<sub>3</sub> and 30 mmol/L NaHCO<sub>3</sub> (pH 9.6) for 2 hours at room temperature. For both AFB1 adducts and 8-OHdG lesions, cells were treated with RNase from MBI Fermentas, Germany, (100 µg/mL) in Tris Buffer (10 mmol/L Trizma Base, 1 mmol/L EDTA, and 0.4 mol/L NaCl; pH 7.5) for 1 h at 37 °C. After washing with PBS, proteinase K from Sigma (10 µg/mL) treatment was done for 7 min at room temperature. After rinsing

with PBS, DNA was denatured with 2N HCl for 10 min and cells were neutralized by soaking coverslips in 50mM Tris Base for 5 min. After blocking for 1 hour, cells were incubated with mouse 6A10 or mouse anti-8-OHdG (Trevigen, MD, USA) monoclonal antibody overnight at 4°C. Anti-mouse HRP-conjugated secondary antibodies (Invitrogen) were used for 30 min for primary antibody detection. Cells were stained with DAB (diaminobenzidine) solution (Dako, Denmark), counterstained with hematoxlin (Sigma), mounted with 80% glycerol, and observed under Olympus light microscope.

### **3.3.9 Indirect immunofluorescence**

Cells were fixed with 4% formaldehyde, and permeabilized with permeabilization solution. After blocking for one hour, cells were incubated overnight at 4°C, with primary antibodies and washed three times with washing solution. Secondary antibodies conjugated to Alexa 568 or Alexa 488 (Invitrogen, USA) incubation was performed for 1h at room temperature. After washing the unbound antibodies slides were counterstained with DAPI (Roche, IN, USA), and observed using Apotome (Zeiss) microscope. Images were captured with a AxioCam HRc color CCD camera (Zeiss) and digitally saved using Axio Imager software (Zeiss).

### **3.3.10 Costaining with immunofluorescence**

Cells were fixed with 4% formaldehyde, and after permeabilization, blocking was performed for one hour. Cells were incubated 2h with the primary antibodies simultaneously, and then washed three times with washing solution. Secondary antibodies conjugated to Alexa 568 or Alexa 488 (Invitrogen, USA) incubation was performed for 1h at room temperature. After washing the unbound antibodies slides were counterstained with DAPI and observed using Apotome (Zeiss) microscope. Images were captured with a AxioCam HRc color CCD camera (Zeiss) and digitally saved using Axio Imager software (Zeiss).



### 3.3.11 Cell cycle analysis and bromodeoxyuridine (BrdU) incorporation assay

Cells were washed twice in PBS and fixed in ice-cold ethanol for 10 min. After two PBS washes, cells were incubated with 20ug/mL of RNase A (MBI Fermentas, USA) at 37°C for 10 minutes and stained with propidium iodide (10 ug/mL in PBS; Sigma). Cell cycle distribution was determined by flow cytometry using FacScan and the CellQuest software (Becton Dickinson, NJ, USA). Cell cycle analysis combined with BrdU incorporation assay was done as described, except that cells were first labeled with 10 µmol/L BrdU (Sigma) for 2 hours prior to each testing time, and cells subjected to anti-BrdU staining after DNA denaturation with 4N HCl for 30 minutes using FITC-conjugated anti-BrdU antibody (BD Bioscience, NJ, USA) at room temperature for 30 minutes in the dark.

### 3.3.12 Single-cell gel electrophoresis (comet) assay

Single strand and double strand DNA breaks were detected using alkaline and neutral comet assays, respectively [262, 263]. Alkaline comet was performed as described [263]. Neutral comet assay was done as described [262], using the lysis protocol described in [264]. Following electrophoresis, slides were rinsed, stained with 5µg/ml DAPI and analyzed under Apotome (Zeiss) microscope. Images were captured with a Axiocam HRc color CCD camera (Zeiss) and digitally saved using Axio Vision software (Zeiss). Data was analyzed by CASP (Comet Assay Software Project) which measures tail moment, using DNA content in the tail and head along with the distance between the means of the head and tail distributions (<http://casplab.com>). At least 30 nuclei were analyzed for each experimental condition.

**Table 3.3.2 Antibodies used for immunoblotting, immunofluorescence and immunoperoxidase assays.** Sec: Secondary antibody; lab; Laboratories.

Antibody	Source
53BP1	Abcam
8-OHdG	Trevigen
Actin	Sigma
AFB1-DNA	Santa Cruz
Alexa anti mouse in goat 488 sec.	Invitrogen

Alexa anti mouse in goat 568 sec.	Invitrogen
Alexa anti rabbit in goat 488 sec.	Invitrogen
Alexa anti rabbit in goat 568 sec.	Invitrogen
ATM	Oncogene Research
ATR	Oncogene Research
Calnexin (Rabbit PAb)	Sigma
Chk1	Santa Cruz
Chk2	Santa Cruz
ERK1/2	cell signaling
H3 K27 Me1	Upstate
H3 K27 Me3	Upstate
H3 K36 Me3	Abcam
H3 K9 Me3	Upstate
H3K27Me2	Abcam
H3K36Me1	Abcam
H3K36Me2	Upstate
H3K4Me3	Abcam
H3R17Me2	Abcam
H3R2Me2	Upstate
H4K20Me1	Abcam
H4K20Me2	Abcam
H4K20Me3	Upstate
H4R3Me2	Upstate
MDM2	Santa Cruz
Mouse in goat sec.	Invitrogen
NFκB	Santa Cruz
p15	Santa Cruz
p16	Santa Cruz
p21 <sup>Cip1</sup>	CalbioChem
p27	Santa Cruz
P38MAPK	Cell Signaling
P53-ser15	cell signaling
phospho-AKT thr308	cell signaling
Phospho-AKT S473	Cell Signaling
phospho-ATMser1981	Cell Signaling
phospho-ATR Ser 428	Cell Signalling
Phospho-cdc25A S124	Abcam
phospho-chk1 ser345	Cell Signaling
phospho-Chk2 thr49	Cell Signaling
Phospho-ERK1/2 T202/Y204	cell signaling
Phospho-IKB	Santa Cruz
Phospho-p38MAPK T180/Y182	Cell Signaling
Phospho-p53 S15	Cell Signaling
Phospho-p53 S20	Cell Signaling
Phospho-SAPK/JNK T183/Y185	cell signaling
Phospho-Stat1 S727	cell signaling
Rabbit in goat sec.	DAKO
SAPK/JNK	cell signaling

Stat1	Transduction Lab.
Total AKT	cell signaling
Total p53	Santa Cruz
Tubulin	CalbioChem
$\gamma$ -H2AX	Milipore
Wee1	UpState

## CHAPTER 4. RESULTS

Reactive oxygen species can be produced from mitochondria, peroxisomes, and inflammatory cell activation [265] endogenously; and exogenously from environmental agents, pharmaceuticals, and industrial chemicals. When ROS are not eliminated by antioxidant defense mechanisms, oxidative stress accumulated in the cell may cause DNA, protein, and/or lipid damage, leading to chromosome instability, genetic mutation, and/or modulation of cell growth that may result in cancer.

In this study, we explored the role of genotoxic stress in the pathogenesis of HCC. In accordance with this objective, we classified the major genotoxic stress causing factors as follows:

1. Selenium deficiency induced oxidative stress
2. Environmental agents: Aflatoxins
3. Therapeutic agents: Adriamycin

First part of the study is mainly focused on understanding the selective tolerance of hepatocellular cell lines to Se-deficiency induced oxidative stress. In the second and third parts of our study, we tried to explore the effects of aflatoxins, the major environmental toxin that is only associated with liver cancer; with a comparative study employing the commonly used chemotherapeutic drug; Adriamycin as a positive control.

### 4.1 Tolerance to selenium-deficient conditions

The exact molecular mechanism of the relation between Se-deficiency with hepatic disease conditions including HCC is poorly understood. Previously our group reported that, *in vitro* Se-deficiency in a subset of HCC cell lines caused oxidative stress along with apoptosis. However, most of HCC cell lines tolerated Se-deficient conditions. There was no oxidative stress and cells escaped apoptotic response [197].

In order to understand the mechanism of this selective survival advantage which is prominent under Se-deficient and oxidative stress conditions, we selected a human hepatoblastoma-derived cell line HepG2 and its isogenic HBV (hepatitis B virus) transfected form HepG2-2.2.15 which are sensitive and resistant to the selenium deficient conditions respectively [197].

#### 4.1.1 Analysis of survival pathways

Several studies reported Se as a suppressor of the JNK, SAPK and p38MAPK pathways after oxidative stress [202, 203]. Therefore, these findings encouraged us to explore the key elements of possible stress activated and survival pathways triggered upon oxidative stress.

We checked the key downstream elements of 3 major pathways; the MAPK/Erk pathway, which is important for cell growth and differentiation, the SAPK/JNK pathway, and the p38MAPK pathway, which are both, activated through various types of environmental stresses. We observed cytoplasmic positivity in total ERK1/2 with no change in HepG2 clones under Se-deficient conditions at 48h while the phosphorylated ERK1/2 was very weakly increased in HepG2-2.2.15 cells in Se-deficient conditions by immunoperoxidase staining (Figure 4.1.1 A). Phosphorylated ERK1/2 levels were high in HepG2-2.2.15 cells when compared to the HepG2 cells, but surprisingly the levels were diminished in a time manner under Se-deficient conditions (Figure 4.1.1 B).

The immunoperoxidase staining pattern with SAPK/JNK demonstrated a weak increase in total levels in HepG2-2.2.15 under Se-deficient conditions at 48h (Figure 4.1.2 A), which was also confirmed by immunoblotting (Figure 4.1.2 B). The total SAPK levels were diminished in HepG2 cells as opposed to the time dependent increase in HepG2-2.2.15 under Se-deficiency (Figure 4.1.2 B). We obtained a very weak signal under the same conditions with p-SAPK/JNK antibody in both cells without any intensity change by immunostaining (Figure 4.1.2 A).

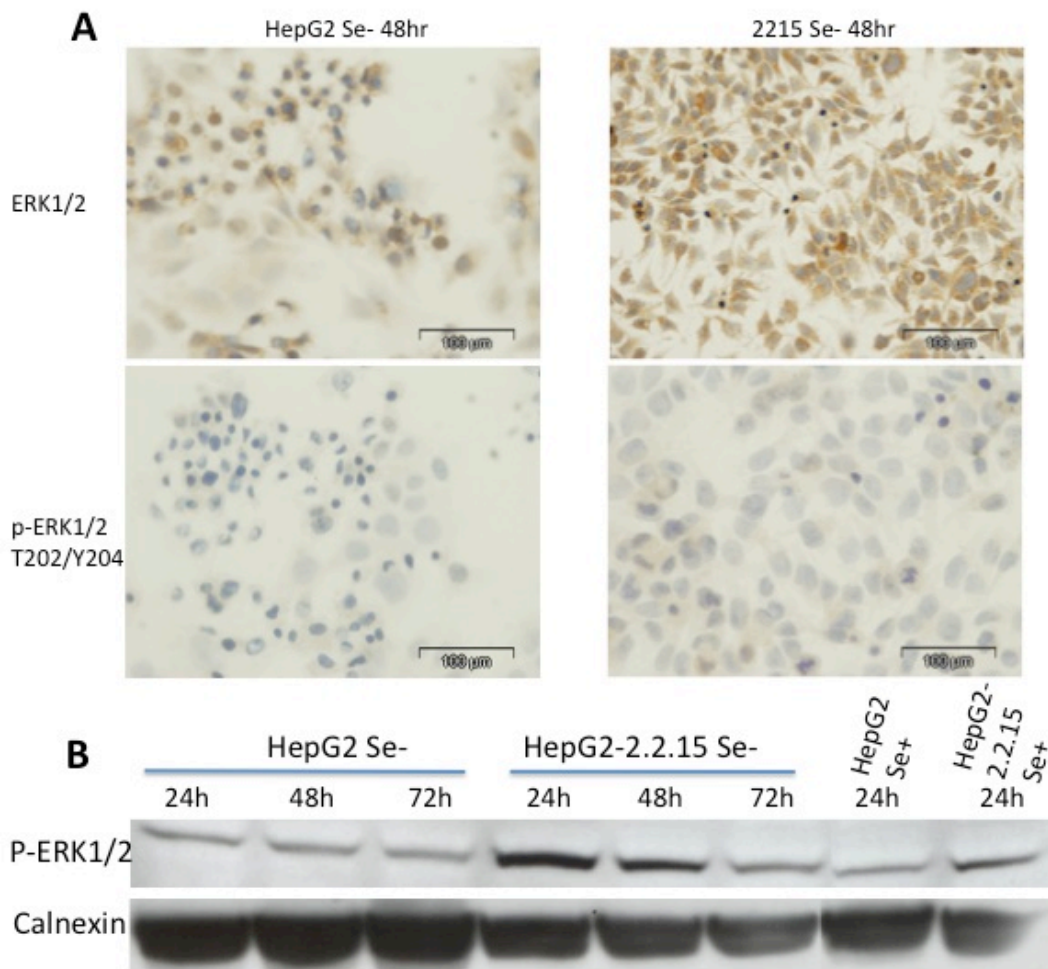


**FIGURE 4.1.1** Analysis of MAPK/ERK signaling pathway under selenium-deficiency. **(A)** HepG2 and HepG2-2.2.15 cells were grown in selenium adequate (Se<sup>+</sup>) or selenium-deficient (Se<sup>-</sup>) conditions for 48 hours and subjected to indirect immunoperoxidase staining with anti-ERK1/2 and anti-phospho ERK1/2. Counterstaining was done with hematoxyline. **(B)** HepG2 and HepG2-2.2.15 cells were grown in selenium adequate (Se<sup>+</sup>) or selenium-deficient (Se<sup>-</sup>) conditions and cells were collected at 24 hours, 48 hours and 72 hours. Immunoblotting was performed with anti-phospho ERK1/2. Cells grown in (Se<sup>+</sup>) for 24 hours were used as control. Calnexin was used as equal loading control.

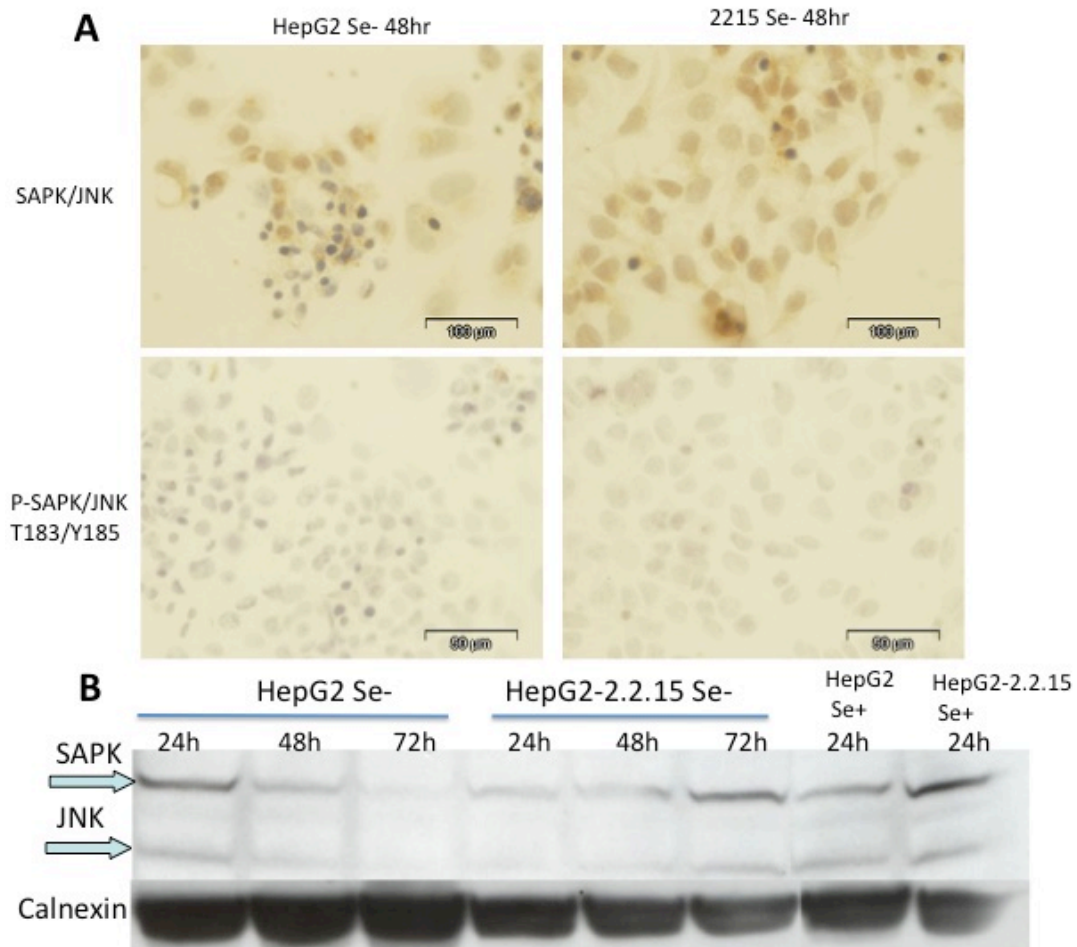


**FIGURE 4.1.2** Analysis of SAPK/JNK signaling pathway under selenium-deficiency. **(A)** HepG2 and HepG2-2.2.15 cells were grown in selenium adequate (Se+) or selenium-deficient (Se-) conditions for 48 hours and subjected to indirect immunoperoxidase staining with antibody against SAPK/JNK and phospho- SAPK/JNK. Counterstaining was performed with hematoxyline. **(B)** HepG2 and HepG2-2.2.15 cells were grown in selenium adequate (Se+) or selenium-deficient (Se-) conditions and cells were collected at 24 hours, 48 hours and 72 hours. Immunoblotting was done with antibody against SAPK/JNK. Cells grown in (Se+) for 24 hours were used as control. Calnexin was used as equal loading control.

Phosphorylated p38MAPK levels were increased in HepG2 cells when compared to the HepG2-2.2.15 cells while the total p38MAPK levels remained the same under Se-deficient conditions. This observation was consistent with the apoptosis in those cells at 48h (Figure 4.1.3). In order to demonstrate the differences observed in the downstream of the p38MAPK signaling pathway, we looked for the activation of a previously reported target of p38MAPK, Stat1 [266]; which has an essential role in oxidative stress induced apoptosis. Nevertheless, our results failed to detect an activation of Stat1 in HepG2 cells under oxidative stress (Figure 4.1.4 A and B).

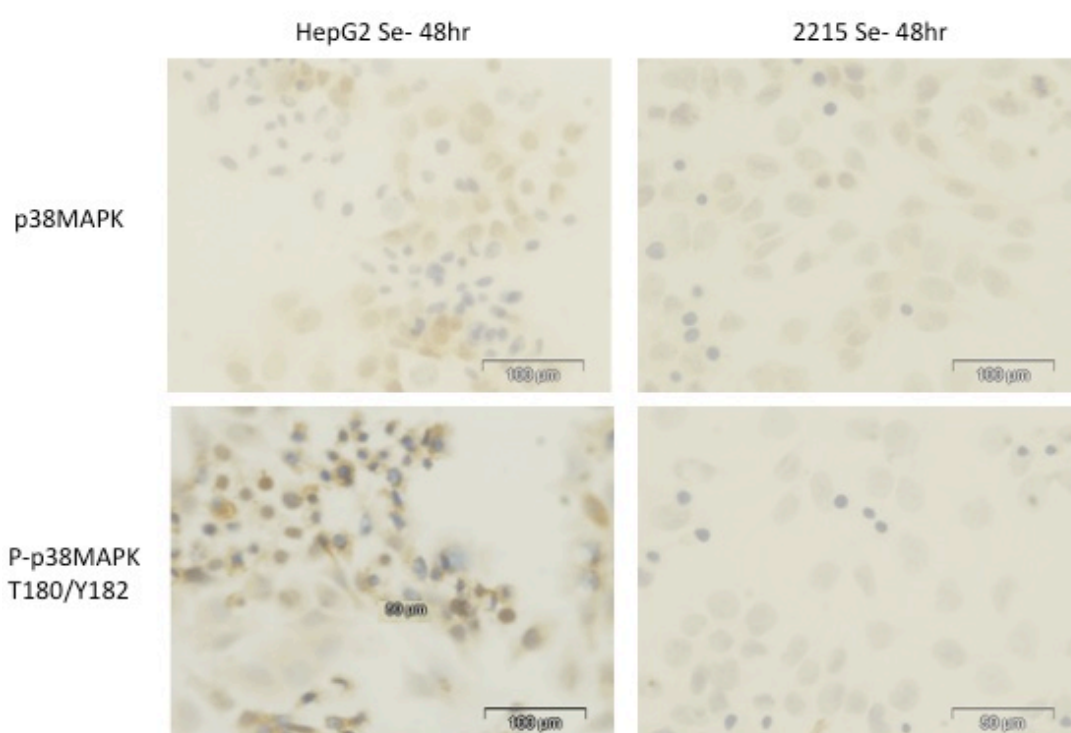


**FIGURE 4.1.3** Analysis of p38MAPK stress signaling pathway under selenium-deficiency. HepG2 and HepG2-2.2.15 cells were grown in selenium adequate (Se+) or selenium-deficient (Se-) conditions for 48 hours and subjected to indirect immunoperoxidase staining with antibody against p38MAPK and phospho-p38MAPK. Counterstaining was performed with hematoxyline.



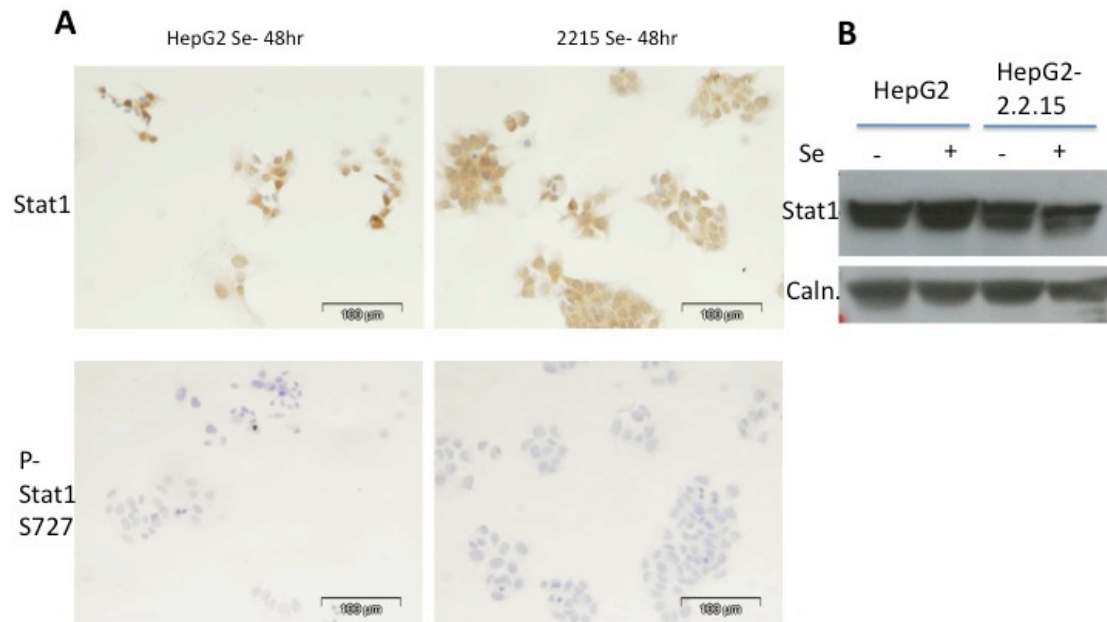


**FIGURE 4.1.4** Analysis of p38MAPK stress signaling pathway downstream apoptosis targets. **(A)** HepG2 and HepG2-2.2.15 cells were grown in selenium adequate (Se+) or selenium-deficient (Se-) conditions for 48 hours and subjected to indirect immunoperoxidase staining with antibody against Stat1 and phospho-Stat1. Counterstaining was performed with hematoxyline. **(B)** HepG2 and HepG2-2.2.15 cells grown in selenium adequate (Se+) or selenium-deficient (Se-) conditions for 48 hours and subjected to western blotting with antibody against Stat1. Calnexin was used as equal loading control.

#### 4.1.2 AKT, as a key for survival under selenium deficient conditions

The PI3K/AKT signal transduction pathway is a crucial regulator of cell proliferation and survival. Activation of Akt1 was reported in HBV-induced HCC [267] and viruses favor the inhibition of apoptosis through the induction of the PI3K/AKT pathway [268]. In our experimental model the only difference that may contribute to the survival advantage under Se-deficiency could be the presence of HBV, therefore we hypothesized AKT could play a role in the process of acquired selective survival mechanism.

In order to test this hypothesis, we incubated HepG2 and HepG2-2.2.15 cells in selenium deficient medium and assessed the AKT activation status by immunostaining and immunoblotting by antibodies against total AKT and phospho-AKT thr308 and phospho-AKT ser473. Both critical residues of AKT required for its full activation

were detected to be phosphorylated in HepG2-2.2.15 cells under Se-deficient conditions (Figure 4.1.4 A), and this data was confirmed by immunoblotting of the samples that were taken at 24, 48 and 72h after incubation with Se-deficient medium with a time-dependent manner (Figure 4.1.4 B). Yet we did not observe any variations in total AKT levels indicating its activation was through phosphorylations.

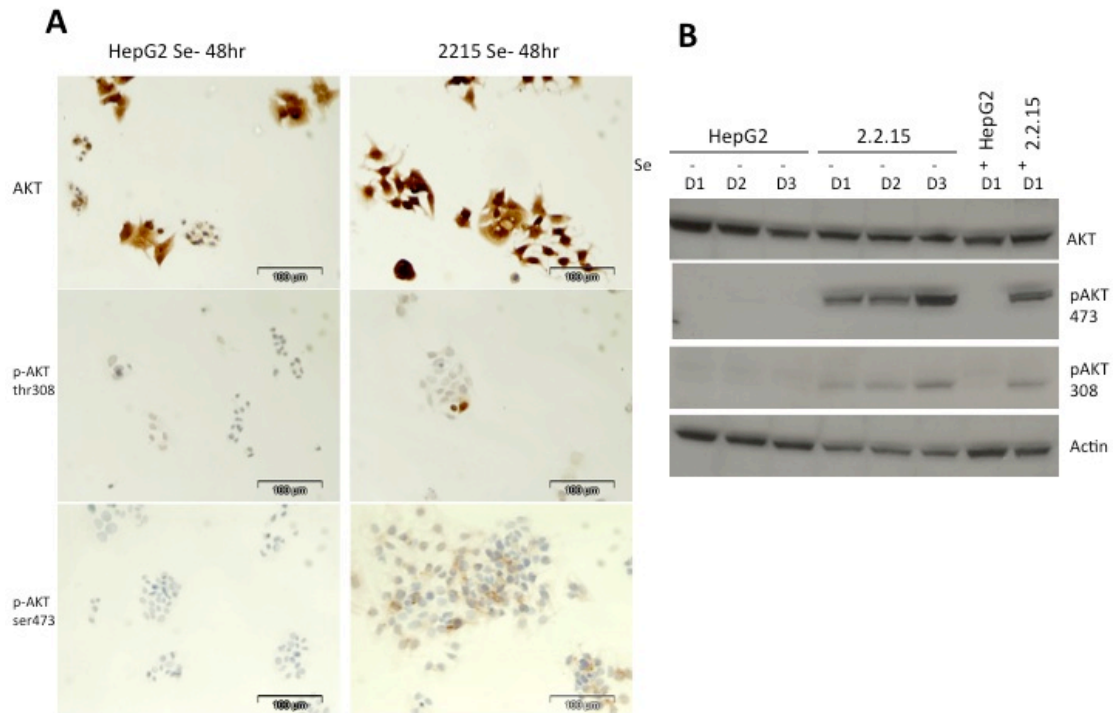


**FIGURE 4.1.5** Phosphorylation of Akt is increased under selenium deficient conditions. **(A)** HepG2 and HepG2-2.2.15 cells were grown in selenium adequate (Se+) or selenium-deficient (Se-) conditions for 48 hours and subjected to indirect immunoperoxidase staining with antibody against AKT, phospho-AKT thr308 and phospho-AKT ser473. Counterstaining was performed with hematoxyline. **(B)** HepG2 and HepG2-2.2.15 cells were grown in selenium adequate (Se+) or selenium-deficient (Se-) conditions and cells were collected at 24 hours, 48 hours and 72 hours and subjected to western blotting with antibodies against AKT, phospho-AKT thr308 and phospho-AKT. Cells grown in (Se+) for 24 hours were used as control. Actin was used as equal loading control.

To identify the mechanism of PI3K/AKT mediated cell survival, we checked for one of the functional targets of AKT; NF- $\kappa$ B [269]. Both clones treated under Se-deficient conditions for 48h were subjected to immunostaining and immunoblotting. We detected a stronger staining pattern (Figure 4.1.6 A) against NF- $\kappa$ B in the apoptosis resistant clone, yet our antibody failed to determine this change in immunoblotting (Figure 4.1.6 B) for both p105 and p50 NF- $\kappa$ B's proteolytic cleavage products. Phosphorylated IKB, which is required for the release of NF- $\kappa$ B, thereby accumulating NF- $\kappa$ B in the nucleus, were remained to be unchanged (Figure 4.1.6 A).

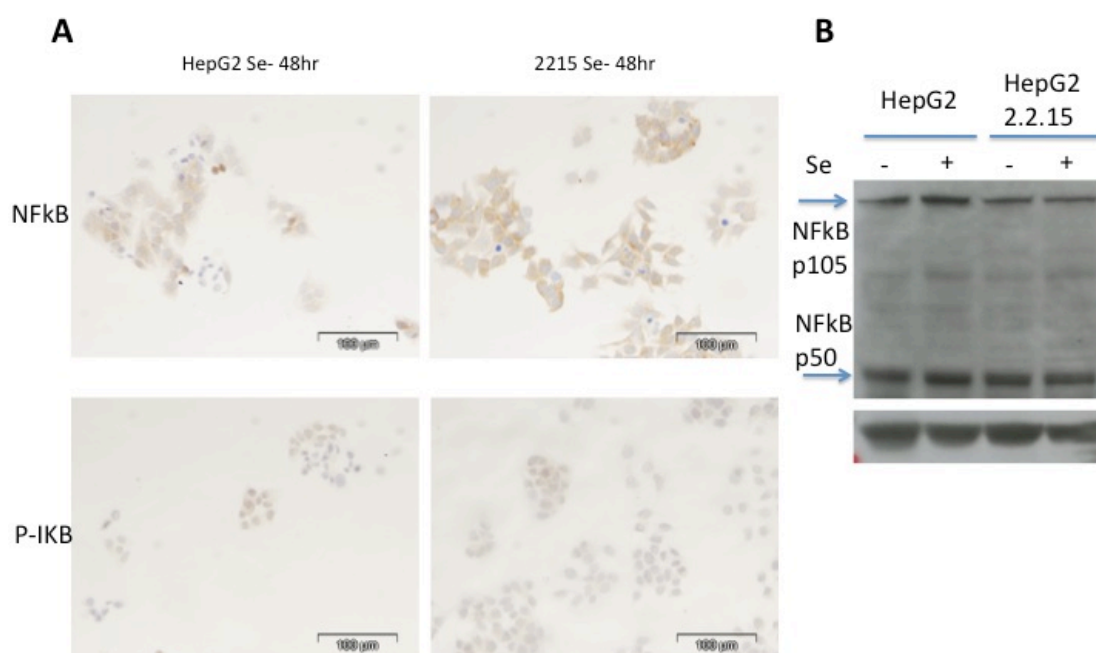


**FIGURE 4.1.6** Analysis of downstream signals in AKT induced survival under selenium deficient conditions. **(A)** HepG2 and HepG2-2.2.15 cells were grown in selenium adequate (Se+) or selenium-deficient (Se-) conditions for 48 hours and subjected to indirect immunoperoxidase staining with antibody against NF $\kappa$ B, phospho-IKB. Counterstaining was performed with hematoxyline. **(B)** HepG2 and HepG2-2.2.15 cells grown in selenium adequate (Se+) or selenium-deficient (Se-) conditions for 48 hours and subjected to western blotting with antibody against NF $\kappa$ B. Calnexin was used as equal loading control.

#### 4.1.3 Inhibition of AKT reverts HepG2-2.2.15 phenotype under Se-deficient conditions.

Our observation of AKT activation through phosphorylation, despite its higher levels in Se-72h samples, was not only due to Se-supplementation, since both phospho-AKT residues were detectable in control HepG2-2.2.15 samples under Se-adequate conditions. This phenomenon, which was reported previously as a consequence of HBV [267], prompted us to further investigate the activation of AKT in the acquired tolerance to the Se-deficient conditions. To rule out the possibility of the requirement of AKT for inhibition of apoptosis, we treated HepG2 and HepG2-2.2.15 cells with Wortmannin, which is a specific and commonly used inhibitor of PI3Ks, at the same time with Se-supplementation. Cells incubated with Se-deficient or Se-adequate medium along with 500nM Wortmannin or its vehicle control DMSO for 48 and 72h, were subjected to immunoblotting to detect the protein levels of phospho-AKT (Figure 4.1.7). We were able to inhibit the ser473 residue phosphorylation of AKT after Wortmannin treatment. Subsequently, we checked for the caspase 3 dependent apoptosis with a specific antibody that recognizes both caspase-3 and its cleaved form. Upon the inhibition of phosphorylation in HepG2-2.2.15 under both Se- and Se+ conditions, cleaved caspase-3 levels were increased (Figure 4.1.7). This data indicated that the inhibition of the PI3K/AKT pathway regardless of Se-supplementation recapitulate apoptosis in HepG2-2.2.15 cells.

#### 4.1.4 Inhibition of constitutively active AKT did not recapitulate apoptosis in Mahlavu and Snu475.

Our previous results indicated that tolerance to selenium deficiency was not only due to the presence of HBV integration but also chronic aflatoxin exposure. In fact, after screening the HCC cell lines with different etiologies, it is concluded that the tolerance to the oxidative stress conditions under selenium deficiency stem from genotoxic stress induced either with HBV infection and/or chronic aflatoxin exposure [197]. Therefore, we wanted to test two different HCC cell lines; Mahlavu (chronic aflatoxin exposure with p53 R249S mutation) and Snu475 (HBV infection) both of which lack PTEN protein expression and have constitutively active PI3K/AKT pathway. We treated Mahlavu and Snu475 with Wortmannin as employed before

along with selenium supplemented or deficient medium for 48 and 72h, and the cell lysates were subjected to immunoblotting to detect the protein levels of phospho-Akt (Figure 4.1.8). We were only able to inhibit the ser473 residue phosphorylation of Akt partially after Wortmannin treatment. Accordingly, we checked the caspase 3 dependent apoptosis with a specific antibody that recognizes both caspase-3 and its cleaved form. Upon the partial inhibition of phosphorylation in Mahlavu (Figure 4.1.8 A) and Snu475 (Figure 4.1.8 B) under both Se- and Se+ conditions, cleaved caspase-3 levels were not detected. This data may suggest that the inhibition of the PI3K/AKT pathway with Wortmannin was not enough to recapitulate apoptosis regardless of Se-supplementation rescue apoptosis in HepG2-2.2.15 cells.

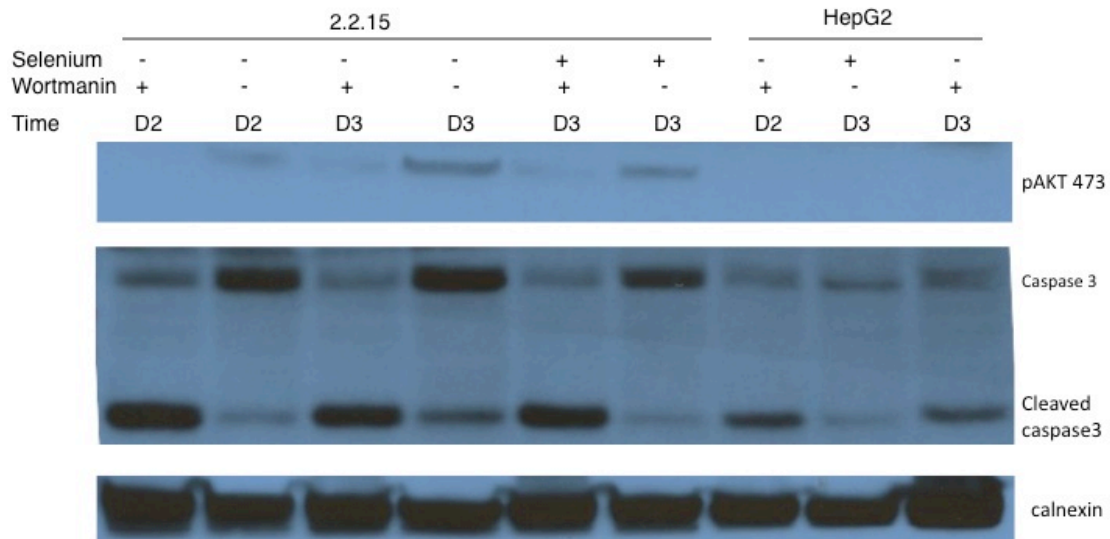


**FIGURE 4.1.7** Inhibition of PI3K/Akt pathway induced apoptosis. HepG2 and HepG2-2.2.15 cells were grown in selenium adequate (Se+) or selenium-deficient (Se-) conditions in the absence/presence of Wortmannin (500nM) for 48 and 72 hours and subjected to indirect western blotting. Phospho-AKT and caspase3 and cleaved caspase3 levels were shown. Calnexin was used as equal loading control.

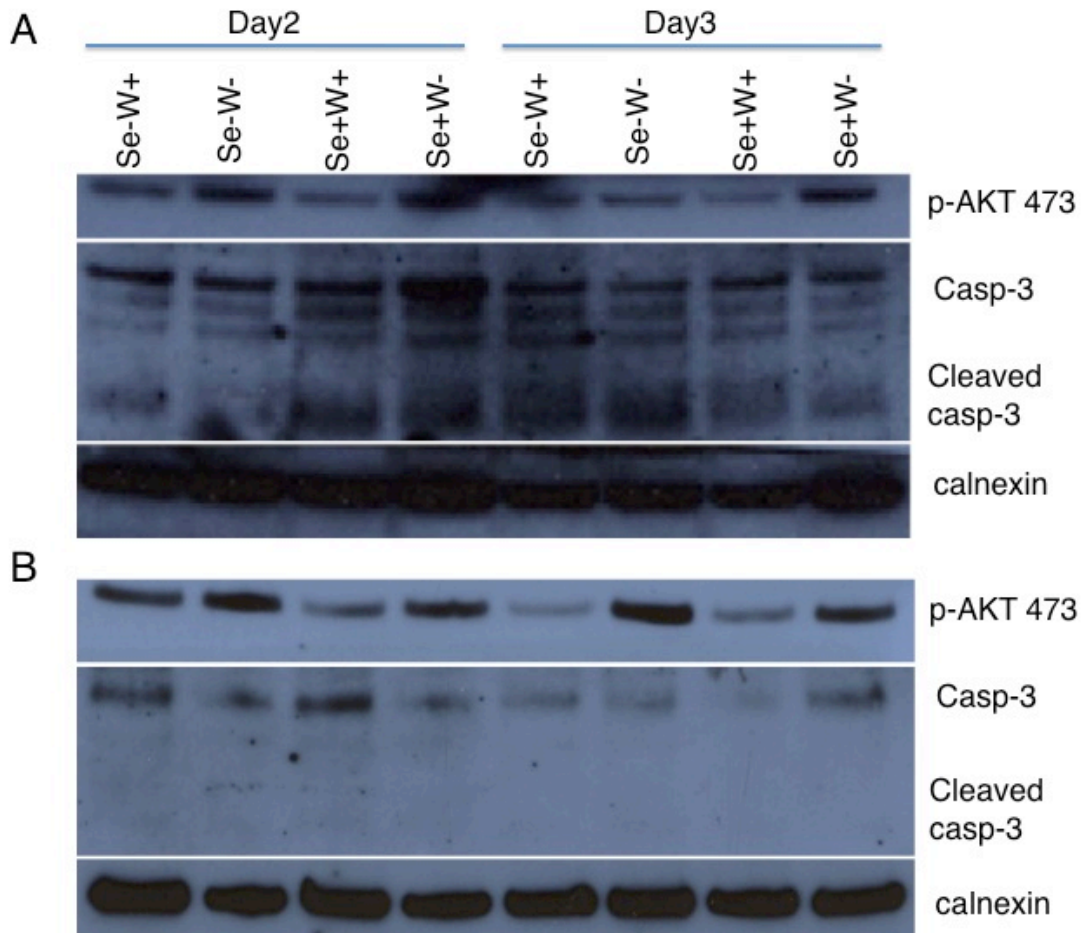


**FIGURE 4.1.8** Inhibition of PI3K/Akt pathway did not induce apoptosis in Mahlavu and Snu475. Mahlavu (A) and Snu475 (B) cells were grown in selenium adequate (Se+) or selenium-deficient (Se-) conditions in the absence/presence of Wortmannin (500nM) for 48 and 72 hours and subjected to indirect western blotting. Phospho-AKT and caspase3 and cleaved caspase3 levels were shown. Calnexin was used as equal loading control.

## 4.2 Exploration of oncogenicity of R249S p53 mutation in HCC

### 4.2.1 Formation and validation of R249S p53 expressing HepG2 clones

In order to investigate the molecular mechanism underlying the oncogenicity of mutant p53-249ser in HCC, HepG2 cells were used as a model. This cell line displays wild-type p53, and transfection with p53-249ser mimics the initial steps of p53-249ser-related hepatocellular carcinogenesis with a heterozygous state for p53 mutation. We transfected HepG2 cell line, with either pCMV-Neo-Bam p53 R249S vector or the empty pCMV-Neo-Bam vector to obtain stable clones bearing R249S mutant p53 in the p53 wild type background. To eliminate the false results that would

stem from clonal selection, six p53-249ser-expressing and four control clones have been selected by mutant p53 expression analysis using RT-PCR followed by 249AGG-<AGT-selective BsuRI and HinfI digestions (Figure 4.2.1A and Figure 4.2.1B). BsuRI is a restriction enzyme with a 5' GG<sup>↓</sup>CC 3' restriction recognition site and cuts if p53 is wild type at codon 249. On the contrary, HinfI has a recognition site at 5' GAN<sup>↓</sup>TC 3' meaning that it cuts p53 when it has 249AGG-<AGT transversion. PLC/PRF/5 cell line with a R249S p53 mutation was used as a positive control.

After this first genotypic validation, we checked the protein level of a cyclin-dependent kinase inhibitor p21<sup>cip1</sup> which is a well-characterized p53 target [270] after the induction of DNA damage. It is a well-known fact that, in wild-type TP53 expressing cell lines, genotoxic treatment induces p53 protein levels and a subsequent transcription of the p21<sup>cip1</sup> gene while in a mutant TP53 background p21<sup>cip1</sup> accumulation is minimum [270-272]. Adriamycin (ADR) is an anti-cancer drug commonly used in the treatment of several human solid cancers including unresectable HCC [273] and its therapeutic effects have been linked to DNA intercalation and topoisomerase inhibition [274]. Therefore, we treated the cell clones with 1 $\mu$ M ADR and checked the nuclear accumulation of p21<sup>cip1</sup> with the clones bearing R249S p53 mutation after DNA damage and manually counted the positive and total number of cells from at least 10 different regions and positive cell percentage was calculated ( $p < 0.01$ ) (Figure 4.2.2).

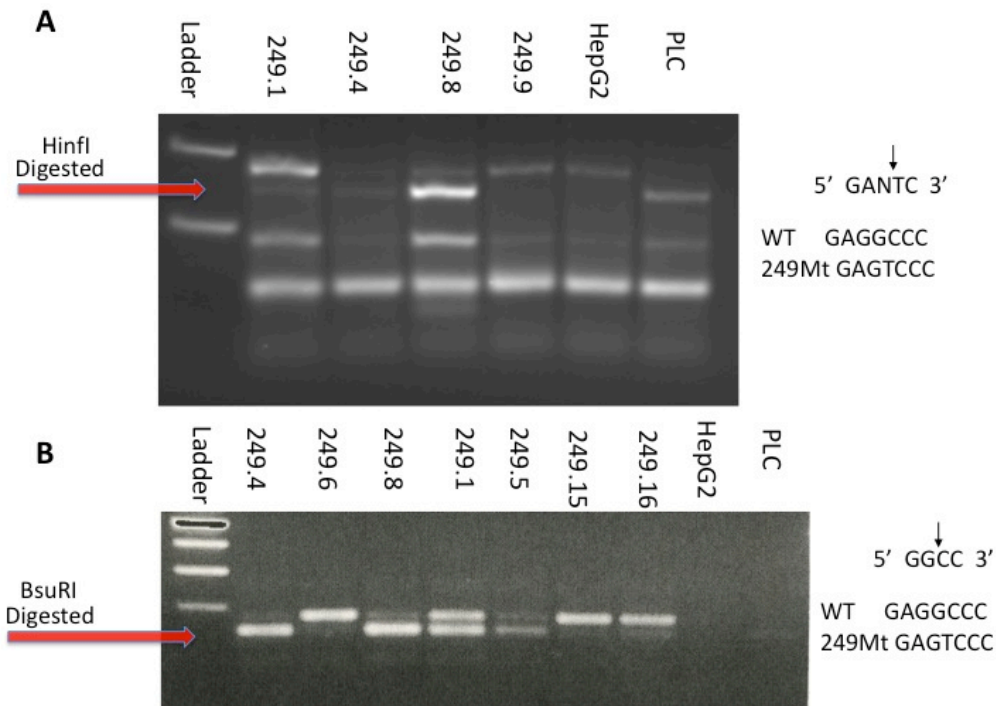


**FIGURE 4.2.1** Validation of transcription of R249S p53 mutation in stable clones. Selected HepG2 R249S p53 clones were subjected to restriction digestions with Hinfl (**A**) and BsuRI (**B**). HepG2 and PLC/PRF/5 were used as negative and positive control respectively. R249S mutant transcripts give 136, 84, 30 and 30bp length and wild-type transcripts give 166, 84, 30 bp fragments subsequently after digestion with Hinfl. R249S mutant transcripts give 280, 138, and 142bp length, since they include wild type p53 also and wild-type transcripts give 138 and 142 bp fragments subsequently after digestion with BsuRI.

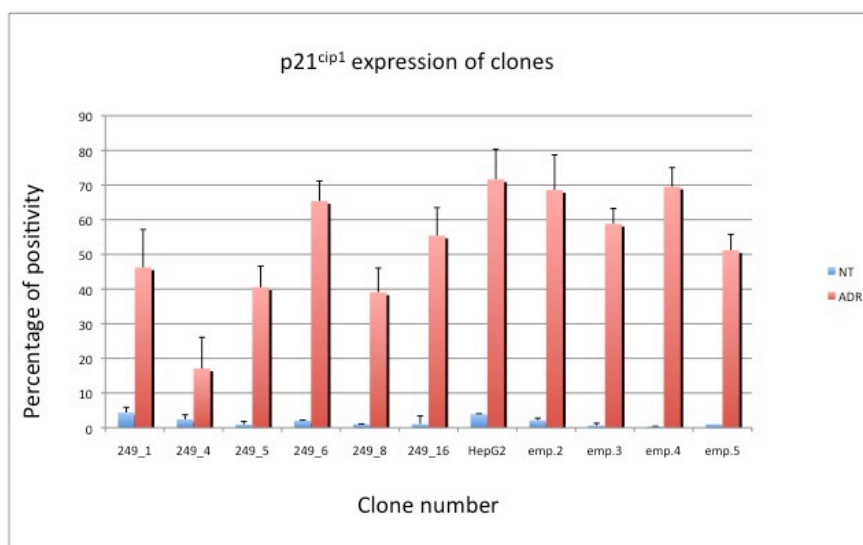


**FIGURE 4.2.2** Expression of p53 target p21<sup>cip1</sup> after treatment with Adriamycin in stable clones. Selected p53 R249S and control clones along with the parental HepG2 cells were treated with 1 $\mu$ M



ADR for 24 hours and then subjected to immunoperoxidase staining with an antibody against p21<sup>cip1</sup>. 150 cells from 10 different places were counted and percentage of positive cells was calculated for non-treated and treated conditions separately. Blue and red bars represent non-treated and ADR treated positivity respectively. Error bars represent standard deviation.

#### 4.2.2 Subcloning of the selected R249S p53 expressing HepG2 clones

Due to some limitations after transfection, cells can lose the ectopic expression of the gene, thus working with a wild type p53 carrying cell line and restrictions of transfection efficiency prompted us to do further subcloning of the selected clones. Our major aim was to ensure the expression of R249S p53 and to obtain a more homogenous population. That's why we selected 2 clones with R249S p53; HepG2\_249.4 and HepG2\_249.8 with the lowest p21<sup>cip1</sup> expression after ADR treatment and 2 control clones HepG2\_emp.4 and HepG2\_emp.5 with the lowest p21<sup>cip1</sup> expression without any treatment to subclone them. After subcloning we tested 15 clones derived from HepG2\_249.4 and HepG2\_249.8 and 7 clones from HepG2\_emp.4 and HepG2\_emp.5. Opposite of what we expect, we could not obtain such a population that is purely negative or positive (Figure 4.2.3A and B) in terms of p21<sup>cip1</sup> expression. This may be either due to the fact that p53-249ser in the presence of wtp53 cannot inhibit wt p53 activity or tumor heterogeneity and/or cell plasticity.

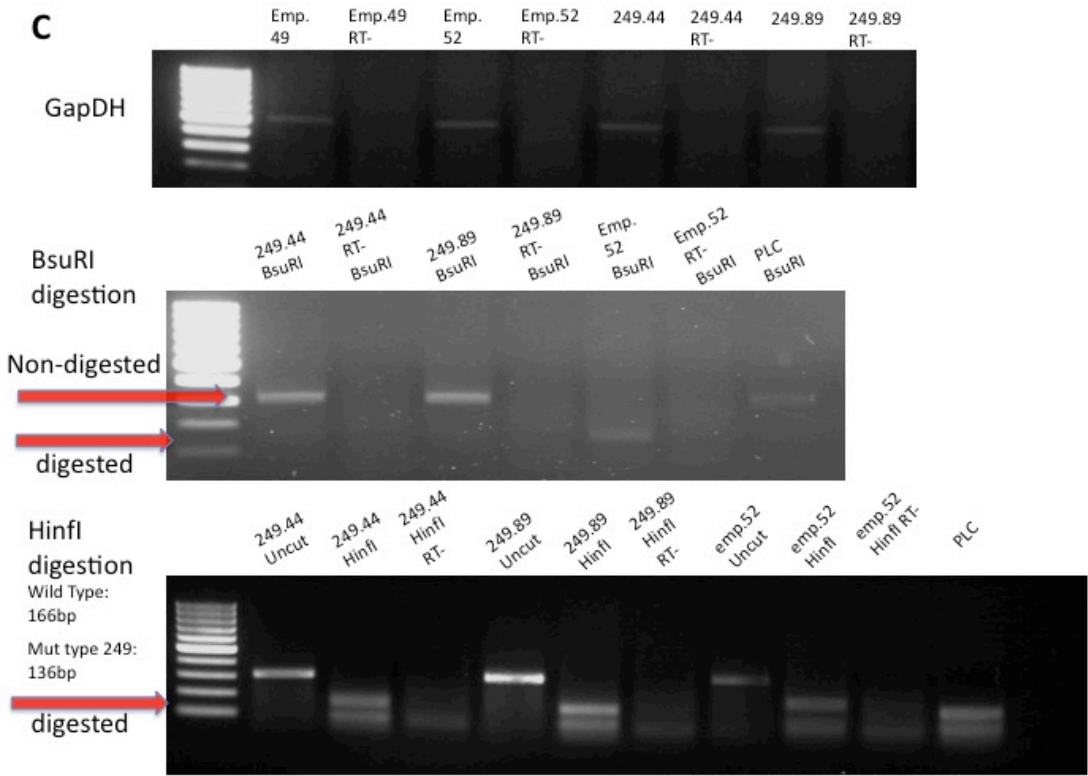
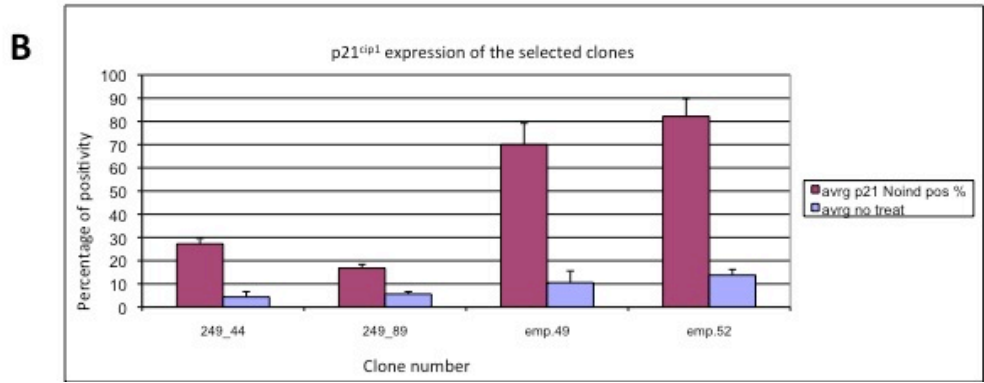
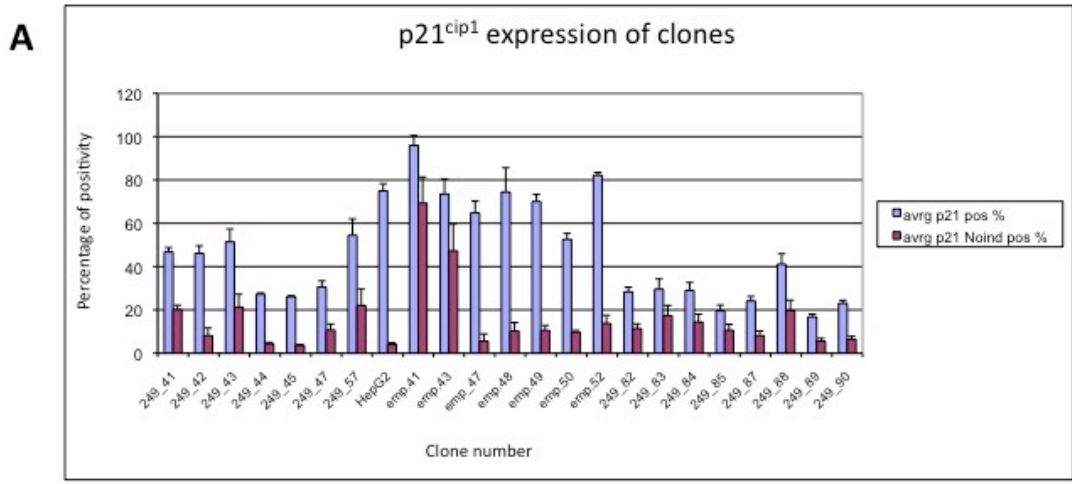


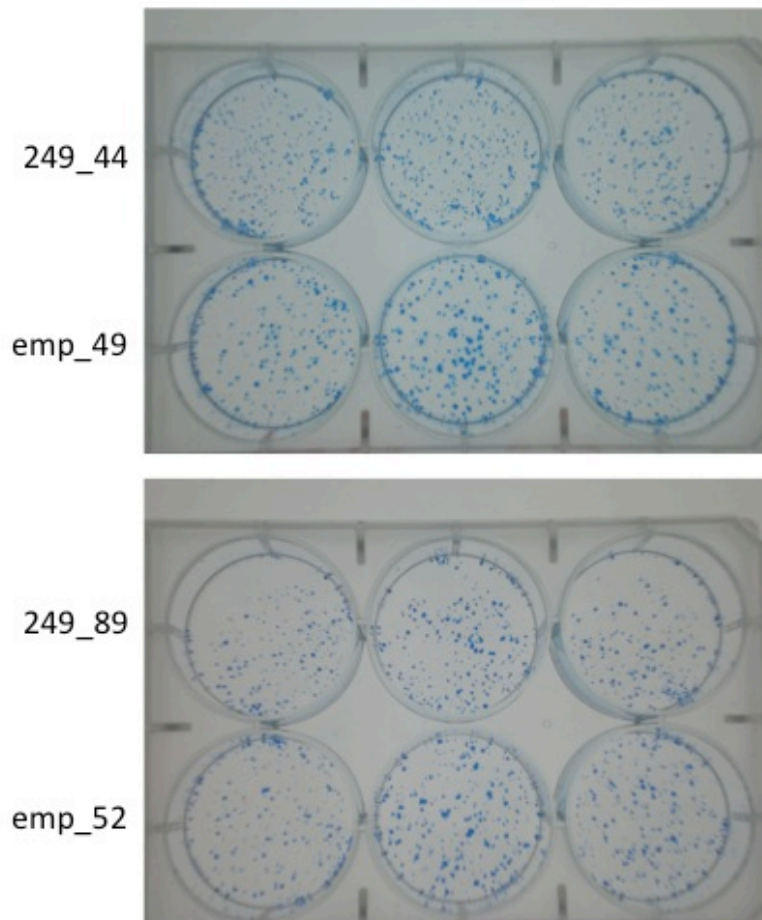
**FIGURE 4.2.3** Validation of transcription of R249S p53 mutation and expression of p21<sup>cip1</sup> after Adriamycin treatment in subclones. Selected p53 R249S and control subclones along with the parental HepG2 cells were treated with 1 $\mu$ M ADR for 24 hours and then subjected to immunoperoxidase staining with an antibody against p21<sup>cip1</sup>. 150 cells from 10 different places were counted and percentage of positive cells was calculated for non-treated and treated conditions separately. Error bars represent standard deviation. **(A)** Blue and red bars represent non-treated and ADR treated positivity respectively. 4 subclones selected from different parental clones were subjected to immunoperoxidase staining with an antibody against p21<sup>cip1</sup> to ensure the expression of p53 target **(B)** and subjected to restriction digestions with BsuRI and HinfI **(C)**. 150 cells from 10 different places were counted and percentage of positive cells was calculated for non-treated and treated conditions separately. Error bars represent standard deviation **(B)**. GAPDH was used as loading control. RT- controls were subjected to the same protocol in order to ensure there is no DNA contamination. PLC/PRF/5 was used as restriction digestion control.

As a result, we selected the lowest p21<sup>cip1</sup> expressing subclones; HepG2\_249.44 and HepG2\_249.89 derived from 2 different parental clones and two control subclones; HepG2\_emp.49 and HepG2\_emp.52 with the lowest background p21<sup>cip1</sup> expression for further analysis and these clones were verified with restriction enzyme digestion method (Figure 4.2.3 C).

#### 4.2.3 Survival advantage of R249S p53

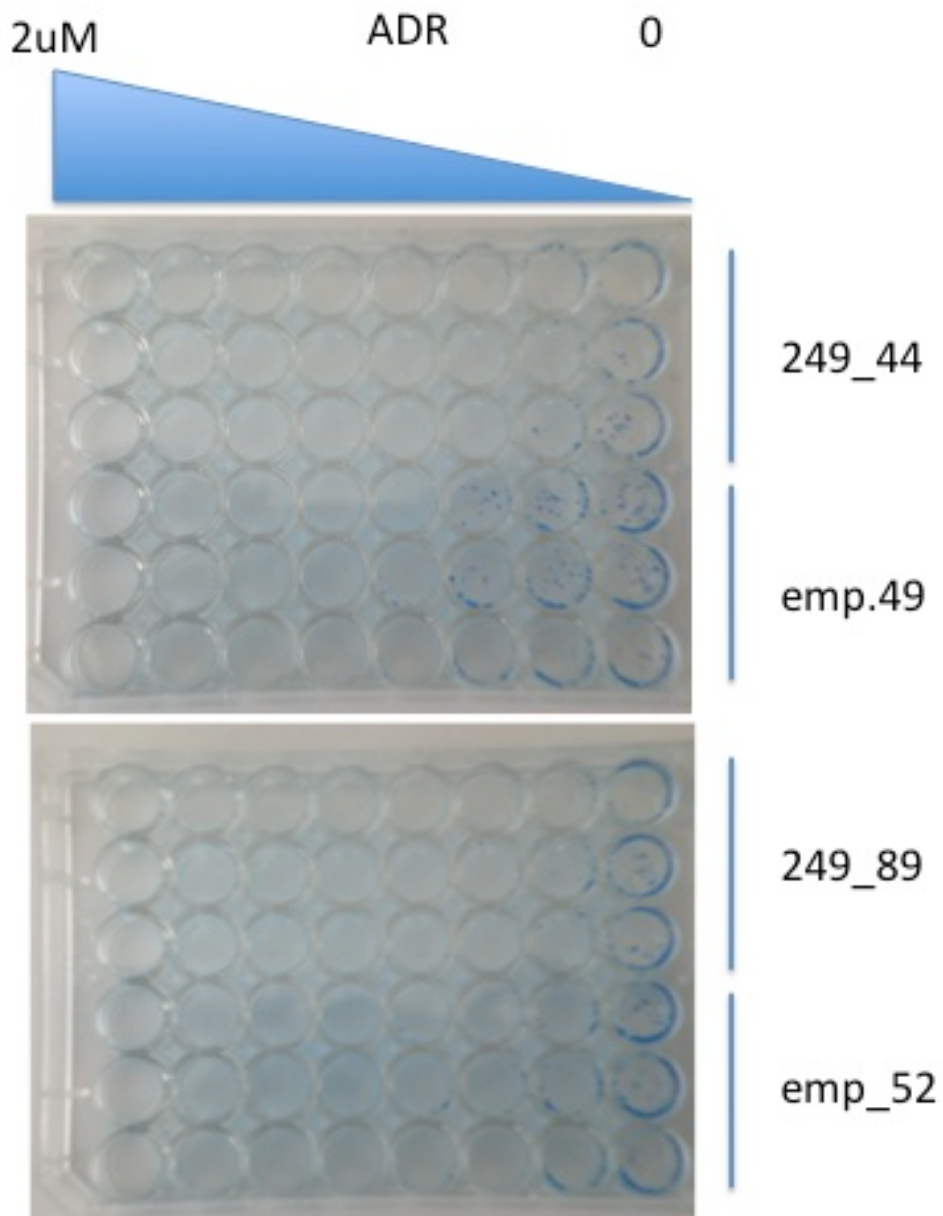
Although the frequent p53 mutations are predominantly involved in the loss of tumor suppressor activity of the protein, there is accumulating evidence that indicates the resulting mutant p53 can contribute to carcinogenesis either with dominant negative effects of the protein or with gain-of-function features. In order to ascertain the role of R249S in tumorigenesis and understand whether, p53-249ser mutation serves as a selective growth advantage thus contributing to the oncogenicity, we performed long term colony formation experiments.

A comparative analysis of *in vitro* growth characteristics of p53-249ser and control subclones was performed in order to assess the duplication capacity of these clones. Control and R429S p53 clones were plated in low density and stained after 15 days of culturing to observe any phenotypic difference between these two different p53 backgrounds. Figure 4.2.4 indicated that the difference of colony number and size were not significant.



**FIGURE 4.2.4** Long-term colony formation assay. Selected subclones for R249S p53 and wild-type p53 were plated on 6-well plates in low density (1000cells/well) in triplicates and after 15 days fixed and stained with Coomassie-Blue. Mediums were changed every 3-4 days.

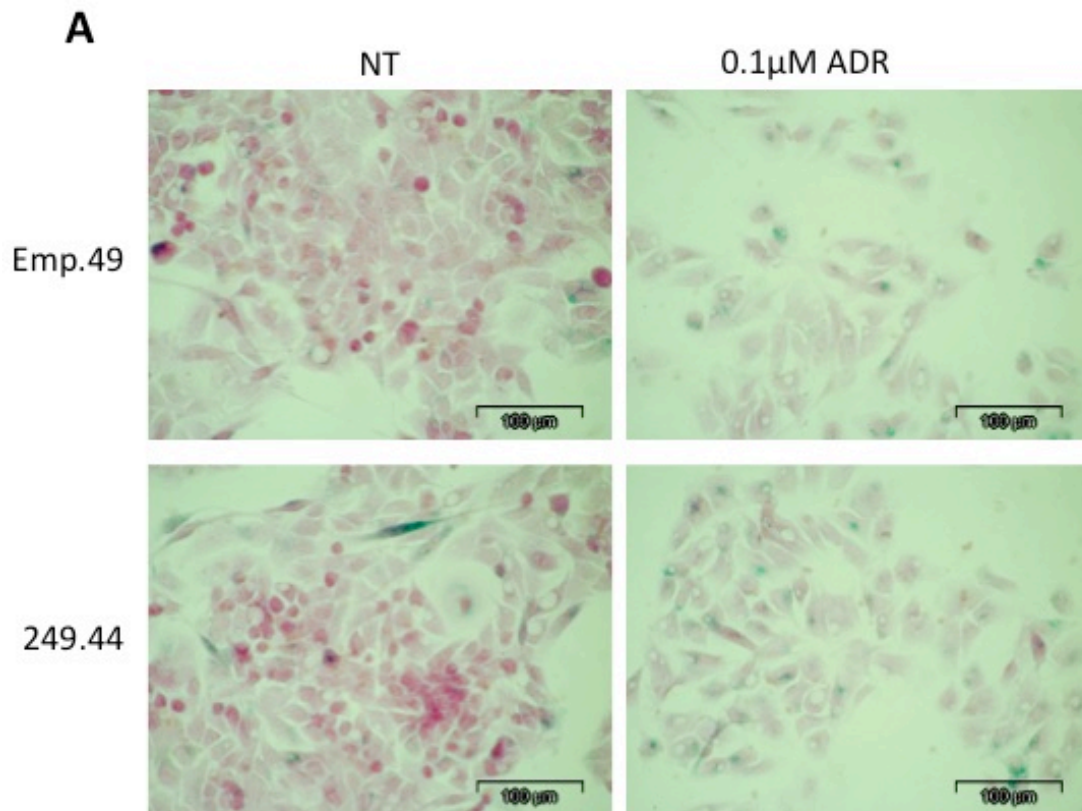
Therefore, as a next step we checked the colony formation after ADR treatment. Cells plated in 48-well plates were treated with 0-2  $\mu\text{M}$  ADR for 24h and then cultured for an additional time of 15 days. We observed that 0.25  $\mu\text{M}$  ADR was a threshold for the clones to survive, after that dose cells were all dead regardless of their p53 status (Figure 4.2.5).



**FIGURE 4.2.5** Long-term colony formation assay after DNA damage induction. Selected subclones for R249S p53 and wild-type p53 were plated on 48-well plates in low density (200cells/well) in triplicates and next day 0, 0.1, 0.25, 0.5, 1, 1.5, 2 $\mu$ M ADR were given for 24 hours and after 15 days fixed and stained with Coomassie-Blue. Mediums were changed every 3-4 days.

Treatment with doses below 0.2  $\mu$ M ADR indicated a slight survival advantage of control clones over R249S p53 ones. Since DNA damage has been identified as potential mediators of cellular senescence and ADR is able to trigger senescence through mitotic catastrophe ([275], Gursoy-Yuzugullu, unpublished data) we checked the senescence response difference after the treatment with two different agents; ADR

and TGF $\beta$ -1 by senescence-associated  $\beta$ -galactosidase (SABG) assays (Figure 4.2.6A and Figure 4.2.6B). We could not conclude a significant senescence response difference with either of those treatments.



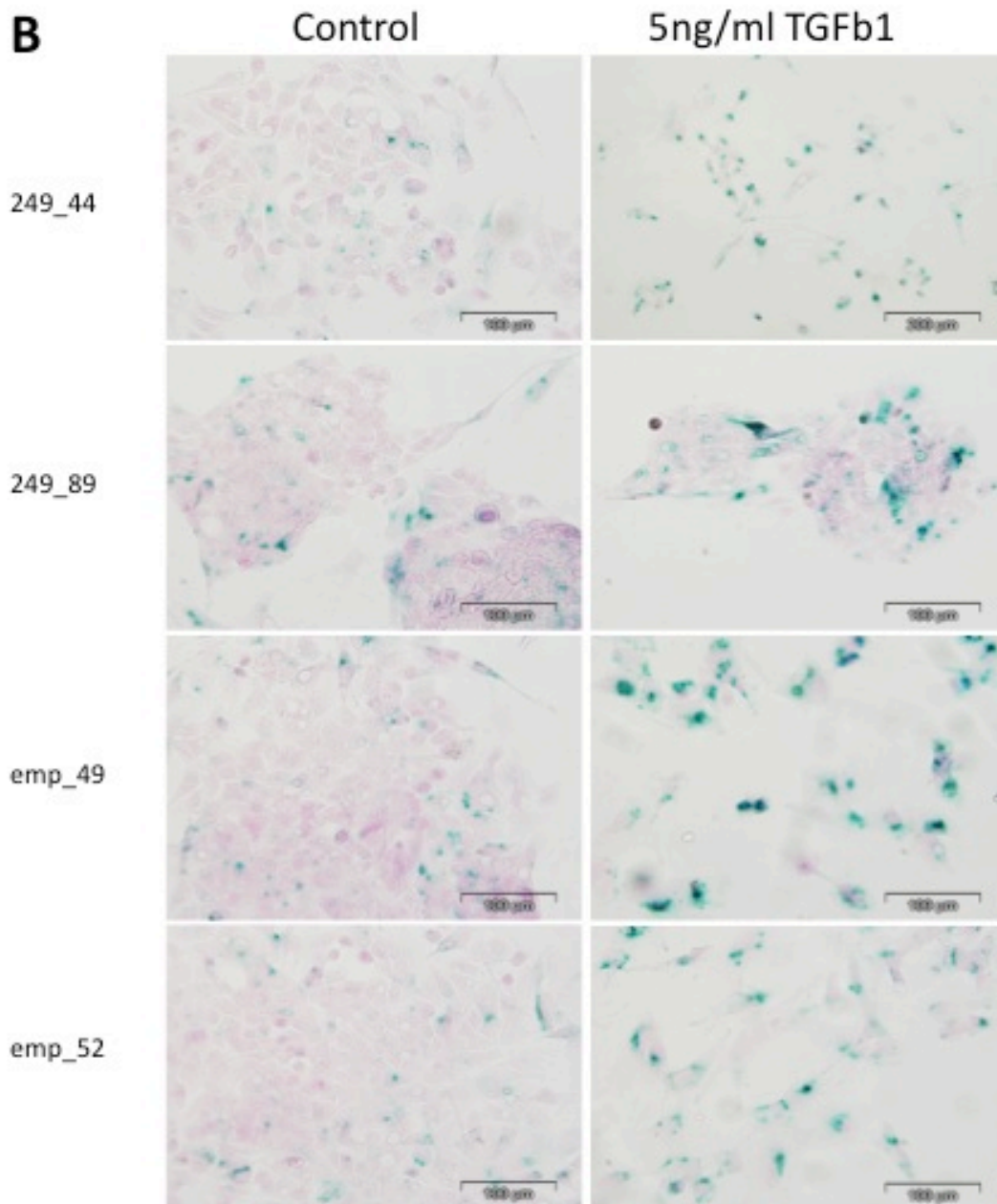


**FIGURE 4.2.6** Difference between senescence response induced by low-dose Adriamycin (A) and TGF-β1 (B). Selected subclones for R249S p53 and wild-type p53 were plated on 6-well plates and treated with either 0.1μM ADR or 5ng/ml TGF-β1 for 72 hours and then subjected to senescence (SABG) assay protocol. Nuclear fast red was used as counterstain. Representative pictures from each condition were taken and compared with each other. Scale bar 100μm.

How a cell line that already has the p53-249ser mutation along with wild type p53 would respond when it is exposed to AFB1 is not known. p53-249ser mutation has been detected in the liver of aflatoxin-exposed people prior to liver cancer development [276]. Thus, people that carry this mutation are being exposed to AFB1 in their diet; therefore their hepatocytes primed with a p53-249 mutation would be

exposed to this toxin in most of the time. This is why we attempted to check the response of p53-249ser and control subclones after AFB<sub>1</sub> treatment *in vitro*. After the exposure of our clones to AFB<sub>1</sub>, we detected aflatoxin-DNA adducts using a specific antibody (6A10). We expected that p53-249ser transfected cells would behave differently upon exposure to AFB<sub>1</sub>, when compared to wt-p53-expressing cells. However, we did not observe a significant difference in AFB<sub>1</sub>-DNA adduct formation in the R249S clones and the controls (Figure 4.2.7).

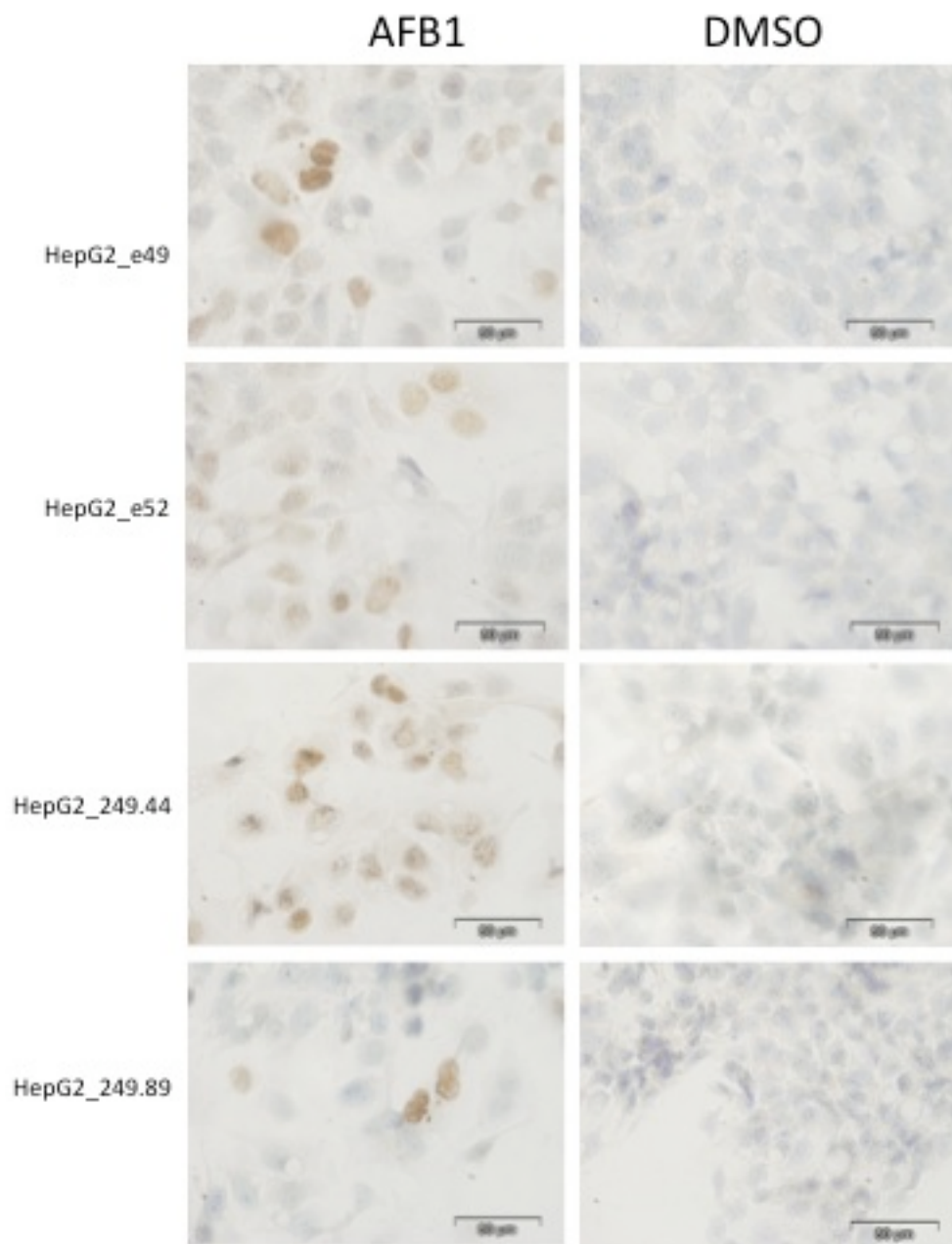


**FIGURE 4.2.7** Aflatoxin induced AFB<sub>1</sub>-DNA adduct detection. Selected subclones for R249S p53 and wild-type p53 were plated on 24-well plates and treated with either 3 $\mu$ M AFB<sub>1</sub> or DMSO (>1:1000) for



24 hours and then subjected to immunoperoxidase detection protocol with the specific antibody against imidazole ring opened form of AFB1-FAPY adducts. Counterstaining was performed with hematoxyline. Representative pictures from each condition were taken and compared with each other. Scale bar 50 $\mu$ m.

Lastly, we treated the clones with 1 $\mu$ M ADR and AFB1 separately for 24h and then incubated with complete medium for 24h and checked for senescence markers such as p53, p21, p15, p16, p27 and also MDM2; an important negative regulator of p53 by immunoblotting (Figure 4.2.8 A and B). Although the protein levels of p53, p21, p15, p16, p27 and MDM2 did not vary much between the p53-249ser and control clones, the response of cells was very different with the ADR and AFB1 treatment. To our surprise, AFB1 treatment did not change the p53 and p21 accumulation; protein levels were significantly lower than the level observed with the ADR treatment (Figure 4.2.8A). MDM2, p15, p16 and p27 protein expression also did not change upon AFB1 treatment, even though we observed a high increase in p15, slight increase in p16, no change in p27 and a diminish in MDM2 protein levels with a correlation with the p53 increase after ADR treatment (Figure 4.2.8 B).

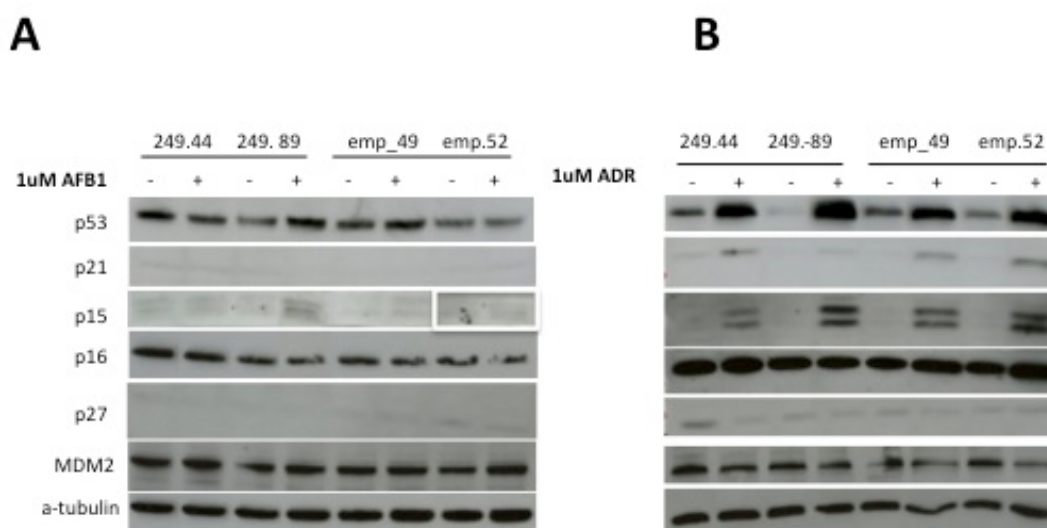


**FIGURE 4.2.8** Comparison of response after AFB<sub>1</sub> (A) and ADR (B) treatment in R249S p53 and wt p53 subclones. Cells treated with either 1 $\mu$ M AFB<sub>1</sub> or DMSO and 1 $\mu$ M ADR for 24 hours and then additional 24 hours without treatment and subjected to immunoblotting with the antibodies against p53, p21, p15, p16, p27 and MDM2.  $\alpha$ -tubulin was used as loading control.

#### 4.2.4 Global histone methylation marker status check

##### 4.2.4.1 Histone methylation marker status in R249S p53 bearing clones

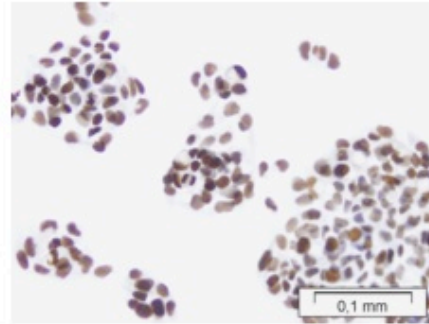
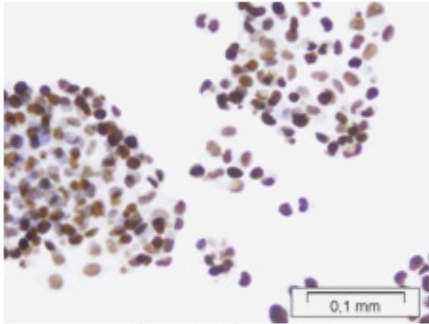
Our results on the survival advantage of genetic modulation of R249S over wild type p53 were not very significant and promising. So we speculated if R249S might be selective due to epigenetic modulation-derived mechanisms. Based on our observation indicating the expression difference of epigenetic related gene groups between senescent and immortal Huh7 clones, epigenetic regulation can play an important role in cell fate determination (Bagislar et al, unpublished data). Hence, we hypothesized that R249S p53 might change the global histone modification markers by itself, thus contribute to carcinogenesis. Therefore we immunostained the p53-249ser and control subclones with polyclonal antibodies against H3K4me3, H3K9me3, H3K27me3, H3K27me1, H3K36me3, H3K36me1, H3R17me2, H4K20me3, H4R3me2.

We tested 6 p53-249ser and 4 control subclones. We obtained positive signal for all the residues tested for both p53 background. In 6 249ser subclones, H3K27me3, H3K36me3, H4K20me3, H3R17me2 and H3K9me3 were observed to be heterogeneously stained and staining was stronger compared to the 4 control subclones, yet the difference was slight in H3K9me3 (Figure 4.2.9 D, F, I, B and H). We did not observe a marked alteration in this comparative study on H3K4me3, H3K27me1, H3K36me1 and H4R3me2 residues, all showing strong heterogenous nuclear staining (Figure 4.2.9 A, C, E, and J).

## A H3K4me3

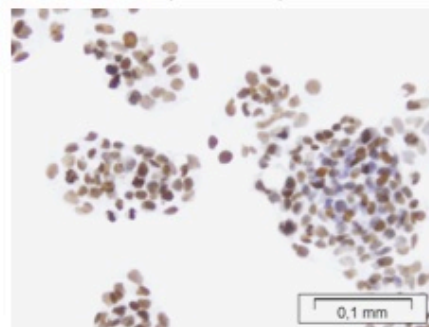
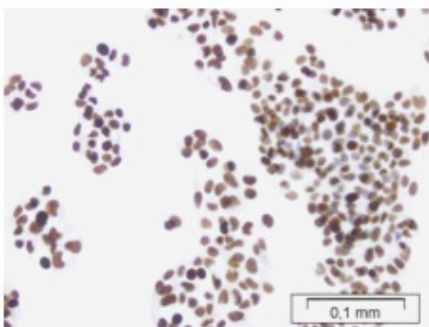
HepG2 249.44

HepG2 emp.49



HepG2 249.89

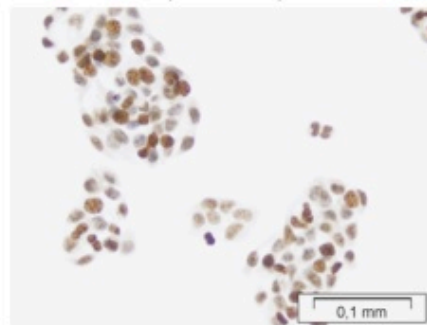
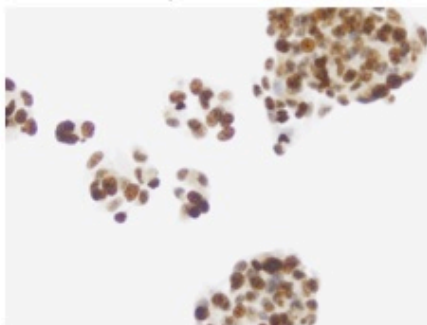
HepG2 emp.52



## B H3K9me3

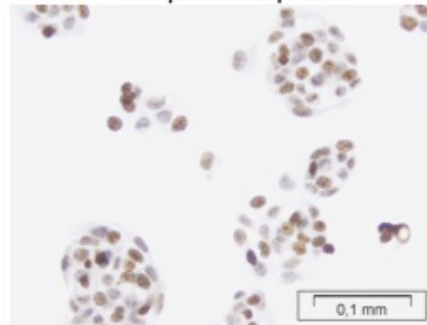
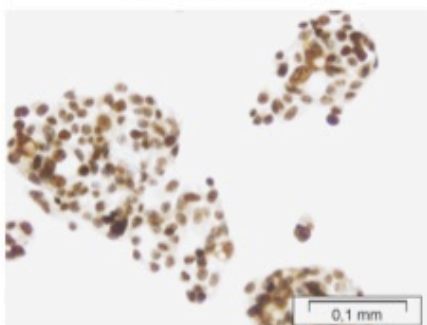
HepG2 249.44

HepG2 emp.49



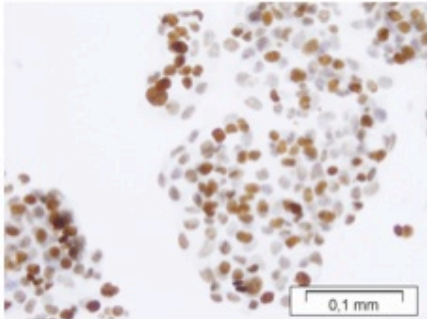
HepG2 249.89

HepG2 emp.52

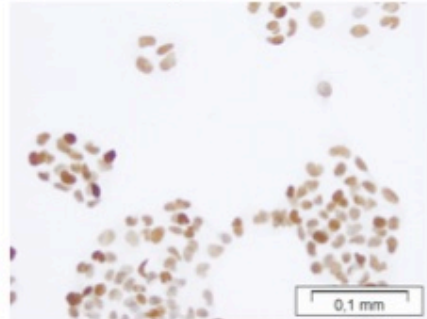


**C** H3K27me1

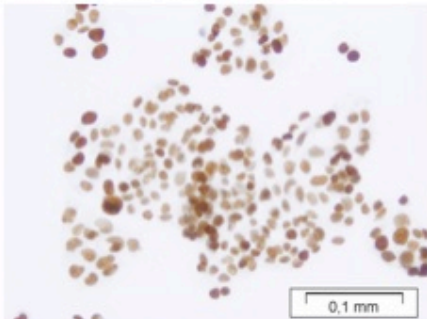
HepG2 249.44



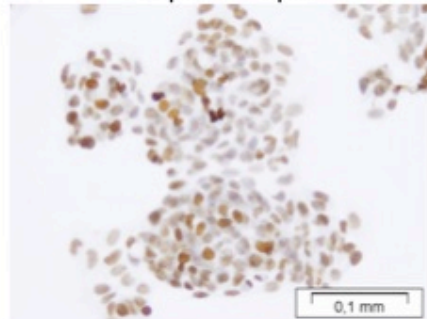
HepG2 emp.49



HepG2 249.89

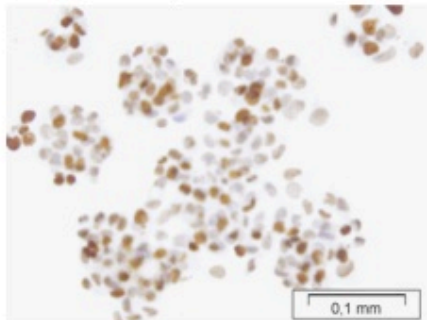


HepG2 emp.52

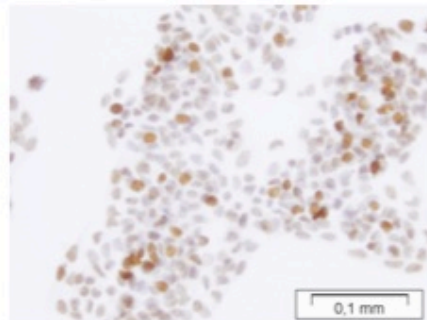


**D** H3K27me3

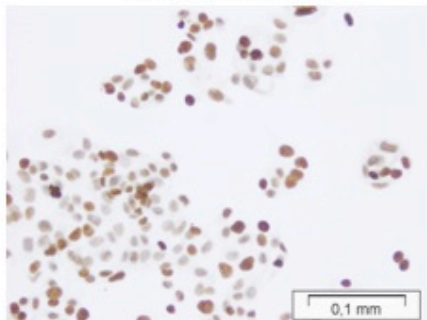
HepG2 249.44



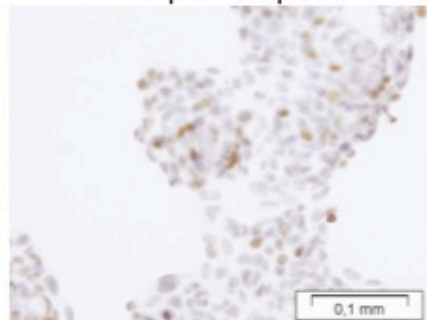
HepG2 emp.49



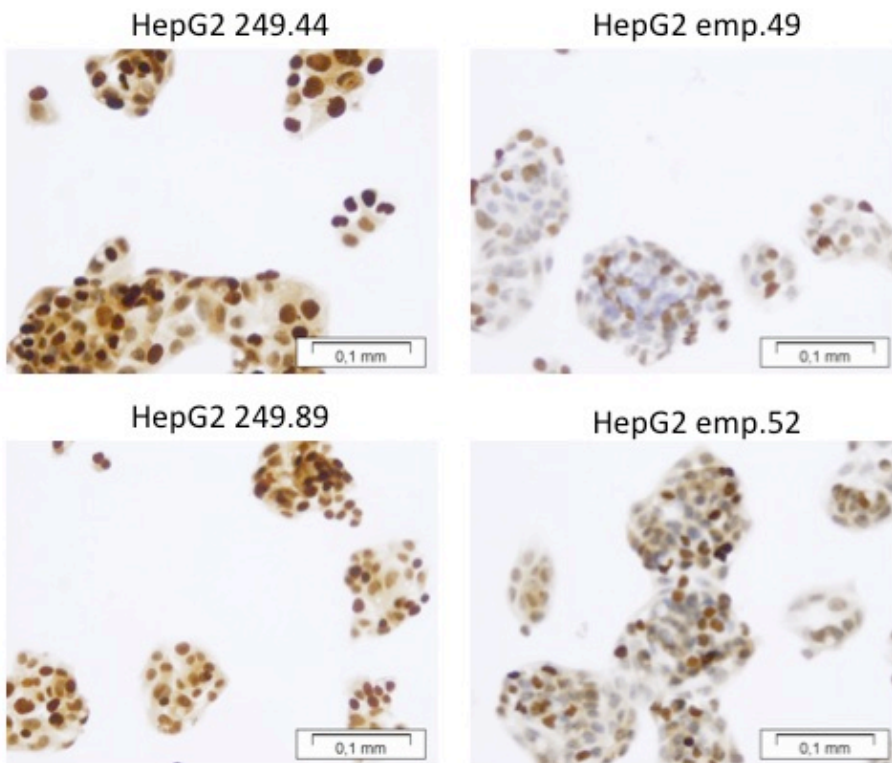
HepG2 249.89



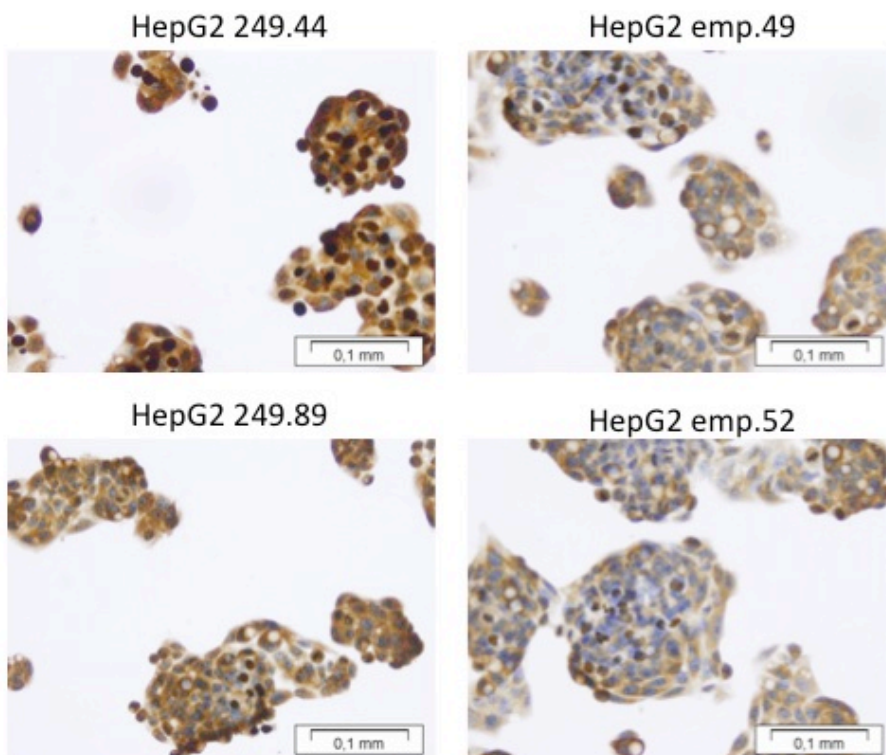
HepG2 emp.52



**E** H3K36me1

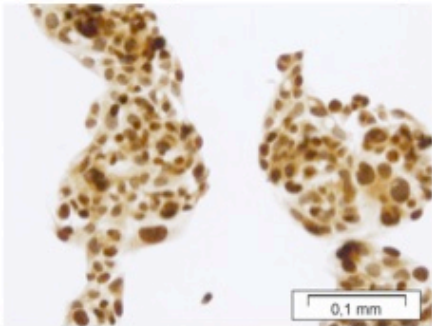


**F** H3K36me3

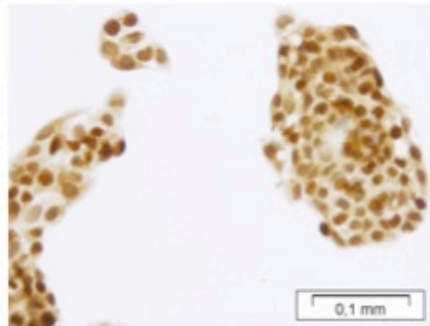


## G H3R2me2

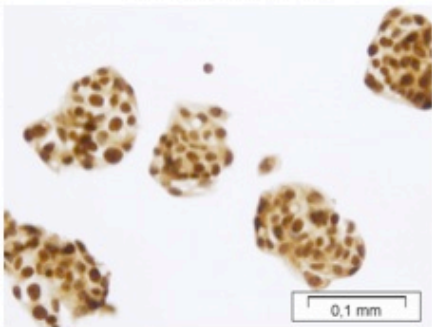
HepG2 249.44



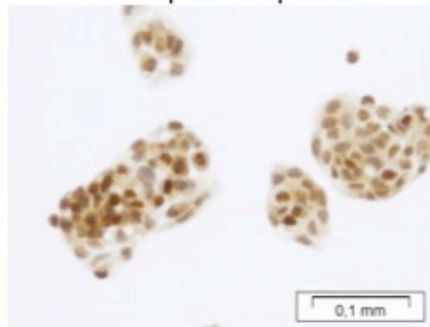
HepG2 emp.49



HepG2 249.89

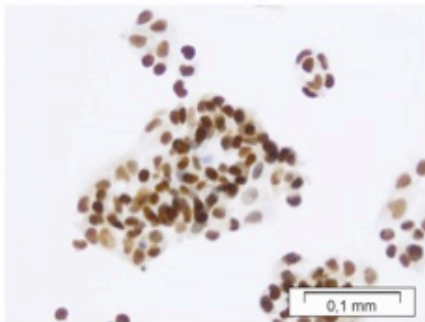


HepG2 emp.52

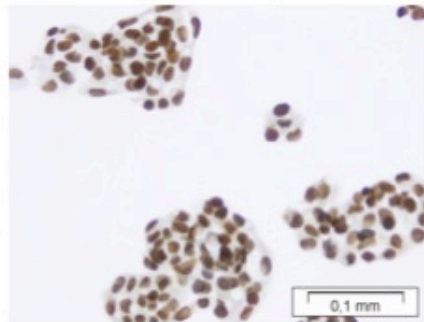


## H H3R17me2

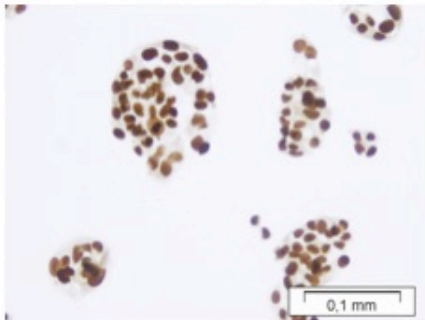
HepG2 249.44



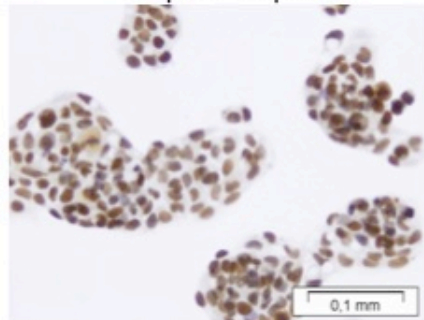
HepG2 emp.49



HepG2 249.89



HepG2 emp.52



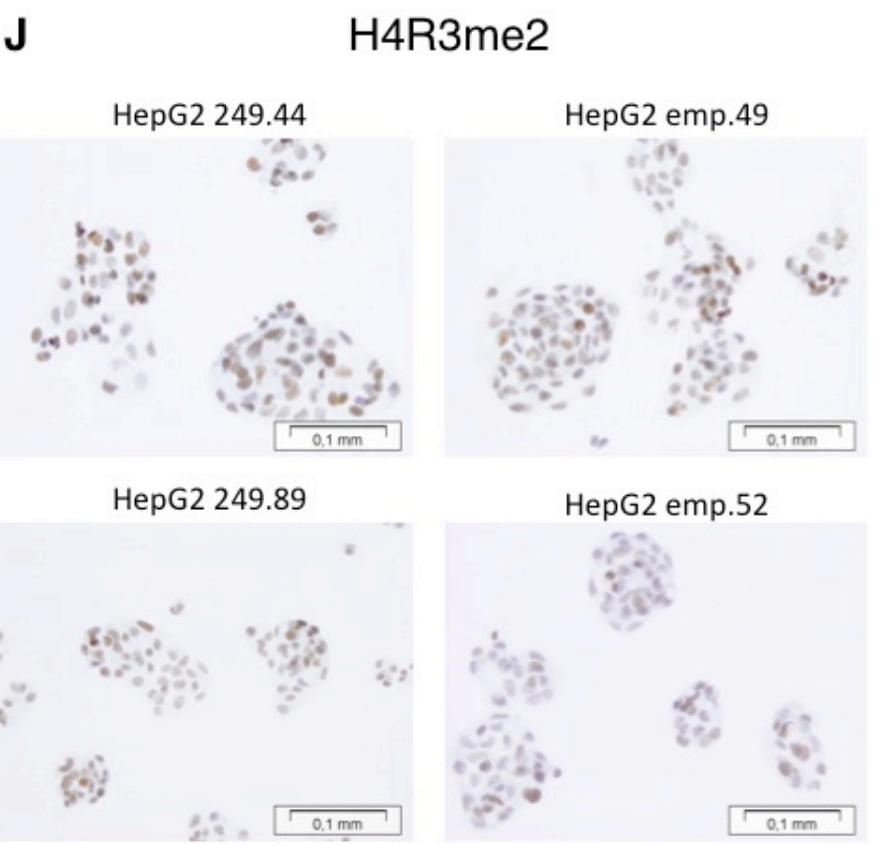
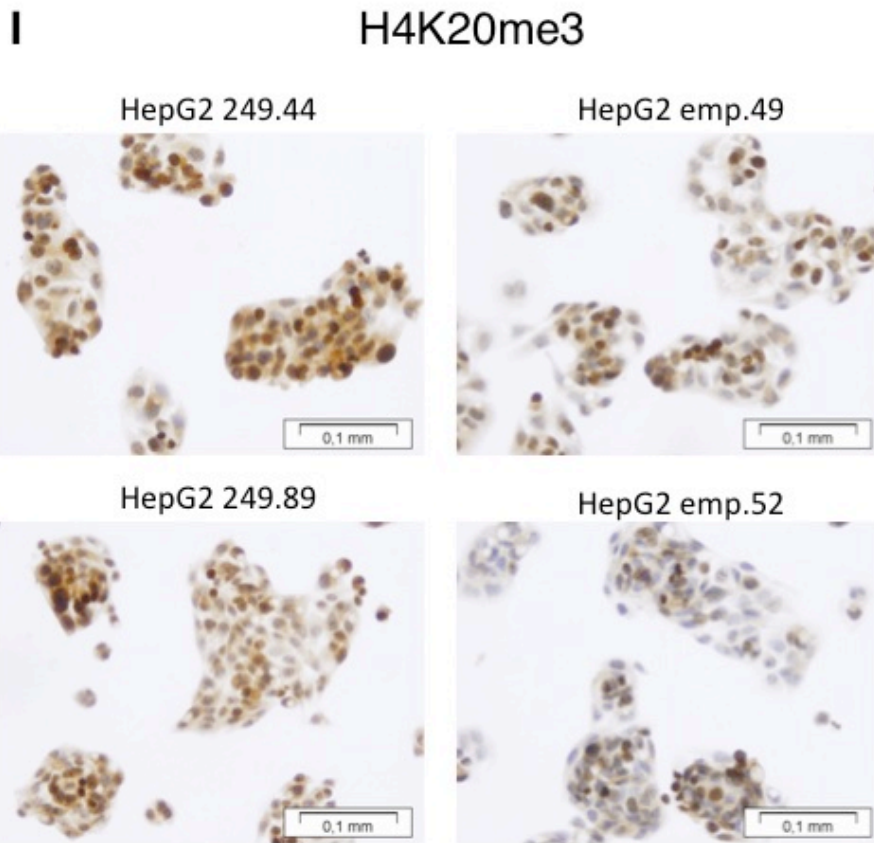


**FIGURE 4.2.9** Global histone methylation marker status check (**A-J**). Selected subclones for R249S p53 and wild-type p53 were plated on 24-well plates and subjected to immunostaining with the specific

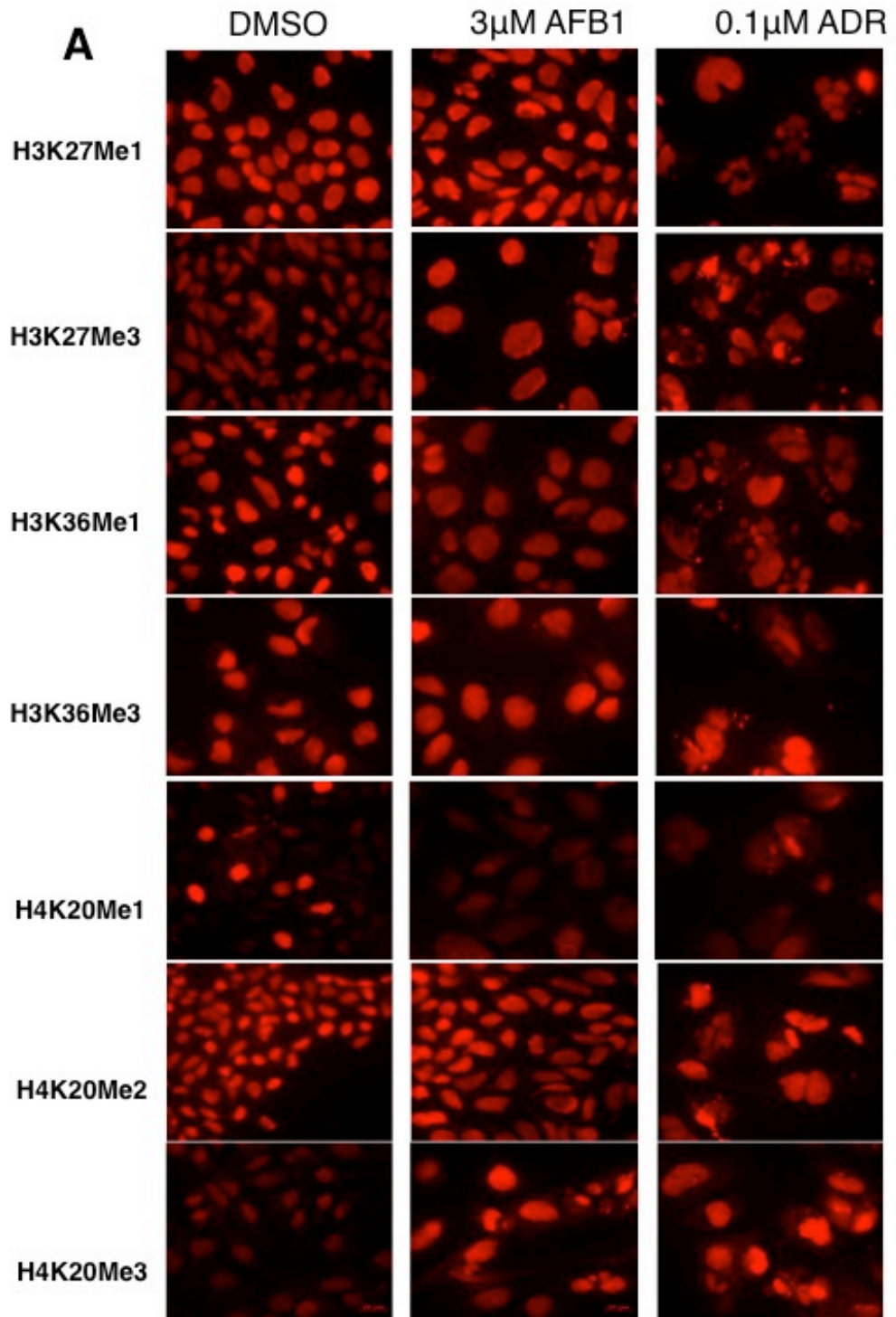
antibodies against H3K4me3, H3K9me3, H3K27me3, H3K27me1, H3K36me3, H3K36me1, H3R17me2, H4K20me3 and H4R3me2. Counterstaining was performed with hematoxyline. Representative pictures from each condition were taken and compared with each other. Scale bar 100 $\mu$ m.

#### 4.2.4.2 Histone methylation marker status check in HCC upon Adriamycin and AFB1 treatment

Our previous studies indicated the increase of H3K27me1, H3K36me3, and H4K20me3 in pre and late senescent Huh7 clones compared to the immortal Huh7 clone and H3K27me3 and H3R2me2 residues indicated a gradual increase with late senescence (Bagislar et. al. unpublished data). Therefore, employing another senescence model based on adriamycin-induced mitotic catastrophe [275], (Gursoy-Yuzugullu et al, unpublished data) we checked the H3K27me1, H3K27me3, H3K36me1, H3K36me2, H3K36me3, H4K20me1, H4K20me2, H4K20me3 residues by indirect immunofluorescence staining. Huh7 cells treated with 0.1 $\mu$ M low dose (LD) ADR and 3 $\mu$ M AFB1 for 72 hours were subjected to staining protocol.

We included AFB1 treatment in the set of experiments for two reasons: the first one is to explore the effect of AFB1 exposure on histone methylation marker status, due to the fact that we previously observed a change in the level of these residues in 249ser p53 bearing clones (Figure 4.2.9), the second one is to find out which modulations in those histone methylation marks were due to DNA damage in common.





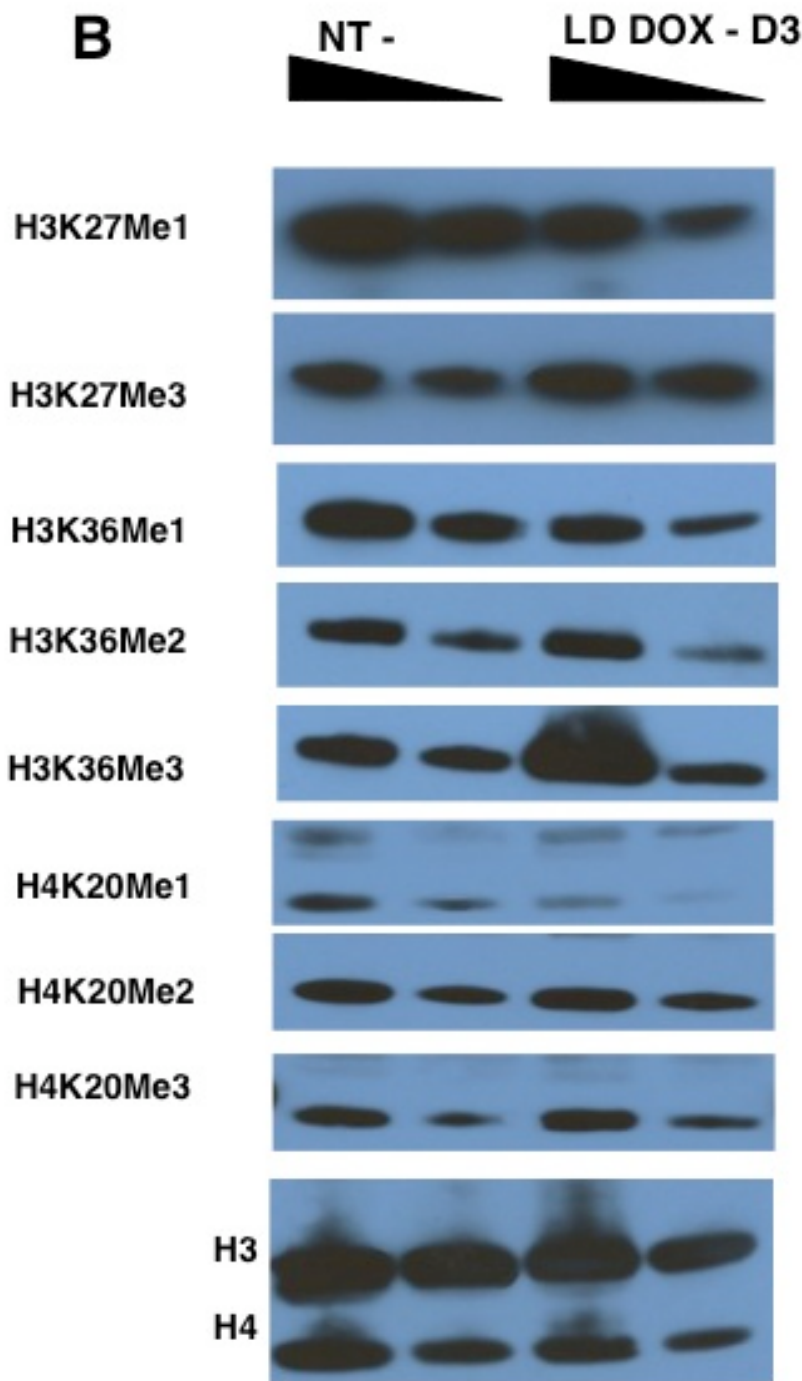


**FIGURE 4.2.10** Global histone methylation marker status check upon DNA damage induction (**A-B**). Huh7 cells were treated with 3 $\mu$ M AFB<sub>1</sub> or DMSO and 0.1 $\mu$ M ADR (low dose) for 72 hours and subjected to immunofluorescence staining with the specific antibodies against H3K27me1, H3K27me3, H3K36me1, H3K36me3, H4K20me1, H4K20me2, and H4K20me3. Representative pictures from each condition were taken and compared with each other (**A**). Huh7 cells treated with 0.1 $\mu$ M ADR (low dose) for 72 hours are subjected to western blotting with the specific antibodies against H3K27me1, H3K27me3, H3K36me1, H3K36me3, H3K36me2, H4K20me1, H4K20me2, and H4K20me3 (**B**). H3 and H4 were used as loading controls.

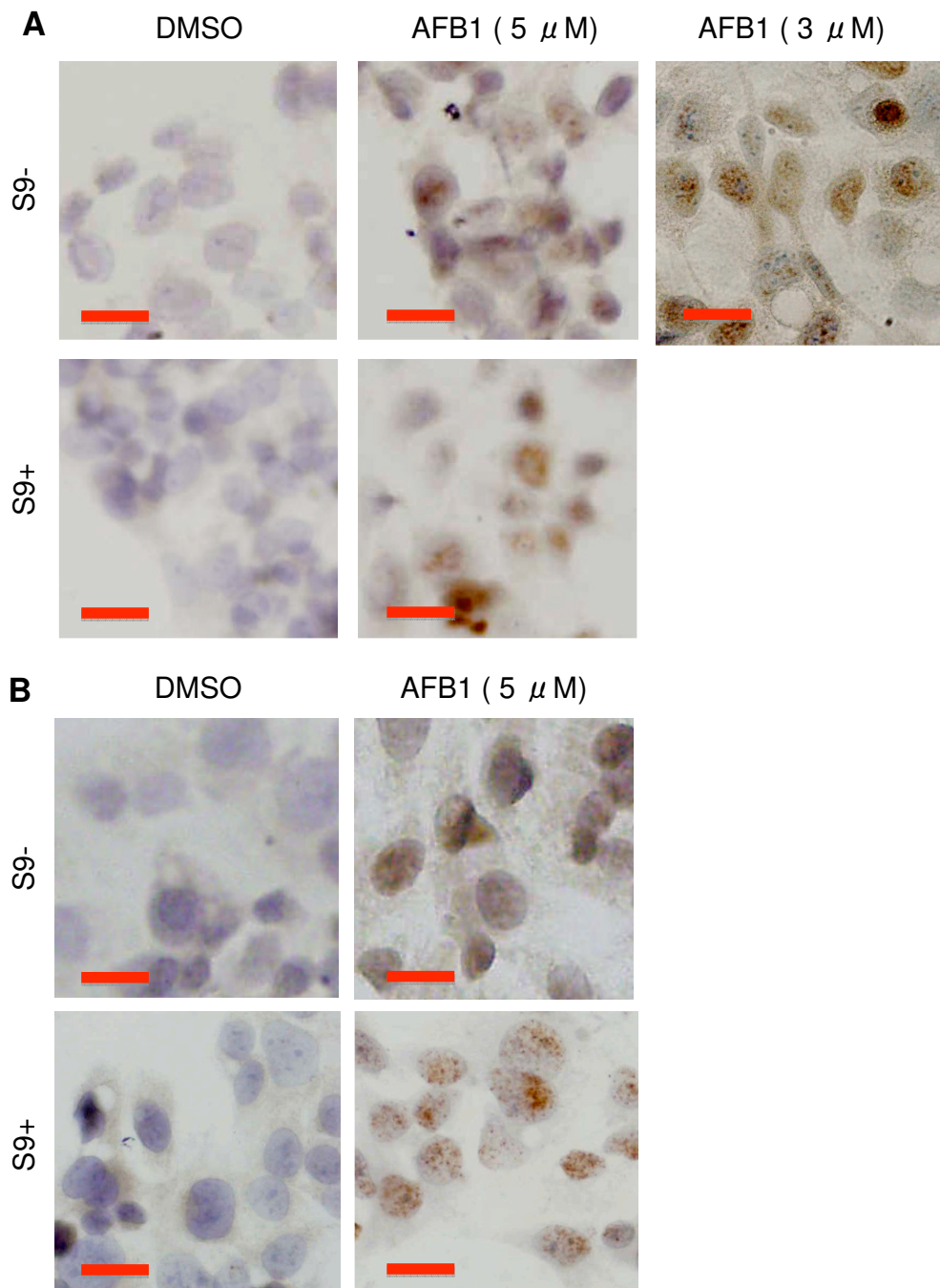
As a result, we observed an increase in H3K27Me3, H3K36Me3 and H4K20Me3 levels and a corresponding decrease in monomethyl forms of these histones, H3K27Me1, H3K36Me1 and H4K20Me1 and no change in dimethyl forms H3K36me2 and H4K20me2 after low dose ADR treatment in Huh7 cells also confirmed by western blotting data (Figure 4.2.10 B). AFB1 treatment also modulated the histone residues H3K27Me3, H3K36Me3, H4K20Me3, monomethyl forms H3K36Me1, H4K20Me1 and dimethyl forms H3K36me2 and H4K20me2 in a same manner as with ADR (Figure 4.2.10 A). These results not only confirmed the alteration in histone methylation phenotype observed in Huh7 senescent and immortal clones, but also pointed out the association with DNA damage response and global changes in histone methylation.

### 4.3 Effects of AFB1-induced genotoxicity in HCC

The predominant adduct Aflatoxin B1 (AFB1)-N7-guanine is formed after the reaction of AFB1-8,9-exo-epoxide with guanine residues in DNA and leads to the formation of more stable imidazole ring-opened AFB1-formamidopyrimidine (AFB1-FAPY) DNA adduct [219]. Since the pseudo-half-life for the loss of AFB1-FAPY is longer, adducts are stable, they remain to be detectable for several weeks in rat liver [218, 222]. Additionally, AFB1 contributes to the oxidative DNA damage, leading to 8-hydroxydeoxyguanosine (8-OHdG) lesions in rat hepatic DNA [223, 225]. Therefore, we first explored AFB1 induced genotoxic effects. Before selecting the dosage range of AFB1, we considered the estimated chronic aflatoxin exposure levels in humans (0.01-0.3 µg/kg/day) [218] and the hepatocarcinogenic doses (0.015-1ppm) in rats [277]. 30 min of exposure to 1.6 µM AFB1 was enough for the induction of p53 R249S mutations in HepG2 cells [278] and 0.2-5 µM doses were sufficient to induce mutations in mouse fibroblasts [279]. Careful consideration of these findings prompted us to use an AFB1 dose range of 3-5µM in our experiments. The dose range we used in this study was at the upper limits of *in vitro* mutagenic activity in mammalian cells.

#### 4.3.1 AFB1 induced DNA adducts and 8-OHdG lesions in hepatocyte-like cells

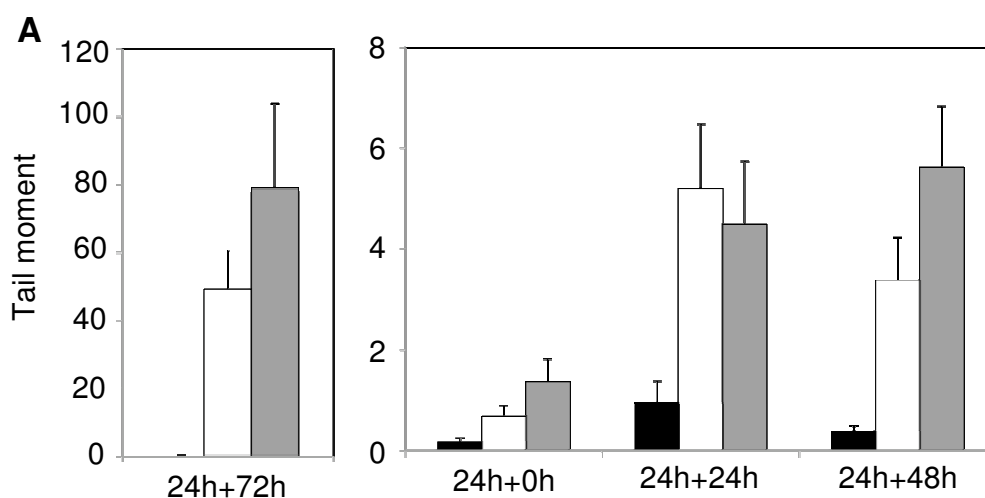
Since we did not observe any difference between the p53-249ser and control clones after AFB1 treatment, we decided to conduct our experiments with hepatocyte-like wild-type p53-expressing parental HepG2 cell line and explore the effects of AFB1 on HCC. Cells were treated with 3-5 µM of AFB1 in the absence or the presence of S9-activating system that allows the activation of AFB1 into AFB1-8,9 epoxide [258]. Following 24 hours of exposure, cells were subjected to immunoperoxidase assays to detect AFB1-FAPY DNA adducts and 8-OHdG DNA lesions. Our results highlighted the presence of AFB1-FAPY adducts in the nuclei of most cells with 3 or 5 µM AFB1 (Fig. 4.3.1A). Adduct detection levels were quite similar between these two doses, indicating that AFB1 was capable of inducing highly abundant DNA adducts when tested at micromolar levels. We observed also the detection of 8-OHdG-positive nuclear foci (Fig. 4.3.1B). Essentially the same results were obtained in the presence or in the absence of S9-activating system in this cell line (Fig.4.3.1).



**Figure 4.3.1** Induction of DNA adducts and 8-hydroxy-deoxyguanosine lesions following aflatoxin B1 (AFB<sub>1</sub>) exposure. HepG2 cells were exposed to AFB<sub>1</sub> or DMSO for 24 hours, in the presence (S9+) or in the absence of S9-activating system (S9-), and then subjected to indirect immunoperoxidase assays using anti AFB<sub>1</sub>-FAPY (**A**) and anti-8OH-dG (**B**) antibodies. Counterstain was performed by using hematoxylin. Scale bar = 20 μm.

### 4.3.2 AFB1 exposure induces single and double strand breaks

Cells were exposed to AFB1 (5  $\mu\text{M}$ ) or ADR (0.5  $\mu\text{M}$ ) as a positive control for 24 hours, and then cultivated in the absence of test chemicals up to 72 hours. Genotoxic effects of AFB1 were studied by alkaline and neutral comet assays that detect single and double strand DNA breaks, respectively [262, 263]. Both AFB1- and ADR-exposed cells, tested by alkaline comet assay at 72 hours post-exposure time displayed statistically significant increase in comet tail moments ( $P < 0.0001$ ), indicating the presence of abundant single strand DNA breaks (Fig. 4.3.2A-left, B). Neutral comet assay also detected statistically significant ( $P < 0.0001$ ) increase in tail moments with both chemicals that lasted at least 48 hours after the removal of chemicals from the cell culture medium (Fig. 4.3.2A-right; C). Tail moments obtained with neutral comet were nearly ten-fold less than those obtained with alkaline comet. Thus, AFB1 induced much more single strand breaks than double strand breaks.



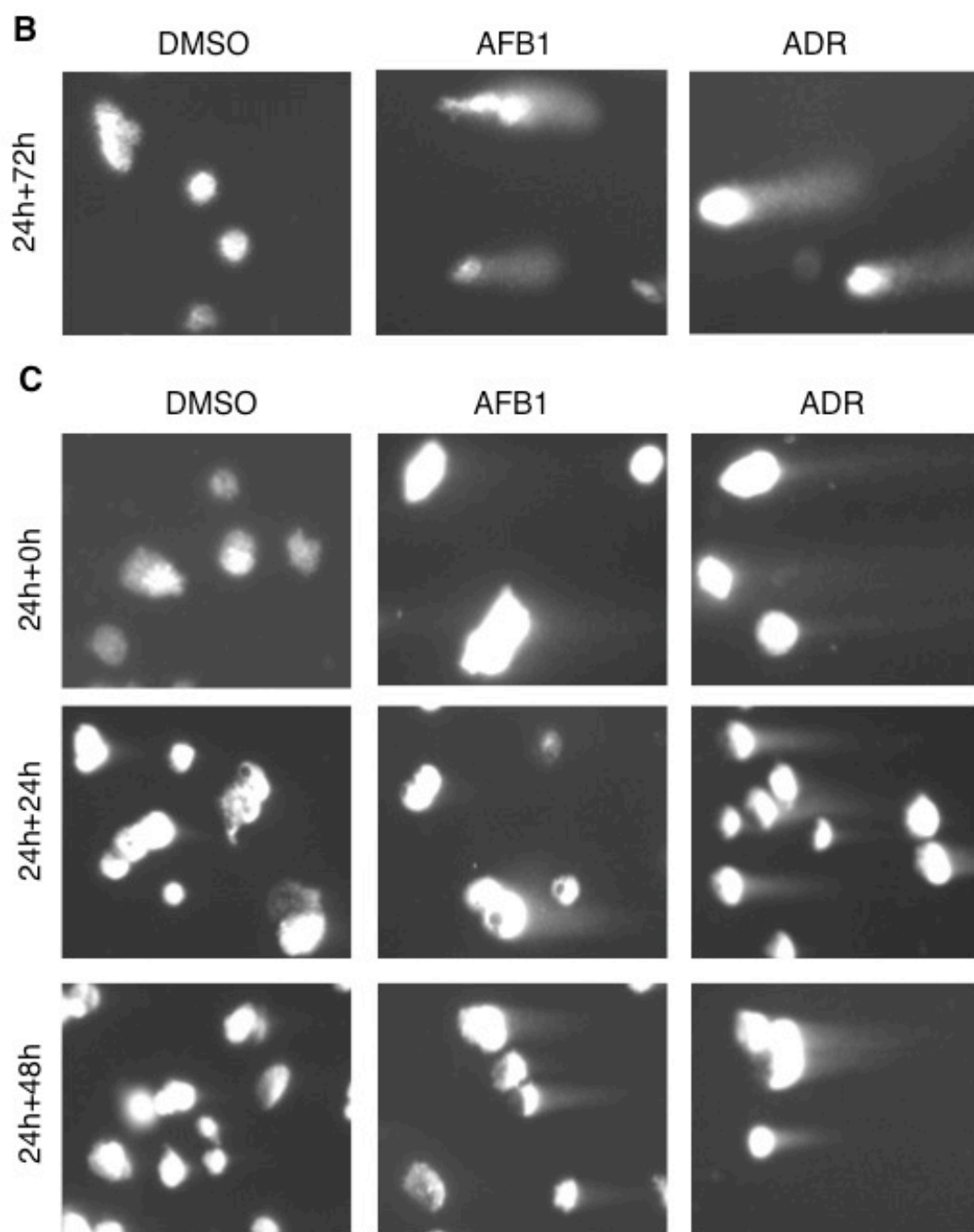
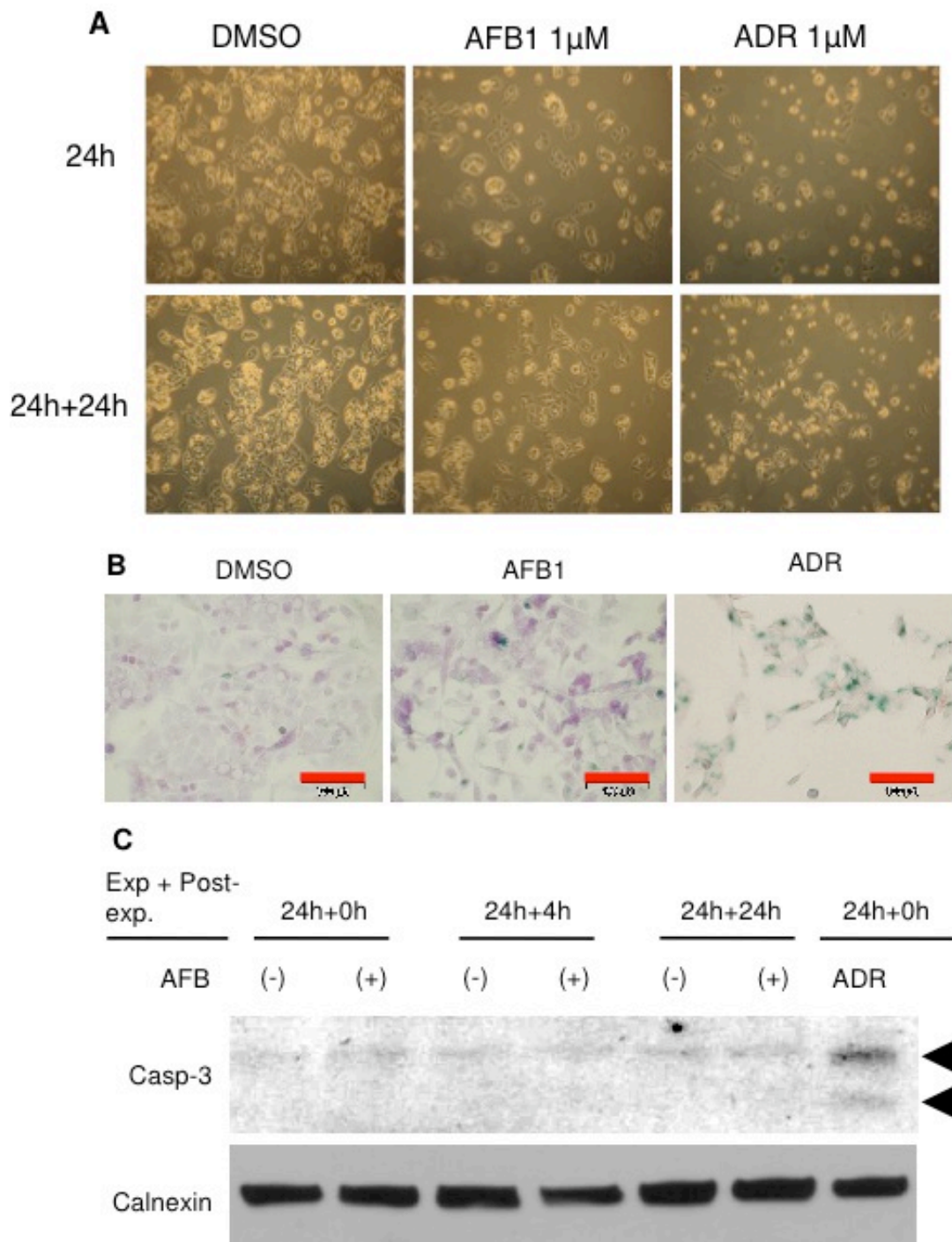


**Figure 4.3.2** Induction of persistent single and double strand DNA breaks after AFB1 treatment. **(A)** HepG2 cells were exposed to DMSO, 5 $\mu$ M AFB1 or 0.5 $\mu$ M ADR as a positive control, for 24 hours, followed by a culture in the absence of test chemicals for up to 72 hours, and subjected to alkaline comet **(A-left)** or neutral comet **(A-right)** assays to detect single and double strand breaks respectively. Black, white and gray columns indicate cells exposed to DMSO, AFB, and ADR, respectively. Error bars indicate SD. AFB1- and ADR-treated cells displayed significantly increased tail moments in all time-points tested ( $P < 0.0001$ ). **(B)** Representative pictures showing comet figures after 5 $\mu$ M AFB1, as compared to ADR exposure. HepG2 cells were treated with chemicals for 24 hours, and then cultivated in the absence of chemical for additional times up to 72 hours. Cells were then subjected to single cell electrophoresis under alkaline **(B)** or neutral **(C)** pH to detect nuclei with single strand and double strand DNA breaks, respectively.

### 4.3.3 AFB1-induced genotoxicity did not affect cell growth and colony survival

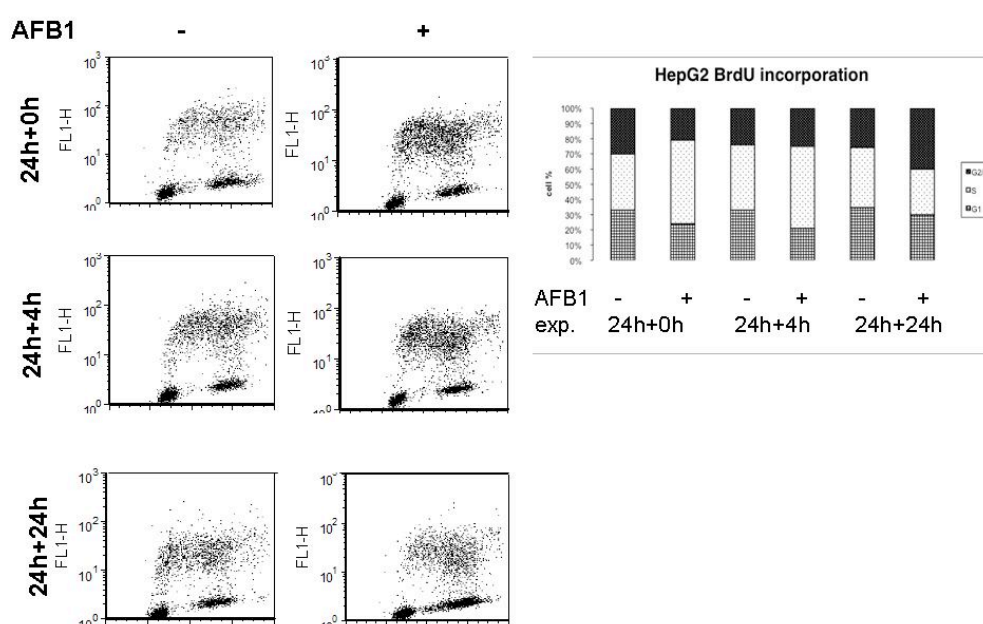
Next, we studied the cellular response to AFB1-induced genotoxicity by cell growth, senescence and apoptosis assays. Three days of exposure to AFB1 (3  $\mu\text{M}$ ) did not induce senescence and had no visible effect on cell growth (Fig. 4.3.3 A-B). AFB1 (5  $\mu\text{M}$ ) was also ineffective for apoptosis induction (Fig. 4.3.3 C). In contrast, a low dose of ADR (0.1  $\mu\text{mol/L}$ ), inhibited cell growth and induced a senescence-associated  $\beta$ -galactosidase (SABG)-positive senescence response (Fig. 4.3.3 B), whereas a high dose (1  $\mu\text{M}$ ) induced activated-procaspase-positive apoptosis response, as evidenced by western blot analysis (Fig. 4.3.3 A and C).



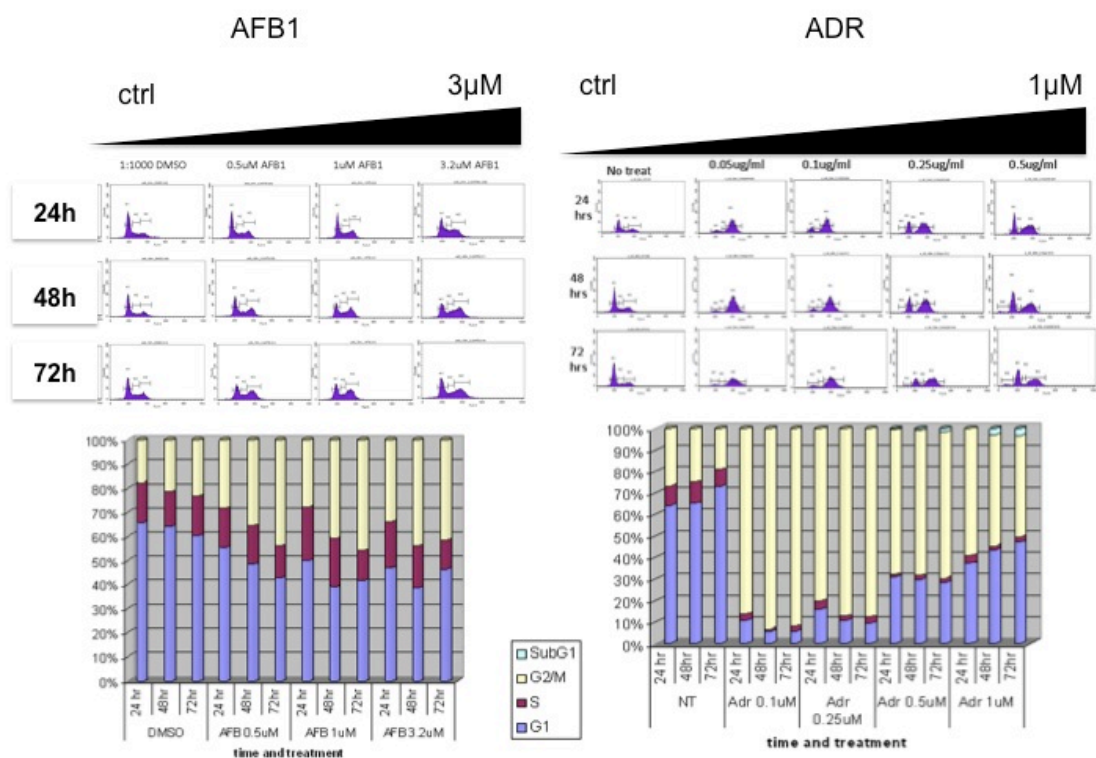


**Figure 4.3.3** Aflatoxin treatment does not induce senescence or apoptosis. HepG2 cells were exposed to 1  $\mu$ M AFB1, or 1 $\mu$ M ADR for 24h and incubated with complete medium for an additional 24 hour period and visualized under light microscope (A). HepG2 cells treated with 3 $\mu$ M AFB1 and 0.1 $\mu$ M ADR were subjected to SABG assay to detect senescent cells (blue). Fast red was used as a counterstain. Scale bar = 100  $\mu$ m (B). HepG2 cells were exposed to 5 $\mu$ M AFB1, or 1 $\mu$ M ADR and then were subjected to Western blot assay to detect apoptosis by active caspase 3. Calnexin was used as a loading control (C).

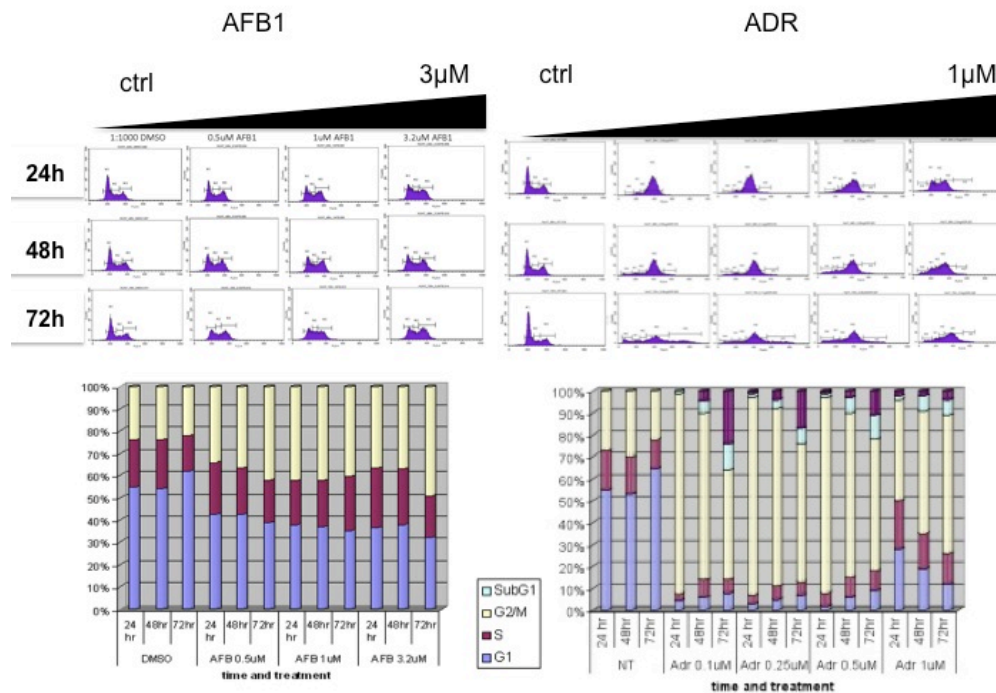
Thus, HepG2 cells were not responsive to AFB1 DNA damage by undergoing a permanent growth arrest such as senescence or apoptosis, but they were partially arrested in the G2/M phase of the cell cycle after 72h of AFB1 exposure (Figure 4.3.4 and 4.3.5- Left) while with ADR exposure, cells respond with either a complete G2/M arrest or apoptosis (Figure 4.3.5-Right). Short term BrdU incorporation rate after AFB1 treatment was not diminished as well, correlating with an incomplete G2/M arrest since the DNA synthesis was continuous (Figure 4.3.4). This partial arrest was not cell context dependent; we observed the same phenomenon with Huh7 (Y220C p53 Mutation) (Figure 4.3.6) and Hep3B (Null p53) (Figure 4.3.7). Since p53 was not playing a key role in the response of cells to AFB1 induced DNA damage, we checked G2/M checkpoint key elements such as *cdc25A*, Wee1 kinase and 14-3-3 [246] (Figure 4.3.8). We observed the nuclear localization of phospho-*cdc25A* (Figure 4.3.8-top), which is inactive when phosphorylated, and 14-3-3 $\sigma$  (Figure 4.3.8-middle), in both AFB1 and ADR exposed cells with weak signal in Wee1 (Figure 4.3.8-bottom), under AFB1 exposure.



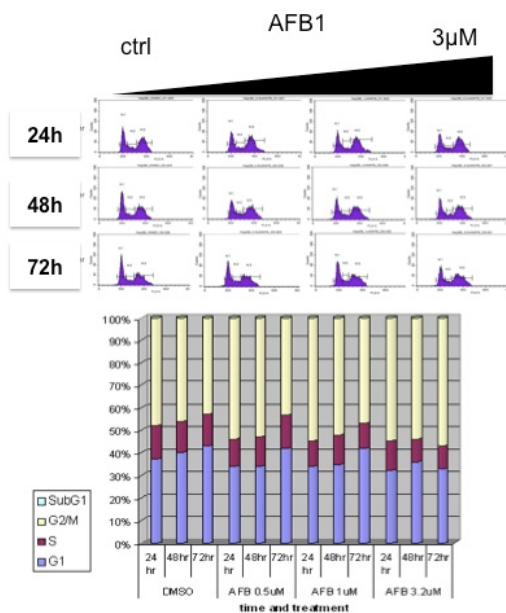
**Figure 4.3.4** Lack of permanent cell cycle arrest in response to AFB1-induced DNA damage. HepG2 cells were treated with AFB1 (5  $\mu$ M) or DMSO (in the presence of S9-activating system) for 24 hours, followed by additional cell culture in the absence of this chemical for another 4h and 24 hours. Cell cycle analysis was performed by flow cytometry after labeling of cells with BrdU and propidium iodide at indicated post-exposure times. On the left, representative flow cytometry plots of AFB-treated (+) and DMSO-treated (-) cells and on the right distribution of cells at G1, S and G2/M phases at different time points after exposure to AFB1 (+) or DMSO (-) is shown.



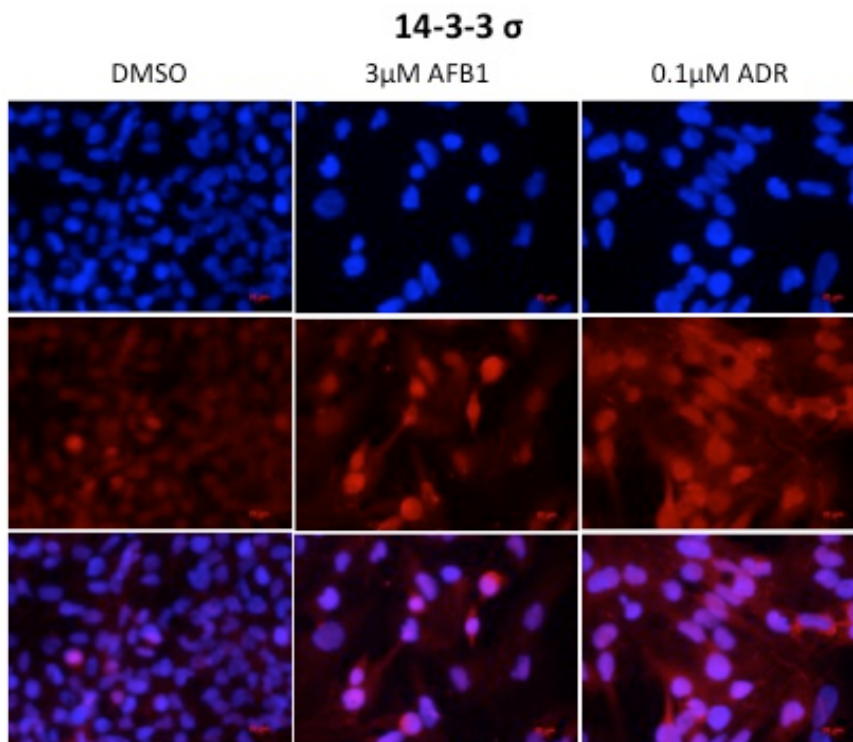
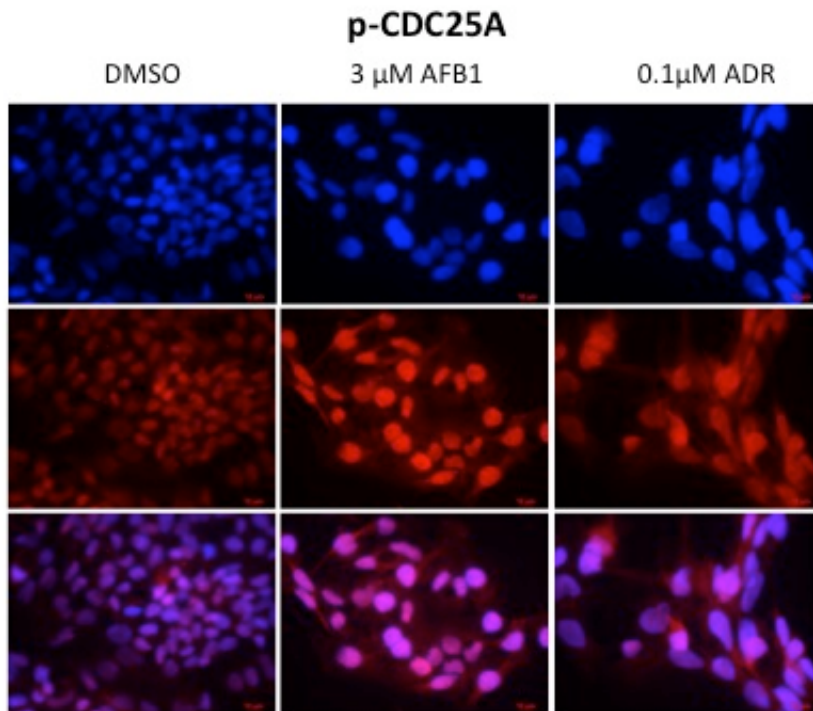
**Figure 4.3.5** Cell cycle analysis of HepG2 cells after Aflatoxin and Adriamycin treatment. HepG2 cells were treated with 0-3 $\mu$ M doses of AFB1 and 0-1 $\mu$ M ADR for 24h, 48h and 72h and cell cycle analysis were performed with Propidium Iodide. Graphs represent the cell cycle distribution of each corresponding condition above the graph. Blue, red, yellow and green bars represent cells in G1, S, G2/M and subG1 phase.



**Figure 4.3.6** Cell cycle analysis of Huh7 cells after Aflatoxin and Adriamycin treatment. Huh7 cells were treated with 0-3 $\mu$ M doses of AFB1 and 0-1 $\mu$ M ADR for 24h, 48h and 72h and cell cycle analysis were performed with Propidium Iodide. Graphs represent the cell cycle distribution of each corresponding condition above the graph. Blue, red, yellow, green and purple bars represent cells in G1, S, G2/M, subG1 and polyploidy phase.



**Figure 4.3.7** Cell cycle analysis of Hep3B cells after Aflatoxin treatment. Hep3B cells were treated with 0-3 $\mu$ M doses of AFB1 for 24h, 48h and 72h and cell cycle analysis were performed with Propidium Iodide. Graphs represent the cell cycle distribution of each corresponding condition above the graph. Blue, red, yellow and green bars represent cells in G1, S, G2/M and subG1 phase



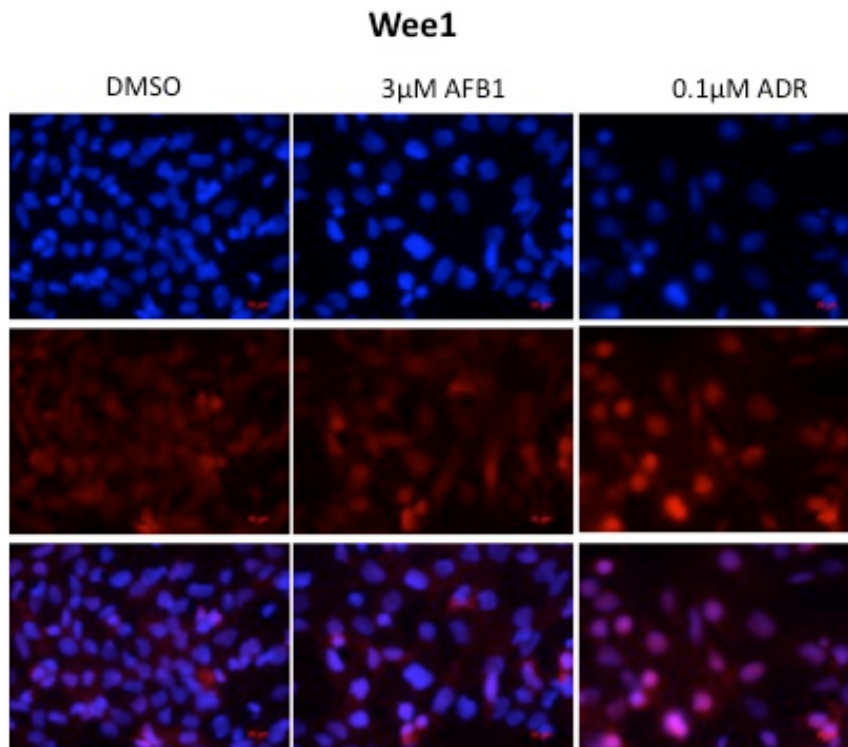


**Figure 4.3.8** Cell cycle checkpoint key players localize into nucleus. HepG2 cells were treated with 3 $\mu$ M of AFB1 and 0.1 $\mu$ M ADR for 72h and then subjected to immunofluorescence staining with the specific antibodies against phospho-cdc25A, 14-3-3 $\sigma$  and Wee1. DAPI is used for nuclear staining. Scale bar: 10 $\mu$ m.

To verify that the effects of G2/M arrest were partial and not permanent, cell survival was determined by assessing colony growth in 100 mm dishes after exposure to AFB1 or ADR. HepG2 cells were seeded in 6-well plates and semi-confluent cells were exposed to AFB1 (0, 1, 3, 5, 10, and 50  $\mu$ M) in the presence of S9-activation system. Control cells were treated with ADR (0, 0.1, 0.3, 0.5, 1, and 5  $\mu$ M). Following 4 hours and 24 hours exposure,  $10^4$  cells were seeded into 100 mm dishes, and colonies were counted 10 days later. Cell survival was calculated as the % ratio of cell numbers in treated versus untreated cells. Survival parameters were determined by plotting survival data on a semilog plot. Aflatoxin B1 did not affect colony survival after 4 hours or 24 hours of treatment, when tested at doses  $\leq 5 \mu$ M. Under similar conditions, ADR displayed strong and time-dependent inhibition of colony survival being active with 50 times less concentrated molar doses (Fig. 4.3.9). Detectable effects of AFB1 were observed only when cells were exposed for 24 hours at very

high doses reaching 50  $\mu\text{M}$  (Fig. 4.3.9, insets). Indeed, the AFB1 was more than 150-fold less cytotoxic than ADR in HepG2 cells (Fig. 4.3.2A).

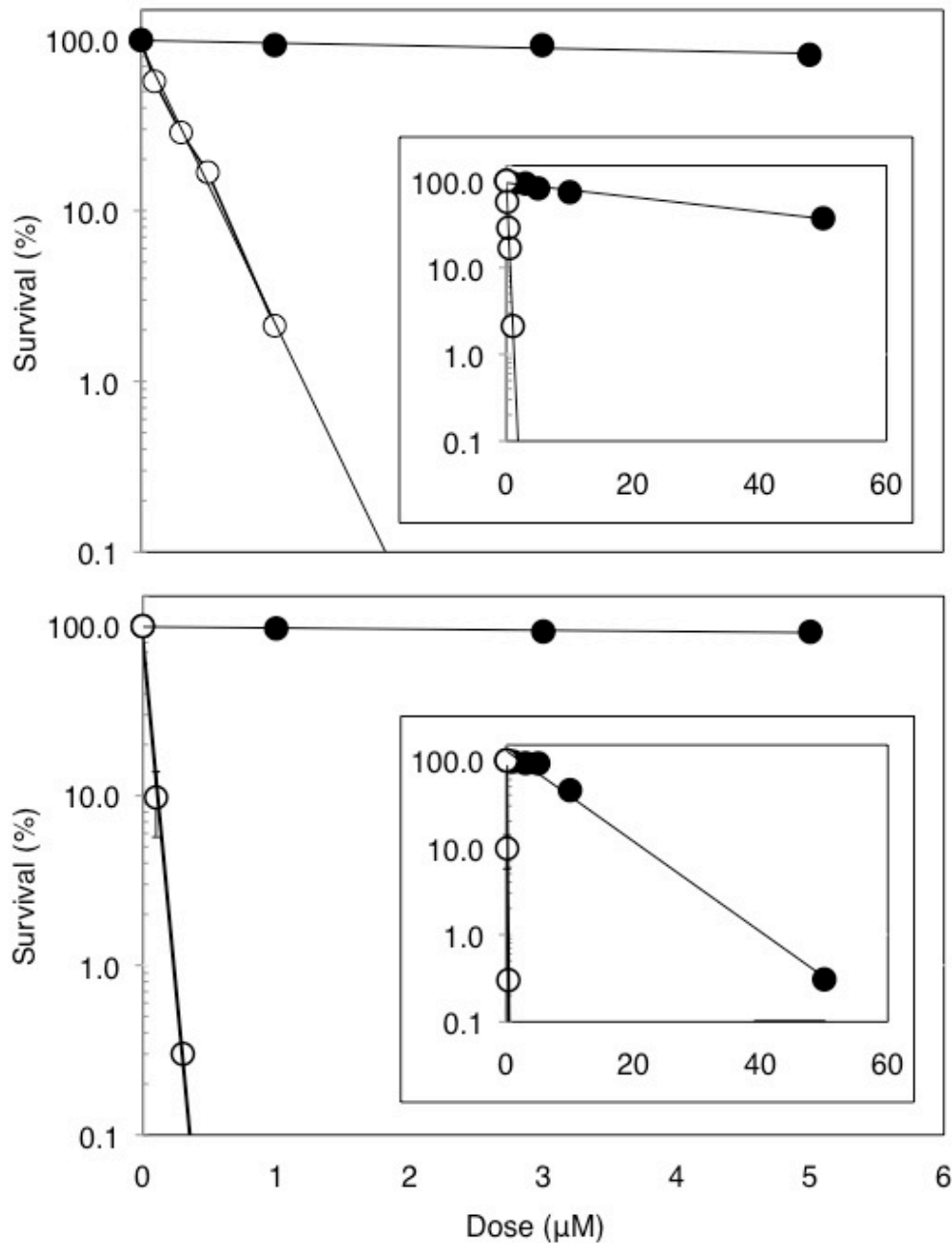


**Figure 4.3.9** The effects of AFB1 (closed circles), or ADR (open circles) treatment of HepG2 cells for 4 hours (top) or 24 hours (bottom) on cell survival-colony forming ability. Cell survival was calculated as the % ratio of cell numbers in treated versus untreated cells ( $n=3$ ). Survival parameters were determined by plotting survival data on a semilog plot. Insets: cell survival at higher AFB1 (up to 50  $\mu\text{M}$ ) and ADR (up to 5  $\mu\text{M}$ ) doses. Error bars: SD. HepG2 cells were seeded in 6-well plates and semi-confluent cells were exposed to aflatoxin (0, 1, 3, 5, 10, and 50  $\mu\text{M}$ ), or adriamycin (0, 0.1, 0.3, 0.5, 1,

and 5  $\mu\text{M}$ ) for 4 hours, or 24 hours. Following exposure,  $10^4$  cells were seeded into 100 mm dishes, and colonies were counted 10 days later.

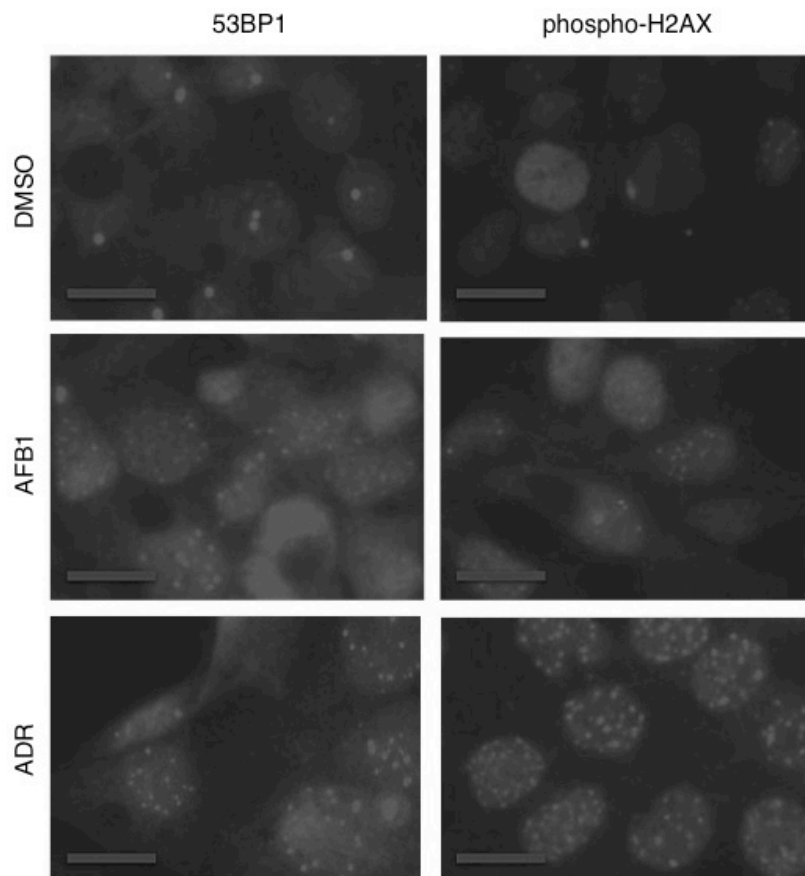
#### 4.4 AFB1-induced DNA damage response in HCC

DNA damage response to AFB1 is poorly known. AFB1-N7-Gua and AFB1-FAPY adducts appear to be removed primarily by NER in mammalian cells, but other repair systems have also been implicated in bacteria and yeast [228]. The mechanisms of DNA damage checkpoint response to AFB1 remain totally unknown. Here, we explored DNA damage checkpoint response of wild-type p53 human cells to AFB1 exposure. Our findings indicate that the checkpoint response to genotoxic and mutagenic doses of AFB1 is incomplete, being unable to activate p53 and to induce cell cycle arrest or apoptosis.

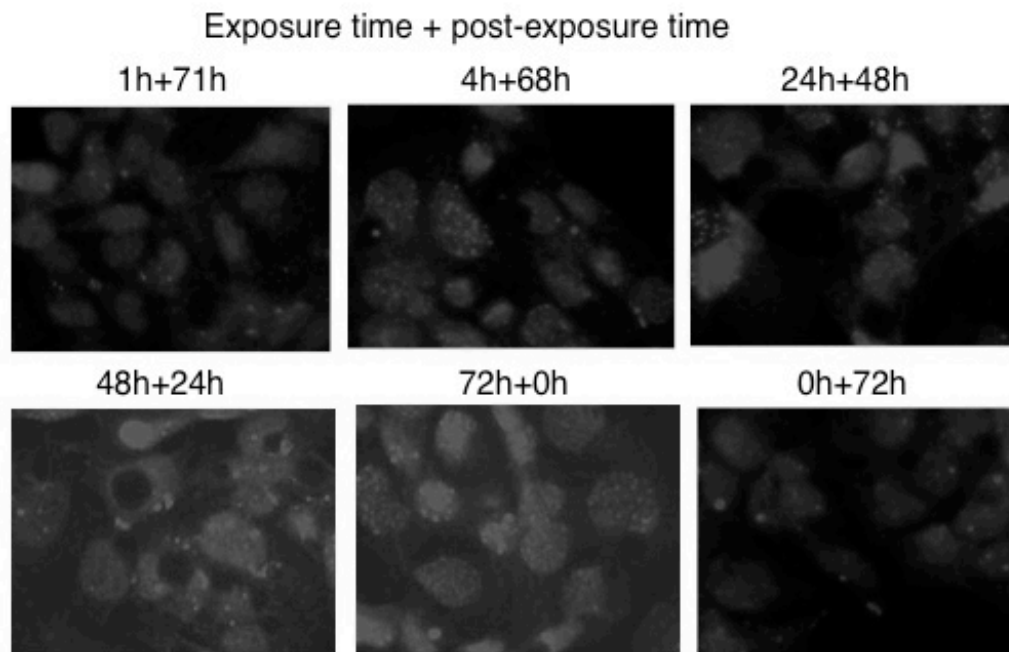
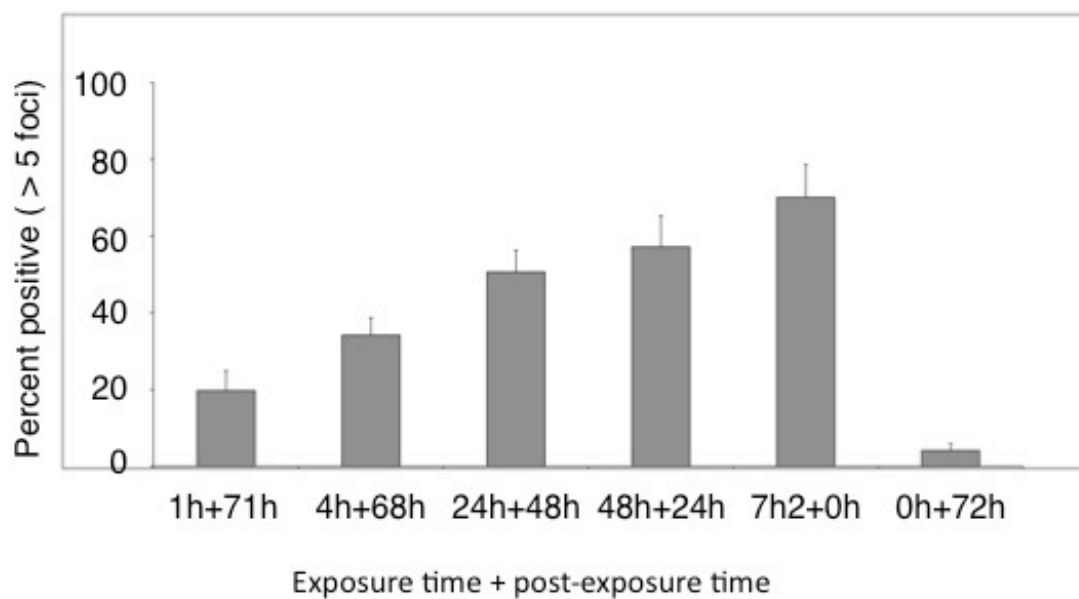
##### 4.4.1 Increased DNA damage checkpoint foci in aflatoxin B1-exposed cells

The lack of a significant effect of AFB1 on cell growth, despite the induction of persistent single and double strand breaks prompted us to test whether the AFB1 can induce a DNA damage response signaling activity. We used 53BP1 and phospho-H2AX foci assays [246] by immunofluorescence following 3 days of exposure to either AFB1 (3  $\mu\text{M}$ ) or ADR (0.1  $\mu\text{M}$ ). Both agents induced 53BP1 and phospho-H2AX foci that were detectable after three days of culture (Fig. 4.4.1), as an indication of double-strand DNA break response [246, 247]. The statistical significance of these observations was tested by counting percent number of cells with 53BP1- positive foci ( $>5$  foci/cell). Cells exposed to AFB1 (3  $\mu\text{M}$ ) between 1 hours and 72 hours showed progressive and statistically significant ( $P<0.0001$ ) accumulation of 53BP1 foci, when tested at 72 hours of cell culture.





**Figure 4.4.1** Induction of 53BP1 and phospho-H2AX foci following aflatoxin B1 exposure. HepG2 cells were treated with AFB1 (3  $\mu$ M) for three days and then subjected to 53BP1 and phospho-H2AX foci detection by indirect immunofluorescence. Control cells were exposed to DMSO only. ADR (0.1  $\mu$ M) was used as a positive control. Scale bar = 20  $\mu$ m.

**A****B**

**Figure 4.4.2** Time-dependent increase in 53BP1 foci-positive cells under aflatoxin B1 exposure. HepG2 cells were treated with AFB1 (3  $\mu$ M) between 1 hour and 72 hours, and then cultivated in the absence of chemical for additional times up to 72 hours. Percent cells with 53BP1 foci (>5 foci) were calculated by manual counting following detection of 53BP1 foci by indirect immunoassay.

(A) Representative examples of 53BP1 immunofluorescence data.

(B). Comparative analysis of AFB1 -treated cells. Error bars indicate SD. The increase in 53BP1 foci positive cells was significant in all time points tested, when compared to DMSO-treated cells ( $P < 0.0001$ ).

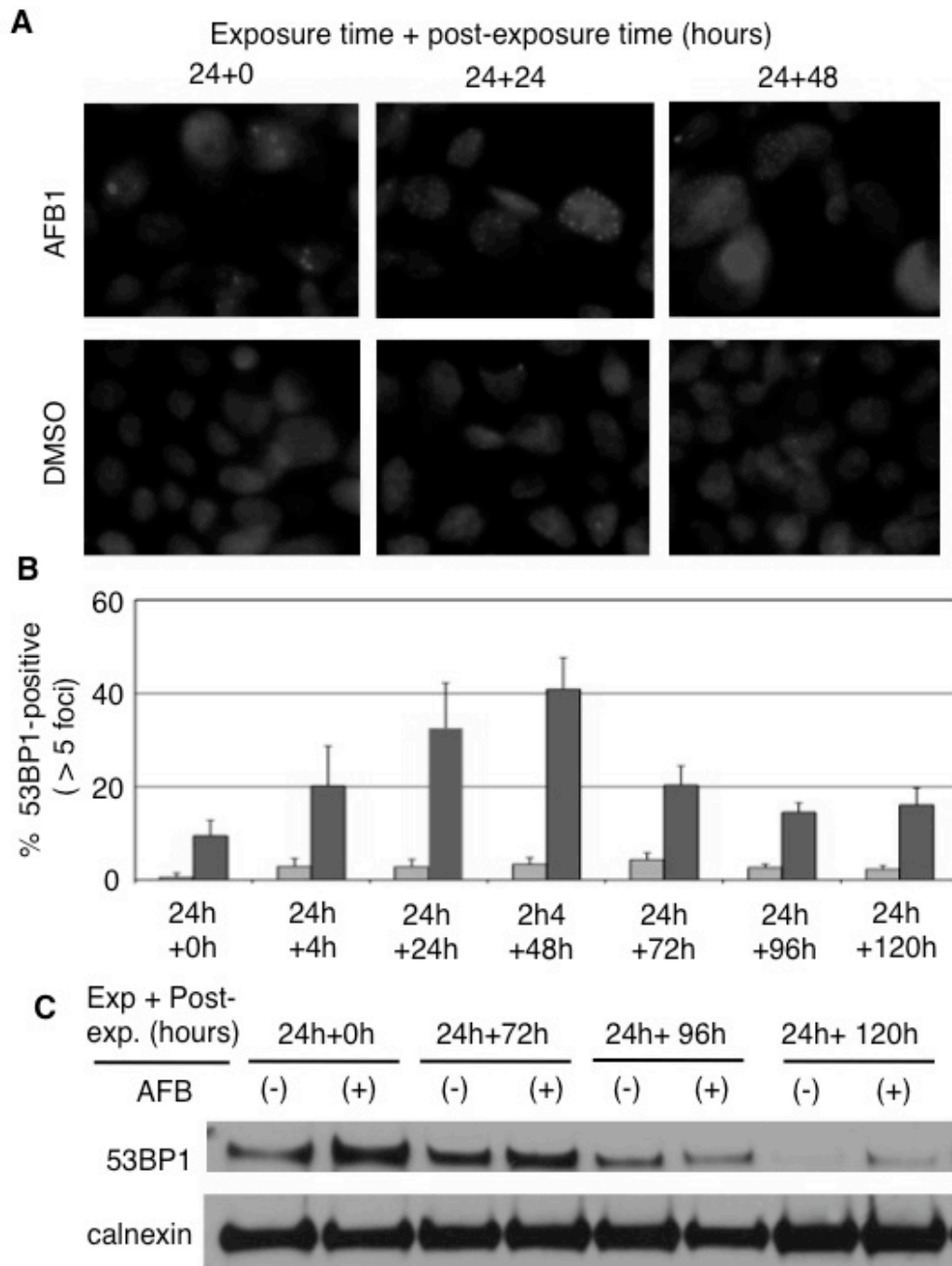


**Figure 4.4.3** The duration of 53BP1 foci after 24 hours of exposure to AFB1. HepG2 cells were treated with AFB1 (5  $\mu$ mol/L) for 24 hours, and then cultivated in the absence of chemical for additional times up to 120 hours. DMSO was used as a negative control. Percent cells with 53BP1 foci (>5 foci) were calculated by manual counting following detection of 53BP1 foci by indirect immunoassay. (A) Representative examples of 53BP1 immunofluorescence data. (B) Comparative analysis of AFB1- and DMSO-treated cells. Error bars indicate SD. The increase in 53BP1 foci positive cells was significant in all time points tested, when compared to DMSO-treated cells ( $P < 0.0001$ ). (C) The accumulation of total 53BP1 protein levels were tested by Western immunoblotting at indicated times. Calnexin was used as a loading control.

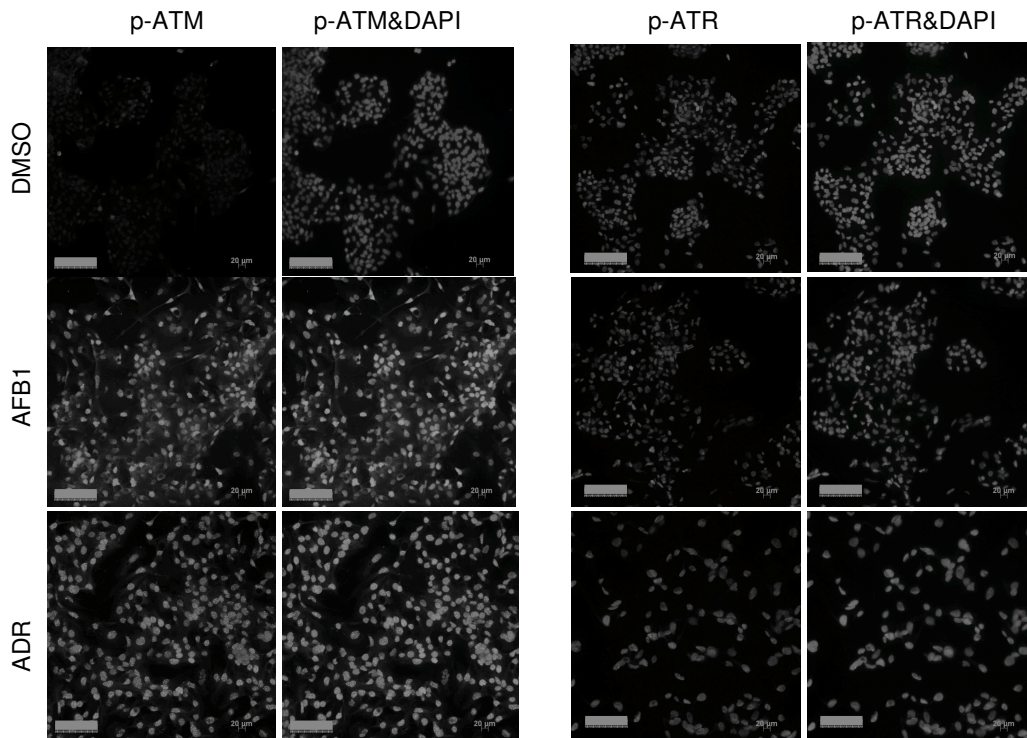


**Figure 4.4.4** Activation of ATM, but not ATR after aflatoxin B1 exposure. HepG2 cells were exposed to AFB1 (3  $\mu\text{mol/L}$ ) or ADR (0.1  $\mu\text{mol/L}$ ), and tested for phosphorylated forms of ATM and ATR (red) three days later, by indirect immunofluorescence assay. DAPI (blue) was used for DNA visualization. p-ATM, phospho-ATM. Scale bar = 100  $\mu\text{m}$ .

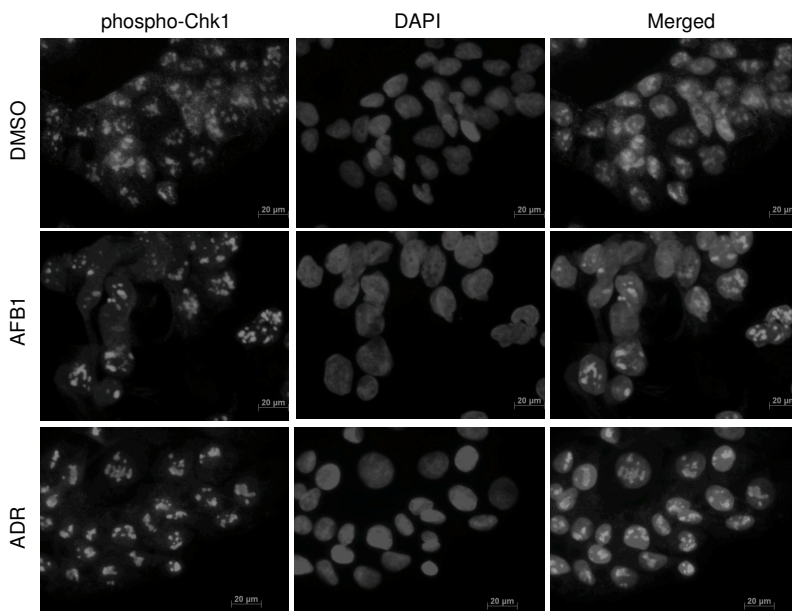


**Figure 4.4.5** Nuclear phospho-Chk1 expression was not affected after exposure AFB1 or ADR. HepG2 cells were exposed to AFB1 (3  $\mu\text{M}$ ) or ADR (0.1  $\mu\text{M}$ ), and tested for phospho-Chk1 three days later, by indirect immunofluorescence assay (red). Counterstain was with DAPI (blue). Scale bar = 20  $\mu\text{m}$ .

We observed a linear increase in the percent ratio of 53BP1 foci- positive cells from 20% to more than 60% between 1 hour and 72 hours of exposure (Figure 4.4.2). To test the duration of 53BP1 foci and phospho-H2AX foci following a fixed time of exposure to AFB1 (5  $\mu$ M), cells were first treated with AFB1 for 24 hours, and then cultivated in the absence of chemical treatment up to 120 hours. Cells with positive 53BP1 foci was detected by indirect immunofluorescence assay (Fig. 4.4.3 A and B), and then counted. The accumulation of foci peaked at 48 hours of post-treatment with 40% positive cells. A residual foci activity with 15-20% positive cells was detectable for at least 120 hours in cells, which are no longer exposed to AFB1, confirmed by western blotting as well (Figure 4.4.3C). In contrast, cells exposed to DMSO only displayed low level foci activity (<5%) throughout the experiment indicating that increased foci formation was due to AFB1 exposure (Figure 4.4.3). Based on the induction of 53BP1 and phospho-H2AX foci by both AFB1 and ADR, we tested the activation states of ATM and ATR response pathways [15], using immunofluorescence analysis of phospho-ATM and phospho-ATR proteins, respectively. HepG2 cells were analyzed after three days of exposure to AFB1 (3  $\mu$ M), ADR (0.1  $\mu$ M), or DMSO. As compared to cells treated with DMSO, both AFB1- and ADR-treated cells displayed increased nuclear signals for phospho-ATM, but there was no detectable change in the nuclear intensity of the phospho-ATR protein (Figure 4.4.4). We also tested phospho-Chk1 nuclear expression under the same experimental conditions. We observed punctuated nuclear staining by immunofluorescence assay with both control and treated cells, with no detectable difference between staining intensities (Figure 4.4.5). The other critical components of DNA damage signaling pathway were tested by immunoblotting using Adriamycin and hydroxyurea as positive controls in both HepG2 (Figure 4.4.6) and Huh7 (Figure 4.4.7) cell lines. Although, Adriamycin treatment triggered a characteristic double strand break response in HepG2 and Huh7 cells by induced phosphorylation of H2AX (Figure 4.4.6 and Figure 4.4.7), HepG2 cells also displayed phosphorylation of Chk2, p53ser15 and p53ser20 weakly (Figure 4.4.6). Hydroxyurea treatment resulted in a phosphorylation of Chk1 in HepG2 and no phosphorylation of Chk1 was observed in Huh7. Inevitably, the response pattern was various in terms of time and cell line. However, after AFB1 exposure the only strong response we observed was with the phosphorylation of H2AX, as the major determinant of DNA damage.

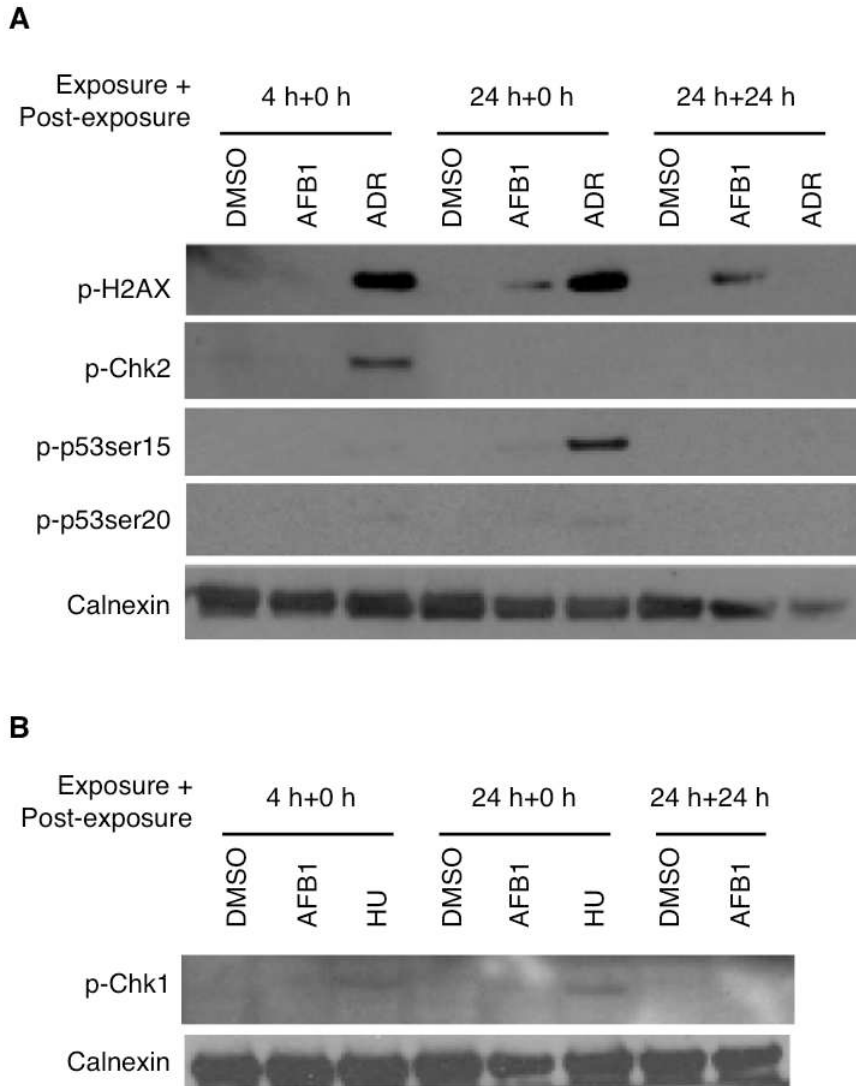


**Figure 4.4.6.** Incomplete DNA damage checkpoint response of HepG2 cells to AFB1. HepG2 cells were treated with DMSO or AFB1 (5  $\mu$ M) for four hours and 24 hours, and tested immediately (4h+0h and 24h+0h), or after 24 hours of incubation without treatment (24h+24h). HepG2 cells treated with 0.5  $\mu$ mol/L Adriamycin (ADR) or 5 mM hydroxyurea (HU) were used as positive controls for experiments shown in A and B, respectively. Total cell lysates were subjected to Western blot analysis. Calnexin was used as a loading control. p-H2AX, phospho-H2AX; p- p53ser15, phospho-p53ser15; p- p53ser20, phospho-p53ser20; p-Chk2, phospho-Chk2; p-Chk1, phospho-Chk1.

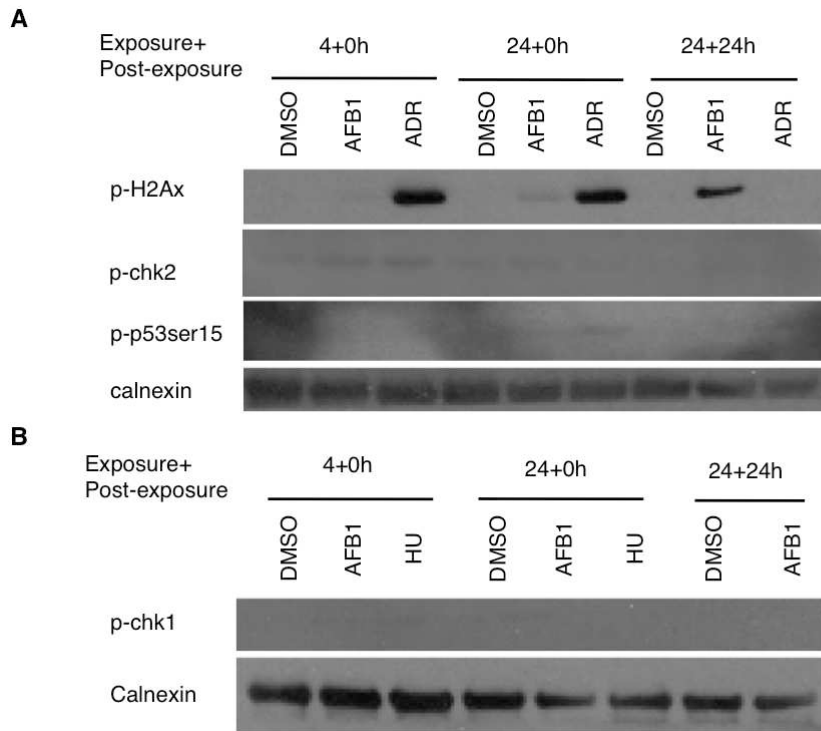


**Figure 4.4.7.** Incomplete DNA damage checkpoint response of Huh7 cells to AFB1.

Huh7 cells were treated with DMSO or AFB1 (5  $\mu$ M) for four hours and 24 hours, and tested immediately (4h+0h and 24h+0h), or after 24 hours of incubation without treatment (24h+24h).

Huh7 cells treated with 0.5  $\mu$ M Adriamycin (ADR) or 5 mM hydroxyurea (HU) were used as positive controls for experiments shown in A and B, respectively. Total cell lysates were subjected to Western blot analysis. Calnexin was used as a loading control. p-H2AX, phospho- H2AX; p-p53ser15, phospho-p53ser15; p-Chk2, phospho-Chk2; p-Chk1, phospho-Chk1.

Derived from these findings, it was exciting to identify whether the DNA damage-induced p53 response has been activated in AFB1 exposed cells. Although, HepG2 cells express wild-type p53, but its p53-deficient isogenic clone is not available. Therefore, we expanded our studies to another cell line, HCT116 with wild-type p53 expression and its p53-deleted isogenic clone [257].

#### 4.5 Recapitulating the effects of AFB1 in isogenic wild-type and p53<sup>-/-</sup> HCT116 cells

We first tested whether the response of HCT116 and HCT116-p53<sup>-/-</sup> cells to AFB1 and ADR exposure induced changes that we have initially identified in HepG2 cells. We performed all AFB1 experiments in these cell lines in the presence of S9-activating system to allow the transformation of AFB1 into epoxy-AFB1 [279]. First, we assessed the formation of DNA lesions following exposure to AFB1 (5 $\mu$ M) and

ADR (1  $\mu$ M). The great majority of cells stained positive for 8-OHdG lesions following 24 hours of exposure to AFB1 or ADR (Figure 4.5.1A). The testing of AFB1-FAPY adducts was not possible, because HCT116 cells loosely attached to coverslips did not resist to the harsh treatment at pH 9.6, prior to antibody incubation. Next, DNA strand breaks were detected using neutral comet assay. Exposed cells were tested either immediately or following culture in the absence of chemical agents up to 48 hours. Both AFB1 and ADR caused comet formation with similar intensities and significant increases ( $P < 0.0001$ ) in tail moments at all tested time-points (Figure 4.5.1B).



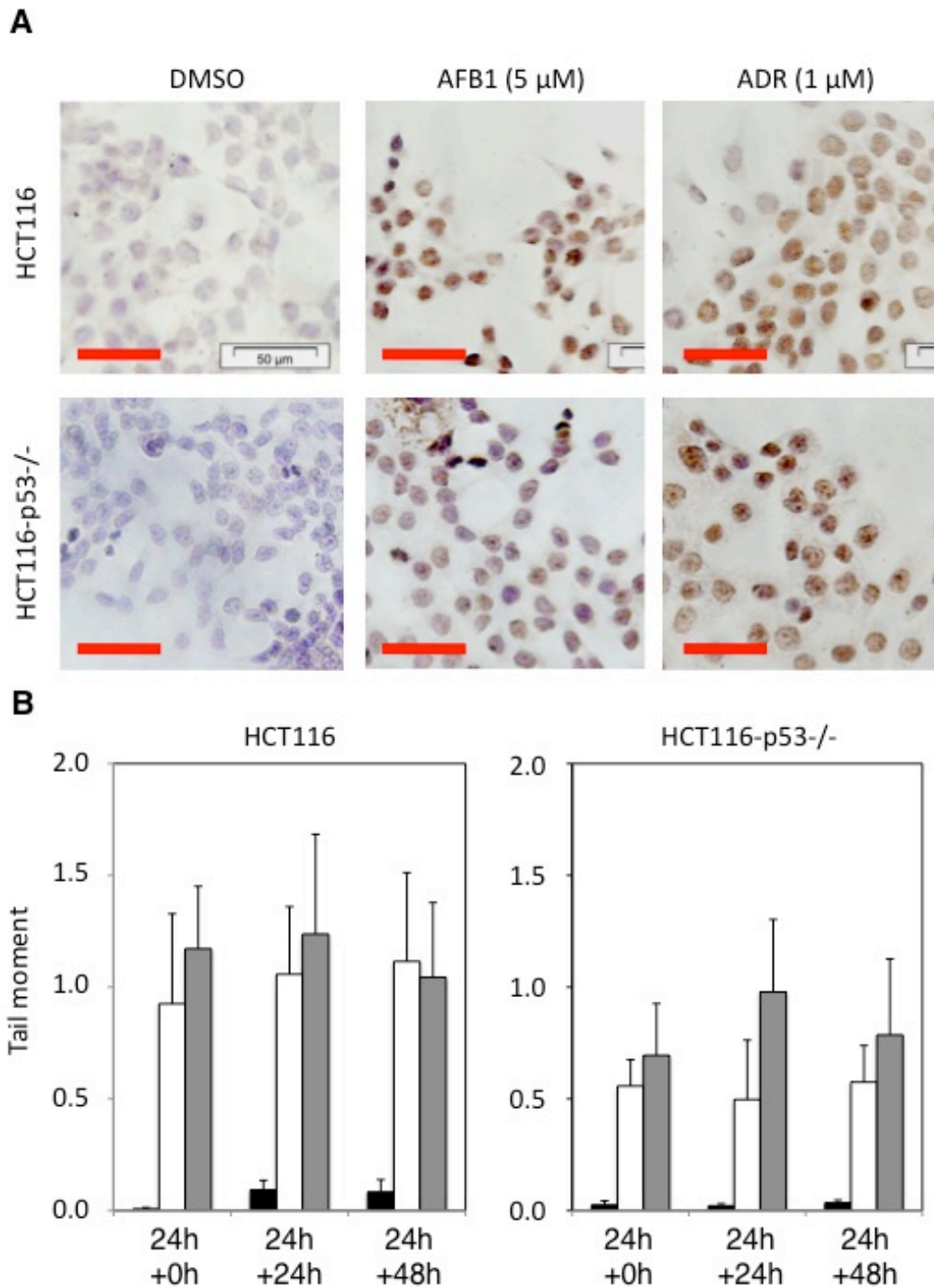


**Figure 4.5.1** Induction of 8-hydroxy-deoxyguanosine lesions and double strand breaks following aflatoxin B1 (AFB1) exposure. HCT116 and HCT116-p53<sup>-/-</sup> cells were exposed to AFB1 (5  $\mu$ M) or DMSO in the presence of S9-activating system. ADR (1  $\mu$ M) treatment was performed in the absence of S9-activating system. Scale bar = 50  $\mu$ m. (A, B).

(A) Cells exposed for 24 hours were subjected to indirect immunoperoxidase assays using anti-8OH-dG antibody. Counterstain was by hematoxylin.

**(B)** Cells were tested immediately after 24 hours of exposure (24h+0h), or after 24 hours (24h+24h) and 48 hours (24h+48h) post-treatment. Neutral comet assay was used to detect double strand breaks. Black, white and gray columns indicate tail moments of cells exposed to DMSO, AFB, and ADR, respectively. Error bars indicate SD. AFB1- and ADR-treated cells displayed significantly increased tail moments in all time-points tested ( $P < 0.0001$ ).

The responses observed with HCT116 and HCT116-p53<sup>-/-</sup> cells were similar to each other, although we observed less double strand breaks in HCT116-p53<sup>-/-</sup> cells. Taken together, these findings indicated that AFB1 and ADR induced genotoxic changes in these cell lines also, in addition to the initially tested HepG2 cell line.

DNA damage foci induction in response to AFB1 exposure was assessed using anti-53BP1 and anti-phospho-H2AX antibodies. Cells exposed to 5  $\mu$ M AFB1 for 24h were examined for foci formation in the absence of AFB1 exposure up to 48 hours. Statistically significant ( $P < 0.0001$ ) increases of both 53BP1 and phospho-H2AX-positive (>5 foci/nuclei) cells were in both HCT116 and HCT116 -p53<sup>-/-</sup> cells in all time-points tested (Figure 4.5.2). Percent number of 53BP1 foci-positive cells remained between 20 % and 50%. In addition, percentages of phospho-H2AX-positive cells were between 30% and 60% for at least 48 hours, after the removal of AFB1 from the cell culture medium.

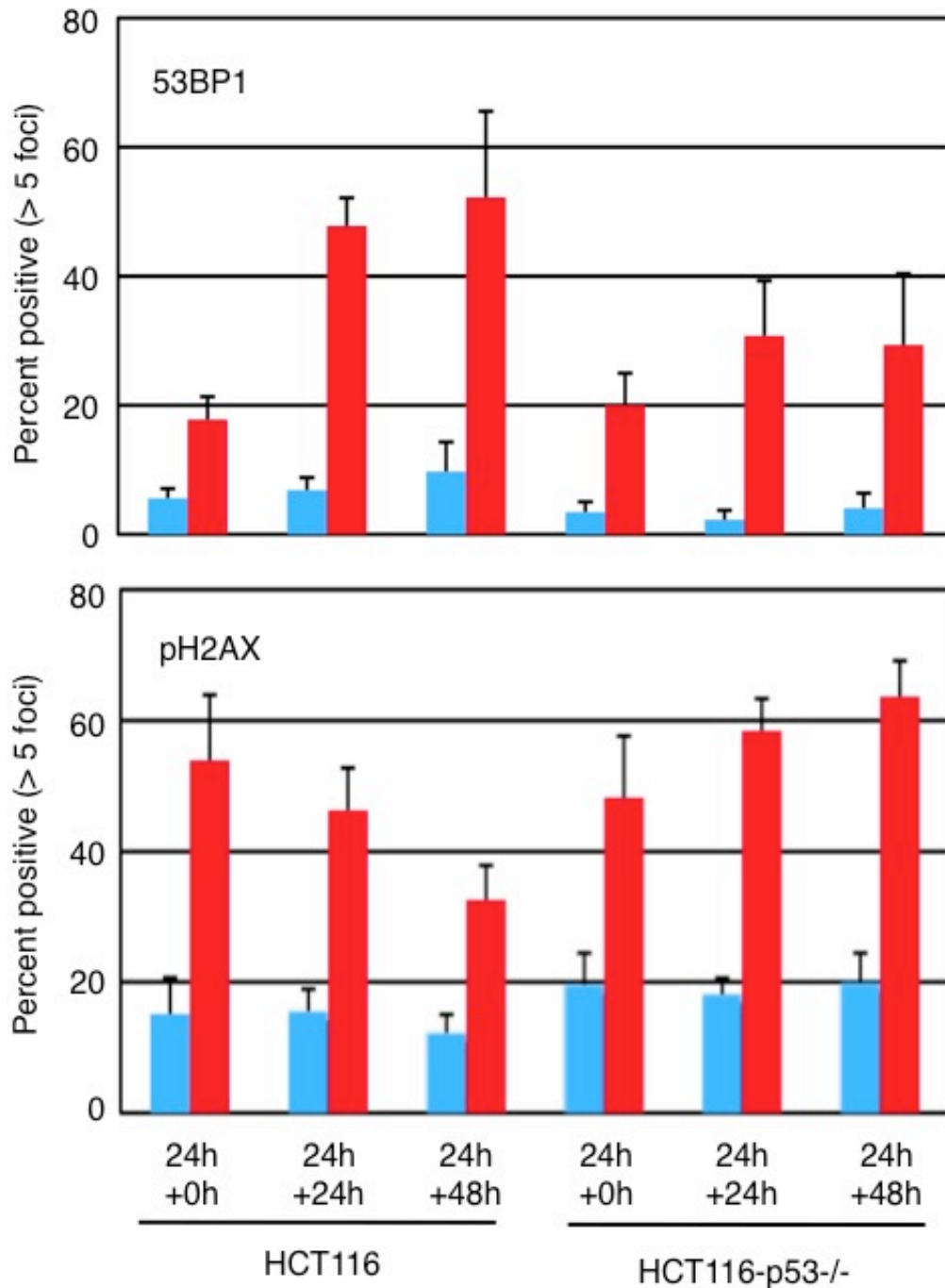


**Figure 4.5.2** Increased DNA damage foci detection after exposure of HCT116 isogenic clones to aflatoxin B1. Cell lines were treated with AFB1 (5  $\mu\text{mol/L}$ ) for 24 hours, followed by further incubation for an additional 48 hours in the absence of the chemical. DNA damage foci-positive cells were detected by indirect immunofluorescence using anti-53BP1 and anti-phospho-H2AX antibodies and percent cells with positive foci (>5 foci per nucleus) were compared. Error bars indicate SD. The increase in aflatoxin B1-treated cells (red columns), compared to DMSO-treated cells (blue columns) was statistically significant ( $P < 0.0001$ ) in all time points tested with both HCT116 and HCT116-p53<sup>-/-</sup> cell lines. pH2AX, phospho-H2AX.

#### 4.5.1 Dose-dependent and differential response of HCT116 and HCT116-p53<sup>-/-</sup> cells to adriamycin treatment

Prior to testing of AFB1 effects on cell cycle checkpoint control, we first examined the responses of HCT116 and HCT116-p53<sup>-/-</sup> cells to ADR. Both p53 and p21Cip1 responded to ADR treatment (0.0 to 0.5  $\mu$ M) with a dose-dependent increase in HCT116 cells. The increase in p21Cip1 levels was p53-dependent, since we did not observe p21Cip1 response in HCT116-p53<sup>-/-</sup> cells (Figure 4.5.3A). HCT116 cells displayed G1 and G2/M arrest in response to ADR, associated with low levels of apoptosis (subG1 peak) and polyploidy formation at higher doses. There was also a depletion of S phase cells, indicating an inhibition of DNA synthesis that lasted at least 48 hours following the removal of ADR from the cell culture medium. The response of HCT116-p53<sup>-/-</sup> cells to ADR was essentially similar with the noticeable absence of the G1 peak (Figure 4.5.3B). Comparative analysis of cell cycle changes in the two tested cell lines indicated that the loss of G1 peak in HCT116-p53<sup>-/-</sup> cell line was associated with a dose-dependent accumulation of nearly all cells at the G2/M phase. Both cell lines also displayed a drop in S phase cells, and an increase in apoptotic (subG1) and polyploidy cells (Figure 4.5.3C). Thus, the major effects of ADR-induced DNA damage in HCT116 cells were a p53-dependent G1 arrest and a p53-independent G2/M arrest.

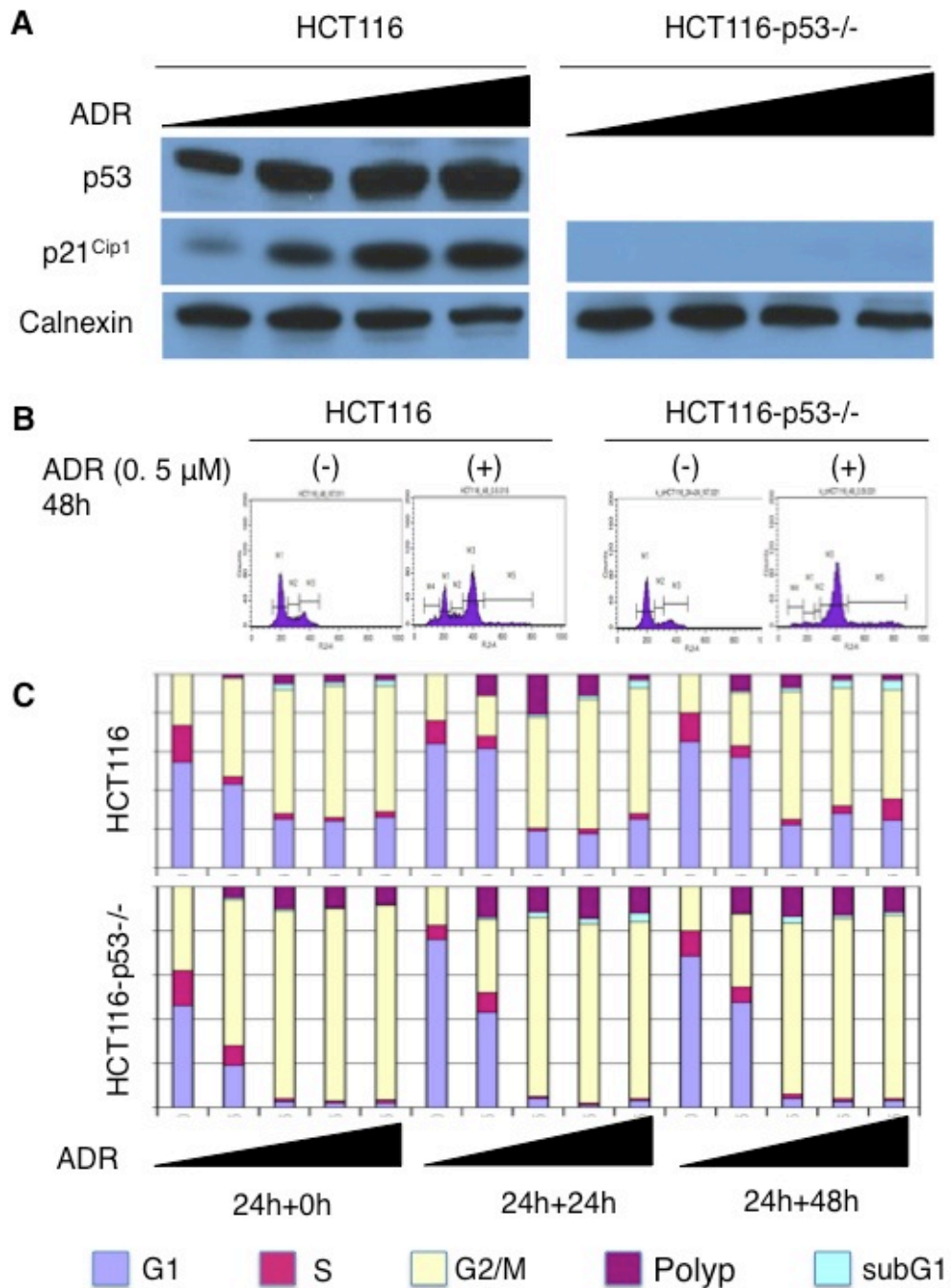


**Figure 4.5.3** p53-dependent and p53-independent cell cycle arrest after adriamycin treatment. **(A)** HCT116 and HCT116-p53<sup>-/-</sup> cells were treated with increasing doses of ADR (0-0.5 μM) for 24 hours. Cell lysates were analyzed for p53 and p21<sup>Cip1</sup> by Western blot. Calnexin was used as loading control. **(B)** Control and ADR-treated cells were subjected to cell cycle analysis by flow cytometry, after 48 hours of post-treatment culture. Loss of G1 peak in ADR-treated HCT116-p53<sup>-/-</sup> was noticed. **(C)** Distribution of cells at different phases of the cell cycle at different post-treatment time points, following exposure to increasing doses of ADR (0.0 to 0.5 μmol/L). Plyp; polyploid cells.

#### 4.5.2 Absence of p53 accumulation and lack of cell cycle arrest in response to AFB1-induced DNA damage

Next, we compared the BrdU incorporation of HCT116 cells and we observed that 5  $\mu\text{M}$  AFB1 treatment for 24 hours did not affect DNA synthesis, regardless of p53 status. The lack of response did not change for an additional 24 hours after the removal of AFB1 from the cell culture medium (Figure 4.5.4A). Comparative analysis of cell cycle changes in HCT116 and HCT116-p53<sup>-/-</sup> cells (Figure 4.5.4B) showed no major change in the fraction of S phase cells in both cell lines after 24 hours of AFB1 treatment, and for an additional 24 hours post-treatment. HCT116 cells displayed a weak decrease in G1 cells associated with a weak increase in G2/M cells at 24 hours. But, this effect was not stable because it vanished during the post-treatment cell growth (Figure 4.5.4B). The response of HCT116-p53<sup>-/-</sup> cells to AFB1 exposure was not remarkable either, except a slight increase in G2/M cells. When we analyzed the response of HCT116 and HCT116-p53<sup>-/-</sup> cells to AFB1 (Figure 4.5.4) in comparison with ADR (Figure 4.5.3), we noticed major discrepancies. While ADR was able to trigger a response with a dose as low as 0.05  $\mu\text{M}$ , AFB1 was ineffective with 60-100-fold higher molar doses (3-5  $\mu\text{M}$ ). This remarkable difference in cellular response contrasted with our other findings that indicated that both AFB1 and ADR induced 8-OHdG lesions (Figure 4.5.1A) and double strand breaks (Figure 4.5.1B) with similar intensities.

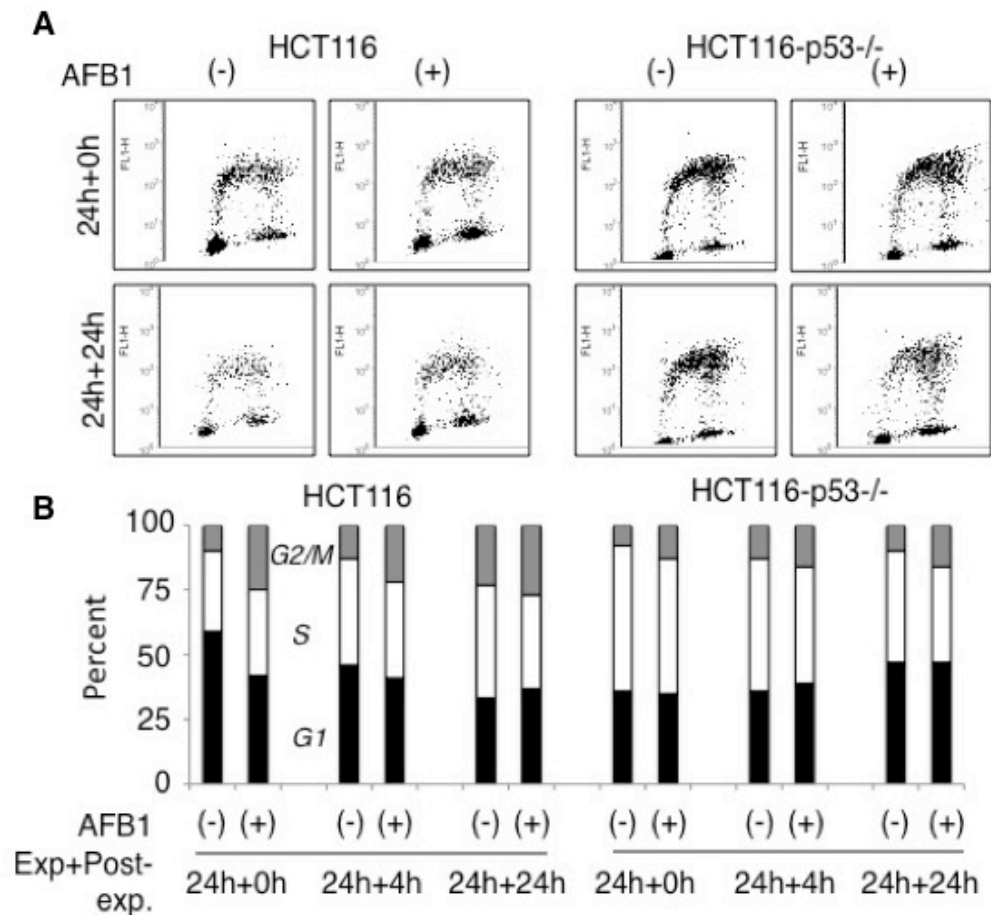


**Figure 4.5.4** Lack of cell cycle arrest in response to AFB1-induced DNA damage. HCT116 and HCT116-p53<sup>-/-</sup> cells were treated with 5  $\mu$ M AFB1 (+) or DMSO (-) in the presence of S9-activating system for 24 hours, followed by additional incubation without treatment up to 24 hours. Cell cycle analysis was performed by flow cytometry after labeling of cells with BrdU and propidium iodide at indicated post-exposure times. **(B)** Representative flow cytometry plots of AFB1-treated (+) and DMSO-treated (-) cells. **(C)** Distribution of cells at G1, S and G2/M phases at different time points after exposure to AFB1 (+) or DMSO (-).

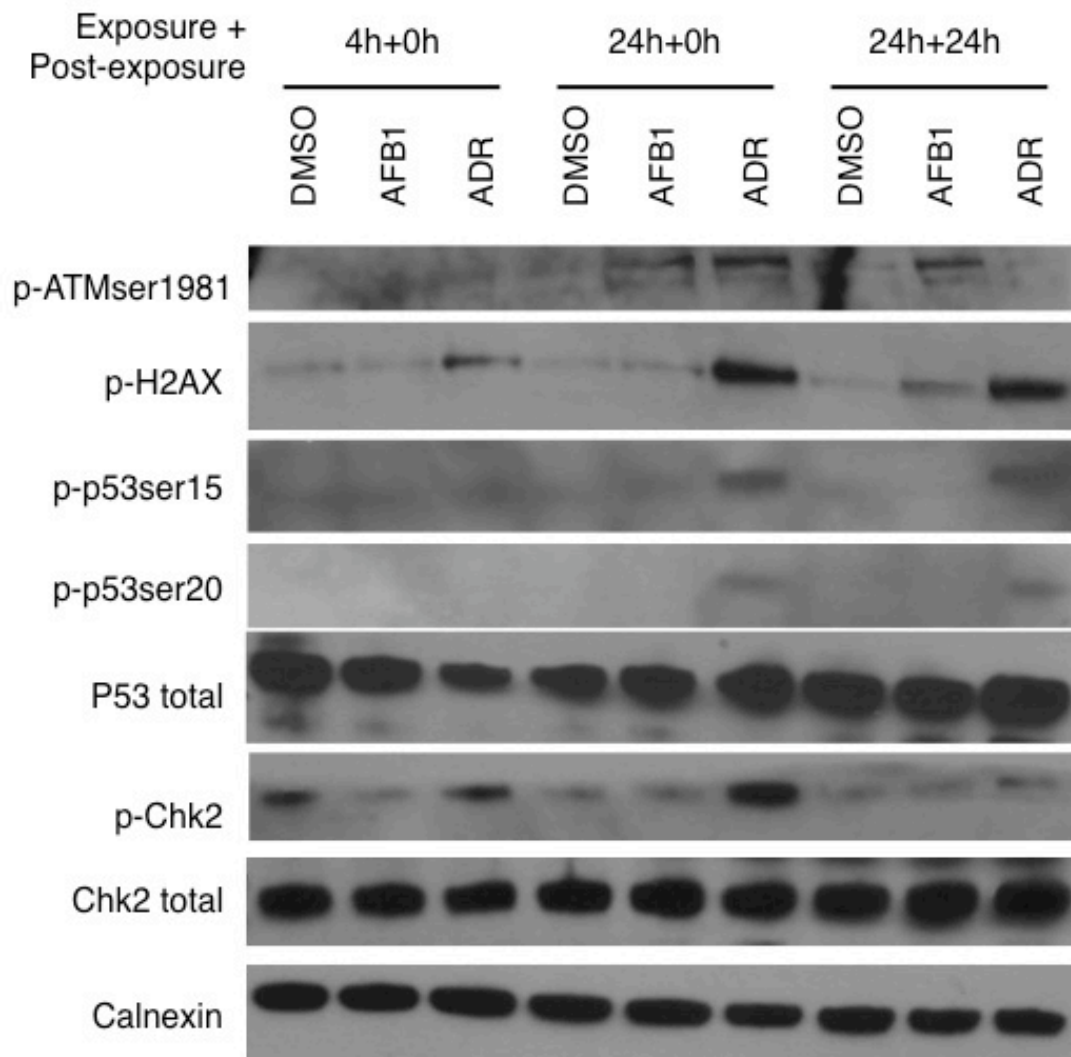
#### 4.5.3 DNA damage checkpoint response to AFB1 was incomplete

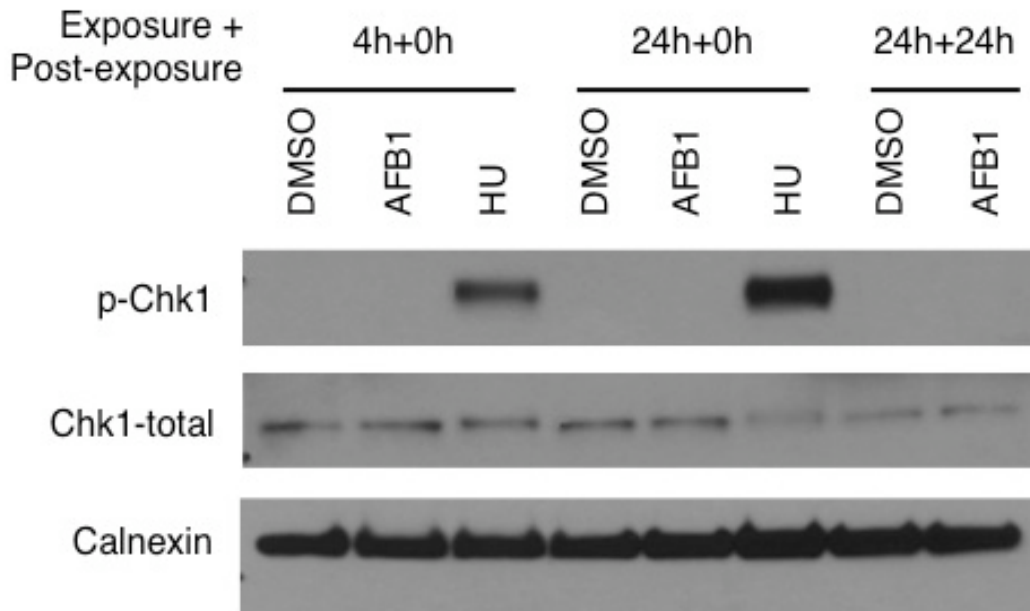
The accumulation of 53BP1 and phospho-H2AX foci after exposure of these cells to AFB1 (Figure 4.5.2) indicated that AFB1-induced DNA damage initiated a checkpoint response, but this initial response did not conduct to a cell cycle arrest or apoptosis response (Figure 4.5.4), despite sustained DNA damage (Figure 4.5.1). Therefore, we examined the status of critical DNA damage signaling proteins in HCT116 cells by Western blot assay following 5  $\mu$ M AFB1 exposure, as compared to 0.5  $\mu$ M ADR exposure (Figure 4.5.5). Following the 24 hours of exposure to AFB1,

we observed a clear increase in phospho-ATM and phospho-H2AX, but not in phospho-Chk2, and phospho-p53ser15 and phospho-p53ser20 levels. The difference between control and AFB1-exposed cells in ATM and H2AX phosphorylation remained discernible, albeit not flagrant, after an additional 24 hours post-treatment. These findings indicated that AFB1-induced DNA damage response was attenuated and incomplete in HCT116 cells. In contrast, a 10-fold lower molar dose of ADR (0.5  $\mu$ M) was sufficient for strong induction of ATM, H2AX, Chk2 and p53ser15 phosphorylation (Figure 4.5.5A). As the ATR/Chk1 activation pathway can also activate p53 through phosphorylation, we also tested the status of Chk1 phosphorylation after the AFB1 exposure. Cells treated with hydroxyurea (HU) were used as positive control. HCT116 cells displayed increased Chk1 phosphorylation upon HU exposure, but they were unresponsive to AFB1 treatment (Figure 4.5.5B). The lack of association between ATM and p53ser15 phosphorylation in AFB1-treated cells was unexpected.



**A**



**B**

**Figure 4.5.5** Incomplete DNA damage checkpoint response to AFB1. HCT116 cells were treated with 5  $\mu$ M AFB1 or DMSO in the presence of S9-activating system for 4 hours and 24 hours, and tested immediately (4h+0h and 24h+0h), or after 24 hours (24h+24h), 24 hours of incubation without treatment. HCT116 cells treated with 0.5  $\mu$ M ADR (**A**) or 5 mM Hydroxyurea (HU) (**B**) were used as positive control. Total cell lysates were subjected to Western blot analysis with the antibodies against phospho-ATM, phospho-H2AX, phospho-Chk2, chk2 total, p53 total, phospho-p53ser15, phospho-p53ser20, phospho-chk1, chk1 total. Calnexin was used as a loading control.

Therefore, we verified the co-expression of these marks using double-immunofluorescence assay with an independent anti-phospho-ATM antibody. As shown in Figure 4.5.6, increased nuclear staining and clearly discernible foci were detected with both AFB1- and ADR-treated cells. Most phospho-ATM-positive nuclei in ADR-treated cells also displayed increased phospho-p53ser15 staining. However, phospho-ATM-positive nuclei in AFB1-treated cells did not show increased phospho-p53 staining.

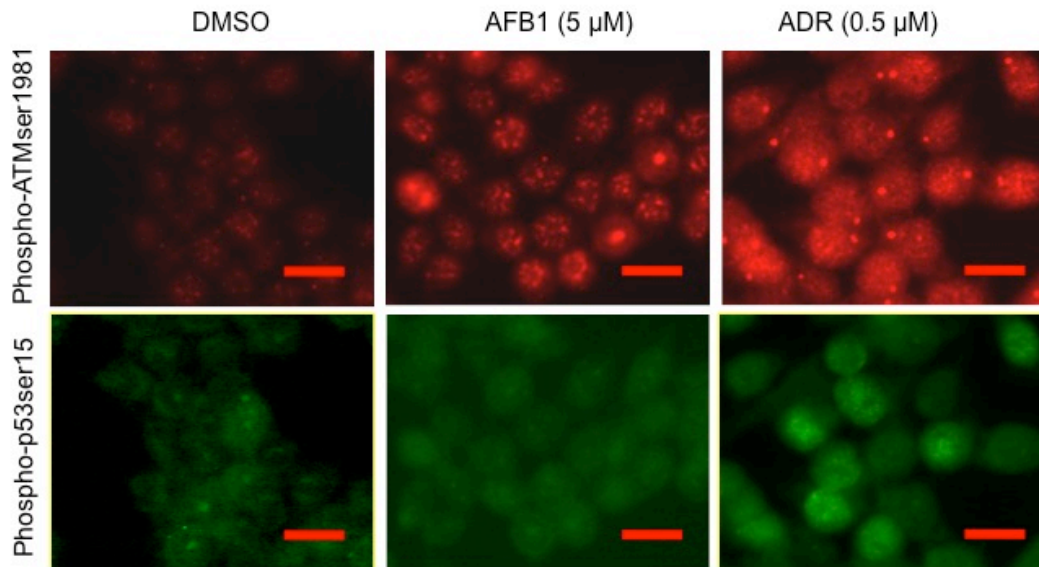


**Figure 4.5.6** Demonstration of the lack of phospho-p53ser15 accumulation in phospho-ATMser1981-positive nuclei after aflatoxin B1 exposure. HCT116 cells were exposed to AFB1 (5  $\mu$ M) or DMSO in the presence of S9-activating system, or treated with ADR (0.5  $\mu$ M) for 24 hours and subjected to rabbit phospho-ATMser1981 and mouse phospho-p53ser15 co-staining. Rabbit anti-phospho-ATM and mouse anti-phospho-p53 antibodies were detected with Alexa-568-conjugated (red) anti-rabbit and Alexa 488-conjugated (green) anti-mouse antibodies, respectively. Scale bar = 20  $\mu$ m.

#### 4.6 Mechanism of p53 activation bypass after AFB1 induced DNA damage

Overall, all the data generated in this study suggested that the AFB1 induced DNA damage response was not enough to generate a complete growth control response. The checkpoint response was either delayed or deficient with the bypass of efficient p53 protein phosphorylation. Hence, we compared the response of HCT116 cells to AFB1-induced DNA damage. First, a 3  $\mu$ M AFB1 treatment for 24 hours did not induce detectable changes in p53 levels in HCT116 cells. In fact, there was no detectable increase in p21<sup>Cip1</sup> levels either in HCT116 or in HCT116-p53<sup>-/-</sup> cells (Figure 4.6.1A). As shown in figure 4.6.1A, after the Adriamycin treatment, both p53 and p21cip1 levels increased in a dose dependent manner in HCT116 cells and the increase in p21cip1 was p53-dependent since no p21cip1 accumulation was observed in HCT116 p53<sup>-/-</sup> cells. On the other hand, AFB1 exposure did not induce any significant p53 accumulation and p21cip1 induction in both HCT116 and HCT116-p53<sup>-/-</sup> cells. Taken together, these data suggested that AFB1 was either implicated in

the inhibition of successful DNA damage induced cell cycle checkpoint response or the damage caused by AFB1 was not enough to accomplish a threshold level that is necessary for the full and efficient checkpoint activation, which was also previously suggested in studies with low-dose ionizing radiation [247]. In order to test our hypothesis, HCT116 cells were co-treated with rising doses of Adriamycin in the presence or in the absence of AFB1. Figure 4.6.1 B indicates that the accumulation of p53 and p21cip1 did not change significantly upon Adriamycin and AFB1 co-treatment. In fact, a slight increase was observed in p21cip1 accumulation after co-treatment. The same response was also observed in HCT116-p53<sup>-/-</sup> cells. These findings suggested that AFB1 did not inhibit the DNA damage checkpoint response under the tested conditions, but increased the checkpoint response to Adriamycin very slightly.

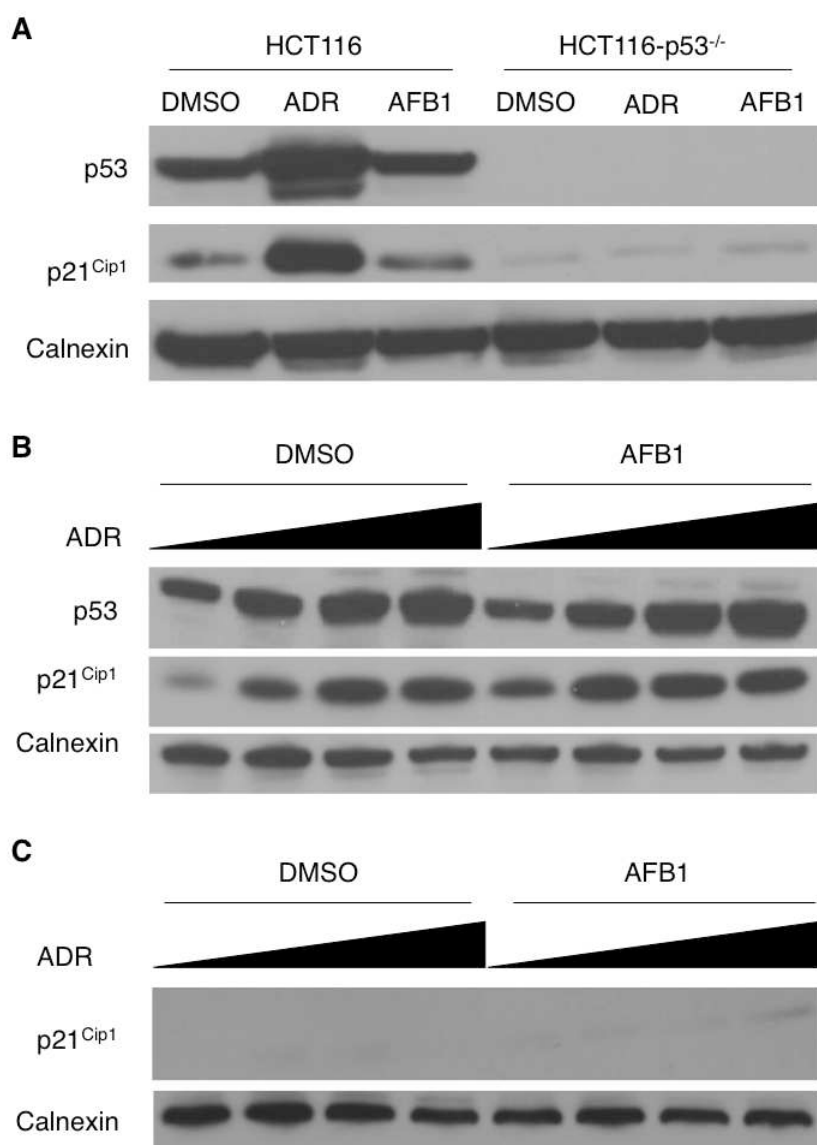


**Figure 4.6.1** Comparative analysis of wild-type p53 response of HCT116 cells to AFB1 and Adriamycin treatment indicates that AFB1 cannot induce effective p53 activation. (A) Wild-type p53 HCT116 and p53-deficient HCT116-p53<sup>-/-</sup> cells were treated with AFB1 (3 μM) or DMSO (in the presence of the S9-activating system) or Adriamycin (ADR; 1 μM) for 24 hours, followed by additional cell culture in the absence of this chemical for another 24 hours. (B, C) HCT116 (B) and HCT116-p53<sup>-/-</sup> (C) cells were co-treated with ADR, increasing doses: 0, 0.1, 0.5 and 1 μM, respectively) in the absence (DMSO) or in the presence of 3 μM AFB1, as described in A for 24 hours (24 hours pre-exposure to AFB1, followed by 24 hours of co-exposure). Total cell lysates were used for Western blot using anti-p53 and anti-p21<sup>Cip1</sup> antibodies. Calnexin was used as a loading control.

## CHAPTER 5. DISCUSSION & FUTURE PERSPECTIVES

### 5.1 AKT activation is required for selenium deficiency induced resistance.

Selenium is essential for human health as a dietary supplement. Many diseases have been reported to be related to selenium deficiency [280]. Consequently, many epidemiological research data indicated an opposite correlation in selenium levels in patients with various cancer types [281-286]. Nevertheless, the mechanism of selenium's protecting effect in cancer especially in HCC is still not well documented.

Our group contributed to the current knowledge related to Se-deficiency and HCC in terms of its association with malignancy. Our *in vitro* model in well-differentiated and poorly-differentiated HCC cell lines demonstrated the selective response of those cell lines to Se-deficiency induced oxidative stress response. Accordingly, our previous data on HCC cell lines with different etiologies showed the close relationship of HBV and genotoxic stress with the selenium deficiency tolerance. 9 out of 10 tolerant HCC cells have HBV integration in their genome. Isogenic cell lines HepG2 and HBV transfected HepG2-2.2.15 cell line also strengthened this association with the observed tolerance of HepG2-2.2.15 to Se-deficiency induced oxidative stress and its deadly consequences.

Apoptosis induced by oxidative stress has been implicated in several biological and pathological processes including senescence, inflammation, and carcinogenesis [287]. Even though the effects of oxidative damage are well known such as mitochondria failure and calcium homeostasis change [288], the underlying mechanism of cell death through oxidative damage is not yet clear. Oxidative stress is important in liver malignancy as well [289]. Selenium deficiency and its contribution to the ROS accumulation are frequent in chronic liver diseases and may cause hepatic malignancies [11, 290]. Therefore, the acquired tolerance of HCC cells to selenium deficiency and ROS accumulation may occur *in vivo* as well.

In this part of our research we aimed to clarify the gained tolerance of HCC to apoptosis under selenium deficient oxidative stress conditions. The results presented here provide the evidence for the involvement of various stress activated cell-signaling pathways under Se-deficiency (Figure 5.1.1).

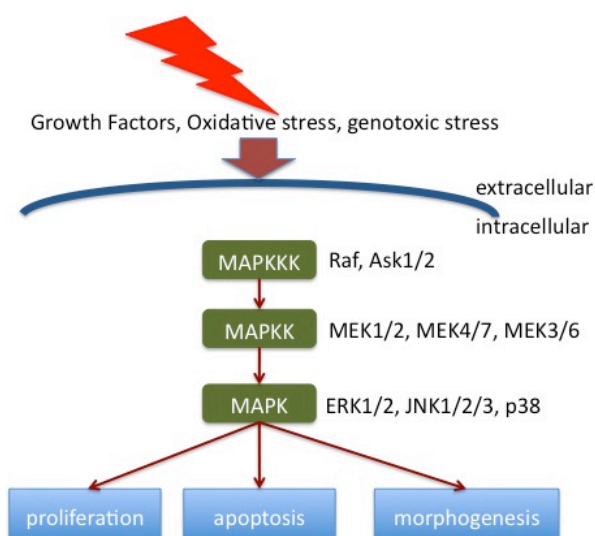


Figure 5.1.1 Activated signaling pathways and cell fate upon oxidative stress

One possible mechanism of Se-deficiency induced apoptosis is through the activation of p38MAPK pathway. Apoptosis observed under oxidative stress was triggered upon the activation of a couple of MAPK signaling elements including the p38MAPK pathway in HepG2 cells. Although STAT1, the transcriptional target of p38MAPK [266] was not activated, other targets or other phosphorylation sites that may be responsible for apoptosis should be checked under these conditions. ERK signaling has a crucial role in numerous steps of tumorigenesis including cancer cell proliferation, migration, and invasion [291, 292]. The MAPK/ERK pathway activation in HepG2-2.2.15 under Se-deficient conditions may contribute to the previously reported resistance to apoptosis. Thus subsequent targets of the ERK pathway such as the well-known Ras oncogene [293] or the anti-apoptotic protein MCL- 1 [294] should be checked.

It is believed that genotoxic stress activate the PI3K/AKT pathway and inhibits apoptosis. In apoptosis resistant HBV integrated HepG2-2.2.15 cell line a time dependant increase in Akt phosphorylation, yet the detectable phosphorylation of Akt

in Se-adequate conditions, pointed out the involvement of HBV in AKT activation. Inhibition of AKT with a specific PI3K inhibitor reactivated the apoptosis phenotype under both Se-deficient and Se-adequate conditions, demonstrating the direct contribution of PI3K/Akt in the acquired selective survival in our model. Other HCC cell lines, which have a PTEN deletion and a constitutively active AKT phosphorylation, were also checked, but we failed to recapitulate apoptosis in those cell lines. This may be due to either the partial inhibition of Akt phosphorylation by Wortmannin or the different etiologies of those cell lines. Additionally, the transcriptional targets of PI3K/Akt in this survival process should be further clarified. We tried to check the targets of the Akt pathway; NFκB and its inhibitor IKK, however we failed to get any significant findings. Other known or novel Akt targets should be checked in order to understand the role of Akt induced survival capacity of some HCC cell lines.

Our *in vitro* model with the unique HBV integration difference and respective apoptosis resistance provided a useful model for the investigation of possible mechanisms of the observed resistance. Therefore, we recently performed a microarray analysis study. We believe that this study would provide evidence for the contribution of MAPK pathway and their target genes with the differential expression profile to the selective survival advantage in HCC. Differential expression of novel targets of both MAPK and Akt survival pathway may be involved in this selective survival ability.

In conclusion, this study further enlightened the association of selenium deficiency and HCC through the activation/inactivation of MAPK and cell survival pathways and provided evidence for its contribution to HCC, nevertheless the transcriptional targets and the exact mechanism needs to be further investigated.

## 5.2 R249S p53 status did not lead to significant growth advantage.

The data presented in this part of our research project is mainly concentrated on the oncogenic functions of R249S p53 mutation. Mutant p53 might trigger different pathways that constitute to the molecular basis of a wide range of gain-of-function



activities, such as resistance to anticancer treatments [241], genomic instability [240], increased cell growth and metastasis [237, 238]. Despite rapidly accumulating evidence, the molecular detail of the transcriptional activity of mutant p53 is still not clarified. In our study, we failed to observe any significant growth advantage of cells bearing this hot spot mutation. Phenotypic changes after various treatments including TGF- $\beta$ 1, Adriamycin and Aflatoxin were remained common in both p53 backgrounds. On contrary to the findings indicating the increased mitotic activity and colony formation in Hep3B cell line transfected with R249S p53, our model presenting the wild type p53 and R249S p53 on the same background failed to show any significant growth advantages. This may be due to the fact that wild type p53 might be still functional and it would be interesting to inactivate the wild type p53 after the transfection of R249S p53, which would mimic the case in real life as well. It is also noteworthy that, due to the clonal selection effects after transfection protocol, 6 selected R249S clones from 2 separate parental clones along with the controls were considered together in each group and the individual phenotypic effects were ignored. Our mutant protein functionality and stability were detected by indirect methods; we were not able to check the exact mutant p53 levels neither after transfection nor after several treatments. There may be no selective pressure in cells to keep exogenous mutant p53; therefore they might lose the ectopic expression after a while.

The lack of significant phenotypic change due to R249S prompted us to check the fact that p53 R249S might be selective via epigenetic modulation-derived mechanisms. In 6 249ser subclones, H3K27me3, H3K36me3, H4K20me3, H3R17me2 and H3K9me3 residues were heterogeneously and strongly stained compared to the 4 control subclones. Global histone methylation might be altered through the presence of R249S hot spot mutation suggesting the possible involvement of p53 mutants in epigenetic modulation.

In conclusion, our findings indicated that R249S does not provide survival advantage at heterozygous state. Therefore the selection of this hot spot mutation could be at the mutation induction stage. The lack of p53 activation in AFB1 exposed HCC cells led us to test the functional DDR induction after AFB1 exposure.

5.3 After AFB1 exposure DNA damage checkpoint response was incomplete without a p53 activation response.

Aflatoxins are the major environmental HCC risk. Aflatoxin's hepatocellular biochemistry, its DNA interacting forms, the types of DNA damage induced by aflatoxins and their repair mechanism by NER, and its *in vitro* and *in vivo* mutagenic specificity for G->T transversions are well established facts [295]. We addressed here a less well understood, but a critical component of aflatoxin genotoxicity, namely DNA damage checkpoint response. The *in vitro* experimental model system used here was designed after careful consideration of previously described features associated with aflatoxin-related carcinogenicity. Human cells with wild-type p53 expression were preferred because of the fact that a specific hotspot mutation of this gene was observed only in human HCC, but not in other aflatoxin-induced mammalian tumors [31]. We considered estimated chronic aflatoxin exposure levels in humans (0.01-0.3 µg/kg/day) [218] and hepatocarcinogenic doses (0.015-1 ppm) in rat [277]. We also considered that 30 minutes exposure to 1.6 µmol/L AFB1 was sufficient to induce p53-249 G->T mutations in HepG2 cells, [278], and 0.2-5 µmol/L doses induced reporter gene mutations in mouse fibroblasts [279]. Thus, AFB1 doses that we used here (3-5 µmol/L) were at the upper limits of *in vitro* mutagenic activity in mammalian cells and they were estimably superior to carcinogenic doses in humans and rats. We performed our cell response studies over a period of several days so that we could determine both immediate and delayed effects.

Our findings demonstrate that AFB1, when tested under conditions comparable to mutagenic and carcinogenic exposure levels, create DNA adducts and oxidative-stress induced DNA lesions, as well as persistent single and double strand breaks. These effects were expected based on previously published findings. AFB1-FAPY adducts are repaired by NER [228]. However, their removal is slow [221], and they remain at maximum levels for several days and are detectable over several weeks in rat liver cells [221, 222]. The unusual stability of AFB1-FAPY adducts together with a slow repair process could account for their sustained genotoxic effects. The lack of a detectable cell cycle arrest or apoptosis response during the same time period was unexpected. Our findings with both HepG2 and HCT116 cell lines clearly indicate that these human cells were unable to develop a protective response to AFB1-induced

genotoxicity, although they responded by cell cycle arrest, senescence and apoptosis to ADR, another genotoxic agent with comparable effects on DNA stability.

Our careful analysis of DNA damage checkpoint proteins provides a plausible explanation for the uncoupling between DNA damage and growth control following AFB1 exposure. The lack of an efficient coordination between DNA damage and growth control was due to an incomplete checkpoint response that occurred selectively after AFB1 exposure, but not after ADR exposure. Studies with both HepG2 and HCT116 cells indicated that DNA damage sensor protein ATM, the adaptor protein 53BP1 and H2AX were activated with both chemicals, probably in response to double strand breaks [246, 247]. ATM/53BP1/H2AX type initiating response was followed by chk2, p53 and p21<sup>Cip1</sup> activation, as well as G1 and G2/M arrest after ADR exposure, but not after AFB1 exposure. Our comparative studies with HCT116 and HCT116-p53<sup>-/-</sup> cells indicated that G1 arrest was p53-dependent, but G2/M arrest was p53-independent. Thus, cells exposed to genotoxic effects of AFB1 failed to develop both p53-dependent G1 and p53-independent G2/M arrest responses. The lack of Chk2 and p53 phosphorylation, associated with a lack of p21<sup>Cip1</sup> accumulation after AFB1 exposure provide evidence for an incomplete transmission of DNA damage signal from ATM and 53BP1.

The mechanisms of checkpoint signal interruption between ATM and Chk2 in AFB1-exposed cells are not known. We first hypothesized an inhibitory effect of AFB1 for the induction of an uninterrupted DNA damage checkpoint response mechanism. However, cotreatment of AFB1 with Adriamycin did not end up with such an inhibition of p53 or p21<sup>Cip1</sup> accumulation. Thus, we would like to speculate that one reason could be the weakness of signal intensity at AFB1 doses used in this study. It has been previously reported that AFB1 exposure could induce p21<sup>Cip1</sup> upregulation in rat liver [296]. Therefore, AFB1 could induce a checkpoint response, presumably mediated by ATM/Chk2/p53 pathway. However AFB1 dose used in this particular study was 5 mg/kg and induced necrosis in the liver, strongly suggesting that it is well above the doses used here, as well as the non-lethal doses that both humans and rats are exposed for a carcinogenic effect. Such a dose would probably cause lethal aflatoxicosis in humans [217]. As stressed earlier, cancer-causing dietary exposure to AFB1 occurs at low levels, a condition that is similar to our in vitro conditions that

provided evidence for a defective checkpoint response. Defective or negligent G2/M checkpoint response to low ionizing radiation exposure has been postulated by Löbrich and Jeggo [247] as a potential cause of genomic instability and cancer risk. The authors also proposed that a master p53-dependent G1 checkpoint might remain effective during negligent G2/M checkpoint for later elimination of escaping cells. Our observations strongly suggest that such a salvage pathway would also be ineffective against AFB1-induced DNA damage.

In conclusion, our findings provide evidence for a negligent G1 and G2/M checkpoint response to AFB1-induced DNA damage. While the permanent G1 and/or G2/M arrest, together with apoptosis after Adriamycin treatment protect cells from the accumulation of DNA damage induced mutations, partial or negligent G2/M arrest and continuation of proliferation of cells in the presence of persistent DNA damage after AFB1 exposure may provide a scaffold to the accumulation of mutations (Figure 5.3.1). This defective response may contribute significantly to potent mutagenicity and carcinogenicity of aflatoxins associated with frequent 249 G->T mutations affecting TP53 tumor suppressor gene in humans.

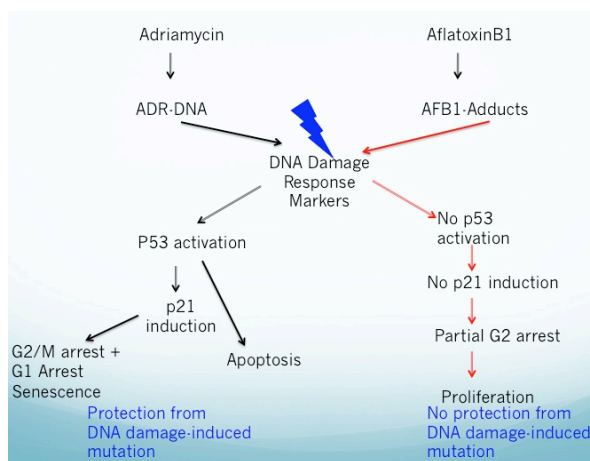


Figure 5.3.1 Schematic representation of proposed mechanism of response after Adriamycin and AFB1 exposure

1. Parkin, D.M., et al., *Estimating the world cancer burden: Globocan 2000*. Int J Cancer, 2001. **94**(2): p. 153-6.
2. Di Bisceglie, A.M., et al., *NIH conference. Hepatocellular carcinoma*. Ann Intern Med, 1988. **108**(3): p. 390-401.
3. Bosch, F.X., J. Ribes, and J. Borrás, *Epidemiology of primary liver cancer*. Semin Liver Dis, 1999. **19**(3): p. 271-85.
4. Parkin, D.M., P. Pisani, and J. Ferlay, *Estimates of the worldwide incidence of 25 major cancers in 1990*. Int J Cancer, 1999. **80**(6): p. 827-41.
5. Deuffic, S., et al., *Trends in primary liver cancer*. Lancet, 1998. **351**(9097): p. 214-5.
6. El-Serag, H.B. and A.C. Mason, *Rising incidence of hepatocellular carcinoma in the United States*. N Engl J Med, 1999. **340**(10): p. 745-50.
7. Edmondson, H.A. and R.L. Peters, *Tumors of the liver: pathologic features*. Semin Roentgenol, 1983. **18**(2): p. 75-83.
8. Chen, C.J., M.W. Yu, and Y.F. Liaw, *Epidemiological characteristics and risk factors of hepatocellular carcinoma*. J Gastroenterol Hepatol, 1997. **12**(9-10): p. S294-308.
9. Hofseth, L.J., et al., *Nitric oxide in cancer and chemoprevention*. Free Radic Biol Med, 2003. **34**(8): p. 955-68.
10. Thorgeirsson, S.S. and J.W. Grisham, *Molecular pathogenesis of human hepatocellular carcinoma*. Nat Genet, 2002. **31**(4): p. 339-46.
11. Ozturk, M., *Genetic aspects of hepatocellular carcinogenesis*. Semin Liver Dis, 1999. **19**(3): p. 235-42.
12. Tannapfel, A. and C. Wittekind, *Genes involved in hepatocellular carcinoma: deregulation in cell cycling and apoptosis*. Virchows Arch, 2002. **440**(4): p. 345-52.
13. Farazi, P.A. and R.A. DePinho, *Hepatocellular carcinoma pathogenesis: from genes to environment*. Nat Rev Cancer, 2006. **6**(9): p. 674-87.
14. Staib, F., et al., *TP53 and liver carcinogenesis*. Hum Mutat, 2003. **21**(3): p. 201-16.
15. Lavanchy, D., *Hepatitis B virus epidemiology, disease burden, treatment, and current and emerging prevention and control measures*. J Viral Hepat, 2004. **11**(2): p. 97-107.
16. Chisari, F.V., *Unscrambling hepatitis C virus-host interactions*. Nature, 2005. **436**(7053): p. 930-2.
17. Bowen, D.G. and C.M. Walker, *Adaptive immune responses in acute and chronic hepatitis C virus infection*. Nature, 2005. **436**(7053): p. 946-52.
18. Aoki, H., et al., *Molecular cloning of a rat chromosome putative recombinogenic sequence homologous to the hepatitis B virus encapsidation signal*. Proc Natl Acad Sci U S A, 1996. **93**(14): p. 7300-4.
19. Dejean, A., et al., *Hepatitis B virus DNA integration in a sequence homologous to v-erb-A and steroid receptor genes in a hepatocellular carcinoma*. Nature, 1986. **322**(6074): p. 70-2.
20. Wang, J., et al., *Hepatitis B virus integration in a cyclin A gene in a hepatocellular carcinoma*. Nature, 1990. **343**(6258): p. 555-7.
21. Murakami, Y., et al., *Large scaled analysis of hepatitis B virus (HBV) DNA integration in HBV related hepatocellular carcinomas*. Gut, 2005. **54**(8): p. 1162-8.
22. Ferber, M.J., et al., *Integrations of the hepatitis B virus (HBV) and human papillomavirus (HPV) into the human telomerase reverse transcriptase*

- (*hTERT*) gene in liver and cervical cancers. *Oncogene*, 2003. **22**(24): p. 3813-20.
23. Horikawa, I. and J.C. Barrett, *Transcriptional regulation of the telomerase hTERT gene as a target for cellular and viral oncogenic mechanisms*. *Carcinogenesis*, 2003. **24**(7): p. 1167-76.
  24. Paterlini-Brechot, P., et al., *Hepatitis B virus-related insertional mutagenesis occurs frequently in human liver cancers and recurrently targets human telomerase gene*. *Oncogene*, 2003. **22**(25): p. 3911-6.
  25. Andrisani, O.M. and S. Barnabas, *The transcriptional function of the hepatitis B virus X protein and its role in hepatocarcinogenesis (Review)*. *Int J Oncol*, 1999. **15**(2): p. 373-9.
  26. Diao, J., R. Garces, and C.D. Richardson, *X protein of hepatitis B virus modulates cytokine and growth factor related signal transduction pathways during the course of viral infections and hepatocarcinogenesis*. *Cytokine Growth Factor Rev*, 2001. **12**(2-3): p. 189-205.
  27. Diao, J., et al., *X protein of hepatitis B virus inhibits Fas-mediated apoptosis and is associated with up-regulation of the SAPK/JNK pathway*. *J Biol Chem*, 2001. **276**(11): p. 8328-40.
  28. Henkler, F., et al., *Erk-independent partial activation of AP-1 sites by the hepatitis B virus HBx protein*. *J Gen Virol*, 1998. **79** ( Pt 11): p. 2737-42.
  29. Feitelson, M.A., et al., *Hepatitis B x antigen and p53 are associated in vitro and in liver tissues from patients with primary hepatocellular carcinoma*. *Oncogene*, 1993. **8**(5): p. 1109-17.
  30. Ueno, Y., et al., *Irregular regeneration of hepatocytes is an important factor in the hepatocarcinogenesis of liver disease*. *Hepatology*, 2001. **33**(2): p. 357-62.
  31. Gouas, D., H. Shi, and P. Hainaut, *The aflatoxin-induced TP53 mutation at codon 249 (R249S): biomarker of exposure, early detection and target for therapy*. *Cancer Lett*, 2009. **286**(1): p. 29-37.
  32. Rehermann, B. and M. Nascimbeni, *Immunology of hepatitis B virus and hepatitis C virus infection*. *Nat Rev Immunol*, 2005. **5**(3): p. 215-29.
  33. Ghosh, A.K., et al., *Hepatitis C virus NS5A protein modulates cell cycle regulatory genes and promotes cell growth*. *J Gen Virol*, 1999. **80** ( Pt 5): p. 1179-83.
  34. Shimotohno, K., *Hepatitis C virus and its pathogenesis*. *Semin Cancer Biol*, 2000. **10**(3): p. 233-40.
  35. Ray, R.B. and R. Ray, *Hepatitis C virus core protein: intriguing properties and functional relevance*. *FEMS Microbiol Lett*, 2001. **202**(2): p. 149-56.
  36. Dubourdeau, M., et al., *Infection of HepG2 cells with recombinant adenovirus encoding the HCV core protein induces p21(WAF1) down-regulation -- effect of transforming growth factor beta*. *J Hepatol*, 2002. **37**(4): p. 486-92.
  37. Shimotohno, K., et al., *Hepatitis C virus and its roles in cell proliferation*. *J Gastroenterol*, 2002. **37** Suppl 13: p. 50-4.
  38. Qadri, I., M. Iwahashi, and F. Simon, *Hepatitis C virus NS5A protein binds TBP and p53, inhibiting their DNA binding and p53 interactions with TBP and ERCC3*. *Biochim Biophys Acta*, 2002. **1592**(2): p. 193-204.
  39. Ray, R.B., et al., *Transcriptional repression of p53 promoter by hepatitis C virus core protein*. *J Biol Chem*, 1997. **272**(17): p. 10983-6.

40. Pontisso, P., et al., *Hepatitis C virus infection associated with human hepatocellular carcinoma: lack of correlation with p53 abnormalities in Caucasian patients*. *Cancer*, 1998. **83**(8): p. 1489-94.
41. Ishido, S. and H. Hotta, *Complex formation of the nonstructural protein 3 of hepatitis C virus with the p53 tumor suppressor*. *FEBS Lett*, 1998. **438**(3): p. 258-62.
42. Majumder, M., et al., *Hepatitis C virus NS5A physically associates with p53 and regulates p21/waf1 gene expression in a p53-dependent manner*. *J Virol*, 2001. **75**(3): p. 1401-7.
43. Suriawinata, A. and R. Xu, *An update on the molecular genetics of hepatocellular carcinoma*. *Semin Liver Dis*, 2004. **24**(1): p. 77-88.
44. Boige, V. and P. Laurent-Puig, *[Genetic alterations associated with hepatocellular carcinoma]*. *Gastroenterol Clin Biol*, 1997. **21**(1): p. 34-44.
45. Nagai, H., et al., *Comprehensive allelotyping of human hepatocellular carcinoma*. *Oncogene*, 1997. **14**(24): p. 2927-33.
46. Piao, Z., et al., *Allelotype analysis of hepatocellular carcinoma*. *Int J Cancer*, 1998. **75**(1): p. 29-33.
47. Okabe, H., et al., *Comprehensive allelotype study of hepatocellular carcinoma: potential differences in pathways to hepatocellular carcinoma between hepatitis B virus-positive and -negative tumors*. *Hepatology*, 2000. **31**(5): p. 1073-9.
48. Laurent-Puig, P., et al., *Genetic alterations associated with hepatocellular carcinomas define distinct pathways of hepatocarcinogenesis*. *Gastroenterology*, 2001. **120**(7): p. 1763-73.
49. Adcox, K., et al., *Suppression of hadrons with large transverse momentum in central Au+Au collisions at root square[s(NN)] = 130 GeV*. *Phys Rev Lett*, 2002. **88**(2): p. 022301.
50. Wang, G., et al., *Allelic loss and gain, but not genomic instability, as the major somatic mutation in primary hepatocellular carcinoma*. *Genes Chromosomes Cancer*, 2001. **31**(3): p. 221-7.
51. Nishimura, T., et al., *Comprehensive allelotyping of well-differentiated human hepatocellular carcinoma with semiquantitative determination of chromosomal gain or loss*. *Genes Chromosomes Cancer*, 2002. **35**(4): p. 329-39.
52. Wong, I.H., et al., *Detection of aberrant p16 methylation in the plasma and serum of liver cancer patients*. *Cancer Res*, 1999. **59**(1): p. 71-3.
53. Marchio, A., et al., *Recurrent chromosomal abnormalities in hepatocellular carcinoma detected by comparative genomic hybridization*. *Genes Chromosomes Cancer*, 1997. **18**(1): p. 59-65.
54. Marchio, A., et al., *Distinct chromosomal abnormality pattern in primary liver cancer of non-B, non-C patients*. *Oncogene*, 2000. **19**(33): p. 3733-8.
55. Kusano, N., et al., *Genetic aberrations detected by comparative genomic hybridization in hepatocellular carcinomas: their relationship to clinicopathological features*. *Hepatology*, 1999. **29**(6): p. 1858-62.
56. Sakakura, C., et al., *Gains, losses, and amplifications of genomic materials in primary gastric cancers analyzed by comparative genomic hybridization*. *Genes Chromosomes Cancer*, 1999. **24**(4): p. 299-305.
57. Guan, X.Y., et al., *Recurrent chromosome alterations in hepatocellular carcinoma detected by comparative genomic hybridization*. *Genes Chromosomes Cancer*, 2000. **29**(2): p. 110-6.

58. Tornillo, L., et al., *Marked genetic similarities between hepatitis B virus-positive and hepatitis C virus-positive hepatocellular carcinomas*. J Pathol, 2000. **192**(3): p. 307-12.
59. Niketeghad, F., et al., *Frequent genomic imbalances suggest commonly altered tumour genes in human hepatocarcinogenesis*. Br J Cancer, 2001. **85**(5): p. 697-704.
60. Miyoshi, Y., et al., *Frequent mutations in the beta-catenin gene in desmoid tumors from patients without familial adenomatous polyposis*. Oncol Res, 1998. **10**(11-12): p. 591-4.
61. Oka, Y., et al., *M6P/IGF2R tumor suppressor gene mutated in hepatocellular carcinomas in Japan*. Hepatology, 2002. **35**(5): p. 1153-63.
62. Lengauer, C., K.W. Kinzler, and B. Vogelstein, *Genetic instabilities in human cancers*. Nature, 1998. **396**(6712): p. 643-9.
63. Yano, M., et al., *Close correlation between a p53 or hMSH2 gene mutation in the tumor and survival of hepatocellular carcinoma patients*. Int J Oncol, 1999. **14**(3): p. 447-51.
64. Kita, R., et al., *Infrequent alterations of the p16INK4A gene in liver cancer*. Int J Cancer, 1996. **67**(2): p. 176-80.
65. Matsuda, Y., et al., *p16(INK4) is inactivated by extensive CpG methylation in human hepatocellular carcinoma*. Gastroenterology, 1999. **116**(2): p. 394-400.
66. Azechi, H., et al., *Disruption of the p16/cyclin D1/retinoblastoma protein pathway in the majority of human hepatocellular carcinomas*. Oncology, 2001. **60**(4): p. 346-54.
67. Tannapfel, A., et al., *INK4a-ARF alterations and p53 mutations in hepatocellular carcinomas*. Oncogene, 2001. **20**(48): p. 7104-9.
68. Kawamura, N., et al., *PTEN/MMAC1 mutations in hepatocellular carcinomas: somatic inactivation of both alleles in tumors*. Jpn J Cancer Res, 1999. **90**(4): p. 413-8.
69. Fujiwara, Y., et al., *PTEN / MMAC1 mutation and frequent loss of heterozygosity identified in chromosome 10q in a subset of hepatocellular carcinomas*. Jpn J Cancer Res, 2000. **91**(3): p. 287-92.
70. Nishida, N., et al., *Amplification and overexpression of the cyclin D1 gene in aggressive human hepatocellular carcinoma*. Cancer Res, 1994. **54**(12): p. 3107-10.
71. Zhang, X., et al., *Deletions of chromosome 13q, mutations in Retinoblastoma 1, and retinoblastoma protein state in human hepatocellular carcinoma*. Cancer Res, 1994. **54**(15): p. 4177-82.
72. Katagiri, T., Y. Nakamura, and Y. Miki, *Mutations in the BRCA2 gene in hepatocellular carcinomas*. Cancer Res, 1996. **56**(20): p. 4575-7.
73. Satoh, S., et al., *AXIN1 mutations in hepatocellular carcinomas, and growth suppression in cancer cells by virus-mediated transfer of AXIN1*. Nat Genet, 2000. **24**(3): p. 245-50.
74. Friend, S.H., et al., *A human DNA segment with properties of the gene that predisposes to retinoblastoma and osteosarcoma*. Nature, 1986. **323**(6089): p. 643-6.
75. Hirai, H., et al., *Novel INK4 proteins, p19 and p18, are specific inhibitors of the cyclin D-dependent kinases CDK4 and CDK6*. Mol Cell Biol, 1995. **15**(5): p. 2672-81.
76. Chellappan, S.P., et al., *The E2F transcription factor is a cellular target for the RB protein*. Cell, 1991. **65**(6): p. 1053-61.



77. Lees, J.A., et al., *The retinoblastoma protein is phosphorylated on multiple sites by human cdc2*. EMBO J, 1991. **10**(13): p. 4279-90.
78. Mittnacht, S., et al., *Distinct sub-populations of the retinoblastoma protein show a distinct pattern of phosphorylation*. EMBO J, 1994. **13**(1): p. 118-27.
79. Conner, E.A., et al., *Dual functions of E2F-1 in a transgenic mouse model of liver carcinogenesis*. Oncogene, 2000. **19**(44): p. 5054-62.
80. Santoni-Rugiu, E., et al., *Evolution of neoplastic development in the liver of transgenic mice co-expressing c-myc and transforming growth factor-alpha*. Am J Pathol, 1996. **149**(2): p. 407-28.
81. Nelsen, C.J., et al., *Transient expression of cyclin D1 is sufficient to promote hepatocyte replication and liver growth in vivo*. Cancer Res, 2001. **61**(23): p. 8564-8.
82. Nelsen, C.J., et al., *Evidence that cyclin D1 mediates both growth and proliferation downstream of TOR in hepatocytes*. J Biol Chem, 2003. **278**(6): p. 3656-63.
83. Nelsen, C.J., et al., *Amino acids regulate hepatocyte proliferation through modulation of cyclin D1 expression*. J Biol Chem, 2003. **278**(28): p. 25853-8.
84. Rickheim, D.G., et al., *Differential regulation of cyclins D1 and D3 in hepatocyte proliferation*. Hepatology, 2002. **36**(1): p. 30-8.
85. Iakova, P., S.S. Awad, and N.A. Timchenko, *Aging reduces proliferative capacities of liver by switching pathways of C/EBPalpha growth arrest*. Cell, 2003. **113**(4): p. 495-506.
86. Kamijo, T., et al., *Functional and physical interactions of the ARF tumor suppressor with p53 and Mdm2*. Proc Natl Acad Sci U S A, 1998. **95**(14): p. 8292-7.
87. Liew, C.T., et al., *Frequent allelic loss on chromosome 9 in hepatocellular carcinoma*. Int J Cancer, 1999. **81**(3): p. 319-24.
88. Akhurst, R.J. and R. Derynck, *TGF-beta signaling in cancer--a double-edged sword*. Trends Cell Biol, 2001. **11**(11): p. S44-51.
89. Schnur, J., et al., *Chemical hepatocarcinogenesis in transgenic mice overexpressing mature TGF beta-1 in liver*. Eur J Cancer, 1999. **35**(13): p. 1842-5.
90. Ghosh, P., et al., *Cardiac reoperations in octogenarians*. Eur J Cardiothorac Surg, 1999. **15**(6): p. 809-15.
91. Im, Y.H., et al., *Heterozygous mice for the transforming growth factor-beta type II receptor gene have increased susceptibility to hepatocellular carcinogenesis*. Cancer Res, 2001. **61**(18): p. 6665-8.
92. Paik, S.Y., et al., *Expression of transforming growth factor-beta1 and transforming growth factor-beta receptors in hepatocellular carcinoma and dysplastic nodules*. Mod Pathol, 2003. **16**(1): p. 86-96.
93. Senturk, S., et al., *Transforming growth factor-beta induces senescence in hepatocellular carcinoma cells and inhibits tumor growth*. Hepatology, 2010.
94. Vivanco, I. and C.L. Sawyers, *The phosphatidylinositol 3-Kinase AKT pathway in human cancer*. Nat Rev Cancer, 2002. **2**(7): p. 489-501.
95. Wang, L., et al., *Epigenetic and genetic alterations of PTEN in hepatocellular carcinoma*. Hepatol Res, 2007. **37**(5): p. 389-396.
96. Villanueva, A., et al., *Pivotal role of mTOR signaling in hepatocellular carcinoma*. Gastroenterology, 2008. **135**(6): p. 1972-83, 1983 e1-11.
97. Bellacosa, A., et al., *Akt activation by growth factors is a multiple-step process: the role of the PH domain*. Oncogene, 1998. **17**(3): p. 313-25.

98. Schmitz, K.J., et al., *Activation of the ERK and AKT signalling pathway predicts poor prognosis in hepatocellular carcinoma and ERK activation in cancer tissue is associated with hepatitis C virus infection*. J Hepatol, 2008. **48**(1): p. 83-90.
99. Amaravadi, R. and C.B. Thompson, *The survival kinases Akt and Pim as potential pharmacological targets*. J Clin Invest, 2005. **115**(10): p. 2618-24.
100. Lee, T.K., et al., *FTY720 induces apoptosis of human hepatoma cell lines through PI3-K-mediated Akt dephosphorylation*. Carcinogenesis, 2004. **25**(12): p. 2397-405.
101. Huynh, H., et al., *RAD001 (everolimus) inhibits tumour growth in xenograft models of human hepatocellular carcinoma*. J Cell Mol Med, 2009. **13**(7): p. 1371-80.
102. Pang, J.Z., et al., *Loss of heterozygosity at D8S298 is a predictor for long-term survival of patients with tumor-node-metastasis stage I of hepatocellular carcinoma*. Clin Cancer Res, 2007. **13**(24): p. 7363-9.
103. Rizell, M., et al., *Effects of the mTOR inhibitor sirolimus in patients with hepatocellular and cholangiocellular cancer*. Int J Clin Oncol, 2008. **13**(1): p. 66-70.
104. Huynh, H., *Tyrosine kinase inhibitors to treat liver cancer*. Expert Opin Emerg Drugs, 2010. **15**(1): p. 13-26.
105. Hussain, S.P. and C.C. Harris, *p53 biological network: at the crossroads of the cellular-stress response pathway and molecular carcinogenesis*. J Nippon Med Sch, 2006. **73**(2): p. 54-64.
106. Lane, D.P., *Cancer. p53, guardian of the genome*. Nature, 1992. **358**(6381): p. 15-6.
107. Venkatachalam, S., et al., *Retention of wild-type p53 in tumors from p53 heterozygous mice: reduction of p53 dosage can promote cancer formation*. EMBO J, 1998. **17**(16): p. 4657-67.
108. Lynch, C.J. and J. Milner, *Loss of one p53 allele results in four-fold reduction of p53 mRNA and protein: a basis for p53 haplo-insufficiency*. Oncogene, 2006. **25**(24): p. 3463-70.
109. Vousden, K.H. and D.P. Lane, *p53 in health and disease*. Nat Rev Mol Cell Biol, 2007. **8**(4): p. 275-83.
110. Hollstein, M., et al., *p53 mutations in human cancers*. Science, 1991. **253**(5015): p. 49-53.
111. Iwakuma, T., G. Lozano, and E.R. Flores, *Li-Fraumeni syndrome: a p53 family affair*. Cell Cycle, 2005. **4**(7): p. 865-7.
112. Harms, K.L. and X. Chen, *The functional domains in p53 family proteins exhibit both common and distinct properties*. Cell Death Differ, 2006. **13**(6): p. 890-7.
113. Oliner, J.D., et al., *Oncoprotein MDM2 conceals the activation domain of tumour suppressor p53*. Nature, 1993. **362**(6423): p. 857-60.
114. Honda, R., H. Tanaka, and H. Yasuda, *Oncoprotein MDM2 is a ubiquitin ligase E3 for tumor suppressor p53*. FEBS Lett, 1997. **420**(1): p. 25-7.
115. Riley, T., et al., *Transcriptional control of human p53-regulated genes*. Nat Rev Mol Cell Biol, 2008. **9**(5): p. 402-12.
116. Bell, H.S., et al., *A p53-derived apoptotic peptide derepresses p73 to cause tumor regression in vivo*. J Clin Invest, 2007. **117**(4): p. 1008-18.
117. Hernandez-Boussard, T., et al., *IARC p53 mutation database: a relational database to compile and analyze p53 mutations in human tumors and cell*

- lines. International Agency for Research on Cancer. Hum Mutat, 1999. 14(1): p. 1-8.*
118. Soussi, T., *p53 alterations in human cancer: more questions than answers. Oncogene, 2007. 26(15): p. 2145-56.*
  119. Bykov, V.J., G. Selivanova, and K.G. Wiman, *Small molecules that reactivate mutant p53. Eur J Cancer, 2003. 39(13): p. 1828-34.*
  120. Cho, Y., et al., *Crystal structure of a p53 tumor suppressor-DNA complex: understanding tumorigenic mutations. Science, 1994. 265(5170): p. 346-55.*
  121. Bossi, G., et al., *Mutant p53 gain of function: reduction of tumor malignancy of human cancer cell lines through abrogation of mutant p53 expression. Oncogene, 2006. 25(2): p. 304-9.*
  122. Cadwell, C. and G.P. Zambetti, *The effects of wild-type p53 tumor suppressor activity and mutant p53 gain-of-function on cell growth. Gene, 2001. 277(1-2): p. 15-30.*
  123. Lang, G.A., et al., *Gain of function of a p53 hot spot mutation in a mouse model of Li-Fraumeni syndrome. Cell, 2004. 119(6): p. 861-72.*
  124. Olive, K.P., et al., *Mutant p53 gain of function in two mouse models of Li-Fraumeni syndrome. Cell, 2004. 119(6): p. 847-60.*
  125. Kastan, M.B. and E. Berkovich, *p53: a two-faced cancer gene. Nat Cell Biol, 2007. 9(5): p. 489-91.*
  126. Qin, L.X. and Z.Y. Tang, *The prognostic molecular markers in hepatocellular carcinoma. World J Gastroenterol, 2002. 8(3): p. 385-92.*
  127. Xue, W., et al., *Senescence and tumour clearance is triggered by p53 restoration in murine liver carcinomas. Nature, 2007. 445(7128): p. 656-60.*
  128. Teoh, N.C., et al., *Defective DNA strand break repair causes chromosomal instability and accelerates liver carcinogenesis in mice. Hepatology, 2008. 47(6): p. 2078-88.*
  129. Farazi, P.A., et al., *Differential impact of telomere dysfunction on initiation and progression of hepatocellular carcinoma. Cancer Res, 2003. 63(16): p. 5021-7.*
  130. Wiemann, S.U., et al., *Hepatocyte telomere shortening and senescence are general markers of human liver cirrhosis. FASEB J, 2002. 16(9): p. 935-42.*
  131. Plentz, R.R., et al., *Hepatocellular telomere shortening correlates with chromosomal instability and the development of human hepatoma. Hepatology, 2004. 40(1): p. 80-6.*
  132. Lund, A.H. and M. van Lohuizen, *Epigenetics and cancer. Genes Dev, 2004. 18(19): p. 2315-35.*
  133. Esteller, M., *Epigenetics in cancer. N Engl J Med, 2008. 358(11): p. 1148-59.*
  134. Kouzarides, T., *Chromatin modifications and their function. Cell, 2007. 128(4): p. 693-705.*
  135. Heintzman, N.D., et al., *Histone modifications at human enhancers reflect global cell-type-specific gene expression. Nature, 2009. 459(7243): p. 108-12.*
  136. Komashko, V.M., et al., *Using ChIP-chip technology to reveal common principles of transcriptional repression in normal and cancer cells. Genome Res, 2008. 18(4): p. 521-32.*
  137. Abbott, D.P. and N.A. Edmondson, *Neuronal ceroid-lipofuscin storage in a cynomolgus monkey (Macaca fascicularis). Lab Anim, 1983. 17(1): p. 18-20.*
  138. Ke, X.S., et al., *Genome-wide profiling of histone h3 lysine 4 and lysine 27 trimethylation reveals an epigenetic signature in prostate carcinogenesis. PLoS One, 2009. 4(3): p. e4687.*

139. Kondo, Y., et al., *Gene silencing in cancer by histone H3 lysine 27 trimethylation independent of promoter DNA methylation*. Nat Genet, 2008. **40**(6): p. 741-50.
140. Yu, J., et al., *A polycomb repression signature in metastatic prostate cancer predicts cancer outcome*. Cancer Res, 2007. **67**(22): p. 10657-63.
141. Wu, J., et al., *Diverse histone modifications on histone 3 lysine 9 and their relation to DNA methylation in specifying gene silencing*. BMC Genomics, 2007. **8**: p. 131.
142. Krivtsov, A.V., et al., *H3K79 methylation profiles define murine and human MLL-AF4 leukemias*. Cancer Cell, 2008. **14**(5): p. 355-68.
143. Fraga, M.F., et al., *Loss of acetylation at Lys16 and trimethylation at Lys20 of histone H4 is a common hallmark of human cancer*. Nat Genet, 2005. **37**(4): p. 391-400.
144. Pogribny, I.P., et al., *Histone H3 lysine 9 and H4 lysine 20 trimethylation and the expression of Suv4-20h2 and Suv-39h1 histone methyltransferases in hepatocarcinogenesis induced by methyl deficiency in rats*. Carcinogenesis, 2006. **27**(6): p. 1180-6.
145. Boffetta, P. and M. Hashibe, *Alcohol and cancer*. Lancet Oncol, 2006. **7**(2): p. 149-56.
146. Donato, F., et al., *Southern Europe as an example of interaction between various environmental factors: a systematic review of the epidemiologic evidence*. Oncogene, 2006. **25**(27): p. 3756-70.
147. Kuper, H., et al., *The risk of liver and bile duct cancer in patients with chronic viral hepatitis, alcoholism, or cirrhosis*. Hepatology, 2001. **34**(4 Pt 1): p. 714-8.
148. Ekstrom, G. and M. Ingelman-Sundberg, *Rat liver microsomal NADPH-supported oxidase activity and lipid peroxidation dependent on ethanol-inducible cytochrome P-450 (P-450IIE1)*. Biochem Pharmacol, 1989. **38**(8): p. 1313-9.
149. Albano, E., S.W. French, and M. Ingelman-Sundberg, *Hydroxyethyl radicals in ethanol hepatotoxicity*. Front Biosci, 1999. **4**: p. D533-40.
150. Dreosti, I.E., et al., *The effect of ethanol and acetaldehyde on DNA synthesis in growing cells and on fetal development in the rat*. Alcohol Clin Exp Res, 1981. **5**(3): p. 357-62.
151. Sun, A.Y., et al., *Ethanol and oxidative stress*. Alcohol Clin Exp Res, 2001. **25**(5 Suppl ISBRA): p. 237S-243S.
152. Lieber, C.S., *Biochemical mechanisms of alcohol-induced hepatic injury*. Alcohol Alcohol Suppl, 1991. **1**: p. 283-90.
153. McKillop, I.H. and L.W. Schrum, *Alcohol and liver cancer*. Alcohol, 2005. **35**(3): p. 195-203.
154. Caldwell, S.H., et al., *Obesity and hepatocellular carcinoma*. Gastroenterology, 2004. **127**(5 Suppl 1): p. S97-103.
155. Bugianesi, E., et al., *Expanding the natural history of nonalcoholic steatohepatitis: from cryptogenic cirrhosis to hepatocellular carcinoma*. Gastroenterology, 2002. **123**(1): p. 134-40.
156. Wolk, A., et al., *A prospective study of obesity and cancer risk (Sweden)*. Cancer Causes Control, 2001. **12**(1): p. 13-21.
157. Bugianesi, E., *Non-alcoholic steatohepatitis and cancer*. Clin Liver Dis, 2007. **11**(1): p. 191-207, x-xi.

158. Navarro-Alarcon, M., et al., *Selenium concentrations in serum of individuals with liver diseases (cirrhosis or hepatitis): relationship with some nutritional and biochemical markers*. *Sci Total Environ*, 2002. **291**(1-3): p. 135-41.
159. Bellinger, F.P., et al., *Regulation and function of selenoproteins in human disease*. *Biochem J*, 2009. **422**(1): p. 11-22.
160. Hartikainen, H., *Biogeochemistry of selenium and its impact on food chain quality and human health*. *J Trace Elem Med Biol*, 2005. **18**(4): p. 309-18.
161. Caurant, F., M. Navarro, and J.C. Amiard, *Mercury in pilot whales: possible limits to the detoxification process*. *Sci Total Environ*, 1996. **186**(1-2): p. 95-104.
162. Thorne, M.C., *Estimation of animal transfer factors for radioactive isotopes of iodine, technetium, selenium and uranium*. *J Environ Radioact*, 2003. **70**(1-2): p. 3-20.
163. Cabanero, A.I., Y. Madrid, and C. Camara, *Mercury-selenium species ratio in representative fish samples and their bioaccessibility by an in vitro digestion method*. *Biol Trace Elem Res*, 2007. **119**(3): p. 195-211.
164. Kibriya, M.G., et al., *Changes in gene expression profiles in response to selenium supplementation among individuals with arsenic-induced pre-malignant skin lesions*. *Toxicol Lett*, 2007. **169**(2): p. 162-76.
165. Mousa, S.A., et al., *Pro-angiogenesis action of arsenic and its reversal by selenium-derived compounds*. *Carcinogenesis*, 2007. **28**(5): p. 962-7.
166. Beck, M.A. and C.C. Matthews, *Micronutrients and host resistance to viral infection*. *Proc Nutr Soc*, 2000. **59**(4): p. 581-5.
167. Beck, M.A., et al., *Selenium deficiency increases the pathology of an influenza virus infection*. *FASEB J*, 2001. **15**(8): p. 1481-3.
168. Beck, M.A., et al., *Benign human enterovirus becomes virulent in selenium-deficient mice*. *J Med Virol*, 1994. **43**(2): p. 166-70.
169. Hori, K., et al., *Selenium supplementation suppresses tumor necrosis factor alpha-induced human immunodeficiency virus type 1 replication in vitro*. *AIDS Res Hum Retroviruses*, 1997. **13**(15): p. 1325-32.
170. Goldstein, B.J., et al., *Role of insulin-induced reactive oxygen species in the insulin signaling pathway*. *Antioxid Redox Signal*, 2005. **7**(7-8): p. 1021-31.
171. Dizdaroglu, M., *Oxidative damage to DNA in mammalian chromatin*. *Mutat Res*, 1992. **275**(3-6): p. 331-42.
172. Papp, L.V., et al., *From selenium to selenoproteins: synthesis, identity, and their role in human health*. *Antioxid Redox Signal*, 2007. **9**(7): p. 775-806.
173. Maiorino, M., et al., *Probing the presumed catalytic triad of selenium-containing peroxidases by mutational analysis of phospholipid hydroperoxide glutathione peroxidase (PHGPx)*. *Biol Chem Hoppe Seyler*, 1995. **376**(11): p. 651-60.
174. Gladyshev, V.N., K.T. Jeang, and T.C. Stadtman, *Selenocysteine, identified as the penultimate C-terminal residue in human T-cell thioredoxin reductase, corresponds to TGA in the human placental gene*. *Proc Natl Acad Sci U S A*, 1996. **93**(12): p. 6146-51.
175. Brigelius-Flohe, R., *Tissue-specific functions of individual glutathione peroxidases*. *Free Radic Biol Med*, 1999. **27**(9-10): p. 951-65.
176. Bjornstedt, M., S. Kumar, and A. Holmgren, *Selenite and selenodiglutathione: reactions with thioredoxin systems*. *Methods Enzymol*, 1995. **252**: p. 209-19.
177. Zhong, L., E.S. Arner, and A. Holmgren, *Structure and mechanism of mammalian thioredoxin reductase: the active site is a redox-active*

- selenolthiol/selenenylsulfide formed from the conserved cysteine-selenocysteine sequence.* Proc Natl Acad Sci U S A, 2000. **97**(11): p. 5854-9.
178. Rubartelli, A., et al., *Secretion of thioredoxin by normal and neoplastic cells through a leaderless secretory pathway.* J Biol Chem, 1992. **267**(34): p. 24161-4.
  179. Rhee, S.G., H.Z. Chae, and K. Kim, *Peroxiredoxins: a historical overview and speculative preview of novel mechanisms and emerging concepts in cell signaling.* Free Radic Biol Med, 2005. **38**(12): p. 1543-52.
  180. Claycombe, K.J. and S.N. Meydani, *Vitamin E and genome stability.* Mutat Res, 2001. **475**(1-2): p. 37-44.
  181. Jackson, M.I. and G.F. Combs, Jr., *Selenium and anticarcinogenesis: underlying mechanisms.* Curr Opin Clin Nutr Metab Care, 2008. **11**(6): p. 718-26.
  182. Squires, J. and M.J. Berry, *Selenium, selenoproteins, and cancer.* Hawaii Med J, 2006. **65**(8): p. 239-40.
  183. Foster, C.B., et al., *Polymorphism analysis of six selenoprotein genes: support for a selective sweep at the glutathione peroxidase 1 locus (3p21) in Asian populations.* BMC Genet, 2006. **7**: p. 56.
  184. Hu, Y., et al., *Allelic loss of the gene for the GPX1 selenium-containing protein is a common event in cancer.* J Nutr, 2005. **135**(12 Suppl): p. 3021S-3024S.
  185. Hu, Y.J. and A.M. Diamond, *Role of glutathione peroxidase 1 in breast cancer: loss of heterozygosity and allelic differences in the response to selenium.* Cancer Res, 2003. **63**(12): p. 3347-51.
  186. Al-Taie, O.H., et al., *Expression profiling and genetic alterations of the selenoproteins GI-GPx and SePP in colorectal carcinogenesis.* Nutr Cancer, 2004. **48**(1): p. 6-14.
  187. Bermano, G., et al., *Evidence that a polymorphism within the 3'UTR of glutathione peroxidase 4 is functional and is associated with susceptibility to colorectal cancer.* Genes Nutr, 2007. **2**(2): p. 225-32.
  188. Jablonska, E., et al., *Association between GPx1 Pro198Leu polymorphism, GPx1 activity and plasma selenium concentration in humans.* Eur J Nutr, 2009. **48**(6): p. 383-6.
  189. Diwadkar-Navsariwala, V. and A.M. Diamond, *The link between selenium and chemoprevention: a case for selenoproteins.* J Nutr, 2004. **134**(11): p. 2899-902.
  190. Geoghegan, M., et al., *Selenium in critical illness.* Curr Opin Crit Care, 2006. **12**(2): p. 136-41.
  191. Berry, M.J., et al., *Selenocysteine incorporation directed from the 3'UTR: characterization of eukaryotic EFsec and mechanistic implications.* Biofactors, 2001. **14**(1-4): p. 17-24.
  192. Czuczejko, J., et al., *Selenium, glutathione and glutathione peroxidases in blood of patients with chronic liver diseases.* Acta Biochim Pol, 2003. **50**(4): p. 1147-54.
  193. Navarro-Alarcon, M. and C. Cabrera-Vique, *Selenium in food and the human body: a review.* Sci Total Environ, 2008. **400**(1-3): p. 115-41.
  194. Yu, S.Y., Y.J. Zhu, and W.G. Li, *Protective role of selenium against hepatitis B virus and primary liver cancer in Qidong.* Biol Trace Elem Res, 1997. **56**(1): p. 117-24.

195. Nakabayashi, H., et al., *Growth of human hepatoma cells lines with differentiated functions in chemically defined medium*. *Cancer Res*, 1982. **42**(9): p. 3858-63.
196. Baker, R.D., et al., *Selenium regulation of glutathione peroxidase in human hepatoma cell line Hep3B*. *Arch Biochem Biophys*, 1993. **304**(1): p. 53-7.
197. Irmak, M.B., et al., *Acquired tolerance of hepatocellular carcinoma cells to selenium deficiency: a selective survival mechanism?* *Cancer Res*, 2003. **63**(20): p. 6707-15.
198. Clark, L.C., et al., *Effects of selenium supplementation for cancer prevention in patients with carcinoma of the skin. A randomized controlled trial. Nutritional Prevention of Cancer Study Group*. *JAMA*, 1996. **276**(24): p. 1957-63.
199. Combs, G.F., Jr., *Chemopreventive mechanisms of selenium*. *Med Klin (Munich)*, 1999. **94 Suppl 3**: p. 18-24.
200. Martindale, J.L. and N.J. Holbrook, *Cellular response to oxidative stress: signaling for suicide and survival*. *J Cell Physiol*, 2002. **192**(1): p. 1-15.
201. Kim, I.Y. and T.C. Stadtman, *Inhibition of NF-kappaB DNA binding and nitric oxide induction in human T cells and lung adenocarcinoma cells by selenite treatment*. *Proc Natl Acad Sci U S A*, 1997. **94**(24): p. 12904-7.
202. Park, H.S., et al., *Selenite inhibits the c-Jun N-terminal kinase/stress-activated protein kinase (JNK/SAPK) through a thiol redox mechanism*. *J Biol Chem*, 2000. **275**(4): p. 2527-31.
203. Park, H.S., et al., *Selenite negatively regulates caspase-3 through a redox mechanism*. *J Biol Chem*, 2000. **275**(12): p. 8487-91.
204. Yoon, S.O., et al., *Selenite suppresses hydrogen peroxide-induced cell apoptosis through inhibition of ASK1/JNK and activation of PI3-K/Akt pathways*. *FASEB J*, 2002. **16**(1): p. 111-3.
205. Lee, Y.C., et al., *Selenite-induced survival of HuH7 hepatoma cells involves activation of focal adhesion kinase-phosphatidylinositol 3-kinase-Akt pathway and Rac1*. *J Biol Chem*, 2003. **278**(41): p. 39615-24.
206. *IARC monographs on the evaluation of carcinogenic risks to humans. Volume 97. 1,3-butadiene, ethylene oxide and vinyl halides (vinyl fluoride, vinyl chloride and vinyl bromide)*. *IARC Monogr Eval Carcinog Risks Hum*, 2008. **97**: p. 3-471.
207. *Cumulative Index to IARC monographs on the evaluation of the carcinogenic risk of chemicals to humans*. *IARC Monogr Eval Carcinog Risk Chem Hum*, 1986. **39**: p. 379-403.
208. Chen, C.J., et al., *Cancer potential in liver, lung, bladder and kidney due to ingested inorganic arsenic in drinking water*. *Br J Cancer*, 1992. **66**(5): p. 888-92.
209. Vainio, H., E. Heseltine, and J. Wilbourn, *Report on an IARC working group meeting on some naturally occurring substances*. *Int J Cancer*, 1993. **53**(4): p. 535-7.
210. Puisieux, A., et al., *Selective targeting of p53 gene mutational hotspots in human cancers by etiologically defined carcinogens*. *Cancer Res*, 1991. **51**(22): p. 6185-9.
211. Barbin, A., et al., *p53 gene mutation pattern in rat liver tumors induced by vinyl chloride*. *Cancer Res*, 1997. **57**(9): p. 1695-8.
212. Bressac, B., et al., *Selective G to T mutations of p53 gene in hepatocellular carcinoma from southern Africa*. *Nature*, 1991. **350**(6317): p. 429-31.

213. Hsu, I.C., et al., *Mutational hotspot in the p53 gene in human hepatocellular carcinomas*. Nature, 1991. **350**(6317): p. 427-8.
214. Lee, Y.I., et al., *Activation of the insulin-like growth factor II transcription by aflatoxin B1 induced p53 mutant 249 is caused by activation of transcription complexes; implications for a gain-of-function during the formation of hepatocellular carcinoma*. Oncogene, 2000. **19**(33): p. 3717-26.
215. Busby, W.F., Jr., et al., *Tumorigenicity of fluoranthene in a newborn mouse lung adenoma bioassay*. Carcinogenesis, 1984. **5**(10): p. 1311-6.
216. Galvano, F., et al., *Survey of the occurrence of aflatoxin M1 in dairy products marketed in Italy: second year of observation*. Food Addit Contam, 2001. **18**(7): p. 644-6.
217. Wild, C.P. and Y.Y. Gong, *Mycotoxins and human disease: a largely ignored global health issue*. Carcinogenesis, 2010. **31**(1): p. 71-82.
218. Liu, Y. and F. Wu, *Global burden of aflatoxin-induced hepatocellular carcinoma: a risk assessment*. Environ Health Perspect, 2010. **118**(6): p. 818-24.
219. Wild, C.P. and R. Montesano, *A model of interaction: aflatoxins and hepatitis viruses in liver cancer aetiology and prevention*. Cancer Lett, 2009. **286**(1): p. 22-8.
220. Smela, M.E., et al., *The chemistry and biology of aflatoxin B(1): from mutational spectrometry to carcinogenesis*. Carcinogenesis, 2001. **22**(4): p. 535-45.
221. Croy, R.G. and G.N. Wogan, *Temporal patterns of covalent DNA adducts in rat liver after single and multiple doses of aflatoxin B1*. Cancer Res, 1981. **41**(1): p. 197-203.
222. Smela, M.E., et al., *The aflatoxin B(1) formamidopyrimidine adduct plays a major role in causing the types of mutations observed in human hepatocellular carcinoma*. Proc Natl Acad Sci U S A, 2002. **99**(10): p. 6655-60.
223. Shen, H.M., et al., *Aflatoxin B1-induced 8-hydroxydeoxyguanosine formation in rat hepatic DNA*. Carcinogenesis, 1995. **16**(2): p. 419-22.
224. Yarborough, A., et al., *Immunoperoxidase detection of 8-hydroxydeoxyguanosine in aflatoxin B1-treated rat liver and human oral mucosal cells*. Cancer Res, 1996. **56**(4): p. 683-8.
225. Wang, J.S. and J.D. Groopman, *DNA damage by mycotoxins*. Mutat Res, 1999. **424**(1-2): p. 167-81.
226. Foster, P.L., E. Eisenstadt, and J.H. Miller, *Base substitution mutations induced by metabolically activated aflatoxin B1*. Proc Natl Acad Sci U S A, 1983. **80**(9): p. 2695-8.
227. Loechler, E.L., *A violation of the Swain-Scott principle, and not SN1 versus SN2 reaction mechanisms, explains why carcinogenic alkylating agents can form different proportions of adducts at oxygen versus nitrogen in DNA*. Chem Res Toxicol, 1994. **7**(3): p. 277-80.
228. Bedard, L.L. and T.E. Massey, *Aflatoxin B1-induced DNA damage and its repair*. Cancer Lett, 2006. **241**(2): p. 174-83.
229. Ozturk, M., *p53 mutation in hepatocellular carcinoma after aflatoxin exposure*. Lancet, 1991. **338**(8779): p. 1356-9.
230. Aguilar, F., et al., *Geographic variation of p53 mutational profile in nonmalignant human liver*. Science, 1994. **264**(5163): p. 1317-9.



231. Kirk, G.D., et al., *249(ser) TP53 mutation in plasma DNA, hepatitis B viral infection, and risk of hepatocellular carcinoma*. *Oncogene*, 2005. **24**(38): p. 5858-67.
232. Bullock, A.N., J. Henckel, and A.R. Fersht, *Quantitative analysis of residual folding and DNA binding in mutant p53 core domain: definition of mutant states for rescue in cancer therapy*. *Oncogene*, 2000. **19**(10): p. 1245-56.
233. Song, H., M. Hollstein, and Y. Xu, *p53 gain-of-function cancer mutants induce genetic instability by inactivating ATM*. *Nat Cell Biol*, 2007. **9**(5): p. 573-80.
234. Finlay, C.A., P.W. Hinds, and A.J. Levine, *The p53 proto-oncogene can act as a suppressor of transformation*. *Cell*, 1989. **57**(7): p. 1083-93.
235. Hinds, P.W., et al., *Mutant p53 DNA clones from human colon carcinomas cooperate with ras in transforming primary rat cells: a comparison of the "hot spot" mutant phenotypes*. *Cell Growth Differ*, 1990. **1**(12): p. 571-80.
236. Preuss, U., R. Kreutzfeld, and K.H. Scheidtmann, *Tumor-derived p53 mutant C174Y is a gain-of-function mutant which activates the fos promoter and enhances colony formation*. *Int J Cancer*, 2000. **88**(2): p. 162-71.
237. Ponchel, F., et al., *Hepatocarcinoma-specific mutant p53-249ser induces mitotic activity but has no effect on transforming growth factor beta 1-mediated apoptosis*. *Cancer Res*, 1994. **54**(8): p. 2064-8.
238. Ghebranious, N. and S. Sell, *The mouse equivalent of the human p53ser249 mutation p53ser246 enhances aflatoxin hepatocarcinogenesis in hepatitis B surface antigen transgenic and p53 heterozygous null mice*. *Hepatology*, 1998. **27**(4): p. 967-73.
239. Schleger, C., et al., *The human p53 gene mutated at position 249 per se is not sufficient to immortalize human liver cells*. *Hepatology*, 1999. **29**(3): p. 834-8.
240. Yin, L., et al., *Control of mouse hepatocyte proliferation and ploidy by p53 and p53ser246 mutation in vivo*. *Hepatology*, 1998. **27**(1): p. 73-80.
241. Shi, H., et al., *In vitro and in vivo cytotoxic effects of PRIMA-1 on hepatocellular carcinoma cells expressing mutant p53ser249*. *Carcinogenesis*, 2008. **29**(7): p. 1428-34.
242. Bykov, V.J., et al., *Restoration of the tumor suppressor function to mutant p53 by a low-molecular-weight compound*. *Nat Med*, 2002. **8**(3): p. 282-8.
243. Hulla, J.E., Z.Y. Chen, and D.L. Eaton, *Aflatoxin B1-induced rat hepatic hyperplastic nodules do not exhibit a site-specific mutation within the p53 gene*. *Cancer Res*, 1993. **53**(1): p. 9-11.
244. Tong, W.M., et al., *Aflatoxin-B exposure does not lead to p53 mutations but results in enhanced liver cancer of Hupki (human p53 knock-in) mice*. *Int J Cancer*, 2006. **119**(4): p. 745-9.
245. Lee, M.K. and K. Sabapathy, *The R246S hot-spot p53 mutant exerts dominant-negative effects in embryonic stem cells in vitro and in vivo*. *J Cell Sci*, 2008. **121**(Pt 11): p. 1899-906.
246. Sancar, A., et al., *Molecular mechanisms of mammalian DNA repair and the DNA damage checkpoints*. *Annu Rev Biochem*, 2004. **73**: p. 39-85.
247. Lobrich, M. and P.A. Jeggo, *The impact of a negligent G2/M checkpoint on genomic instability and cancer induction*. *Nat Rev Cancer*, 2007. **7**(11): p. 861-9.
248. Oleykowski, C.A., et al., *Repair of aflatoxin B1 DNA adducts by the UvrABC endonuclease of Escherichia coli*. *J Biol Chem*, 1993. **268**(11): p. 7990-8002.

249. Guo, Y., et al., *Expression of a human cytochrome p450 in yeast permits analysis of pathways for response to and repair of aflatoxin-induced DNA damage*. Mol Cell Biol, 2005. **25**(14): p. 5823-33.
250. Keller-Seitz, M.U., et al., *Transcriptional response of yeast to aflatoxin B1: recombinational repair involving RAD51 and RAD1*. Mol Biol Cell, 2004. **15**(9): p. 4321-36.
251. Leadon, S.A., R.M. Tyrrell, and P.A. Cerutti, *Excision repair of aflatoxin B1-DNA adducts in human fibroblasts*. Cancer Res, 1981. **41**(12 Pt 1): p. 5125-9.
252. Levy, D.D., et al., *Sequence specificity of aflatoxin B1-induced mutations in a plasmid replicated in xeroderma pigmentosum and DNA repair proficient human cells*. Cancer Res, 1992. **52**(20): p. 5668-73.
253. Friedberg, E.C., R. Wagner, and M. Radman, *Specialized DNA polymerases, cellular survival, and the genesis of mutations*. Science, 2002. **296**(5573): p. 1627-30.
254. Bedard, L.L., et al., *Susceptibility to aflatoxin B1-induced carcinogenesis correlates with tissue-specific differences in DNA repair activity in mouse and in rat*. Cancer Res, 2005. **65**(4): p. 1265-70.
255. Bailey, E.A., et al., *Mutational properties of the primary aflatoxin B1-DNA adduct*. Proc Natl Acad Sci U S A, 1996. **93**(4): p. 1535-9.
256. Cagatay, T. and M. Ozturk, *P53 mutation as a source of aberrant beta-catenin accumulation in cancer cells*. Oncogene, 2002. **21**(52): p. 7971-80.
257. Bunz, F., et al., *Requirement for p53 and p21 to sustain G2 arrest after DNA damage*. Science, 1998. **282**(5393): p. 1497-501.
258. Dreiem, A. and F. Fonnum, *Thiophene is toxic to cerebellar granule cells in culture after bioactivation by rat liver enzymes*. Neurotoxicology, 2004. **25**(6): p. 959-66.
259. Erexson, G.L., M.V. Periago, and C.S. Spicer, *Differential sensitivity of Chinese hamster V79 and Chinese hamster ovary (CHO) cells in the in vitro micronucleus screening assay*. Mutat Res, 2001. **495**(1-2): p. 75-80.
260. Dimri, G.P., et al., *A biomarker that identifies senescent human cells in culture and in aging skin in vivo*. Proc Natl Acad Sci U S A, 1995. **92**(20): p. 9363-7.
261. Hsieh, L.L., et al., *Immunological detection of aflatoxin B1-DNA adducts formed in vivo*. Cancer Res, 1988. **48**(22): p. 6328-31.
262. Olive, P.L. and J.P. Banath, *Detection of DNA double-strand breaks through the cell cycle after exposure to X-rays, bleomycin, etoposide and 125IdUrd*. Int J Radiat Biol, 1993. **64**(4): p. 349-58.
263. Olive, P.L., et al., *Gel electrophoresis of individual cells to quantify hypoxic fraction in human breast cancers*. Cancer Res, 1993. **53**(4): p. 733-6.
264. Chandna, S., *Single-cell gel electrophoresis assay monitors precise kinetics of DNA fragmentation induced during programmed cell death*. Cytometry A, 2004. **61**(2): p. 127-33.
265. Klaunig, J.E. and L.M. Kamendulis, *The role of oxidative stress in carcinogenesis*. Annu Rev Pharmacol Toxicol, 2004. **44**: p. 239-67.
266. Kim, H.S. and M.S. Lee, *Essential role of STAT1 in caspase-independent cell death of activated macrophages through the p38 mitogen-activated protein kinase/STAT1/reactive oxygen species pathway*. Mol Cell Biol, 2005. **25**(15): p. 6821-33.
267. Boyault, S., et al., *Transcriptome classification of HCC is related to gene alterations and to new therapeutic targets*. Hepatology, 2007. **45**(1): p. 42-52.

268. Cooray, S., *The pivotal role of phosphatidylinositol 3-kinase-Akt signal transduction in virus survival*. J Gen Virol, 2004. **85**(Pt 5): p. 1065-76.
269. Ozes, O.N., et al., *NF-kappaB activation by tumour necrosis factor requires the Akt serine-threonine kinase*. Nature, 1999. **401**(6748): p. 82-5.
270. el-Deiry, W.S., et al., *WAF1, a potential mediator of p53 tumor suppression*. Cell, 1993. **75**(4): p. 817-25.
271. el-Deiry, W.S., et al., *WAF1/CIP1 is induced in p53-mediated G1 arrest and apoptosis*. Cancer Res, 1994. **54**(5): p. 1169-74.
272. Waldman, T., K.W. Kinzler, and B. Vogelstein, *p21 is necessary for the p53-mediated G1 arrest in human cancer cells*. Cancer Res, 1995. **55**(22): p. 5187-90.
273. Schwartz, J.D. and A.S. Beutler, *Therapy for unresectable hepatocellular carcinoma: review of the randomized clinical trials-II: systemic and local non-embolization-based therapies in unresectable and advanced hepatocellular carcinoma*. Anticancer Drugs, 2004. **15**(5): p. 439-52.
274. Gewirtz, D.A., *A critical evaluation of the mechanisms of action proposed for the antitumor effects of the anthracycline antibiotics adriamycin and daunorubicin*. Biochem Pharmacol, 1999. **57**(7): p. 727-41.
275. Park, S.S., Y.W. Eom, and K.S. Choi, *Cdc2 and Cdk2 play critical roles in low dose doxorubicin-induced cell death through mitotic catastrophe but not in high dose doxorubicin-induced apoptosis*. Biochem Biophys Res Commun, 2005. **334**(4): p. 1014-21.
276. Soini, Y., et al., *An aflatoxin-associated mutational hotspot at codon 249 in the p53 tumor suppressor gene occurs in hepatocellular carcinomas from Mexico*. Carcinogenesis, 1996. **17**(5): p. 1007-12.
277. Newberne, P.M. and G.N. Wogan, *Sequential morphologic changes in aflatoxin B carcinogenesis in the rat*. Cancer Res, 1968. **28**(4): p. 770-81.
278. Aguilar, F., S.P. Hussain, and P. Cerutti, *Aflatoxin B1 induces the transversion of G-->T in codon 249 of the p53 tumor suppressor gene in human hepatocytes*. Proc Natl Acad Sci U S A, 1993. **90**(18): p. 8586-90.
279. Besaratinia, A., et al., *In vitro recapitulating of TP53 mutagenesis in hepatocellular carcinoma associated with dietary aflatoxin B1 exposure*. Gastroenterology, 2009. **137**(3): p. 1127-37, 1137 e1-5.
280. Rayman, M.P., *The importance of selenium to human health*. Lancet, 2000. **356**(9225): p. 233-41.
281. Duffield-Lillico, A.J., et al., *Selenium supplementation, baseline plasma selenium status and incidence of prostate cancer: an analysis of the complete treatment period of the Nutritional Prevention of Cancer Trial*. BJU Int, 2003. **91**(7): p. 608-12.
282. Duffield-Lillico, A.J., et al., *Selenium supplementation and secondary prevention of nonmelanoma skin cancer in a randomized trial*. J Natl Cancer Inst, 2003. **95**(19): p. 1477-81.
283. Yoshizawa, K., et al., *Study of prediagnostic selenium level in toenails and the risk of advanced prostate cancer*. J Natl Cancer Inst, 1998. **90**(16): p. 1219-24.
284. Knekt, P., et al., *Is low selenium status a risk factor for lung cancer?* Am J Epidemiol, 1998. **148**(10): p. 975-82.
285. Willett, W.C., et al., *Prediagnostic serum selenium and risk of cancer*. Lancet, 1983. **2**(8342): p. 130-4.

286. Corrocher, R., et al., *Reduction of liver glutathione peroxidase activity and deficiency of serum selenium in patients with hepatocellular carcinoma*. Tumori, 1986. **72**(6): p. 617-9.
287. Chandra, J., A. Samali, and S. Orrenius, *Triggering and modulation of apoptosis by oxidative stress*. Free Radic Biol Med, 2000. **29**(3-4): p. 323-33.
288. Hyslop, P.A., et al., *Mechanisms of oxidant-mediated cell injury. The glycolytic and mitochondrial pathways of ADP phosphorylation are major intracellular targets inactivated by hydrogen peroxide*. J Biol Chem, 1988. **263**(4): p. 1665-75.
289. Toyokuni, S., et al., *Persistent oxidative stress in cancer*. FEBS Lett, 1995. **358**(1): p. 1-3.
290. Lieber, C.S., *Role of oxidative stress and antioxidant therapy in alcoholic and nonalcoholic liver diseases*. Adv Pharmacol, 1997. **38**: p. 601-28.
291. Voisin, L., et al., *Activation of MEK1 or MEK2 isoform is sufficient to fully transform intestinal epithelial cells and induce the formation of metastatic tumors*. BMC Cancer, 2008. **8**: p. 337.
292. Balmano, K. and S.J. Cook, *Tumour cell survival signalling by the ERK1/2 pathway*. Cell Death Differ, 2009. **16**(3): p. 368-77.
293. Schubbert, S., K. Shannon, and G. Bollag, *Hyperactive Ras in developmental disorders and cancer*. Nat Rev Cancer, 2007. **7**(4): p. 295-308.
294. Huang, H.M., C.J. Huang, and J.J. Yen, *Mcl-1 is a common target of stem cell factor and interleukin-5 for apoptosis prevention activity via MEK/MAPK and PI-3K/Akt pathways*. Blood, 2000. **96**(5): p. 1764-71.
295. Groopman, J.D., T.W. Kensler, and C.P. Wild, *Protective interventions to prevent aflatoxin-induced carcinogenesis in developing countries*. Annu Rev Public Health, 2008. **29**: p. 187-203.
296. Ellinger-Ziegelbauer, H., et al., *Characteristic expression profiles induced by genotoxic carcinogens in rat liver*. Toxicol Sci, 2004. **77**(1): p. 19-34.

## BASIC STUDIES

**Aflatoxin genotoxicity is associated with a defective DNA damage response bypassing p53 activation**Ozge Gursoy-Yuzugullu<sup>1,2</sup>, Haluk Yuzugullu<sup>1,2</sup>, Mustafa Yilmaz<sup>2</sup> and Mehmet Ozturk<sup>1,2</sup><sup>1</sup> Centre de Recherche INSERM, Institut Albert Bonniot, Université Joseph Fourier U823, Grenoble, France<sup>2</sup> Department of Molecular Biology and Genetics, BilGen Genetics and Biotechnology Research Center, Bilkent University, Ankara, Turkey**Keywords**

aflatoxin – checkpoint – DNA damage response – liver cancer – p53

**Abbreviations**AFB1, aflatoxin B<sub>1</sub>; DMSO, dimethyl sulphoxide; HCC, hepatocellular carcinoma.**Correspondence**

Mehmet Ozturk, PhD, Centre de Recherche INSERM/UJF U823, Institut Albert Bonniot, Université Joseph Fourier U823, Grenoble, France

Tel: +33476549410

Fax: +33476549413

e-mail: ozturkm@ujf-grenoble.fr

Received 14 September 2010

Accepted 10 January 2011

DOI:10.1111/j.1478-3223.2011.02474.x

**Abstract**

**Background:** Hepatocellular carcinoma (HCC) is a leading cause of cancer deaths. Aflatoxins, which may play a causative role in 5–28% of HCCs worldwide, are activated in liver cells and induce principally G → T mutations, including the TP53 codon 249(G → T) hotspot mutation. The DNA damage checkpoint response acts as an antitumour mechanism against genotoxic agents, but its role in aflatoxin-induced DNA damage is unknown. **Aim:** We studied the DNA damage checkpoint response of human cells to aflatoxin B<sub>1</sub> (AFB<sub>1</sub>). **Methods and results:** The treatment of HepG2 hepatoma cells with mutation-inducing doses (3–5 μmol/l) of AFB<sub>1</sub> induced DNA adducts, 8-hydroxyguanine lesions and DNA strand breaks that lasted several days. Persistent phospho-H2AX and 53BP1 foci were also detected, but cell growth was not affected. AFB<sub>1</sub>-exposed HepG2 cells formed phospho-H2AX and 53BP1 foci, but failed to phosphorylate both Chk1 and Chk2. Huh7 hepatoma and HCT116 colorectal cancer cell lines also exhibited a similarly incomplete checkpoint response. p53 phosphorylation also failed, and AFB<sub>1</sub>-exposed cells did not show p53-dependent G1 arrest or a sustained G2/M arrest. These observations contrasted sharply with the fully functional DNA damage response of cells to Adriamycin. Cotreatment of cells with AFB<sub>1</sub> did not inhibit p53 and p21<sup>CIP1</sup> accumulation induced by Adriamycin. Thus, the deficient checkpoint response to AFB<sub>1</sub> was not due to an inhibitory effect, but could be explained by an inefficient activation. **Conclusion:** Genotoxic doses of AFB<sub>1</sub> induce an incomplete and inefficient checkpoint response in human cells. This defective response may contribute to the mutagenic and carcinogenic potencies of aflatoxins.

More than 600 000 people die each year from hepatocellular carcinoma (HCC), mostly (> 80%) in developing countries (1). Dietary exposure to aflatoxins and infection with the hepatitis B virus are the major risk factors for HCC, the most frequent liver cancer in these areas (2). According to a recent study, about 25 200–155 000 of global HCCs may be attributable to aflatoxin exposure. Most cases occur in sub-Saharan Africa, Southeast Asia and China, where populations suffer both from a high hepatitis B virus prevalence and largely uncontrolled aflatoxin exposure in food. Thus, aflatoxins may play a causative role in 5–28% of all global HCC cases (3).

Aflatoxins are potent liver toxins, lethal when consumed in large doses. Sublethal exposures can induce chronic toxicity, and low levels of chronic exposure can result in neoplasia, primarily HCC, in many animal species (4). Aflatoxin exposure in humans may occur at high or low levels, depending on the level of dietary *Aspergillus* contamination. Acute exposure to high levels leads to lethal aflatoxicosis associated with liver necrosis. Chronic exposure to low levels of aflatoxin is not lethal, but highly hepatocarcinogenic. Acute exposure to high levels of aflatoxins (> 20 μg/kg/day) with aflatoxicosis rarely occurs (5).


In contrast, > 90% of people at a high risk for aflatoxin-caused HCC are exposed to very low doses (0.01–0.3 μg/kg/day), but the exposition is chronic (3, 5).

Aflatoxin B<sub>1</sub> (AFB<sub>1</sub>), the major aflatoxin product, is metabolized mainly in the liver to AFB<sub>1</sub>-8,9-*exo*-epoxide and 8,9-*endo*-epoxide. The *exo*-epoxide form of AFB<sub>1</sub> binds to DNA to form the predominant 8,9-dihydro-8-(N7-guanyl)-9-hydroxy AFB<sub>1</sub> adduct, leading to a more stable imidazole ring-opened AFB<sub>1</sub>-formamidopyrimidine adduct (5). The pseudo-half-life for loss of 8,9-dihydro-8-(N7-guanyl)-9-hydroxy AFB<sub>1</sub> is short, but AFB<sub>1</sub>-formamidopyrimidine adducts are stable, accumulate for several days and remain detectable for several weeks in rat liver (6, 7). The initial 8,9-dihydro-8-(N7-guanyl)-9-hydroxy AFB<sub>1</sub> adduct and AFB<sub>1</sub>-formamidopyrimidine adduct, individually or collectively, represent the likely chemical precursors responsible for the genotoxic effects of AFB<sub>1</sub> (8). In addition, common oxidative DNA damage, leading to 8-hydroxydeoxyguanosine lesions, was observed in rat hepatic DNA following exposure to AFB<sub>1</sub> (4, 9). AFB<sub>1</sub> induces mainly G:C to T:A transversions (4). We (10, 11) and others

Liver International (2011)  
© 2011 John Wiley & Sons A/S

1

LIV 247

	L I V	2 4 7 4	B	Dispatch: 31.1.11	Journal: LIV	CE: xx
	Journal Name	Manuscript No.		Author Received:	No. of pages: 11	Op:

(12) have identified a hotspot G → T mutation at codon 249 of the *TP53* gene (encoding the mutant p53ser249 protein) in HCC tissues in patients exposed to aflatoxins. Later studies demonstrated that this mutation was also detectable in non-tumour liver samples (13), as well as in the plasma of 6% of healthy individuals, 15% of cirrhotic patients and 40% of HCC patients living in aflatoxin-contaminated areas (14). Thus, the AFB1-specific G → T mutation of *TP53* is frequently present in people exposed to aflatoxins before any clinically detectable liver tumour. Taken together, these observations provide strong evidence that low levels of AFB1 are highly mutagenic in people chronically exposed to this hepatocarcinogenic agent.

Eukaryotic cells have developed a powerful DNA damage response system to protect their genome integrity. DNA damage induces several cellular responses that enable the cell either to eliminate the damage or to activate senescence and apoptosis processes. DNA damage checkpoint proteins play a central role in coordinating repair and cell cycle progression to prevent mutation. Several kinases, including ATM, ATR, Chk1 and Chk2, adaptor proteins such as 53BP1 and downstream cell cycle control proteins such as p53 and Cdc25, are involved in damage sensing and cell cycle control. DNA repair mechanisms include direct repair, base excision repair, nucleotide excision repair, double-strand break repair and cross-link repair (15, 16).

8,9-Dihydro-8-(*N*7-guanyl)-9-hydroxy AFB1 and AFB1-formamidopyrimidine adducts appear to be removed primarily by nucleotide excision repair in mammalian cells, but other repair systems have also been implicated in bacteria and yeast (8). The mechanisms of the DNA damage checkpoint response to AFB1 are poorly known. Here, we explored the DNA damage checkpoint response of wild-type p53 human cells to AFB1 exposure. Our findings indicate that the checkpoint response to genotoxic and mutagenic doses of AFB1 is incomplete. AFB1-exposed cells failed to activate p53 and did not undergo cell cycle arrest or apoptosis, despite the presence of DNA adducts and the accumulation of DNA strand breaks.

## Material and methods

### Cell lines

HepG2 and Huh7 cell lines were cultivated as described previously (10). HCT116 and HCT116-p53<sup>-/-</sup> cell lines (17), gifts from B. Vogelstein, were cultivated in McCoy's cell growth medium (Gibco) supplemented with 10% heat-inactivated fetal calf serum and 1% penicillin and streptomycin solution (Gibco).

### Cell treatment

Aflatoxin B1 (Sigma) was dissolved in dimethyl sulphoxide (DMSO, Carlo Erba). Adriamycin (Sigma) and hydroxyurea (Sigma) were dissolved in distilled water. Aliquots were stored at -20 °C. Working dilutions were prepared fresh and added in a complete cell culture

medium. DMSO (< 10<sup>-3</sup> v/v dilution) and distilled water were used for negative control experiments. AFB1 treatment was performed in the presence of the S9-activation system for all HCT116, HCT116-p53<sup>-/-</sup> and some HepG2 experiments for enzymatic activation into the AFB1-8,9-*exo*-epoxide form. The S9 activation system was prepared as described previously (18, 19), with minor changes. Briefly, the S9-activation mixture was prepared with 0.20 g/l S9 fraction from Sprague-Dawley rat liver (Xenotech), 10.5 mmol/l isocitric acid (Sigma) and 1.8 mmol/l β-nicotinamide adenine dinucleotide phosphate sodium salt hydrate (Sigma). This mixture was filtered (0.45 μm) and used at a 1:10 dilution in the cell culture medium.

### Aflatoxin B1-DNA adduct and 8-hydroxy-deoxyguanosine immunoperoxidase assays

Aflatoxin B1-DNA adducts and 8-hydroxydeoxyguanosine lesions were detected by immunoperoxidase assays, as described previously (20), with minor changes. Briefly, cells were treated with AFB1 or DMSO on coverslips, washed with phosphate-buffered saline and then fixed in ice-cold methanol. AFB1-DNA adducts were detected using a monoclonal antibody (6A10) against an imidazole ring-opened persistent form of the major *N*7-guanine adduct of AFB1 (21). Before the immunoperoxidase assay of AFB1 adducts, cells were treated with a buffer containing 15 mmol/l Na<sub>2</sub>CO<sub>3</sub> and 30 mmol/l NaHCO<sub>3</sub> (pH 9.6) for 2 h at room temperature. For the AFB1 adducts and 8-hydroxydeoxyguanosine lesions, cells were treated with RNase (100 μg/ml) in Tris buffer (10 mmol/l Trizma Base, 1 mmol/l EDTA and 0.4 mol/l NaCl; pH 7.5) for 1 h at 37 °C. After washing with phosphate-buffered saline, proteinase K (10 μg/ml) treatment was carried out for 7 min at room temperature. After rinsing with phosphate-buffered saline, DNA was denatured with 2N HCl for 10 min and cells were neutralized by soaking coverslips in 50 mmol/l Tris base for 5 min. After blocking for 1 h, cells were incubated with mouse 6A10 (Santa Cruz) or mouse anti-8-hydroxydeoxyguanosine (Trevigen) monoclonal antibody overnight at 4 °C. Anti-mouse HRP-conjugated secondary antibodies (Invitrogen) were used for 30 min for primary antibody detection. Cells were stained with diaminobenzidine solution (Dako), counterstained with haematoxylin (Sigma), mounted with 80% glycerol and observed under an Olympus light microscope.

### Post-treatment cell survival – colony-forming ability assay

Cell survival was determined by assessing cell growth in 100 mm dishes after exposure to AFB1 or Adriamycin. HepG2 cells were seeded in six-well plates and semiconfluent cells were exposed to AFB1 (0–50 μmol/l) in the presence of the S9-activation system for 4 and 24 h respectively. Control cells were exposed to Adriamycin (0–5 μmol/l) in parallel experiments. Following

1 exposure,  $10^4$  cells were seeded into 100 mm dishes. After  
 2 10 days of cell culture, colonies were fixed in cold  
 3 methanol, stained with Crystal Violet (Sigma) and  
 4 counted in triplicate experiments. Cell survival was  
 5 calculated as the percent ratio of cell numbers in treated  
 6 vs untreated cells. Survival parameters were determined  
 7 by plotting survival data on a semi-log plot.

#### 8 Western immunoblotting

10 These experiments were carried out as described previously  
 11 (22). Proteins were subjected to electrophoresis using 10%  
 12 or 4–12% Bis-Tris NuPAGE Novex Mini gel systems  
 13 (Invitrogen), according to the manufacturer's instructions.  
 14 For the detection of phosphorylated proteins, cell lysates  
 15 were prepared according to the protocol provided by the  
 16 supplier using the following lysis buffer: 20 mmol/l Tris  
 17 (pH 7.5), 150 mmol/l NaCl, 1 mmol/l EDTA, 1 mmol/l  
 18 EGTA, 1% Triton X-100, 1 mmol/l  $\text{Na}_3\text{VO}_4$ , 1  $\mu\text{g}/\text{ml}$   
 19 leupeptin and 1 mmol/l phenylmethylsulphonyl fluoride.  
 20 Following electrophoresis, proteins were transferred onto  
 21 nitrocellulose membranes and analysed using antibodies  
 22 against cleaved caspase-3 (Cell Signaling), total p53 (Santa  
 23 Cruz), p21<sup>Cip1</sup> (Calbiochem), phospho-H2AX (Millipore),  
 24 phospho-Chk2, phospho-p53ser15, phospho-p53ser20  
 25 (all from Cell Signaling) and Calnexin (Sigma).

#### 28 Senescence-associated $\beta$ -galactosidase assay

29 Senescence-associated  $\beta$ -galactosidase activity was de-  
 30 tected as described previously (22), using a senescent cell  
 31 staining kit (Sigma).

#### 34 Single-cell gel electrophoresis (comet) assay

35 Single- and double-strand DNA breaks were detected  
 36 using alkaline and neutral comet assays respectively (23,  
 37 24). The alkaline comet was performed exactly as de-  
 38 scribed (23). The neutral comet assay was conducted as  
 39 described (24), using the lysis protocol described by  
 40 Chandna (25). Following electrophoresis, slides were  
 41 rinsed, stained with 5  $\mu\text{g}/\text{ml}$  4',6-diamidino-2-phenylin-  
 42 dole (Roche) and analysed under an Apotome (Zeiss)  
 43 microscope. Images were captured with an Axiocam HRC  
 44 colour CCD camera (Zeiss) and digitally saved using AXIO  
 45 VISION software (Zeiss). Data were analysed by CASP  
 46 (Comet Assay Software Project), which measures tail  
 47 moment, using the DNA content in the tail and head  
 48 along with the distance between the means of the head  
 49 and tail distributions (<http://casplab.com>). At least 30  
 50 nuclei were analysed for each experimental condition.

#### 52 Indirect immunofluorescence

53 Cells were fixed with 4% formaldehyde and permeabilized  
 54 with phosphate-buffered saline supplemented with 0.5%  
 55 saponin (Sigma) and 0.3% Triton X-100 (Sigma). After  
 56 blocking for 1 h, cells were incubated overnight at 4°C,  
 57 with antibodies against Ser139-phosphorylated H2AX

(phospho-H2AX; Millipore) or against 53BP1 (Abcam).  
 After incubation with Alexa 568-conjugated secondary  
 antibodies (Invitrogen), cells were counterstained with  
 4',6-diamidino-2-phenylindole (Roche) and observed  
 using an Apotome (Zeiss) microscope. Images were cap-  
 tured with an Axiocam HRC colour CCD camera (Zeiss)  
 and digitally saved using AXIO VISION software (Zeiss).

#### Cell cycle analysis and bromodeoxyuridine incorporation assay

Cells were washed twice in phosphate-buffered saline and  
 fixed in ice-cold ethanol for 10 min. After two phosphate-  
 buffered saline washes, cells were incubated with 20  $\mu\text{g}/\text{ml}$   
 of RNase A (Fermentas) at 37°C for 10 min and stained  
 with propidium iodide (10  $\mu\text{g}/\text{ml}$ ; Sigma). Cell cycle  
 distribution was determined by flow cytometry using  
 FACSCAN and CELLQUEST software (Becton Dickinson). Cell  
 cycle analysis combined with the bromodeoxyuridine  
 incorporation assay was performed using cells first labelled  
 with 10  $\mu\text{mol}/\text{l}$  bromodeoxyuridine (Sigma) for 2 h before  
 each testing time. Cells were incubated with FITC-con-  
 jugated antibromodeoxyuridine antibody (BD Bioscience)  
 at room temperature in the dark, following DNA denatura-  
 tion with 4N HCl for 30 min (26).

## Results

### Induction of DNA adducts, 8-hydroxydeoxyguanosine lesions and DNA breaks by aflatoxin B1 in HepG2 cells

The human hepatoma line HepG2 has retained the activ-  
 ities of various phase I and phase II enzymes that play a  
 crucial role in the activation and detoxification of geno-  
 toxic procarcinogens. It has been used successfully for  
 genotoxicity assays for various classes of environmental  
 carcinogens including aflatoxins, nitrosamines, aromatic  
 and heterocyclic amines and polycyclic aromatic hydro-  
 carbons, as well as for antimutagenicity studies (27).  
 Furthermore, HepG2 has retained the wild-type activity of  
 the p53 gene, a well-established DNA damage response  
 gene (28, 29). Therefore, we first used the HepG2 cell line  
 to test the genotoxic effects of AFB1. Cells were treated  
 with 3–5  $\mu\text{mol}/\text{l}$  of AFB1 in the absence or the presence of  
 the S9-activating system that allows the activation of AFB1  
 into AFB1-8,9 epoxide (18). Following 24 h of exposure,  
 cells were subjected to immunoperoxidase assays to  
 detect the imidazole ring-opened persistent form of the  
 major N7-guanine adduct of AFB1 and 8-hydroxydeoxy-  
 guanosine DNA lesions. Our results verified the detection  
 of AFB1 adducts in the nuclei of most cells with 3 or  
 5  $\mu\text{mol}/\text{l}$  AFB1 (Fig. S1A). Adduct detection levels were  
 quite similar between these two doses, indicating  
 that AFB1 was capable of inducing highly abundant  
 DNA adducts when tested at micromolar levels. We also  
 observed the detection of 8-hydroxydeoxyguanosine-posi-  
 tive nuclear foci (Fig. S1B). The same results were obtained  
 in the presence or in the absence of the S9-activating  
 system (Fig. S1).

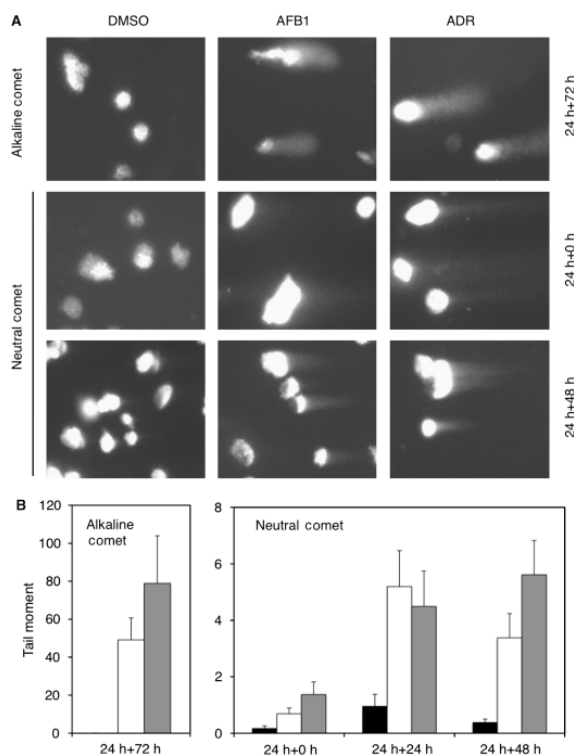


**Fig. 1.** Induction of persistent single- and double-strand DNA breaks in HepG2 cells following AFB1 exposure. (A) HepG2 cells were exposed to DMSO, AFB1 (5  $\mu\text{mol/l}$ ) or Adriamycin (0.5–1  $\mu\text{mol/l}$ ) as a positive control for 24 h, followed by a culture in the absence of test chemicals for up to 72 h, and subjected to alkaline comet or neutral comet assays to detect single- and double-strand breaks respectively. (B) Quantitative analysis of AFB1-induced DNA breaks by automated tail moment measurement. Black, white and grey columns indicate cells exposed to DMSO, AFB1 and Adriamycin respectively. Error bars indicate SD. AFB1- and Adriamycin-treated cells displayed significantly increased tail moments at all time-points tested ( $P < 0.0001$ ). AFB1, aflatoxin B1; DMSO, dimethyl sulphoxide; SD, standard deviation.

The genotoxic effects of AFB1 were studied by alkaline and neutral comet assays that detect single- and double-strand DNA breaks respectively (23, 24). Examples of comet assay results are shown in Figure 1A. Both AFB1- and Adriamycin-exposed cells, tested by an alkaline comet assay at 72 h post-exposure time, displayed a statistically significant increase in comet tail moments ( $P < 0.0001$ ), indicating the presence of abundant single-strand DNA breaks (Fig. 1B, left). A neutral comet assay also detected a statistically significant ( $P < 0.0001$ ) increase in tail moments with both chemicals that lasted at least 48 h after the removal of chemicals from the cell

culture medium (Fig. 1B, right). Tail moments obtained with the neutral comet were nearly 10-fold fewer than those obtained with the alkaline comet (Fig. 1B). Thus, AFB1 induced many more single-strand breaks than double-strand breaks

#### Lack of significant growth inhibition in response to aflatoxin B1 exposure

Next, we studied the cellular response to AFB1-induced genotoxicity using cell growth, senescence and apoptosis assays. Cell survival was determined by assessing colony



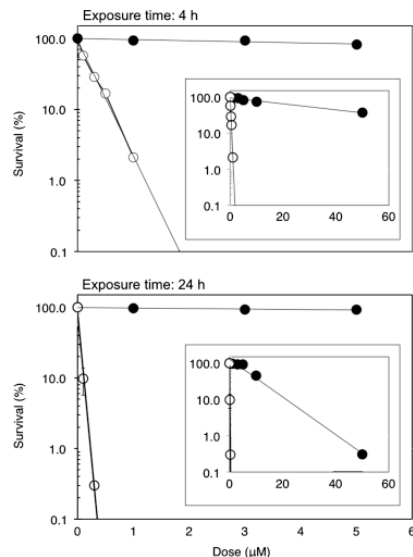


**Fig. 2.** The effects of AFB1 (closed circles) or Adriamycin (open circles) treatment of HepG2 cells for 4 h (top) or 24 h (bottom) on cell survival colony-forming ability. Cell survival was calculated as the per cent ratio of cell numbers in treated vs untreated cells ( $n = 3$ ). Survival parameters were determined by plotting survival data on a semi-log plot. Insets: cell survival at higher AFB1 (up to 50  $\mu\text{mol/l}$ ) and Adriamycin (up to 5  $\mu\text{mol/l}$ ) doses. Error bars: SD. cell survival was determined by assessing cell growth in 100 mm dishes after exposure to AFB1 or Adriamycin. HepG2 cells were seeded in six-well plates and semiconfluent cells were exposed to AFB1 (0, 1, 3, 5, 10 and 50  $\mu\text{mol/l}$ ) or Adriamycin (0, 0.1, 0.3, 0.5, 1 and 5  $\mu\text{mol/l}$ ) for 4 or 24 h. Following exposure,  $10^4$  cells were seeded into 100-mm dishes and colonies were counted 10 days later. AFB1, aflatoxin B1; SD, standard deviation.

growth in 100 mm dishes after exposure to AFB1 or Adriamycin. HepG2 cells were seeded in six-well plates and semiconfluent cells were exposed to AFB1 (0–50  $\mu\text{mol/l}$ ) in the presence of the S9-activation system. Control cells were treated with Adriamycin (0–5  $\mu\text{mol/l}$ ). Following 4 and 24 h of exposure,  $10^4$  cells were seeded into 100-mm dishes and colonies were counted 10 days later. Cell survival was calculated as the percent ratio of cell numbers in treated vs untreated cells. Survival parameters were determined by plotting survival data on a semi-log plot. AFB1 did not affect colony survival after 4 or 24 h of treatment at doses  $\leq 5 \mu\text{mol/l}$  (Fig. 2, closed circles). In contrast, Adriamycin displayed a strong inhibition of colony survival, even with 50 times less concentrated molar doses (Fig. 2, open circles).

Detectable effects of AFB1 were observed only when cells were exposed for 24 h at doses reaching 50  $\mu\text{mol/l}$  (Fig. 2, bottom, inset).

We noticed that both AFB1 and Adriamycin displayed genotoxic effects that caused DNA breaks at comparable intensities (Fig. 1), but their effects on cell survival were highly different (Fig. 2). DNA damage usually triggers a strong cytotoxic response as observed here with Adriamycin (Fig. 2, open circles). This was not the case for AFB1-induced DNA damage that resulted in only a weak colony-inhibitory effect (Fig. 2, closed circles). In confirmation of these observations, 3 days of exposure to AFB1 did not induce a senescence response as tested by a senescence-associated  $\beta$ -galactosidase assay (Fig. S2A) nor apoptosis as tested by an activated caspase-3 assay (Fig. S2B). These findings prompted us to further explore the DNA damage response of HepG2 cells to AFB1.

#### DNA damage checkpoint foci induction by aflatoxin B1

To test the checkpoint response, we first used 53BP1 and phospho-H2AX foci assays (15) by immunofluorescence. Both AFB1 and Adriamycin induced 53BP1 and phospho-H2AX foci that were detectable after 3 days of culture, but AFB1-induced foci formation appeared to be less strong (Fig. 3). These findings provided evidence for a double-strand DNA break response (15, 16) to both agents, although the response appeared to be slightly different. We tested the statistical significance of AFB1-induced foci formation by counting cells with 53BP1-positive foci ( $> 5$  foci/cell). Cells exposed to AFB1 between 1 and 72 h showed a progressive and statistically significant ( $P < 0.0001$ ) accumulation of 53BP1 foci (Fig. S3). To test the duration of 53BP1 foci following a fixed time of exposure to AFB1, cells were first treated with AFB1 for 24 h and then cultivated in the absence of chemical treatment for up to 120 h. Cells with positive 53BP1 foci were detected by an indirect immunofluorescence assay (Fig. S4A) and then counted. As shown in Fig. S4B, the accumulation of 53BP1 foci peaked at 48 h of post-treatment, with 40% positive cells. A residual foci activity with 15–20% positive cells was detectable for at least 120 h in cells no longer exposed to AFB1. In contrast, cells exposed to DMSO only displayed low foci activity ( $< 5\%$ ) throughout the experiment, indicating that increased foci formation was because of AFB1 exposure. Western blot analysis of the total 53BP1 protein demonstrated its higher expression in cells exposed to AFB1 for at least 72 h (Fig. S4C). Taken together, our findings indicated that following exposure to AFB1, HepG2 cells develop persistent 53BP1 foci that are compatible with a double-strand DNA break response lasting for several days.

#### Effects of aflatoxin B1 on HepG2 cell cycle progression

Based on observations indicating a defective growth response to AFB1 (Fig. 2), despite the formation of

1  
2  
3  
4  
5  
6  
7  
8  
9  
10  
11  
12  
13  
14  
15  
16  
17  
18  
19  
20  
21  
22  
23  
24  
25  
26  
27  
28  
29  
30  
31  
32  
33  
34  
35  
36  
37  
38  
39  
40  
41  
42  
43  
44  
45  
46  
47  
48  
49  
50  
51  
52  
53  
54  
55  
56  
57  
58

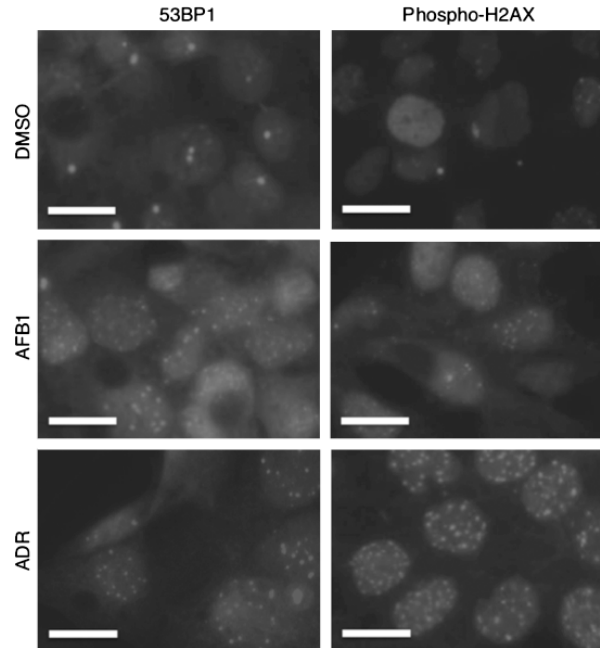


**Fig. 3.** Induction of 53BP1 and phospho-H2AX foci following AFB1 exposure in HepG2. Cells were treated with AFB1 (3  $\mu\text{mol/l}$ ) for 3 days and then subjected to 53BP1 and phospho-H2AX foci detection by indirect immunofluorescence. Control cells were exposed to DMSO only. Adriamycin (0.1  $\mu\text{mol/l}$ ) was used as a positive control. Scale bar = 20  $\mu\text{m}$ . ADR, Adriamycin; AFB1, aflatoxin B1; DMSO, dimethyl sulphoxide.

persistent AFB1-DNA adducts (Fig. S1), DNA strand breaks (Fig. 1) and DNA damage foci (Figs. 3, S3 and S4), we performed time-course studies on cell cycle progression of HepG2 cells following AFB1 exposure. As shown in Figure 4, AFB1 exposure resulted in a transient accumulation of cells at the S phase (up to 26% from 13%, one-fold increase) at 24 h, followed by a return to control levels at 48 and 72 h. These changes were accompanied by a slight increase (40%) in G2/M-phase cells at 48 and 72 h, together with a slight decrease (18–26%) in G1-phase cells. These observations provided evidence for a transient and weak growth inhibition in HepG2 cells following AFB1 exposure (Fig. 4). The lack of a total cell cycle block under AFB1 exposure was compatible with a nearly complete colony survival after 5  $\mu\text{mol/l}$  AFB1 exposure (Fig. 2). Of particular interest, AFB1-exposed HepG2 cells did not undergo G1 arrest despite the expression of wild-type p53, strongly suggesting that AFB1-induced DNA damage did not trigger a p53-dependent DNA damage response in these cells.

#### Incomplete DNA damage checkpoint response to aflatoxin B1 in different cell types

p53-dependent response to DNA damage is a strong mechanism protecting cells against the accumulation of deleterious mutations (15, 17, 30). Based on the current model for p53 activation upon DNA damage (15), we tested the status of critical components of DNA damage signalling after AFB1 exposure. Adriamycin and hydroxyurea were used for control experiments. As shown in Figure 5, Adriamycin treatment induced a typical double-strand break response in HepG2 cells by induced phosphorylations of H2AX, Chk2 and p53ser15, together with a weak induction of p53ser20 phosphorylation. Hydroxyurea treatment resulted in a weak phosphorylation of Chk1. As expected, we noted time-dependent differences in these responses. The response to AFB1 was globally weak or even absent. The only detectable response was observed with H2AX phosphorylation that was detectable after 24 h of AFB1 exposure, as well as

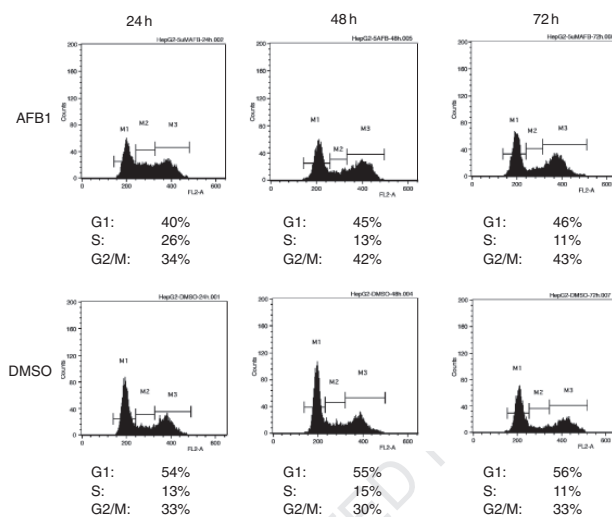


**Fig. 4.** The effects of AFB1 on HepG2 cell cycle distribution. Cells were treated with either 5  $\mu\text{mol/l}$  AFB1 or DMSO up to 72 h, and cell cycle distribution was analysed by flow cytometry at 24, 48 and 72 h. AFB1, aflatoxin B1; DMSO, dimethyl sulphoxide.

after 24 h post-exposure. We performed additional studies with Huh7, an HCC cell line with retained activities for AFB1 activation (31), but displaying a homozygous p53 mutation (28). As shown in Fig. S5, Huh7 cells responded to Adriamycin by upregulation of phospho-H2AX levels only, and there was no phospho-Chk1 phosphorylation in response to hydroxyurea treatment. AFB1 did not affect phosphorylations of Chk1, Chk2 or p53ser15, and the effect on H2AX phosphorylation was weakly detectable at 24 h of exposure. Taken together, these studies indicated that, apart from H2AX phosphorylation, critical components of DNA damage checkpoint proteins were not affected in hepatoma cells. In addition, the induction of p53 phosphorylation in response to DNA damage by Adriamycin appeared to be dependent on the wild type of the mutant status of p53 gene (see Fig. 5 in comparison with Fig. S5).

In order to further investigate the role of AFB1 in DNA damage response induction, we decided to explore wild-type p53-expressing HCT116 colorectal cancer cells and their p53 knockout HCT116-p53<sup>-/-</sup> derivatives (17). We performed all AFB1 experiments in these cell lines in the presence of the S9-activating system to allow the transformation of AFB1 into epoxy-AFB1 (32). First, we assessed the formation of DNA lesions following exposure to AFB1 (5  $\mu\text{mol/l}$ ) and Adriamycin (1  $\mu\text{mol/l}$ ). The response of HCT116 cells to both AFB1 and Adriamycin treatment was not different from the observations

obtained with HepG2 cells. The great majority of cells stained positive for 8-hydroxydeoxyguanosine lesions following drug exposure (Fig. S6A) and displayed DNA double-strand breaks as tested by a neutral comet assay (Fig. S6B). Furthermore, HCT116 cells exposed to 5  $\mu\text{mol/l}$  AFB1 for 24 h displayed a statistically significant ( $P < 0.0001$ ) increase in both 53BP1 and phospho-H2AX-positive foci that lasted at least 48 h post-exposure, independent of TP53 status (Fig. S7). Western blot analysis of critical components of DNA damage checkpoint response also provided results quite similar to that of HepG2. As shown in Fig. S8 and in comparison with Adriamycin and hydroxyurea, AFB1 treatment induced only a weak upregulation of phospho-H2AX levels at 24 h of exposure, with a more pronounced increase at 24 h of post-exposure.

Taken together, our observations with three different cell lines indicated that AFB1 induced a weak and delayed accumulation of phospho-H2AX. The phosphorylation of H2AX strongly suggested that AFB1-induced DNA damage triggered ATM activation by double-strand DNA breaks (15, 33). However, this ATM response was not accompanied by phosphorylations of Chk1, Chk2 or p53, three key proteins involved in the DNA damage checkpoint response. The lack of Chk1 phosphorylation after AFB1 exposure also suggested that the ATR/Chk1 pathway response was also inactive against AFB1-induced DNA damage.

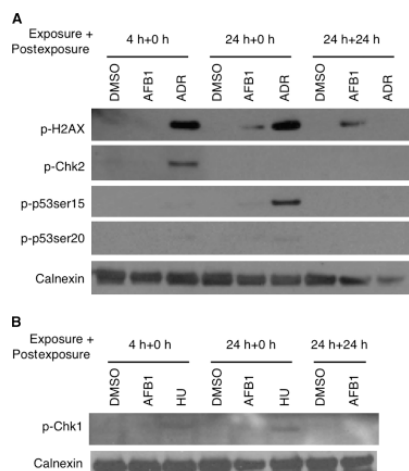


**Fig. 5.** Incomplete DNA damage checkpoint response of HepG2 cells to aflatoxin B1 (AFB1). HepG2 cells were treated with dimethyl sulphoxide (DMSO) or AFB1 (5  $\mu\text{mol/l}$ ) for 4 and 24 h, and tested immediately (4+0 h and 24+0 h) or after 24 h of incubation without treatment (24+24 h). HepG2 cells treated with 0.5  $\mu\text{mol/l}$  Adriamycin (ADR) or 5 mmol/l hydroxyurea (HU) were used as positive controls for experiments shown in (A) and (B) respectively. Total cell lysates were subjected to western blot analysis. Calnexin was used as a loading control. p-H2AX, phospho-H2AX; p-p53ser15, phospho-p53ser15; p-p53ser20, phospho-p53ser20; p-Chk2, phospho-Chk2; p-Chk1, phospho-Chk1.

#### The mechanism of the inefficient DNA damage response to aflatoxin B1

As we observed similar responses of HCT116 and hepatoma cells to both AFB1 and Adriamycin treatment, we decided to further explore AFB1 effects using the isogenic HCT116 model, allowing us to better define its potential implications in p53-mediated DNA damage response. Before testing of AFB1 effects, we first examined the cell cycle responses of HCT116 and HCT116-p53<sup>-/-</sup> cells to Adriamycin. HCT116 cells displayed G1 and G2/M arrests in response to Adriamycin, associated with low levels of apoptosis (subG1 peak) and polyploidy formation at higher doses (Fig. S9A). There was also a depletion of S-phase cells as an indication of DNA synthesis inhibition that lasted at least 48 h following the removal of Adriamycin from the cell culture medium. The response of HCT116-p53<sup>-/-</sup> cells to Adriamycin was essentially similar, with the noticeable absence of a G1 peak (Fig. S9A). Based on Fig. S9B, which compares Adriamycin-induced cell cycle changes in wild-type and p53 knockout HCT116 cells, we concluded that DNA damage induced by Adriamycin is associated with a p53-dependent G1 arrest and a p53-independent G2/M arrest.

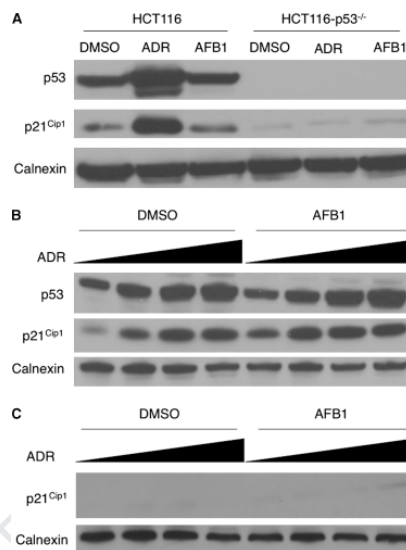


**Fig. 6.** Comparative analysis of the wild-type p53 response of HCT116 cells to AFB1 and Adriamycin treatment indicates that AFB1 cannot induce effective p53 activation. (A) Wild-type 53 HCT116 and p53-deficient HCT116-p53<sup>-/-</sup> cells were treated with AFB1 (3  $\mu\text{mol/l}$ ) or DMSO (in the presence of the S9-activating system) or Adriamycin (ADR; 1  $\mu\text{mol/l}$ ) for 24 h, followed by an additional cell culture in the absence of this chemical for another 24 h. (B and C) HCT116 (B) and HCT116-p53<sup>-/-</sup> (C) cells were cotreated with Adriamycin (ADR, increasing doses: 0, 0.1, 0.5 and 1  $\mu\text{mol/l}$  respectively) in the absence (DMSO) or in the presence of 3  $\mu\text{mol/l}$  AFB1, as described in (A) for 24 h (24 h pre-exposure to AFB1, followed by 24 h of co-exposure). Total cell lysates were used for western blot using anti-p53 and anti-p21<sup>Cip1</sup> antibodies. Calnexin was used as a loading control. AFB1, aflatoxin B1; DMSO, dimethyl sulphoxide.

Our cell cycle studies with AFB1 treatment in the same cell lines are shown in Fig. S10. Unlike HepG2 cells, the HCT116 cell lines did not display a significant increase in S-phase cells. However, they displayed a weak decrease in the G1 phase, in parallel to a weak increase in G2/M cells, as observed with HepG2 cells. The response of HCT116-p53<sup>-/-</sup> cells to AFB1 exposure was not remarkable either, except for a slight increase in G2/M cells.

Taken together, these observations strongly suggested that human cells exposed to AFB1 could not develop a growth control response. The most likely reason for this was a delayed and deficient checkpoint response, including a lack of efficient phosphorylation of p53 protein. Therefore, we also compared the effects of AFB1 and Adriamycin on p53 and p21<sup>Cip1</sup>. As shown in Figure 6A,

1 both p53 and p21<sup>Cip1</sup> responded to Adriamycin treatment  
 2 with a dose-dependent increase in HCT116 cells. The  
 3 increase in p21<sup>Cip1</sup> levels was p53-dependent, because we  
 4 did not observe p21<sup>Cip1</sup> response in HCT116-p53<sup>-/-</sup> cells.  
 5 In contrast, AFB1 treatment did not produce any detect-  
 6 able change in p53 levels in HCT116 cells. As a result, there  
 7 was no detectable increase in p21<sup>Cip1</sup> in both HCT116 and  
 8 HCT116-p53<sup>-/-</sup> cells. These findings suggested that either  
 9 the AFB1 was actively involved in the inhibition of an  
 10 effective DNA damage checkpoint response or the damage  
 11 inflicted by AFB1 did not reach a threshold that is  
 12 necessary for checkpoint activation, similar to previous  
 13 observations with low-dose ionizing radiation (16). To test  
 14 whether AFB1 inhibits the checkpoint response, we co-  
 15 treated HCT116 cells with increasing doses of Adriamycin  
 16 (0, 0.1, 0.5 and 1 µmol/l respectively) in the absence or  
 17 presence of 3 µmol/l AFB1. As shown in Figure 6B and C,  
 18 the accumulation of p53 and p21<sup>Cip1</sup> after Adriamycin  
 19 exposure was not inhibited by AFB1 in HCT116 cells.  
 20 Indeed, there was a slight increase in the accumulation  
 21 p21<sup>Cip1</sup> after 0.1 µmol/l Adriamycin treatment in the pre-  
 22 sence of AFB1. The p21<sup>Cip1</sup> response of HCT116-p53<sup>-/-</sup>  
 23 cells to Adriamycin was not affected by AFB1, except for a  
 24 weak accumulation that was observed when cells were  
 25 cotreated with 1 µmol/l Adriamycin and 3 µmol/l AFB1.  
 26 These findings showed that AFB1 did not inhibit DNA  
 27 damage checkpoint response under the conditions tested.  
 28 Instead, AFB1 slightly stimulated the checkpoint response  
 29 to Adriamycin.

### Discussion

33 Hepatocellular cancer risk from aflatoxins, as well as  
 34 aflatoxins' hepatocellular biochemistry, DNA interacting  
 35 forms, the types of DNA damage and their repair by  
 36 nucleotide excision, and their *in vitro* and *in vivo*  
 37 mutagenic specificity for G → T transversions are  
 38 well-established facts (34). Here, we addressed a less  
 39 well-understood, but critical component of aflatoxin  
 40 genotoxicity, namely the DNA damage checkpoint re-  
 41 sponse. The *in vitro* experimental model system used  
 42 here was designed after carefully considering previously  
 43 described features associated with aflatoxin-related car-  
 44 cinogenicity. Human cells with a wild-type p53 expression  
 45 were preferred because of the fact that a specific hotspot  
 46 mutation of this gene was observed only in human HCC,  
 47 not in other aflatoxin-induced mammalian tumours  
 48 (35). We considered estimated chronic aflatoxin expo-  
 49 sure levels in humans (0.01–0.3 µg/kg/day) (3) and  
 50 hepatocarcinogenic doses (0.015–1 ppm) in rats (36).  
 51 We also considered that 30 min of exposure to 1.6 µmol/  
 52 l AFB1 was sufficient to induce p53-249 G → T muta-  
 53 tions in HepG2 cells (37) and 0.2–5 µmol/l doses induced  
 54 reporter gene mutations in mouse fibroblasts (32). Thus,  
 55 the AFB1 doses that we used here (3–5 µmol/l) were at  
 56 the upper limits of *in vitro* mutagenic activity in mam-  
 57 malian cells and were estimably superior to carcinogenic  
 58 doses in humans and rats. We performed our cell

response studies over a period of several days so that we  
 could determine both immediate and delayed effects.

Our findings demonstrate that AFB1, when tested under  
 conditions comparable with mutagenic and carcinogenic  
 exposure levels, creates DNA adducts, 8-hydroxy-deoxy-  
 guanosine lesions and persistent strand breaks, but it does  
 not lead to a sustained cell cycle arrest and/or an apoptosis  
 response. AFB1 adducts are repaired by nucleotide excision  
 repair (8); however, their removal is slow (6) and they  
 remain at maximum levels for several days and are  
 detectable over several weeks in rat liver cells (6, 7). The  
 unusual stability of AFB1 adducts together with a slow  
 repair process could account for their strong genotoxic  
 effects. The expansion of cells with unrepaired DNA lesions  
 could cause mutations in their genomes. Therefore, such  
 cells are under the strict control of DNA damage check-  
 point proteins that block cell cycle and/or induce apoptosis  
 (15, 16, 30). Our *in vitro* findings and previously reported  
*in vivo* studies strongly suggest that cells exposed to  
 mutagenic doses of AFB1 cannot develop a strong cell cycle  
 arrest and/or apoptosis response. Our detailed analysis of  
 DNA damage checkpoint proteins provides a plausible  
 explanation for the uncoupling between DNA damage  
 and growth control following AFB1 exposure. AFB1-  
 exposed cells displayed DNA damage foci formation with  
 both 53BP1 and phospho-H2AX marker proteins. These  
 findings suggest that AFB1-induced DNA damage might  
 trigger a checkpoint response compatible with a double-  
 strand break-type response involving ATM. However, this  
 response was weak and delayed, as indicated by phospho-  
 H2AX levels tested by western blot analysis. Our western  
 blot studies for phospho-ATM levels after AFB1 exposure  
 provided inconsistent results with or without an increase  
 (data not shown), further indicating that ATM is not  
 activated consistently following AFB1-induced DNA da-  
 mage. In confirmation of this hypothesis, AFB1-induced  
 DNA damage failed to activate Chk2 and p53ser15 phos-  
 phorylations. The alternative DNA damage checkpoint  
 response mediated by ATR and Chk1 was also ineffective,  
 as tested by Chk1 and p53ser20 phosphorylation. The most  
 important outcome of a deficient response to AFB1 was a  
 lack of cell growth control. Apart from a slight and  
 transient increase in the G2/M phase, cells did not undergo  
 stable cell cycle arrest, senescence and/or apoptosis. Con-  
 sequently, the overall cell survival was not affected even  
 after exposure to 5 µmol/l AFB1. It was necessary to expose  
 cells to 50 µmol/l AFB1 for at least 24 h in order to observe  
 a cytotoxic effect. Such a high dose represents a more than  
 150-fold higher value when compared with effective doses  
 of Adriamycin in the same type of cells.

The mechanisms of the failing checkpoint response to  
 AFB1 are currently unknown. We speculate that AFB1 is  
 able to induce DNA damage, without triggering an effective  
 damage response signal at doses ≤ 5 µmol/l. The delayed  
 and defective DNA damage response to AFB1 could be  
 related to the type of DNA and protein adducts that it  
 forms in exposed cells (5, 8). AFB1 DNA adducts that are  
 known to be repaired primarily by nucleotide excision

repair (8) may not be sufficient to trigger directly a strong DNA damage response, which usually requires single- and double-strand DNA breaks (15, 16). Instead, the DNA breaks could occur during the repair process causing a delayed response, as suggested by a weak and delayed occurrence of phospho-H2AX accumulation observed here. Alternatively, or in addition, adducts of AFB1 formed with critical cellular proteins may hamper an effective damage response. This alternative is highly unlikely, as suggested by the inability of AFB1 cotreatment to inhibit Adriamycin-induced accumulation of p53 and p21<sup>Cip1</sup> as an end-point reporter for checkpoint response. Thus, our findings favour the hypothesis that AFB1-induced DNA damage, tested here at doses  $\leq 5 \mu\text{mol/l}$ , did not reach the threshold for an efficient induction of checkpoint response. At higher doses, AFB1 is probably effective to trigger a DNA damage response. Indeed, it has been reported previously that HepG2 cells exposed to  $10 \mu\text{mol/l}$  AFB1 can elicit a cell cycle arrest response (38). When tested with  $5 \text{ mg/kg}$  dose, AFB1 exposure could induce p21<sup>Cip1</sup> upregulation in rat liver (39). However, as stressed earlier, cancer-causing dietary exposure to AFB1 occurs at low levels, a condition that is similar to our *in vitro* conditions that provided evidence for a defective checkpoint response.

A defective or a negligent G2/M checkpoint response to low ionizing radiation exposure has been postulated by Löbrich and Jeggo (16) as a potential cause of genomic instability and cancer risk. The authors also proposed that a master p53-dependent G1 checkpoint might remain effective during a negligent G2/M checkpoint for later elimination of escaping cells. Our findings strongly suggest that the DNA damage checkpoint in response to low doses of AFB1 is defective, negligent or delayed. In addition, a p53-dependent salvage pathway is apparently ineffective against AFB1-induced DNA damage. The lack of an efficient response to AFB1-induced DNA damage may be because of the type of lesion(s) induced at the DNA and/or protein levels by activated AFB1 in exposed cells. It will be interesting to further investigate these issues in future studies.

In conclusion, our findings provide *in vitro* evidence for a negligent G1 and G2/M checkpoint response to AFB1-induced DNA damage. This defective response may contribute to the mutagenic and carcinogenic potencies of aflatoxins.

#### Acknowledgements

O. G. Y. and H. Y. were supported by short-term European Molecular Biology Organization (EMBO), and O. G. Y., H. Y. and M. Y. by long-term The Scientific and Technological Research Council of Turkey (TUBITAK) PhD fellowships respectively. We would like to thank Stefan Dimitrov for his critical reading of the manuscript and helpful suggestions.

**Funding:** this work was supported by grants from the Institut National de Cancer (France), The Scientific and Technological Research Council of Turkey (TUBITAK)

and State Planning Office of Turkey (DPT). Additional support was provided by the Turkish Academy of Sciences. The funders had no role in the study design, data collection and analysis, decision to publish or preparation of the manuscript.

**Conflict of interest statement:** none declared.

#### References

- Parkin DM. The global health burden of infection-associated cancers in the year 2002. *Int J Cancer* 2006; **118**: 3030–44.
- Wild CP, Montesano R. A model of interaction: aflatoxins and hepatitis viruses in liver cancer aetiology and prevention. *Cancer Lett* 2009; **286**: 22–8.
- Liu Y, Wu F. Global burden of aflatoxin-induced hepatocellular carcinoma: a risk assessment. *Environ Health Perspect*. Q14
- Wang JS, Groopman JD. DNA damage by mycotoxins. *Mutat Res* 1999; **424**: 167–81.
- Wild CP, Gong YY. Mycotoxins and human disease: a largely ignored global health issue. *Carcinogenesis* 31: 71–82. Q15
- Croy RG, Wogan GN. Temporal patterns of covalent DNA adducts in rat liver after single and multiple doses of aflatoxin B1. *Cancer Res* 1981; **41**: 197–203.
- Smela ME, Hamm ML, Henderson PT, et al. The aflatoxin B(1) formamidopyrimidine adduct plays a major role in causing the types of mutations observed in human hepatocellular carcinoma. *Proc Natl Acad Sci USA* 2002; **99**: 6655–60.
- Bedard LL, Massey TE. Aflatoxin B1-induced DNA damage and its repair. *Cancer Lett* 2006; **241**: 174–83.
- Shen HM, Ong CN, Lee BL, Shi CY. Aflatoxin B1-induced 8-hydroxydeoxyguanosine formation in rat hepatic DNA. *Carcinogenesis* 1995; **16**: 419–22.
- Bressac B, Kew M, Wands J, Ozturk M. Selective G to T mutations of p53 gene in hepatocellular carcinoma from southern Africa. *Nature* 1991; **350**: 429–31.
- Ozturk M. P53 mutation in hepatocellular carcinoma after aflatoxin exposure. *Lancet* 1991; **338**: 1356–9.
- Hsu IC, Metcalf RA, Sun T, et al. Mutational hotspot in the p53 gene in human hepatocellular carcinomas. *Nature* 1991; **350**: 427–8.
- Aguilar F, Harris CC, Sun T, Hollstein M, Cerutti P. Geographic variation of p53 mutational profile in non-malignant human liver. *Science* 1994; **264**: 1317–9.
- Kirk GD, Lesi OA, Mendy M, et al. 249(ser) TP53 mutation in plasma DNA, hepatitis B viral infection, and risk of hepatocellular carcinoma. *Oncogene* 2005; **24**: 5858–67.
- Sancar A, Lindsey-Boltz LA, Unsal-Kacmaz K, Linn S. Molecular mechanisms of mammalian DNA repair and the DNA damage checkpoints. *Annu Rev Biochem* 2004; **73**: 39–85.
- Löbrich M, Jeggo PA. The impact of a negligent G2/M checkpoint on genomic instability and cancer induction. *Nat Rev Cancer* 2007; **7**: 861–9.
- Bunz F, Dutriaux A, Lengauer C, et al. Requirement for p53 and p21 to sustain G2 arrest after DNA damage. *Science* 1998; **282**: 1497–501.
- Dreiem A, Fonnum F. Thiophene is toxic to cerebellar granule cells in culture after bioactivation by rat liver enzymes. *Neurotoxicology* 2004; **25**: 959–66.

- 1  
2  
3  
4  
5  
6  
7  
8  
9  
10  
11  
12  
13  
14  
15  
16  
17  
18  
19  
20  
21  
22  
23  
24  
25  
26  
27  
28  
29  
30  
31  
32  
33  
34  
35  
36  
37  
38  
39  
40  
41  
42  
43  
44  
45  
46  
47  
48  
49
19. Erexson GL, Periago MV, Spicer CS. Differential sensitivity of Chinese hamster V79 and Chinese hamster ovary (CHO) cells in the *in vitro* micronucleus screening assay. *Mutat Res* 2001; **495**: 75–80.
20. Yarborough A, Zhang YJ, Hsu TM, Santella RM. Immunoperoxidase detection of 8-hydroxydeoxyguanosine in aflatoxin B1-treated rat liver and human oral mucosal cells. *Cancer Res* 1996; **56**: 683–8.
21. Hsieh LL, Hsu SW, Chen DS, Santella RM. Immunological detection of aflatoxin B1-DNA adducts formed *in vivo*. *Cancer Res* 1988; **48**: 6328–31.
22. Ozturk N, Erdal E, Mumcuoglu M, *et al.* Reprogramming of replicative senescence in hepatocellular carcinoma-derived cells. *Proc Natl Acad Sci USA* 2006; **103**: 2178–83.
23. Olive PL, Durand RE, Le Riche J, Olivetto IA, Jackson SM. Gel electrophoresis of individual cells to quantify hypoxic fraction in human breast cancers. *Cancer Res* 1993; **53**: 733–6.
24. Olive PL, Banath JP. Detection of DNA double-strand breaks through the cell cycle after exposure to X-rays, bleomycin, etoposide and 125I-dUrd. *Int J Radiat Biol* 1993; **64**: 349–58.
25. Chandna S. Single-cell gel electrophoresis assay monitors precise kinetics of DNA fragmentation induced during programmed cell death. *Cytometry A* 2004; **61**: 127–33.
26. Senturk S, Mumcuoglu M, Gursay-Yuzugullu O, *et al.* Transforming growth factor-beta induces senescence in hepatocellular carcinoma cells and inhibits tumor growth. *Hepatology* 2010. **Q16**
27. Knasmuller S, Parzefall W, Sanyal R, *et al.* Use of metabolically competent human hepatoma cells for the detection of mutagens and antimutagens. *Mutat Res* 1998; **402**: 185–202.
28. Puisieux A, Ji J, Guillot C, *et al.* P53-mediated cellular response to DNA damage in cells with replicative hepatitis B virus. *Proc Natl Acad Sci USA* 1995; **92**: 1342–6.
29. Puisieux A, Galvin K, Troalen F, *et al.* Retinoblastoma and p53 tumor suppressor genes in human hepatoma cell lines. *FASEB J* 1993; **7**: 1407–13.
30. Meek DW. Tumour suppression by p53: a role for the DNA damage response? *Nat Rev Cancer* 2009; **9**: 714–23.
31. Sivertsson L, Ek M, Darnell M, *et al.* CYP3A4 catalytic activity is induced in confluent Huh7 hepatoma cells. *Drug Metab Dispos* 38: 995–1002. **Q17**
32. Besaratinia A, Kim SI, Hainaut P, Pfeifer GP. *In vitro* recapitulating of TP53 mutagenesis in hepatocellular carcinoma associated with dietary aflatoxin B1 exposure. *Gastroenterology* 2009; **137**: 1127–37, 37 e1–5.
33. Burma S, Chen BP, Murphy M, Kurimasa A, Chen DJ. ATM phosphorylates histone H2AX in response to DNA double-strand breaks. *J Biol Chem* 2001; **276**: 42462–7.
34. Groopman JD, Kensler TW, Wild CP. Protective interventions to prevent aflatoxin-induced carcinogenesis in developing countries. *Annu Rev Public Health* 2008; **29**: 187–203.
35. Gouas D, Shi H, Hainaut P. The aflatoxin-induced TP53 mutation at codon 249 (R249S): biomarker of exposure, early detection and target for therapy. *Cancer Lett* 2009; **286**: 29–37.
36. Newberne PM, Wogan GN. Sequential morphologic changes in aflatoxin B carcinogenesis in the rat. *Cancer Res* 1968; **28**: 770–81.
37. Aguilar F, Hussain SP, Cerutti P. Aflatoxin B1 induces the transversion of G → T in codon 249 of the p53 tumor suppressor gene in human hepatocytes. *Proc Natl Acad Sci USA* 1993; **90**: 8586–90.
38. Ricordy R, Gensabella G, Cacci E, Augusti-Tocco G. Impairment of cell cycle progression by aflatoxin B1 in human cell lines. *Mutagenesis* 2002; **17**: 241–9.
39. Ellinger-Ziegelbauer H, Stuart B, Wahle B, Bommann W, Ahr HJ. Characteristic expression profiles induced by genotoxic carcinogens in rat liver. *Toxicol Sci* 2004; **77**: 19–34.

### Supporting information

Additional supporting information may be found in the online version of this article:

**Figure S1.** Induction of DNA adducts and 8-hydroxydeoxyguanosine lesions following AFB1 exposure in HepG2.

**Figure S2.** Induction of senescence arrest and apoptosis in HepG2 cells by Adriamycin, but not AFB1 in HepG2.

**Figure S3.** Time-dependent increase in 53BP1 foci-positive HepG2 cells under AFB1 exposure.

**Figure S4.** The duration of 53BP1 foci after 24 h of exposure to AFB1 in HepG2.

**Figure S5.** Incomplete DNA damage checkpoint response of Huh7 hepatoma cells to AFB1.

**Figure S6.** Induction of 8-hydroxydeoxyguanosine lesions and double-strand breaks in HCT116 isogenic clones following AFB1 exposure.

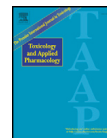
**Figure S7.** Increased DNA damage-induced foci detection after exposure of HCT116 isogenic clones to AFB1.

**Figure S8.** Incomplete DNA damage checkpoint response of wild-type p53 HCT116 cells to AFB1.

**Figure S9.** p53-dependent and p53-independent cell cycle arrest in HCT116 isogenic clones after Adriamycin treatment.

**Figure S10.** Lack of cell cycle arrest of HCT116 isogenic clones in response to AFB1-induced DNA damage.

Please note: Wiley-Blackwell is not responsible for the content or functionality of any supporting materials supplied by the authors. Any queries (other than missing material) should be directed to the corresponding author for the article.



## Evaluation of cytotoxicity and oxidative DNA damaging effects of di(2-ethylhexyl)-phthalate (DEHP) and mono(2-ethylhexyl)-phthalate (MEHP) on MA-10 Leydig cells and protection by selenium

Pinar Erkekoglu<sup>a,b</sup>, Walid Rachidi<sup>a</sup>, Ozge Gursoy Yuzugullu<sup>c,d</sup>, Belma Giray<sup>b</sup>, Alain Favier<sup>a</sup>, Mehmet Ozturk<sup>c,d</sup>, Filiz Hincal<sup>b,\*</sup>

<sup>a</sup> CEA Grenoble, INAC/SCIB/LAN, 17 Rue des Martyrs, 38054 Grenoble Cedex 9, France

<sup>b</sup> Hacettepe University, Faculty of Pharmacy, Department of Toxicology, 06100 Ankara, Turkey

<sup>c</sup> Department of Molecular Biology and Genetics, Bilkent University, 06800 Ankara, Turkey

<sup>d</sup> Centre de Recherche INSERM-Université Joseph Fourier UR23, Institut Albert Bonniot, 38042 Grenoble, France

### ARTICLE INFO

#### Article history:

Received 30 April 2010

Revised 14 July 2010

Accepted 19 July 2010

Available online 24 July 2010

#### Keywords:

Di(2-ethylhexyl)-phthalate

Mono(2-ethylhexyl)-phthalate

Selenium

Oxidative stress

p53

Cytotoxicity

Antioxidant enzymes

Comet assay

### ABSTRACT

Di(2-ethylhexyl)-phthalate (DEHP) is the most abundantly used phthalate derivative, inevitable environmental exposure of which is suspected to contribute to the increasing incidence of testicular dysgenesis syndrome in humans. Oxidative stress and mitochondrial dysfunction in germ cells are suggested to contribute to phthalate-induced disruption of spermatogenesis in rodents, and Leydig cells are one of the main targets of phthalates' testicular toxicity. Selenium is known to be involved in the modulation of intracellular redox equilibrium, and plays a critical role in testis, sperm, and reproduction. This study was aimed to investigate the oxidative stress potential of DEHP and its consequences in testicular cells, and examine the possible protective effects of selenium using the MA-10 mouse Leydig tumor cell line as a model. In the presence and absence of selenium compounds [30 nM sodium selenite (SS), and 10 μM selenomethionine (SM)], the effects of exposure to DEHP and its main metabolite mono(2-ethylhexyl)-phthalate (MEHP) on the cell viability, enzymatic and non-enzymatic antioxidant status, ROS production, p53 expression, and DNA damage by alkaline Comet assay were investigated. The overall results of this study demonstrated the cytotoxicity and genotoxicity potential of DEHP, where MEHP was found to be more potent than the parent compound. SS and SM produced almost the same level of protection against antioxidant status modifying effects, ROS and p53 inducing potentials, and DNA damaging effects of the two phthalate derivatives. It was thus shown that DEHP produced oxidative stress in MA-10 cells, and selenium supplementation appeared to be an effective redox regulator in the experimental conditions used in this study, emphasizing the critical importance of the appropriate selenium status.

© 2010 Elsevier Inc. All rights reserved.

**Abbreviations:** BCA, bicinchoninic acid assay.; CDNB, 1-chloro-2,4 dinitrobenzene.; CM-H<sub>2</sub>DCFDA, 5-(and 6-) chloromethyl-2,7'-dichlorodihydrofluorescein diacetate.; DAB, 3,3'-diaminobenzidine.; DCFH, 2,7'-dichlorofluorescein.; DCF, 2,7'-dichlorofluorescein.; DEHP, di(2-ethylhexyl) phthalate.; DMEM/F-12, Dulbecco's Modified Eagle Medium (1:1) Nutrient Mixture.; DMSO, dimethyl sulfoxide.; DTNB, 5,5'-dithiobis(2-nitrobenzoic acid).; FBS, fetal bovine serum.; GPx1, cytosolic glutathione peroxidase.; GPx4, phospholipid hydroperoxide glutathione peroxidase.; GR, glutathione reductase.; GSH, glutathione.; GSSG, oxidized glutathione.; GST, glutathione S-transferase.; H<sub>2</sub>Se, hydrogen selenide.; hCG, human chorionic gonadotropin.; MEHP, mono(2-ethylhexyl) phthalate.; MTT, 3-(4,5-dimethyl-thiazol-2-yl)-2,5-diphenyl-tetrazolium bromide.; Na<sub>2</sub>-EDTA, disodium ethylenediaminetetraacetic acid.; NADPH, nicotinamide adenine dinucleotide phosphate, reduced form.; p53, protein 53.; PBS, phosphate-buffered saline.; PP, peroxisome proliferators.; PPARα, peroxisome proliferator-activated receptor α.; PPARβ, peroxisome proliferator-activated receptor β.; PPARγ, peroxisome proliferator-activated receptor γ.; ROS, reactive oxygen species.; Se, selenium.; SEM, standard error of mean.; Sepp1, selenoprotein P.; SM, selenomethionine.; SS, sodium selenite.; TNB, 5-thio-2-nitrobenzoic acid.; TrxR, thioredoxin reductase.

\* Corresponding author. Fax: +90 3123092958.

E-mail address: fhincal@t.net (F. Hincal).

0041-008X/\$ – see front matter © 2010 Elsevier Inc. All rights reserved.

doi:10.1016/j.taap.2010.07.016

### Introduction

Phthalic acid esters are the most abundantly produced plasticizers, and known as endocrine disruptors and peroxisome proliferators (PP). Their inevitable environmental exposures in humans have been suspected to contribute to the increasing incidence of testicular dysgenesis syndrome (TDS) that is a range of reproductive defects including cryptorchidism and hypospadias in newborn boys, and testicular cancer and reduced sperm quality in adult males (Swan, 2008). In fact, TDS has been shown to develop in male rats that are exposed to phthalates *in utero* (Fisher et al., 2003). Di(2-ethylhexyl)-phthalate (DEHP) is the most important phthalate derivative with its high production, use and occurrence in the environment. It is mainly used in polyvinyl chloride plastics in the form of numerous consumer and personal care products and medical devices. The typical human exposure to DEHP ranges from 3 to 30 μg/kg/day (Doull et al., 1999) but, can be exceeded in specific medical conditions reaching 1.5 mg/



kg/day exposure in hemodialysis patients, or as high as 10–20 mg/kg/day during neonatal transfusion or parenteral nutrition (Loff et al., 2000; Kavlock et al., 2005).

The mechanisms by which phthalates and specifically DEHP exert their toxic effects in reproductive system are not yet fully elucidated. Some of the effects of phthalate are related to their anti-androgenic potential (Ge et al., 2007; Noriega et al., 2009). A peroxisome proliferator-activated receptor  $\alpha$  (PPAR $\alpha$ )-mediated pathway based on their PP activity (Gazouli et al., 2002), and activation of metabolizing enzymes leading to free radical production and oxidative stress have also been suggested (O'Brien et al., 2005). Although Sertoli cells were thought to be the primary targets of phthalate exposure in testis (Grasso et al., 1993), available data suggest that Leydig cells are one of the main targets (Ge et al., 2007). Leydig cells are the primary source of testosterone production in males, and differentiation of Leydig cells in the testes is one of the primary events in the development of the male body and fertility (Zhang et al., 2008). Using the MA-10 mouse Leydig tumor cell line as a model system may, therefore, offer a valuable model in studying the direct effects of environmental chemicals, particularly those of endocrine disruptors on Leydig cell function *in vitro*. MA-10 cells are by far the best characterized and more widely used lines of cultured Leydig tumor cells that were independently derived from the M5480 tumor, a hormonally responsive mouse Leydig tumor (Ascoli, 1981).

The essential trace element selenium (Se), is the important component of cellular antioxidant defense and is involved in the modulation of intracellular redox equilibrium with its some 25 forms of cellular selenoproteins, particularly with glutathione peroxidases (GPx), and thioredoxin reductases (TrxR) (Oberley et al., 2000). Se is actively involved in many fundamental biological processes ranging from immune functions to apoptosis, and protection and repair of DNA (Ganther, 1999). It is essential for the production of normal spermatozoa and thus plays a critical role in testis, sperm, and reproduction (Flohé, 2007). The major role of Se in fertility is mediated by the membrane bound phospholipid hydroperoxide glutathione peroxidase (GPx4) which is the most abundant selenoprotein in testis (Flohé, 2007; Ursini et al., 1999). Testis Se is known to be remarkably and preferentially maintained in Se deficiency. Severe and prolonged deficiency results in sterility as spermatogenesis was arrested, whereas in less severe Se deprivation reduced sperm motility leading to impaired fertilization capacity and abnormal sperm morphology were reported (Maiorino et al., 2006). On the other hand, epidemiological studies have suggested that low serum Se levels were associated with an increase in the incidence of cancer (Clark et al., 1991). The chemopreventive and chemotherapeutic mechanisms of Se still remain unclear. Protection against oxidative damage, induction of apoptosis secondary to production of reactive oxygen species (ROS), and regulation of the thioredoxin (Trx) redox system are among the many potential mechanisms proposed (Combs and Gray, 1998; Ganther, 1999; Kitahara et al., 1993) which also seem to be closely related to the roles of Se in the reproductive system.

Oxidative stress and, thus, ROS play an important role in the modulation of several important physiological functions, but also accounts for changes that can be detrimental to the cells (Dröge, 2002). ROS are shown to contribute to cellular damage, apoptosis and cell death, but also involved in regulation of gene expression by controlling signal transduction through direct participation in cell signaling, and/or modulation of cell redox state (Dalton et al., 1999; Finkel, 1998). ROS have also been suspected of being involved in the formation of testicular atrophy in phthalate-exposed rats (Kasahara et al., 2002). On the other hand, p53 tumor suppressor protein is a redox sensitive protein known to play important roles in controlling the integrity and correctness of all processes in each individual cell. Activation of p53 by ROS and exogenous DNA damages can lead to growth arrest of the cell, DNA repair induction or apoptosis (Kim et al., 2009). Several environmental chemicals including phthalates have

been shown to induce apoptosis in the reproductive tract of rodents through p53 induction (Chandrasekaran and Richburg, 2005).

On the basis of these knowledge and available data, it seems useful to examine modulation of cellular redox by Se and whether Se supplementation is effective on the effects of phthalates in rat reproductive system. In the current study, MA-10 mouse Leydig cells cultured with and without Se supplementation were used as a model, and the effects of exposure to DEHP and its major metabolite MEHP on the viability, enzymatic and non-enzymatic antioxidant status, ROS production, p53 expression and DNA damage were investigated.

## Materials and methods

**Chemicals.** MEHP was obtained from Cambridge Isotope Laboratories® (Andover, MA, USA). The protein assay kit was from Uptima Interchim® (Montluçon, France). NaOH was purchased from Carlo Erba® (Rodano, Italy). Dulbecco's modified Eagle medium (1:1) nutrient mixture (DMEM/F-12) was purchased from Gibco® (Courbevoie, France). 5-(and 6-) chloromethyl-2',7'-dichlorodihydrofluorescein diacetate (CM-H<sub>2</sub>DCFDA) was purchased from Molecular Probes Detection Technologies, Invitrogen® (Eugene, OR, USA). The EnVision Plus staining kit was purchased from Dako® (Carpinteria, CA, USA). All the other chemicals including DEHP, sodium selenite (SS), selenomethionine (SM), dimethyl sulfoxide (DMSO), 3-(4,5-dimethylthiazol-2-yl)-2,5-diphenyl-tetrazolium bromide (MTT), 5,5'-dithiobis (2-nitrobenzoic) acid (DTNB), 1-chloro-2,4-dinitrobenzene (CDNB), fetal bovine serum (FBS), Mayers hematoxylin nuclear stain, and saponin from quillaja bark; colorimetric assay kits for thioredoxin reductase (TrxR), and glutathione (GSH) measurements; Cell Lytic M cell lysis reagent, protease inhibitor cocktail, were obtained from Sigma-Aldrich® (St. Louis, MO, USA). Anti-p53, the mouse monoclonal antibody, sc-263 was obtained from Santa Cruz Biotechnology Inc® (Santa Cruz, California, USA). The goat anti-mouse horseradish peroxidase (HRP) conjugated secondary antibody was purchased from Invitrogen Molecular Probes® (Oregon, USA).

**Cell culture and treatment.** MA-10 mouse Leydig tumor cells were a generous gift from Prof. Mario Ascoli (Department of Pharmacology, University of Iowa College, Iowa City, USA) and maintained in Waymouth medium containing 15% (v/v) heat-inactivated horse serum, and 50 µg/mL gentamicin as previously described (Ascoli, 1981). Culturing of the MA-10 cells were accomplished in DMEM/F-12 (1:1) medium supplemented with 15% horse serum and gentamicin (50 µg/ml) using gelatin-coated culture flasks, at 37 °C in a humidified incubator under 5% CO<sub>2</sub>. For sub-cultivation cells were trypsinized, washed with sterile phosphate-buffered saline (PBS) and centrifuged at 1500 × g for 5 min. For the experiments only the cells of 10–12 passages were used.

SS and SM stock solutions were prepared in sterile, deionized water. DEHP (50 mM) and MEHP (100 µM) stock solution were prepared in 0.1% DMSO, and fresh dilutions were made using culture medium to achieve final concentrations ranging from 1 to 10 mM for DEHP and from 1 to 10 µM for MEHP. Cell viability measurements were performed in MA-10 cells incubated with various concentrations of DEHP or MEHP for 24 h. For the assessment of protective effect of Se, MA-10 cells supplemented with 30 nM SS or 10 µM SM were cultured for 72 h, then exposed to various concentrations of DEHP or MEHP for 24 h while continuing the Se supplementation. The doses of Se in the form of SS and SM used in this study were chosen from preliminary experiments (not shown) as concentrations do not inhibit cell growth and do not cause cytotoxicity, but result in maximal GPx1 induction after 72 h of incubation.

For the measurement of enzyme activities, ROS and total GSH levels, p53 expression, and for alkaline single-cell gel electrophoresis (SCGE, Comet assay), following treatment groups of MA-10 cells were prepared: Non-treated cells (NT-C): MA-10 cells were cultured

without any treatment for 72 h; SS-supplemented cells (SS-S): MA-10 cells were cultured with 30 nM SS for 72 h; SM-supplemented cells (SM-S): MA-10 cells were cultured with 10  $\mu$ M SM for 72 h; DEHP-treated cells (DEHP-T): MA-10 cells were cultured with 3 mM DEHP for 24 h; DEHP-treated SS-S cells (SS/DEHP-T): SS-S cells were cultured with 3 mM DEHP for 24 h; DEHP-treated SM-S cells (SM/DEHP-T): SM-S cells were cultured with 3 mM DEHP for 24 h; MEHP-treated cells (MEHP-T): MA-10 cells were cultured with 3  $\mu$ M MEHP for 24 h; MEHP-treated SS-S cells (SS/MEHP-T): SS-S cells were cultured with 3  $\mu$ M MEHP for 24 h; MEHP-treated SM-S cells (SM/MEHP-T): SM-S cells were cultured with 3  $\mu$ M MEHP for 24 h.

**Determination of cell viability.** Cell viability was determined by a modified MTT assay (Cory et al., 1991), in conjunction with trypan blue counting. 3000 cells per well were plated onto 96-well microtiter plates in 200  $\mu$ L medium with or without DEHP, MEHP, SS or SM. After incubation for specified times at 37 °C in a humidified incubator, the medium was removed, cells were washed twice with PBS and 20  $\mu$ L of MTT (5 mg/mL in PBS) was added to each well. The medium was removed 2 h later, 200  $\mu$ L of DMSO was added to dissolve the formazan product and the absorbance was read at 570 nm using Multiscan Ascent microtiter plate reader (Labsystems, France). The absorbance was proportional to viable cell number, and cell survival was calculated as the percentage of the staining values of untreated cultures. The percentage viability was calculated as "% specific viability = [(A - B) / (C - B)] / 100" where A = absorbance of the treated cells at 570 nm, B = absorbance of the medium at 570 nm, and C = absorbance of the control cells at 570 nm.

**Antioxidant enzyme assays and glutathione levels.** After specified incubation periods and trypsinization, cells were lysed using Cell Lysis M Cell Lysis agent with a protease inhibitor cocktail, and then centrifuged at 4000 rpm, 4 °C for 10 min. After further centrifugation at 13,000 rpm, 4 °C, for 20 min, antioxidant enzyme activities and GSH levels were measured in the supernatant.

The activity of cytosolic GPx (GPx1) was measured in a coupled reaction with glutathione reductase (GR) as described earlier (Flohé and Günzler, 1984; Günzler et al., 1974). The assay is based on the instant and continuous reduction of oxidized glutathione (GSSG) formed during GPx1 reaction by an excess of GR activity providing for a constant level of GSH. As a substrate, t-butyl hydroperoxide used and concomitant oxidation of NADPH was monitored spectrophotometrically at 340 nm. One unit of enzyme was defined as the amount of GPx1 that transformed 1  $\mu$ mol of NADPH to NADP per minute at 37 °C.

Cytosolic TrxR activity was determined colorimetrically using ThioRedoxin Reductase Assay kit. As described previously (Arner et al., 1999), the method is based on the reduction of DTNB with NADPH to 5-thio-2-nitrobenzoic acid (TNB) that is measured at 412 nm. One unit of TrxR activity was defined as the enzyme that caused an increase in  $A_{412}$  of 1.0 per minute per mL at pH 7.0 at 25 °C.

Cytosolic glutathione-S-transferase (GST) activity was determined according to the method of Habig et al. (1974) using CDNB as a substrate and measuring the change in absorbance at 340 nm. The results were given as nmol/min/mg protein.

For the measurement of the total GSH levels, cells were diluted with 5-sulphosalicylic acid for protein precipitation, and centrifuged at 4000 rpm, 4 °C, for 10 min. Supernatants were used for total GSH determinations by using Glutathione Assay kit. The assay was based on the reduction of DTNB by NADPH by a reaction catalyzed by GR using GSH at 412 nm (Akerboom and Sies, 1981). The results were given as pmol GSH/mg protein.

Protein content of the samples was determined by bicinchoninic acid assay (BCA) using a protein assay kit (Krieg et al., 2005). The results were given as mg/mL protein.

**Measurement of intracellular ROS production.** Total intracellular ROS production was measured using peroxide sensitive fluorescent probe CM-H<sub>2</sub>DCFDA as described earlier (Loikkanen et al., 1998). The study was conducted in the dark, and 70–80% confluent cells were used. MA-10 cells seeded in 96-well plates with/without SS (30 nM) and SM (10  $\mu$ M) incubated at 37 °C in a humidified incubator under 5% CO<sub>2</sub> for 72 h. After removal of the culture media, cells were loaded with CM-H<sub>2</sub>DCFDA in PBS buffer for 30 min at room temperature. The cellular esterase activity results in the formation of the nonfluorescent compound, the 2',7'-dichlorofluorescein (DCFH). DCFH is rapidly oxidized in the presence of ROS to a highly fluorescent 2',7'-dichlorofluorescein (DCF). The cells were washed, then incubated with with/without DEHP (3 mM) or MEHP (3  $\mu$ M) at 37 °C in a humidified incubator under 5% CO<sub>2</sub> for 0, 30 and 60 min. DCF fluorescence was measured with a PerkinElmer Victor 3 1420 multiwell fluorometer (Perkin Elmer®, Buckinghamshire, UK) at an excitation wavelength of 485 nm and an emission wavelength of 535 nm. After data acquisition, Wallac 1420 Manager software was used to analyze ROS production. Background fluorescence was obtained from cell-free wells containing 5  $\mu$ M DCF in 0.5 mL of PBS and subtracted from the fluorescence values found. The multiwell plate was kept in a cell culture incubator between the measurements. The exposures were repeated 3–4 times with three parallel measurements. Fluorescence values were normalized to the cell numbers. For each condition, 8-wells with triplicate measurements were used and the mean of three independent experiments was given as a result.

**p53 evaluation by immunocytochemistry.** The expression of p53 in MA-10 cells was examined immunocytochemically using the EnVision Plus System. MA-10 cells, treated and cultured as described above, were washed with PBS for 3 min shaking on a shaker gently, and fixed with 4% formaldehyde in PBS at room temperature. Cells were rinsed with ddH<sub>2</sub>O once, and washed with PBS for 3 min as were done between each step, then permeabilized with PBS/0.5% saponin/0.3% Triton X-100 for 3 times, each 5 min on the shaker. Cells were blocked with PBS/10% FBS/0.3% Triton X-100 at 37 °C for 1 h, then PBS washed cells were incubated with diluted primary antibody overnight at 4 °C. Secondary antibody was used directly and cells were incubated at 25 °C for 30 min. Cells were again washed with 1 $\times$  PBS and later with 1 $\times$  PBS/2% FBS/0.3% Triton X-100 3 times, and stained with 3,3'-diaminobenzidine (DAB) Chromogen solution. The staining was stopped by adding ddH<sub>2</sub>O, and then hematoxylin was used as a nuclear stain. Images were acquired with a DC490 digital camera (Leica, Wetzlar, Germany). Cells were considered to be positive when the brown staining was present in the nucleus. For each condition 3 slides were counted and the results were given as percentage of p53 nuclear stainings.

**Alkaline single-cell gel electrophoresis (Comet assay).** DNA damage was evaluated using the alkaline Comet assay that allows the measurement of single- and double-strand breaks together with alkali-labile sites. The assay was performed as described earlier (Singh et al., 1988; Tice et al., 2000) and measurements were made in two consecutive days on triplicate slides and the results were given as the mean value of the two days. Immediately after the treatments, the cells were isolated, washed and re-suspended in PBS at a density of  $\sim 2.5 \times 10^6$  cells/mL. 50  $\mu$ L of this suspension was mixed with 450  $\mu$ L solution of low melting point agarose (0.6% in PBS), and 100  $\mu$ L of the solution was spread on a microscope slide covered with 1% agarose. Cells were lysed (2.5 M NaCl, 0.5 M Na<sub>2</sub>-EDTA, 10 mM Tris, 1% sodium lauryl sulfate, 1% Triton X-100, 10% DMSO, pH 10) at 4 °C in the dark for 1 h. After lysis, cells were immersed in freshly prepared alkaline electrophoresis buffer (300 mM NaOH, 1 mM Na<sub>2</sub>-EDTA, pH 13) for 30 min to allow DNA unwinding. Electrophoresis was then performed at 25 V/300 mA for 30 min. Slides were rinsed three times for 5 min with neutralization buffer (0.4 M Tris-HCl, pH 7.4), and stained with

ethidium bromide (20 µg/mL) in PBS. For quantification, fluorescence microscope (Carl Zeiss®, Germany) was used which was connected to a charge-coupled device (CDC) and a computer-based analysis system (Comet assay IV software, Perceptive Instruments Ltd), and the extent of DNA damage was determined after electrophoretic migration of DNA fragments in the agarose gel. For each condition, 50 randomly selected comets on each slide were scored, and the tail% intensities (percentage of DNA in the tail) and the tail moments (product of comet length and tail intensity) were determined as an average of triplicate slides.

**Statistical analysis.** The data were expressed as mean ± standard error (SEM). Statistical significances of differences among treatment groups were determined by use of one-way analysis of variance and covariance (ANOVA), followed by Student's *t*-test using a Statistical Package for Social Sciences Program (SPSS). A *p*-value < 0.05 was considered as statistically significant.

**Results**

**Cell viability**

In Fig. 1, cell viability data produced by MTT assay for DEHP-, and MEHP-treated MA-10 cells were presented as relative to zero dose of DEHP or MEHP. DEHP had a flat dose-cell viability response curve, so that MA-10 cells showed ~80 to 60% survival at a dose range of 10 µM to 0.5 mM DEHP (Fig. 1A). Whereas MEHP was highly toxic at µM range with a very sharp dose-response curve, so that there was no cell survival at doses 10 µM and higher (Fig. 1B). The IC<sub>50</sub> values for DEHP and MEHP were found to be approximately 3 mM and 3 µM, respectively. This demonstrated that MEHP, the main metabolite of DEHP, was the main active form in MA-10 cells with an almost ~1000-fold higher cytotoxicity than the parent compound.

Se supplementation of the cells with either SS (30 nM) or SM (10 µM) was protective against the cytotoxic effects of DEHP, and MEHP.

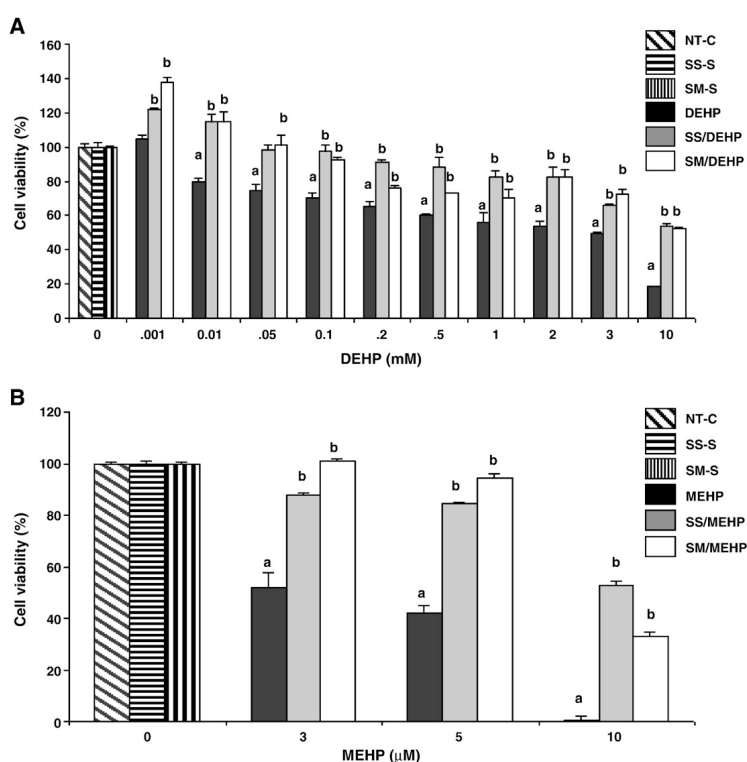


**Fig. 1.** Cell viability in phthalate-exposed MA-10 mouse Leydig tumor cell line, and protective effect of selenium supplementation. Cell viability was determined by MTT assay and data were presented as relative to zero dose of DEHP or MEHP. Values are given as mean ± SEM of *n* = 3 independent experiments and triplicate measurements. A. Cytotoxicity of various concentrations of DEHP on MA-10 Leydig cells cultured with or without selenium supplementation. NT-C: non-treated MA-10 cells cultured for 72 h; SS-S: MA-10 cells supplemented and cultured with 30 nM SS for 72 h; SM-S: MA-10 cells supplemented and cultured with 10 µM SM for 72 h; DEHP: MA-10 cells treated with various concentrations of DEHP for 24 h; SS/DEHP: SS-S cells cultured with various concentrations of DEHP for 24 h; SM/DEHP: SM-S cells cultured with various concentrations of DEHP for 24 h. 24 h. <sup>a</sup>*p* < 0.05 vs. NT-C. <sup>b</sup>*p* < 0.05 vs. DEHP. B. Cytotoxicity of various concentrations of MEHP exposure on MA-10 Leydig cells cultured with or without selenium supplementation. MEHP: MA-10 cells cultured with various concentrations of MEHP for 24 h; SS/MEHP: SS-S cells cultured with various concentrations of MEHP for 24 h; SM/MEHP: SM-S cells cultured with various concentrations of MEHP for 24 h. <sup>a</sup>*p* < 0.05 vs. NT-C. <sup>b</sup>*p* < 0.05 vs. MEHP.

In DEHP-exposed cells, for concentrations up to 2 mM, Se was highly protective providing  $\geq 50\%$  higher viability, and the effects of SS was higher ( $p < 0.05$ ) than SM at 0.2, 0.5 and 1 mM DEHP exposures. In cells exposed to an  $IC_{50}$  dose of DEHP, both SS and SM forms of Se provided higher viability ( $\sim 36$  and  $48\%$ , respectively,  $p > 0.05$ ) than DEHP-treated cells (Fig. 1A). Whereas a complete viability as control cells was observed with SM supplementation in MA-10 cells exposed to an  $IC_{50}$  dose of MEHP (Fig. 1B), supplementation with SS maintained the cell viability at a level of  $\sim 85\%$  of control cells (NT-C), and the difference of SS and SM effects was significant ( $p < 0.05$ ).

#### Enzymatic and non-enzymatic antioxidants

The results of the antioxidant status assessment of MA-10 cells are illustrated in Fig. 2. Se supplementation of MA-10 cells with either SS or SM (that is SS-S and SM-S cells) significantly increased the activities of GPx1 (1.7- and 1.6-fold, respectively) and TrxR ( $\sim 1.6$ - and  $1.7$ -fold, respectively) compared to non-treated control cells (NT-C); but did not cause any change on the total GSH level and GST activity. The difference between the effects of SS and SM was insignificant.

In cells exposed to DEHP or MEHP, GPx1 activity decreased  $\sim 2.5$  and  $\sim 4$ -fold, respectively (Fig. 2A). Thus, the effect of MEHP was much higher. Se supplementation either with SS or SM in DEHP-exposed cells was able to enhance the GPx1 activity significantly even up to those of SS-S and SM-S cells. In MEHP-exposed cells, SS supplementation maintained the GPx1 activity almost at the control level,

whereas the effect of SM was significantly higher than that of SS, elevating the activity of GPx1 to the level of SM-S cells.

The same level of decrease ( $\sim 2.4$ -fold) was observed in cytosolic TrxR activity of MA-10 cells exposed to the parent phthalate or the main metabolite (Fig. 2B). Supplementation of Se with SS was able to elevate the cytosolic TrxR activity of MEHP-exposed cells to the levels of SS-S cells, and with SM to the level of control cells. However, in DEHP-exposed cells, the increase of TrxR activity with Se supplementation was rather low reaching only  $\sim 75$ – $80\%$  of that of control cells.

GST activity also decreased significantly in DEHP-T (60%) and MEHP-T (53%) cells. Neither SS nor SM supplementation restored the activity of the cytosolic GST in phthalate-exposed cells. In contrast, Se supplementation in both SS and SM forms decreased the enzyme activity in MEHP-exposed cells. Whereas, GST activity remained the same with the presence of SS, but was found even lower with SM supplementation in DEHP-exposed cells (Fig. 2C).

Total GSH levels decreased significantly in DEHP-T ( $\sim 40\%$ ) and MEHP-T ( $\sim 42\%$ ) cells (Fig. 2D). Se supplementation provided significant restoration in both groups elevating the GSH content up to  $\sim 75$ – $80\%$  of the NT-C levels.

#### ROS production

Fig. 3 illustrates the intracellular production of ROS in MA-10 cells at different time points. As shown in Fig. 3A, there was no significant ROS production in NT-C cells at time point 30 min, but after 60 min of

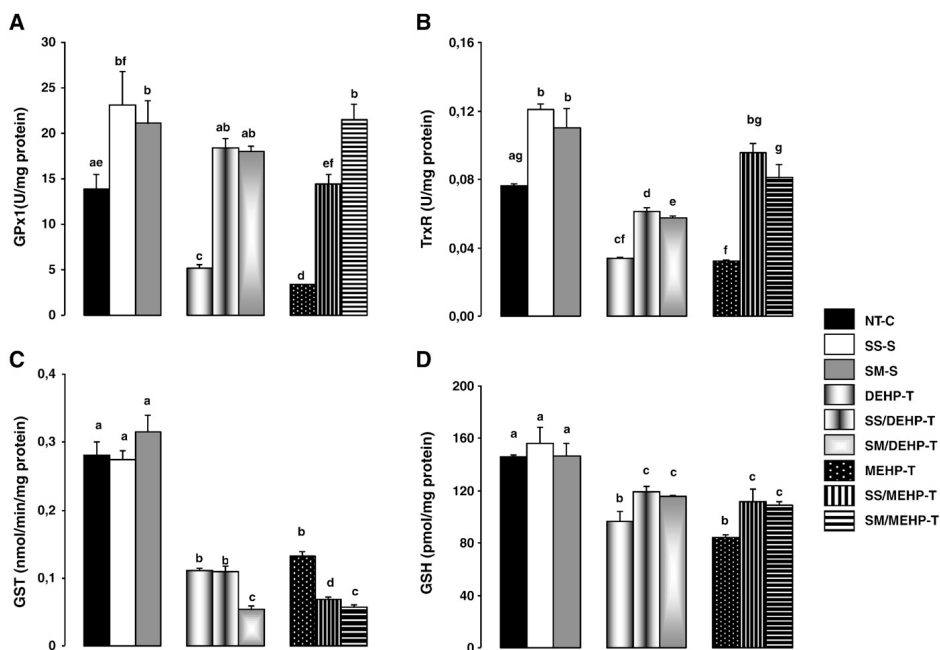


**Fig. 2.** Enzymatic and non-enzymatic antioxidant status in DEHP- or MEHP-treated MA-10 Leydig cells and effects of selenium supplementation. A. GPx1 activity. B. TrxR activity. C. GST activity. D. Total GSH level. Values are given as mean  $\pm$  SEM of  $n = 3$  independent experiments and triplicate measurements. Bars that do not share same letters (superscripts) are significantly different from each other ( $p < 0.05$ ). Measurements were performed in the following treatment groups of cells: NT-C: non-treated MA-10 cells cultured for 72 h; SS-S: MA-10 cells supplemented and cultured with 30 nM SS for 72 h; SM-S: MA-10 cells supplemented and cultured with 10  $\mu$ M SM for 72 h; DEHP-T: MA-10 cells cultured with 3 mM DEHP for 24 h; SS/DEHP-T: SS-S cells cultured with 3 mM DEHP for 24 h; SM/DEHP-T: SM-S cells cultured with 3 mM DEHP for 24 h; MEHP-T: MA-10 cells cultured with 3  $\mu$ M MEHP for 24 h; SS/MEHP-T: SS-S cells cultured with 3  $\mu$ M MEHP for 24 h; SM/MEHP-T: SM-S cells cultured with 3  $\mu$ M MEHP for 24 h.

incubation ROS production increased ~1.7-fold. Presence of Se in SS or SM forms did not change the intracellular ROS levels when compared to NT-C cells neither after 30 min nor 60 min of incubations.

DEHP and MEHP exposures caused strongly amplified production of ROS. At time point 30 min, ROS levels of the DEHP-exposed cells increased significantly, reaching ~2.4-fold of the level of time zero, and after 60 min of incubation the increase was ~3.5-fold (Fig. 3B). Whereas in MEHP-treated MA-10 cells, very sharp elevation of ROS production was observed reaching ~2.3-fold and ~11.4-fold of the initial level, at time points 30 min and 60 min, respectively (Fig. 3C).

Both SS and SM supplementations were highly effective against the generation of intracellular ROS induced by both phthalate derivatives. In the presence of SS, ROS levels in DEHP-exposed cells decreased ~2-fold and ~2.2-fold, at 30 and 60 min, respectively. Whereas, the decrease with SM supplementation was ~1.4-fold at both time points (Fig. 3B).

In MEHP-T cells, SS supplementation caused ~3.5-fold and ~1.8-fold decrease of ROS production at 30 min and 60 min, respectively. Whereas presence of Se in SM form provided ~2.6-fold and ~2.1-fold decrease of ROS generation at 30 min and 60 min, respectively (Fig. 3C).

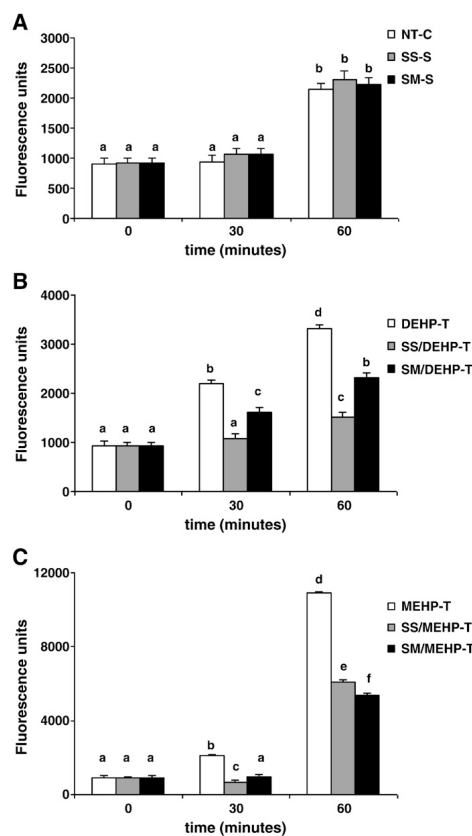


**Fig. 3.** ROS production in DEHP- or MEHP-exposed MA-10 Leydig cells and effects of selenium supplementation. Total intracellular ROS was measured using peroxide sensitive fluorescent probe CM-H<sub>2</sub>DCEFA at 0, 30, and 60 min. Values are given as mean  $\pm$  SEM of  $n = 3$  independent experiments and triplicate measurements. Bars that do not share same letters (superscripts) are significantly different from each other ( $p < 0.05$ ). A. ROS production in cells without phthalate exposure (NT-C: non-treated MA-10 cells cultured for 72 h; SS-S: MA-10 cells supplemented and cultured with 30 nM SS for 72 h; SM-S: MA-10 cells supplemented and cultured with 10  $\mu$ M SM for 72 h). B. ROS production in DEHP-treated cells (DEHP-T: MA-10 cells cultured with 3 mM DEHP for 24 h; SS/DEHP-T: SS-S cells cultured with 3 mM DEHP for 24 h; SM/DEHP-T: SM-S cells cultured with 3 mM DEHP for 24 h). C. ROS production in MEHP-treated cells (MEHP-T: MA-10 cells cultured with 3  $\mu$ M MEHP for 24 h; SS/MEHP-T: SS-S cells cultured with 3  $\mu$ M MEHP for 24 h; SM/MEHP-T: SM-S cells cultured with 3  $\mu$ M MEHP for 24 h).

#### p53 immunocytochemistry

As shown in Table 1, p53 protein expression in Se treated MA-10 cells was significantly lower (~65%) than the steady state level of the control cells (NT-C), and there was no difference between the protective effects of SS and SM. In MA-10 cells exposed to an IC<sub>50</sub> dose of DEHP, p53 expression was not induced. But a significant induction (~1.7-fold) of p53 expression was observed in MA-10 cells exposed to an IC<sub>50</sub> dose of MEHP. SS or SM supplementation enabled the phthalate-exposed cells to maintain the p53 expression almost at the basal level, or even lower as in the case of SS/DEHP-T cells. Fig. 4 shows the images of p53 expression in MEHP-treated cells along with the images of control groups.

#### DNA damage—Comet assay

Fig. 5 shows the results of the alkaline Comet assay performed on MA-10 cells exposed to an IC<sub>50</sub> dose of DEHP (3 mM) or MEHP (3  $\mu$ M) in the presence or absence of Se, with the illustrations of the examples of comet images.

Both DEHP and MEHP produced high level of DNA damage as evidenced by significantly increased tail intensity (%) (~3.4-fold and ~3.8-fold, respectively), and tail moment (~4.2-fold and ~3.8-fold, respectively) compared to non-treated MA-10 cells. The difference between the DNA damaging effects of the parent compound and the metabolite was insignificant.

Se supplementation itself did not cause any alteration on the steady state levels of the DNA damage biomarkers of MA-10 cells. But Se was highly effective to decrease the genotoxic effects of phthalate esters. Increased tail % intensities by DEHP and MEHP exposure were lowered ~50–55% with SS supplementation, whereas SM treatment

**Table 1**  
p53 immunocytochemistry scorings for the study groups.

Study group	% of nuclear p53 stained cells
NT-C	8.77 <sup>a</sup>
SS-S	2.99 <sup>b</sup>
SM-S	3.14 <sup>b</sup>
DEHP-T	9.38 <sup>a</sup>
SS/DEHP-T	6.72 <sup>c</sup>
SM/DEHP-T	8.76 <sup>a</sup>
MEHP-T	15.03 <sup>d</sup>
SS/MEHP-T	8.86 <sup>a</sup>
SM/MEHP-T	9.85 <sup>a</sup>

p53 expression was determined using EnVision Plus staining kit as described in Materials and Methods. Results were given as the percentage of p53 nuclear staining (mean  $\pm$  SEM). Means that do not share same letters (superscripts) are significantly different from each other ( $p < 0.05$ ).

Measurements were performed in the following treatment groups of cells: NT-C: non-treated MA-10 cells cultured for 72 h; SS-S: MA-10 cells supplemented and cultured with 30 nM SS for 72 h; SM-S: MA-10 cells supplemented and cultured with 10  $\mu$ M SM for 72 h; DEHP-T: MA-10 cells cultured with 3 mM DEHP for 24 h; SS/DEHP-T: SS-S cells cultured with 3 mM DEHP for 24 h; SM/DEHP-T: SM-S cells cultured with 3 mM DEHP for 24 h; MEHP-T: MA-10 cells cultured with 3  $\mu$ M MEHP for 24 h; SS/MEHP-T: SS-S cells cultured with 3  $\mu$ M MEHP for 24 h; SM/MEHP-T: SM-S cells cultured with 3  $\mu$ M MEHP for 24 h.

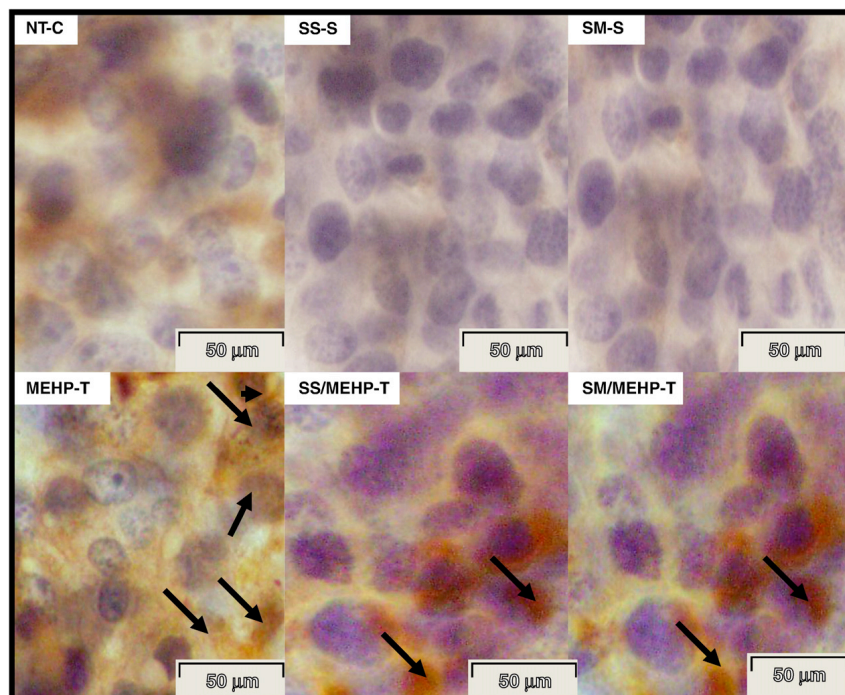


**Fig. 4.** Immunocytochemistry of p53 expression, using EnVision Plus staining kit, in MEHP-treated MA-10 Leydig cells in the presence and absence of selenium p53 was visualized as brown precipitate in the nucleus of the cells. Arrows indicate MA-10 cells with p53 positive staining. For each condition 3 slides were counted and the results were given as the percentage of p53 nuclear staining. The images represent the p53 protein of the following treatment groups of cells: NT-C: non-treated MA-10 cells cultured for 72 h; SS-S: MA-10 cells supplemented and cultured with 30 nM SS for 72 h; SM-S: MA-10 cells supplemented and cultured with 10  $\mu$ M SM for 72 h; MEHP-T: MA-10 cells cultured with 3  $\mu$ M MEHP for 24 h; SS/MEHP-T: SS-S cells cultured with 3  $\mu$ M MEHP for 24 h; SM/MEHP-T: SM-S cells cultured with 3  $\mu$ M MEHP for 24 h.

provided ~30–40% protection. SS decreased the tail moments of the DEHP- or MEHP-exposed cells by ~55–65%, whereas the protective effect of SM on tail moments was significantly lower than SS as being ~45% and ~34% for the effects of DEHP and MEHP, respectively. However, both SS and SM reduced the tail moments of the DEHP- and MEHP-exposed cells down to the levels that were not significantly different than that of control cells.

#### Discussion

DEHP is a well-known peroxisome proliferator, and regarded as a non-classic type endocrine disruptor, that is, in contrast to the classical endocrine disruptors which interfere with endocrine process at the receptor level, alters reproductive function by affecting hormone synthesis (Akingbemi et al., 2004; Gazouli et al., 2002; Wilson et al., 2004). Exposures to DEHP or its main metabolite MEHP have been found to result in decreased testicular testosterone levels in mice, indicating that testosterone producing Leydig cells were also the target of the phthalates, besides Sertoli cells (Jones et al., 1993). In fact, inhibition of LH-stimulated testosterone secretion by MEHP in MA-10 Leydig cells was previously demonstrated (Freeman and Ascoli, 1983; Gazouli et al., 2002), and co-administration of testosterone with DEHP was reported to prevent the DEHP-induced testicular toxicity (Parma et al., 1987).

The induction of oxidative stress was previously suggested to represent a common mechanism in endocrine disruptor-mediated dysfunction, specific to certain testicular cells (Latchoumycandane and Mathur, 2002). Recent data have also shown that phthalates were able to produce free radicals by several pathways in germ cells including activation of PPAR $\alpha$ , suggesting the possibility that oxidative stress and mitochondrial dysfunction in germ cells may contribute to phthalate-induced disruption of spermatogenesis (Gazouli et al., 2002; Suna et al., 2007). DEHP treatment, indeed, was reported to provoke oxidative stress as measured by increases in ROS in subsequently isolated rat spermatocytes (Kasahara et al., 2002). MEHP was reported to increase peroxiredoxin 3 and cyclooxygenase-2 levels in germ cells indicating that the disruption of cellular redox mechanisms in spermatocytes (Onorato et al., 2008). Thus, at least one of the mechanisms underlying the reproductive toxicity of DEHP might be the induction of intracellular ROS and/or to cause alterations on intracellular enzymatic and non-enzymatic antioxidants, thereby to produce oxidative stress.

In the current study, using a well-established cell model, the MA-10 mouse Leydig tumor cell line (Ascoli, 1981), the effects of direct exposure to DEHP and MEHP on Leydig cells, including cytotoxicity, genotoxicity and oxidative stress potential were investigated. MA-10 cells produce more progesterone than testosterone, but otherwise resemble normal Leydig cells (Mylchreest et al., 2002). They contain

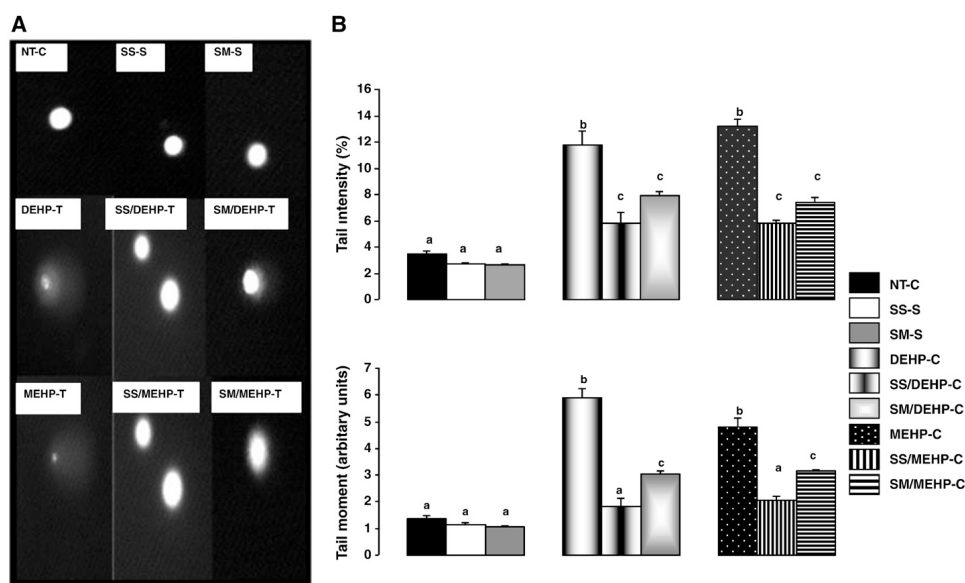


**Fig. 5.** Results of alkaline Comet assay in DEHP- or MEHP-treated MA-10 Leydig cells and effects of selenium supplementation. A. Typical images of Comets. B. Tail % intensities and tail moments as a measure of DNA damage. Values are given as mean  $\pm$  SEM of  $n = 2$  independent experiments and triplicate measurements. Bars that do not share same letters (superscripts) are significantly different from each other ( $p < 0.05$ ). Measurements were performed in the following treatment groups of cells: NT-C; non-treated MA-10 cells cultured for 72 h; SS-S; MA-10 cells supplemented and cultured with 30 nM SS for 72 h; SM-S; MA-10 cells supplemented and cultured with 10  $\mu$ M SM for 72 h; DEHP-T; MA-10 cells cultured with 3 mM DEHP for 24 h; SS/DEHP-T; SS-S cells cultured with 3 mM DEHP for 24 h; SM/DEHP-T; SM-S cells cultured with 3 mM DEHP for 24 h; MEHP-T; MA-10 cells cultured with 3  $\mu$ M MEHP for 24 h; SS/MEHP-T; SS-S cells cultured with 3  $\mu$ M MEHP for 24 h; SM/MEHP-T; SM-S cells cultured with 3  $\mu$ M MEHP for 24 h.

both PPAR $\alpha$  and PPAR $\beta$ , but not PPAR $\gamma$  (Dostal et al., 1988) as in the case of both Leydig and Sertoli cells of adult rats (Braissant et al., 1996).

Cytotoxicity, in the current study, was assessed using the MTT assay of mitochondrial integrity, a marker of cell viability. Significantly decreased cell viability was observed with 10  $\mu$ M and higher concentrations of DEHP. However, in agreement with earlier reports (Kambia et al., 2004), and with the results of our recent study conducted on LNCaP cells (Erkekoglu et al., 2010), cytotoxicity of MEHP was much higher than the parent compound, indicating the toxicity of DEHP is mostly based on the activity of MEHP. In fact, the difference between the  $IC_{50}$  values of the two agents was almost three orders of magnitude. However, the toxicity range of MEHP reported by two studies was significantly different than ours. Dees et al. (2001) examined the effects of various concentrations of MEHP on progesterone production, cell viability, protein content and cell morphology in MA-10 cells in the presence of hCG, and they observed no effect for the range of 0.3  $\mu$ M to 1 mM MEHP, and markedly decreased cell viability (to 16%) at 3 mM–10 mM. In a very recent study which was published during the submission of the present study, it was also reported that at concentrations as high as 300  $\mu$ M, MEHP was not toxic to the MA-10 cells (Fan et al., 2010). The reason for this discrepancy is not known, however, might be due to the differences in the experimental designs, the cell culturing conditions, particularly cell density/number, and source and purity of the MEHP, and may be the presence or absence of hCG.

Se supplementation was highly effective in maintaining the viability of MA-10 cells exposed to various doses of DEHP, and MEHP. The protective effect of 30 nM SS supplementation on the cell

survival was almost as the same level as the protection provided by 10  $\mu$ M SM. Thus, more SM was required to achieve a similar effect as was obtained with the more bioavailable form of Se, selenite. The doses of Se in the form of SS and SM used in this study were chosen from preliminary experiments (not shown) as the concentrations did not inhibit cell growth and did not cause cytotoxicity, but result in maximal GPx1 induction after 72 h of incubation. These concentrations were also in the same range as those concentrations of SS and SM that were shown previously with the same properties for several other cell types (Bhamre et al., 2003; Chu et al., 1990; Mansur et al., 2000). SS is commonly used for cell culture and animal studies, and SM is the most common form of Se obtained from the diet. SM is converted to H<sub>2</sub>Se through transsulfuration and  $\beta$ -lyase cleavage, whereas SS interacts with GSH to form GSSeSG which is subsequently reduced to H<sub>2</sub>Se. H<sub>2</sub>Se derived via both pathways can be converted to selenophosphate which is then used in the synthesis of selenoproteins. This difference in Se metabolism is likely to account for the greater efficiency of SS over SM, as has been reported for a variety of cell types (Zhuo et al., 2009).

Se plays a critical role in testis, sperm, and reproduction. In rodent testis, Se concentrations are typically higher than for any other tissue except kidney, and unlike most other tissues except brain and endocrine tissues, generally do not decrease even with prolonged Se deficiency, showing that Se is preferentially maintained in the rodent testis (Behne and Höfer-Bosse, 1984; Behne et al., 1988). Selenoprotein P (Sepp1) is the responsible molecule for the targeted trafficking of Se to testis (Hill et al., 2003; Schomburg et al., 2003). When Se supply is limited due to Se deficiency, incoming Se as Sepp1 would be delivered preferentially to the Sertoli cells, thereby maintaining testis Se

concentrations. Selenoproteins identified in testis are Sepp1, mitochondrial and cytosolic TrxR, GPx1, and GPx4 as the most abundantly present selenoprotein in rat testis (Maiorino et al., 2006; Roveri et al., 1992; Tramer et al., 1998). Leydig cells, on the other hand, do not contain appreciable Sepp1 protein (Olson et al., 2007), but they are the major cells expressing Sepp1 mRNA in testis (Koga et al., 1998; Steinert et al., 1998). GPx1 has been implicated in antioxidant defense in Leydig cells that are presumed to produce H<sub>2</sub>O<sub>2</sub> during steroid hormone synthesis (Peltola et al., 1996). It is thought that the seminiferous epithelium and mature sperm also require a particularly efficient protection against oxidative stress (Tramer et al., 1998; Zini and Schlegel, 1997). GPx1, as the selenoperoxidase most efficient in H<sub>2</sub>O<sub>2</sub> reduction would indeed be the enzyme of choice to meet this demand (Ursini et al., 1995).

The induction of GPx1 activity in MA-10 cells that we observed with Se supplementation was previously demonstrated in several tissues, and reported as being due to enhanced translation and not transcription of the enzyme (Hu and Diamond, 2003). The Se-containing cytosolic enzyme GPx1 plays an important role in the defense mechanisms of mammals against damage by catalyzing the reduction of H<sub>2</sub>O<sub>2</sub> and a large variety of hydroperoxides (Ursini et al., 1995). GPx1, in addition to affecting GSH/GSSG, controls the cellular content of H<sub>2</sub>O<sub>2</sub> (or other organic hydroperoxides) and NADPH/NADP<sup>+</sup>, so that it may regulate the cellular redox status. Taking into account the critical importance of GPx1 activity and expression, the GPx1 activity reducing effects of DEHP (~2.5-fold) and MEHP (~4-fold) shown in this study in MA-10 cells might be considered as having important implications in testicular function. Intracellular GSH is a key redox regulator that is crucial for multiple biological functions. The decrease of GSH we observed in phthalate treated cells was further supportive of the occurrence of oxidative stress and disturbance of the intracellular redox equilibrium, because removal of H<sub>2</sub>O<sub>2</sub> by GPx1 requires GSH as a cofactor. Loss of GSH also occurs through conjugation to endogenous and exogenous electrophilic centers in reactions catalyzed by GSTs, the enzymes capable of detoxifying genotoxic electrophilic compounds by catalyzing their conjugation to GSH, and thus inactivate several environmental chemicals (Hayes and Pulford, 1995). However, in this study the activity of cytosolic GST was found to be reduced more than 50% in DEHP, and MEHP-treated cells, indicating that the phthalate exposure disturbed the GST expression and/or activity in MA-10 cells as it disturbed GPx1. Se supplementation was not effective in restoring the GST activity and even lowered more, a finding that remained to be explained.

The Trx system, together with TrxR enzymes and NADPH, comprises an important defense system against oxidative stress and involved in many biological processes, such as DNA metabolism and repair, apoptosis, protein folding and degradation, regulation of several transcription factors and signal transduction (Björnstedt et al., 1997; Watson et al., 2004). Multiple TrxR enzymes are present, and cytosolic TrxR is a predominant form known for its antioxidant properties. Like GPx1, it plays a role in reducing oxidative species either directly or by regeneration of cellular antioxidants (Xia et al., 2003), and maintain the redox balance in the cell (Mustacich and Powis, 2000). Available data also indicate that cytosolic TrxR is regulated by the redox state of the cell (Gandin et al., 2009), and its specific activity is highly sensitive to concentration of Se in cellular milieu. Our findings showing ~2.4-fold decrease in cytosolic TrxR activity by both DEHP and MEHP exposures and significant restoration by Se supplementation, thus, provided more evidence for the alterations of cellular redox state induced by these two phthalates. Interestingly, protection by Se supplementation was complete only in MEHP-exposed cells. Our results also suggested the possibility that the decrease of TrxR activity contributes to the cytotoxicity of DEHP, and MEHP in MA-cells, as TrxR is essential for the normal growth of the cell, and inhibition of TrxR activity to below normal level has been reported to cause inhibited cell growth (Mustacich and Powis, 2000).

Various recent data have shown that ROS were involved in the modulation of cell redox state, and redox regulation of protein functions is now accepted as an additional regulatory mechanism of

normal cell physiology (D'Autreaux and Toledano, 2007; Veal et al., 2007). Thus, ROS recently gained attention as important second messengers. However, excessive production of ROS may lead to oxidative stress, loss of cell function, and cell death by apoptosis or necrosis (Nose, 2000). The increased intracellular ROS production with phthalate exposure in the current study, along with the observation of decrease in intracellular GSH level, is the predominant evidence of a shift in the redox equilibrium towards oxidation, thus occurrence of oxidative stress. In agreement with our results, Fan et al. (2010) also observed an increase in ROS generation with MEHP exposure in MA-10 cells, and demonstrated that the increase of ROS production even with the highest concentration of MEHP (300 μM) used in their study was blocked by preincubation of the cells with *N*-acetylcysteine (NAC). In this very recent study, the authors suggested that the MEHP-induced expression of *Cyp11a1* might be associated with the excess ROS generation.

Alteration of cell redox status by ROS can also change thiol groups in proteins and alter the activation of cell signaling proteins (Dalton et al., 1999; Finkel, 1998). p53 tumor suppressor protein is one of those various cell signaling proteins and known to be redox sensitive (Hainaut and Milner, 1993). When cells are exposed to oxidative stress, p53 is expressed at high levels by post-translational modifications (Burns and El-Deiry, 1999). These modifications occur rapidly and lead to the activation of p53, resulting in cell cycle arrest or apoptosis. Therefore, ROS are reported to function as p53 activators or p53 downstream effectors (Zhao et al., 2006). In fact, our results showed significant increase in nuclear p53 expression in MEHP-exposed cells further evidencing the alteration of intracellular redox state by phthalate exposure. Thus, our data suggested that MEHP, the main metabolite of DEHP, and possibly at proper doses DEHP itself induce nuclear p53 activation by producing ROS to activate p53. Determination of nuclear p53 is a good indicator of cell cycle arrest or apoptosis, because after the transfer of p53 to nucleus or after its overexpression, it is bound to the promoter regions of several genes including p21, thus, p53 acts as a transcriptional regulator (Ozturk et al., 2009). The ultimate results of all these alterations were the modulation of redox sensitive enzymes, DNA damage as evidenced with the results of alkaline Comet assay, and decreased cell viability. Our data also showed that, at the dose levels and forms we used, Se supplementation was protective against those adverse effects of DEHP and MEHP suggesting that Se exerted its protective effect by regulating the intracellular redox equilibrium of MA-10 cells.

Thus, the results of this study clearly showed the genotoxic potential of DEHP, and its main metabolite MEHP in MA-10 Leydig cells. This might have a contributory role on the overall effects of these compounds which are known as nongenotoxic rodent carcinogens (Rusyn et al., 2006). On the other hand, Se is known as bimodal in nature. At low concentrations, Se compounds are antigenotoxic and anticarcinogenic, whereas at high concentrations, they are mutagenic, toxic, and possibly carcinogenic (Letavayová et al., 2006). In this regard, it appears that the doses and the chemical forms of Se we used in this study were appropriate, did not exert any genotoxicity, but provided protection against the genotoxic effects of DEHP and MEHP on MA-10 cells at doses used within the study. The protection of DNA damages by Se might be through its involvement in DNA repair, but may also be due to a preventive effect in relation to its intracellular redox modulation.

In conclusion, the overall results of this study demonstrated the cytotoxicity and genotoxicity of DEHP, and its main metabolite MEHP in MA-10 mouse Leydig tumor cells indicating the oxidative stress induction as a main mechanism. Oxidative stress might also be one of the mechanisms underlying the testicular testosterone suppressing effect in Leydig cells, and in turn, the reproductive toxicity of DEHP. Generated data also emphasized the critical role of Se in modulation of the redox state in the testicular cells and the importance of the appropriate Se status. Therefore, it will be meaningful to study the consequences of oxidative stress on the steroidogenic functions of the MA-10 Leydig cells and particularly the primary Leydig cells; to



examine whether there is a link between oxidative stress, cytotoxicity, genotoxicity and functional role of those cells; and the regulatory effects of various doses of Se.

#### Acknowledgments

The authors would like to thank Prof. Dr. Mario Ascoli for generously providing the MA-10 mouse Leydig tumor cells. Pinar Erkekoglu, PhD, is a receiver of Erasmus and CEA grants and completed this work in INAC/SCIB/LAN, CEA in Grenoble, France. This study was presented as a poster in XII International Congress of Toxicology – IUTOX 2010, Barcelona, Spain.

#### References

- Akerboom, T.P., Sies, H., 1981. Assay of glutathione, glutathione disulfide, and glutathione mixed disulfides in biological samples. *Meth. Enzymol.* 77, 373–382.
- Akingbemi, B.T., Ge, R., Kimefelter, G.R., Zikrin, B.R., Hardy, M.P., 2004. Phthalate-induced Leydig cell hyperplasia is associated with multiple endocrine disturbances. *Proc. Natl. Acad. Sci. USA* 101, 775–780.
- Arner, E.S., Zhong, L., Holmgren, A., 1999. Preparation and assay of mammalian thioredoxin and thioredoxin reductase. *Meth. Enzymol.* 300, 226–239.
- Ascoli, M., 1981. Characterization of several clonal lines of cultured Leydig tumor cells: gonadotropin receptors and steroidogenic responses. *Endocrinology* 108, 88–95.
- Behne, D., Höfer-Bosse, T., 1984. Effects of a low selenium status on the distribution and retention of selenium in the rat. *J. Nutr.* 114, 1289–1296.
- Behne, D., Hilmert, H., Scheid, S., Gessner, H., Elger, W., 1988. Evidence for specific selenium target tissues and new biologically important selenoproteins. *Biochim. Biophys. Acta* 966, 12–21.
- Bhamre, S., Whithin, J.C., Cohen, H.J., 2003. Selenomethionine does not affect PSA secretion independent of its effect on LNCaP cell growth. *Prostate* 54, 315–321.
- Björnstedt, M., Kumar, S., Björkhem, I., Spyrou, G., Holmgren, A., 1997. Selenium and the thioredoxin and glutaredoxin systems. *Biomed. Environ. Sci.* 10, 271–279.
- Braissant, O., Foufelle, F., Scott, C., Duaca, M., Wahli, W., 1996. Differential expression of peroxisome proliferator-activated receptors (PPARs): tissue distribution of PPAR- $\alpha$ , - $\beta$ , and - $\gamma$  in the adult rat. *Endocrinology* 137, 354–366.
- Burns, T.F., El-Deiry, W.S., 1999. The p53 pathway and apoptosis. *J. Cell. Physiol.* 181, 231–239.
- Chandrasekaran, Y., Richburg, J.H., 2005. The p53 protein influences the sensitivity of testicular germ cells to mono-(2-ethylhexyl) phthalate-induced apoptosis by increasing the membrane levels of Fas and DR5 and decreasing the intracellular amount of c-FLIP. *Biol. Reprod.* 72, 206–213.
- Chu, F.F., Esworthy, R.S., Akman, S., Doroshov, J.H., 1990. Modulation of glutathione peroxidase expression by selenium: effect on human MCF-7 breast cancer cell transfectants expressing a cellular glutathione peroxidase cDNA and doxorubicin-resistant MCF-7 cells. *Nucleic Acids Res.* 18, 1531–1539.
- Clark, L.C., Cantor, K.P., Allaway, W.H., 1991. Selenium in forage crops and cancer mortality in US counties. *Arch. Environ. Health* 46, 37–42.
- Combs Jr., G.F., Gray, W.P., 1998. Chemopreventive agents: selenium. *Pharmacol. Ther.* 79, 179–192.
- Cory, A.H., Owen, T.C., Barltrop, J.A., Cory, J.G., 1991. Use of an aqueous soluble tetrazolium/formazan assay for cell growth assays in culture. *Cancer Commun.* 3, 207–212.
- Dalton, T.P., Shertzer, H.G., Puge, A., 1999. Regulation of gene expression by reactive oxygen. *Annu. Rev. Pharmacol. Toxicol.* 39, 67–101.
- D'Autreaux, B., Toledano, M.B., 2007. ROS as signalling molecules: mechanisms that generate specificity in ROS homeostasis. *Nat. Rev. Mol. Cell Biol.* 8, 813–824.
- Dees, J.H., Gazouli, M., Papadopoulos, V., 2001. Effect of mono-ethylhexyl phthalate on MA-10 Leydig tumor cell structure and function. *Reprod. Toxicol.* 15, 171–187.
- Dostal, L.A., Chapin, R.E., Stefanski, S.A., Harris, M.W., Schwetz, B.A., 1988. Testicular toxicity and reduced Sertoli cell numbers in neonatal rats by di(2-ethylhexyl)phthalate and the recovery of fertility as adults. *Toxicol. Appl. Pharmacol.* 95, 104–121.
- Doull, J., Cattley, R., Elcombe, C., Lake, B.G., Swenberg, J., Wilkinson, C., Van Williams, G., Gernert, M., 1999. A cancer risk assessment of di(2-ethylhexyl) phthalate: application of the new U.S. EPA risk assessment guidelines. *Regul. Toxicol. Pharmacol.* 29, 327–357.
- Dröge, W., 2002. Free radicals in the physiological control of cell function. *Physiol. Rev.* 82, 47–95.
- Erkekoglu, P., Rachidi, W., De Rosa, V., Giray, B., Favier, A., Hincal, F., 2010. Protective effect of selenium supplementation on the genotoxicity of di(2-ethylhexyl) phthalate and mono(2-ethylhexyl)phthalate treatment in LNCaP cells. *Free Radic. Biol. Med.* 49, 559–566.
- Fan, J., Traore, K., Li, W., Anni, H., Huang, H., Wu, C., Chen, H., Zirkin, B., Papadopoulos, V., 2010. Molecular mechanisms mediating the effect of mono-(2-ethylhexyl) phthalate on hormone-stimulated steroidogenesis in MA-10 mouse tumor Leydig cells. *Endocrinology* 151, 3348–3362.
- Finkel, T., 1998. Oxygen radicals and signaling. *Curr. Opin. Cell Biol.* 10, 248–253.
- Fisher, J.S., Macpherson, S., Marchetti, N., Sharpe, R.M., 2003. Human testicular dysgenesis syndrome: a possible model using in-utero exposure of the rat to dibutyl phthalate. *Hum. Reprod.* 18, 1383–1394.
- Flohé, L., 2007. Selenium in mammalian spermiogenesis. *Biol. Chem.* 388, 987–995.
- Flohé, L., Günzler, W.A., 1984. Assays of glutathione peroxidase. *Meth. Enzymol.* 105, 114–121.
- Freeman, D.A., Ascoli, M., 1983. The low-density lipoprotein pathway of cultured Leydig tumor cells: utilization of low-density lipoprotein-derived cholesterol for steroidogenesis. *Biochim. Biophys. Acta* 754, 72–81.
- Gandin, V., Nyström, C., Rundlöf, A.K., Jönsson-Videsäter, K., Schönlau, F., Hörkkö, J., Björnstedt, M., Fernandes, A.P., 2009. Effects of the antioxidant Pycnogenol on cellular redox systems in U1285 human lung carcinoma cells. *FEBS J.* 276, 532–540.
- Ganther, D.E., 1999. Selenium metabolism, selenoproteins and mechanisms of cancer prevention: complexities with thioredoxin reductase. *Carcinogenesis* 20, 1657–1666.
- Gazouli, M., Yao, Z.X., Boujrad, N., Corton, J.C., Culty, M., Papadopoulos, V., 2002. Effect of peroxisome proliferators on Leydig cell peripheral-type benzodiazepine receptor gene expression, hormone-stimulated cholesterol transport, and steroidogenesis: role of the peroxisome proliferator-activator receptor  $\alpha$ . *Endocrinology* 143, 2571–2583.
- Ge, R.S., Chen, G.R., Tanrikut, C., Hardy, M.P., 2007. Phthalate ester toxicity in Leydig cells: developmental timing and dosage considerations. *Reprod. Toxicol.* 23, 366–373.
- Grasso, P., Heindel, J.J., Powell, C.J., Reichert Jr., L.E., 1993. Effects of mono(2-ethylhexyl) phthalate, a testicular toxicant, on follicle-stimulating hormone binding to membranes from cultured rat Sertoli cells. *Biol. Reprod.* 48, 454–459.
- Günzler, W.A., Kremers, H., Flohé, L., 1974. An improved coupled test procedure for glutathione peroxidase (EC 1-11-1-9-) in blood. *Z. Klin. Chem. Klin. Biochem.* 12, 444–481.
- Habig, W.H., Pabst, M.J., Jakoby, W.B., 1974. Glutathione S-transferases, the first enzymatic step in mercapturic acid formation. *Biol. Chem.* 249, 7130–7139.
- Hainaut, P., Milner, J., 1993. Redox modulation of p53 conformation and sequence-specific DNA binding in vitro. *Cancer Res.* 53, 4469–4473.
- Hayes, J.D., Pulford, D.J., 1995. The glutathione S-transferase supergene family: regulation of GST and the contribution of the isoenzymes to cancer chemoprotection and drug resistance. *Crit. Rev. Biochem. Mol. Biol.* 30, 445–600.
- Hill, K.E., Zhou, J., McMahan, W.J., Motley, A.K., Atkins, J.F., Gesteland, R.F., Burk, R.F., 2003. Deletion of selenoprotein P alters distribution of selenium in the mouse. *J. Biol. Chem.* 278, 13640–13646.
- Hu, Y.J., Diamond, A.M., 2003. Role of glutathione peroxidase 1 in breast cancer: loss of heterozygosity and allelic differences in the response to selenium. *Cancer Res.* 63, 3347–3351.
- Jones, H.B., Garside, D.A., Liu, R., Roberts, J.C., 1993. The influence of phthalate esters on Leydig cell structure and function in vitro and in vivo. *Exp. Mol. Pathol.* 58, 179–193.
- Kambia, K., Dine, T., Gressier, B., Dupin-Spriet, T., Luyckx, M., Brunet, C., 2004. Evaluation of the direct toxicity of trioctyltrimellitate (TOTM), di(2-ethylhexyl) phthalate (DEHP) and their hydrolysis products on isolated rat hepatocytes. *Int. J. Artif. Organs* 27, 971–978.
- Kasahara, E., Sato, E.F., Miyoshi, M., Konaka, R., Hiramoto, K., Sasaki, J., Tokuda, M., Nakano, Y., Inoue, M., 2002. Role of oxidative stress in germ cell apoptosis induced by di(2-ethylhexyl)phthalate. *Biochem. J.* 365, 849–856.
- Kavlock, R., Boekelheide, K., Chapin, R., Cunningham, M., Faustman, E., Foster, P., Golub, M., Henderson, R., Hinberg, L., Little, R., Seed, J., Shea, K. NTP-CERHR Expert panel update on the reproductive and developmental toxicity of di(2-ethylhexyl) phthalate. 2005. (URL: <http://cerhr.niehs.nih.gov/chemicals/dehp/DEHP-Monograph.pdf>). (Novem-ber, 2006).
- Kim, E., Giese, A., Deppert, W., 2009. Wild-type p53 in cancer cells: when a guardian turns into a blackguard. *Biochem. Pharmacol.* 77, 11–20.
- Kitahara, J., Seko, Y., Imura, N., 1993. Possible involvement of active oxygen species in selenite toxicity in isolated rat hepatocytes. *Arch. Toxicol.* 67, 497–501.
- Koga, M., Tanaka, H., Yomogida, K., Tsuchida, J., Uchida, K., Kitamura, M., Sakoda, S., Matsumiya, K., Okuyama, A., Nishimune, Y., 1998. Expression of selenoprotein-P messenger ribonucleic acid in the rat testis. *Biol. Reprod.* 58, 261–265.
- Krieg, R.C., Dong, Y., Schwaborn, K., Knuechel, R., 2005. Protein quantification and its tolerance for different interfering reagents using the BCA-method with regard to 2D SDS PAGE. *J. Biochem. Biophys. Meth.* 65, 13–19.
- Latchoumycandane, C., Mathur, P.P., 2002. Induction of oxidative stress in the rat testis after short-term exposure to the organochlorine pesticide methoxychlor. *Arch. Toxicol.* 76, 692–698.
- Letavayová, L., Vlcková, V., Broznanová, J., 2006. Selenium: from cancer prevention to DNA damage. *Toxicology* 227, 1–14.
- Loff, S., Kabs, F., Witt, K., Sartoris, J., Mandl, B., Niessen, K.H., Waag, K.L., 2000. Polyvinylchloride infusion lines expose infants to large amounts of toxic plasticizers. *J. Pediatr. Surg.* 35, 1775–1781.
- Loikkanen, J.J., Naarala, J., Savolainen, K.M., 1998. Modification of glutamate-induced oxidative stress by lead: the role of extracellular calcium. *Free Radic. Biol. Med.* 24, 377–384.
- Maiorino, M., Roveri, A., Ursini, F., 2006. Selenium and male reproduction. Chapter 28 In: Hatfield, D.L., Berry, M.J., Gladyshev, V.N. (Eds.), Selenium. Its molecular biology and role in human health. Springer Science + Business Media, New York, pp. 323–331.
- Mansur, D.B., Hao, H., Gladyshev, V.N., Korotkov, K.V., Hu, Y., Moustafa, M.E., El-Saadani, M.A., Carlson, B.A., Hatfield, D.L., Diamond, A.M., 2000. Multiple levels of regulation of selenoprotein biosynthesis revealed from the analysis of human glioma cell lines. *Biochem. Pharmacol.* 60, 489–497.
- Mustachich, D., Powis, G., 2000. Thioredoxin reductase. *Biochem. J.* 346Pt (1), 1–8.
- Mylchreest, E., Sar, M., Wallace, D.G., Foster, P.M., 2002. Fetal testosterone insufficiency and abnormal proliferation of Leydig cells and gonocytes in rats exposed to di(n-butyl) phthalate. *Reprod. Toxicol.* 16, 19–28.
- Noriega, N.C., Howdeshell, K.L., Furr, J., Lambright, C.R., Wilson, V.S., Gray Jr., L.E., 2009. Pubertal administration of DEHP delays puberty, suppresses testosterone production, and inhibits reproductive tract development in male Sprague-Dawley and Long-Evans rats. *Toxicol. Sci.* 111, 163–178.
- Nose, K., 2000. Role of reactive oxygen species in the regulation of physiological functions. *Biol. Pharm. Bull.* 23, 897–903.
- O'Brien, M.L., Spear, B.T., Glauer, H.P., 2005. Role of oxidative stress in peroxisome proliferator-mediated carcinogenesis. *Crit. Rev. Toxicol.* 35, 61–88.

- Oberley, T.D., Zhong, W., Swzeda, L.I., Oberley, L.W., 2000. Localization of antioxidant enzymes and oxidative damage products in normal and malignant prostate epithelium. *Prostate* 44, 144–155.
- Olson, G.E., Winfrey, V.P., Nagdas, S.K., Hill, K.E., Burk, R.F., 2007. Apolipoprotein E receptor-2 (ApoER2) mediates selenium uptake from selenoprotein P by the mouse testis. *J. Biol. Chem.* 282, 12290–12297.
- Onorato, T.M., Brown, P.W., Morris, P.L., 2008. Mono-(2-ethylhexyl) phthalate increases spermatocyte mitochondrial peroxiredoxin 3 and cyclooxygenase 2. *J. Androl.* 29, 293–303.
- Ozturk, M., Arslan-Ergul, A., Bagislar, S., Senturk, S., Yuzugullu, H., 2009. Senescence and immortality in hepatocellular carcinoma. *Cancer Lett.* 286, 103–113.
- Pama, D., Srivastava, S.P., Singh, G.B., Seth, P.K., 1987. Effect of testosterone on the testicular atrophy caused by di(2-ethylhexyl) phthalate (DEHP). *Toxicol. Lett.* 36, 297–308.
- Peltola, V., Huhtaniemi, I., Metsä-Ketela, T., Ahotupa, M., 1996. Induction of lipid peroxidation during steroidogenesis in the rat testis. *Endocrinology* 137, 105–112.
- Roveri, A., Casasco, A., Maiorino, M., Dalan, P., Calligaro, A., Ursini, F., 1992. Phospholipid hydroperoxide glutathione peroxidase of rat testis. Gonadotropin dependence and immunocytochemical identification. *J. Biol. Chem.* 267, 6142–6146.
- Rusyn, I., Peters, J.M., Cunningham, M.L., 2006. Modes of action and species-specific effects of di-(2-ethylhexyl)phthalate in the liver. *Crit. Rev. Toxicol.* 36, 459–479.
- Schomburg, L., Schweizer, U., Holtmann, B., Flohé, L., Sendtner, M., Köhrle, J., 2003. Gene disruption discloses role of selenoprotein P in selenium delivery to target tissues. *Biochem. J.* 370, 397–402.
- Singh, N.P., McCoy, M.T., Tice, R.R., Schneider, E.L., 1988. A simple technique for quantitation of low levels of DNA damage in individual cells. *Exp. Cell Res.* 175, 184–191.
- Steinert, P., Bächner, D., Flohé, L., 1998. Analysis of the mouse selenoprotein P gene. *Biol. Chem.* 379, 683–691.
- Suna, S., Yamaguchi, F., Kimura, S., Tokuda, M., Jitsunari, F., 2007. Preventive effect of D-psicose, one of rare ketohexoses, on di-(2-ethylhexyl) phthalate (DEHP)-induced testicular injury in rat. *Toxicol. Lett.* 173, 107–117.
- Swan, S.H., 2008. Environmental phthalate exposure in relation to reproductive outcomes and other health endpoints in humans. *Environ. Res.* 108, 177–184.
- Tice, R.R., Agurell, E., Anderson, D., Burlinson, B., Hartmann, A., Kobayashi, H., Miyamae, Y., Rojas, E., Ryu, J.C., Sasaki, Y.F., 2000. Single cell gel/comet assay: guidelines for in vitro and in vivo genetic toxicology testing. *Environ. Mol. Mutagen.* 35, 206–221.
- Tramer, F., Rocco, F., Micali, F., Sandri, G., Panfilii, E., 1998. Antioxidant systems in rat epididymal spermatozoa. *Biol. Reprod.* 59, 753–758.
- Ursini, F., Maiorino, M., Brigelius-Flohé, R., Aumann, K.D., Roveri, A., Schomburg, D., Flohé, L., 1995. Diversity of glutathione peroxidases. *Meth. Enzymol.* 252, 38–53.
- Ursini, F., Heim, S., Kiess, M., Maiorino, M., Roveri, A., Wissing, J., Flohé, L., 1999. Dual function of the selenoprotein PHGPx during sperm maturation. *Science* 285, 1393–1396.
- Veal, E.A., Day, A.M., Morgan, B.A., 2007. Hydrogen peroxide sensing and signaling. *Mol. Cell* 26, 1–14.
- Watson, W.H., Yang, X., Choi, Y.E., Jones, D.P., Kehrer, J.P., 2004. Thioredoxin and its role in toxicology. *Toxicol. Sci.* 78, 3–14.
- Wilson, V.S., Lambright, C., Furr, J., Ostby, J., Wood, C., Held, G., Gray Jr., L.E., 2004. Phthalate ester-induced gubernacular lesions are associated with reduced *insl3* gene expression in the fetal rat testis. *Toxicol. Lett.* 146, 207–215.
- Xia, L., Nordman, T., Olsson, J.M., Damiopoulos, A., Björkhem-Bergman, L., Nalvarte, I., Eriksson, L.C., Arnér, E.S., Spyrou, G., Björnstedt, M., 2003. The mammalian cytosolic selenoenzyme thioredoxin reductase reduces ubiquinone. A novel mechanism for defense against oxidative stress. *Biol. Chem.* 278, 2141–2146.
- Zhang, Y.H., Lin, L., Liu, Z.W., Jiang, X.Z., Chen, B.H., 2008. Disruption effects of monophthalate exposures on inter-Sertoli tight junction in a two-compartment culture model. *Environ. Toxicol.* 23, 302–308.
- Zhao, R., Domann, F.E., Zhong, W., 2006. Apoptosis induced by selenomethionine and methioninase is superoxide mediated and p53 dependent in human prostate cancer cells. *Mol. Cancer Ther.* 5, 3275–3284.
- Zhuo, P., Goldberg, M., Herman, L., Lee, B.S., Wang, H., Brown, R.L., Foster, C.B., Peters, U., Diamond, A.M., 2009. Molecular consequences of genetic variations in the glutathione peroxidase 1 selenoenzyme. *Cancer Res.* 69, 8183–8190.
- Zini, A., Schlegel, P.N., 1997. Expression of glutathione peroxidases in the adult male rat reproductive tract. *Fertil. Steril.* 68, 689–695.

# Transforming Growth Factor-Beta Induces Senescence in Hepatocellular Carcinoma Cells and Inhibits Tumor Growth

Serif Senturk,<sup>1</sup> Mine Mumcuoglu,<sup>1</sup> Ozge Gursoy-Yuzugullu,<sup>1,2</sup> Burcu Cingoz,<sup>1</sup> Kamil Can Akcali,<sup>1</sup> and Mehmet Ozturk<sup>1,2</sup>

Senescence induction could be used as an effective treatment for hepatocellular carcinoma (HCC). However, major senescence inducers (p53 and p16<sup>Ink4a</sup>) are frequently inactivated in these cancers. We tested whether transforming growth factor- $\beta$  (TGF- $\beta$ ) could serve as a potential senescence inducer in HCC. First, we screened for HCC cell lines with intact TGF- $\beta$  signaling that leads to small mothers against decapentaplegic (Smad)-targeted gene activation. Five cell lines met this condition, and all of them displayed a strong senescence response to TGF- $\beta$ 1 (1-5 ng/mL) treatment. Upon treatment, c-myc was down-regulated, p21<sup>Cip1</sup> and p15<sup>Ink4b</sup> were up-regulated, and cells were arrested at G<sub>1</sub>. The expression of p16<sup>Ink4a</sup> was not induced, and the senescence response was independent of p53 status. A short exposure of less than 1 minute was sufficient for a robust senescence response. Forced expression of p21<sup>Cip1</sup> and p15<sup>Ink4b</sup> recapitulated TGF- $\beta$ 1 effects. Senescence response was associated with reduced nicotinamide adenine dinucleotide phosphate oxidase 4 (Nox4) induction and intracellular reactive oxygen species (ROS) accumulation. The treatment of cells with the ROS scavenger N-acetyl-L-cysteine, or silencing of the NOX4 gene, rescued p21<sup>Cip1</sup> and p15<sup>Ink4b</sup> accumulation as well as the growth arrest in response to TGF- $\beta$ . Human HCC tumors raised in immunodeficient mice also displayed TGF- $\beta$ 1-induced senescence. More importantly, peritumoral injection of TGF- $\beta$ 1 (2 ng) at 4-day intervals reduced tumor growth by more than 75%. In contrast, the deletion of TGF- $\beta$  receptor 2 abolished *in vitro* senescence response and greatly accelerated *in vivo* tumor growth. **Conclusion:** TGF- $\beta$  induces p53-independent and p16<sup>Ink4a</sup>-independent, but Nox4-dependent, p21<sup>Cip1</sup>-dependent, p15<sup>Ink4b</sup>-dependent, and ROS-dependent senescence arrest in well-differentiated HCC cells. Moreover, TGF- $\beta$ -induced senescence *in vivo* is associated with a strong antitumor response against HCC. (HEPATOLOGY 2010;52:966-974)

Abbreviations: BrdU, bromodeoxyuridine; cDNA, complementary DNA; NAC, N-acetyl-L-cysteine; Nox4, NADPH oxidase-4; ROS, reactive oxygen species; SA- $\beta$ -Gal, senescence-associated- $\beta$ -galactosidase; siRNA, small interfering RNA; TERT, telomerase reverse transcriptase; TGF- $\beta$ , transforming growth factor- $\beta$ ; TGF- $\beta$ R1, TGF- $\beta$  receptor 1.

From the <sup>1</sup>BilGen Research Center and Department of Molecular Biology and Genetics, Bilkent University, Ankara, Turkey; and <sup>2</sup>Centre de Recherche, Institut National de la Santé et de la Recherche Médicale (INSERM)-Université Joseph Fourier U823, Institut Albert Bonniot, La Tronche, France.

Received March 16, 2010; accepted May 9, 2010.

This work was supported by grants from the TUBITAK and State Planning Office (Turkey) and the Institut National de Cancer (France). Additional support was provided by the Turkish Academy of Sciences.

Address reprint requests to: Mehmet Ozturk, Ph.D., Centre de Recherche INSERM/UJF U823, Institut Albert Bonniot, Grenoble, France.  
E-mail: ozturkm@ujf-grenoble.fr; Fax: +33476549413.

Copyright © 2010 by the American Association for the Study of Liver Diseases.

View this article online at wileyonlinelibrary.com.

DOI 10.1002/hep.23769

Potential conflict of interest: Nothing to report.

Additional Supporting Information may be found in the online version of this article.

Cellular senescence is a permanent withdrawal from the cell cycle in response to diverse stress conditions such as dysfunctional telomeres, DNA damage, strong mitotic signals, and disrupted chromatin. Senescence is considered to be a major cause of aging, but also a strong anticancer mechanism.<sup>1</sup> The relevance of senescence in chronic liver diseases is poorly known, but it may play a central role. Hepatocyte telomeres undergo shortening during chronic liver disease progression,<sup>2</sup> and this is accompanied by a progressive decline of hepatocyte proliferation.<sup>3</sup> Senescence-associated  $\beta$ -galactosidase (SA- $\beta$ -Gal)-positive cells have been detected in 3%-7% of normal liver, 50% of chronic hepatitis, 70%-100% of cirrhosis, and up to 60% of hepatocellular carcinoma (HCC) tissues.<sup>2,4-7</sup> Highly abundant senescence observed in cirrhosis has been confined to hepatocytes<sup>2</sup> and stellate cells.<sup>8</sup> Because telomere-deficient mice

develop cirrhosis,<sup>9</sup> and cirrhotic hepatocytes display shortened telomeres, telomere dysfunction was proposed to cause senescence in cirrhosis.<sup>2</sup> It is assumed that HCC tumor cells bypass hepatocellular senescence to become immortalized. Frequent inactivation of *TP53* (encoding the tumor protein p53) and *CDKN2A* (cyclin-dependent kinase inhibitor 2A, encoding p16<sup>Ink4a</sup> protein) genes in these tumors supports this hypothesis.<sup>10</sup> Nevertheless, the detection of senescent cells in some HCC tumors suggests that transformed and presumably immortal hepatocytes have maintained the capacity to undergo senescence arrest under appropriate conditions.

With this regard, immortal HCC cell lines can spontaneously generate progeny that undergo replicative senescence<sup>11</sup>; murine HCC tumors generated by the expression of a mutant *Ras* gene in p53-deficient hepatoblasts can be cleared by a massive senescence response upon reactivation of p53 expression<sup>12</sup>; *c-myc* oncogene inactivation in murine HCCs results in senescence-mediated tumor regression.<sup>13</sup> One of our goals is to identify novel mechanisms of senescence induction in HCC cells. Here, we identify the transforming growth factor-beta (TGF- $\beta$ ) as a major cytokine that is able to trigger a massive senescence response in well-differentiated HCC cell lines. Reduced nicotinamide adenine dinucleotide phosphate oxidase-4 (Nox4) and reactive oxygen species (ROS) were key intermediates of TGF- $\beta$ -induced growth arrest that was mediated by p21<sup>Cip1</sup> and p15<sup>Ink4b</sup>.

## Materials and Methods

Detailed materials and methods are described in the Supporting Information Materials and Methods. Cell lines were tested under standard culture conditions in the presence of 10% fetal bovine serum. Total RNA was isolated using a NucleoSpin RNA II Kit (Macherey-Nagel, Duren, Germany), and first-strand complementary DNA (cDNA) was synthesized using RevertAid First Strand cDNA synthesis kit (MBI Fermentas, Leon-Rot, Germany). Genomic DNA was extracted as described,<sup>11</sup> and polymerase chain reaction (PCR) assays were done using appropriate primers. Quantitative PCR was performed using SYBR Green I (Invitrogen, Carlsbad, CA). Glyceraldehyde 3-phosphate dehydrogenase and  $\beta$ -actin were used as internal controls. The SA- $\beta$ -Gal assay was performed as described.<sup>11</sup> Commercial and homemade antibodies were used. Western blot assays were performed as described,<sup>11</sup> using  $\alpha$ -tubulin or calnexin as internal controls. For immunoperoxidase and immunofluorescence assays, cells were fixed with 4% formaldehyde,

permeabilized with phosphate-buffered saline supplemented with 0.5% saponin and 0.3% TritonX-100 (Sigma, St. Louis, MO), and subjected to indirect immunofluorescence and immunoperoxidase assays. To test permanent cell cycle arrest, cells were labeled with bromodeoxyuridine (BrdU) for 24 hours in freshly added culture media, and the anti-BrdU immunofluorescence assay was performed as described.<sup>11</sup> Human p15<sup>Ink4b</sup> and p21<sup>Cip1</sup> were cloned into pcDNA3.1C/Neo and pcDNA3.1(+)/hygromycin (Invitrogen), respectively. Cells were transfected with Lipofectamine 2000 (Invitrogen) and selected with either Geneticin G418 (Gibco) or hygromycin-B (Roche, Indianapolis, IN) for 8 days. The *NOX4* gene was silenced using previously described Nox4-specific small interfering RNAs (siRNAs).<sup>14</sup> A negative control siRNA was used in parallel experiments. The siRNAs were transfected with Lipofectamine RNAiMAX (Invitrogen). The pSBE4-luc reporter was cotransfected with pRL-TK (plasmid Renilla luciferase, with thymidine kinase promoter; Promega, Madison, WI), using Lipofectamine 2000. The luciferase assay was performed using a Dual-Glo luciferase kit (Promega). For cell cycle studies, fixed cells were labeled with propidium iodide and analyzed using FACSCalibur Flow Cytometer (BD Biosciences, San Jose, CA). Intracellular ROS were detected with 2',7'-dichlorofluorescein diacetate (DCFH-DA; Sigma), using MitoTracker Red (Invitrogen) as a counterstain. Apoptosis was tested by Negative in Apoptosis (NAPO)<sup>15</sup> and active caspase-3 antibody (Asp-175; Cell Signaling Technology, Danvers, MA) immunoassays. Subcutaneous human HCC tumors were obtained in CD1 *nude* mice using  $5 \times 10^6$  live cells per injection. All animals received care according to the Guide for the Care and Use of Laboratory Animals. Results were expressed as mean  $\pm$  standard deviation from at least three independent experiments. Data between groups were analyzed by one-tailed *t* test. A *P* value <0.05 was considered statistically significant. TGF- $\beta$ 1 expression in liver disease was analyzed using a publicly available global gene expression data,<sup>16</sup> which were normalized using JustRMA tool from the Bioconductor group.<sup>17</sup> A two-sample *t* test with random variance model was used with a 0.05 nominal significance level of each univariate test.

## Results

**Differential Expression of TGF- $\beta$ 1 in Normal Liver, Cirrhosis, and HCC.** We first analyzed TGF- $\beta$ 1 expression in normal liver, cirrhosis, and HCC, using the publicly available clinical data sets.<sup>16</sup> TGF- $\beta$ 1 expression displayed a bell-shaped distribution with

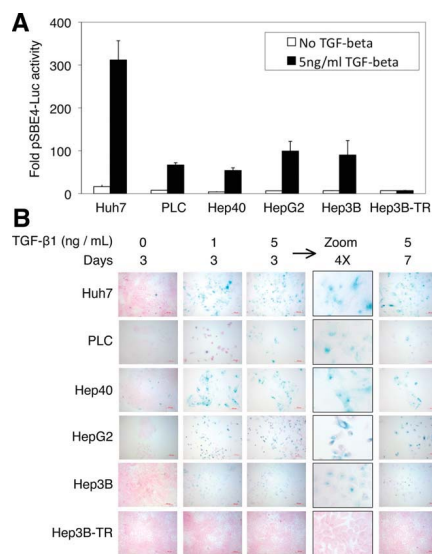


Fig. 1. Well-differentiated HCC cell lines are competent for TGF- $\beta$  signaling activity and they respond to TGF- $\beta$  by potent senescence-like growth arrest. (A) Cells were cotransfected with pSBE4-Luc and control pRL-TK plasmids, and treated with or without TGF- $\beta$ 1 (5 ng/mL) for 24 hours. The luciferase activity was measured and expressed as fold-activity of pSBE4-Luc/pRL-TK (mean  $\pm$  standard deviation; n = 3). (B) Cells were plated at low density and treated with 1 or 5 ng/mL TGF- $\beta$ 1, and tested for SA- $\beta$ -Gal activity (blue) at days 3 and 7. Counterstain: Fast Red. TGFBR2-deleted Hep3B-TR cells were used as negative controls in (A) and (B).

a sharp increase in cirrhosis (cirrhosis versus normal liver,  $P < 0.001$ ), followed by a progressive decrease in early HCC (early HCC versus cirrhosis,  $P < 0.02$ ) and advanced HCCs (Supporting Information Fig. 1). This expression pattern closely correlated with reported frequencies of SA- $\beta$ -Gal activities in normal liver, cirrhosis, and HCC.<sup>2,4-7</sup>

**TGF- $\beta$  Is an Autocrine Cytokine Inducing a Senescence-Like Response in Well-Differentiated HCC Cell Lines.** We hypothesized that TGF- $\beta$  signaling can induce hepatocellular senescence response, because it is a potent inducer of G<sub>1</sub> arrest.<sup>18</sup> To test this hypothesis, we first formed a panel of "well-differentiated" HCC cell lines that display E-cadherin expression, epithelial-like morphology, and hepatocyte-like gene expression.<sup>19</sup> Well-differentiated cell lines also share the same TGF- $\beta$  early response gene expression patterns with normal hepatocytes.<sup>20</sup> All selected cell lines expressed all critical components of TGF- $\beta$  signaling including

TGF- $\beta$ 1, TGF- $\beta$  receptor 1 (TGFBR1), TGFBR2, small mothers against decapentaplegic homolog 2 (SMAD2), SMAD3, and SMAD4 (Supporting Information Fig. 2A). Hep3B-TR clone displaying homozygous deletion of *TGFBR2*<sup>21</sup> was used as a negative control (Supporting Information Fig. 2). All cell lines, except Hep3B-TR displayed intact TGF- $\beta$  signaling activity (Fig. 1A), as tested by pSBE4-Luc reporter activity.<sup>22</sup> Treatment of cells with TGF- $\beta$ 1 (5 ng/mL) yielded 9-fold to 19-fold induction of pSBE4-Luc reporter activity in responsive cell lines. The expression of endogenous plasminogen activator inhibitor-1 (*PAI-1*), a well-known TGF- $\beta$  target gene,<sup>23</sup> was also induced (Supporting Information Fig. 3). TGF- $\beta$ 1-treated cell lines were kept in culture with medium changes (without TGF- $\beta$ 1) every 3 days, examined morphologically, and subjected to SA- $\beta$ -Gal assay. All cell lines tested, except Hep3B-TR, displayed growth inhibition associated with flattened cell morphology and >50% positive SA- $\beta$ -Gal activity, as early as 3 days after TGF- $\beta$ 1 treatment (Fig. 1B).

Expression of TGF- $\beta$ 1 in all tested cell lines suggested that it could act as an autocrine cytokine. Therefore, we exposed Huh7 cells to either anti-TGF- $\beta$ 1 antibody (5  $\mu$ g/mL) or TGF- $\beta$ 1 (5 ng/mL) and tested for total and SA- $\beta$ -Gal-positive cells in isolated colonies 10 days later. Cells treated with anti-TGF- $\beta$ 1 antibody displayed two-fold increased colony size ( $P < 0.04$ ) and 50% decreased SA- $\beta$ -Gal activity ( $P < 0.02$ ; Supporting Information Fig. 4). In contrast, ectopic TGF- $\beta$ 1 treatment caused a seven-fold decrease in colony size ( $P < 0.005$ ) and five-fold increase in SA- $\beta$ -Gal activity ( $P < 0.0001$ ). Thus, Huh7 cells produced TGF- $\beta$ 1 acting as a weak autocrine senescence-inducing signal that was inhibited by anti-TGF- $\beta$ 1 antibody, and amplified by ectopic TGF- $\beta$ 1.

**A Brief Exposure to TGF- $\beta$  for a Robust Senescence Response.** To test the shortest time of exposure to TGF- $\beta$ 1 for a full senescence response, three cell lines were treated with TGF- $\beta$ 1 for durations between <1 minute (~20 seconds) and 72 hours, and subjected to SA- $\beta$ -Gal staining. To our surprise, <1 minute exposure was sufficient for a robust senescence response (Fig. 2). Thus, the senescence-initiating effect of TGF- $\beta$ 1 was immediate, even though the senescence phenotype (>50% SA- $\beta$ -Gal-positive and flattened cells) was manifested 3 days later.

**Lack of Evidence for TGF- $\beta$ -Induced Apoptosis.** Earlier studies indicated that TGF- $\beta$  induces apoptosis in hepatocytes and some HCC cell lines under serum-free conditions.<sup>24-27</sup> Under our experimental conditions using 10% fetal bovine serum, all five cell lines tested failed to enter apoptosis following TGF- $\beta$

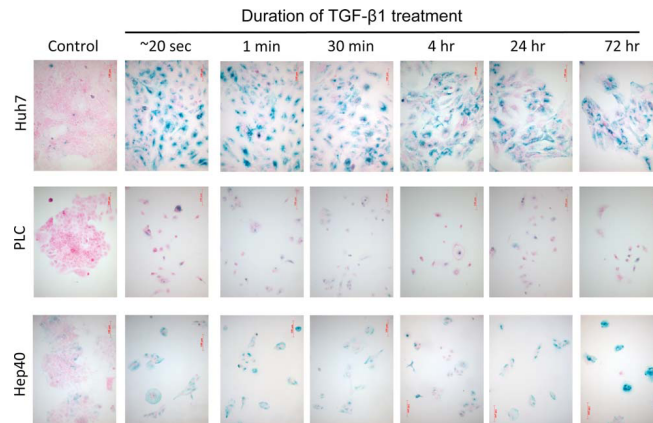


Fig. 2. Induction of a strong senescence-like response by TGF- $\beta$  after a very short exposure. Cells were treated with TGF- $\beta$ 1 (5 ng/mL) for the indicated times, and SA- $\beta$ -Gal activity (blue) was tested at 72 hours. Control: no TGF- $\beta$ 1 treatment. Counterstain: Fast Red.

treatment, as examined by NAPO antibody<sup>15</sup> and activated caspase-3-specific antibody tests (Supporting Information Figs. 5 and 6).

**TGF- $\beta$ -Induced Senescence Is Associated with Sustained Induction of p21<sup>Cip1</sup> and p15<sup>Ink4b</sup>.** Cellular senescence is usually associated with cell cycle arrest induced by p53, p21<sup>Cip1</sup>, p16<sup>Ink4a</sup>, and/or p15<sup>Ink4b</sup>.<sup>1,28</sup> TGF- $\beta$ 1 caused c-myc repression and p15<sup>Ink4b</sup> and p21<sup>Cip1</sup> induction (Fig. 3; Supporting Information Fig. 7A). Decreased pRb phosphorylation, together with decreased p107 and increased p130 protein levels, was also observed. These changes in retinoblastoma family proteins correlate with exit from the cell cycle.<sup>29</sup> The

TGF- $\beta$  response was independent of p53. All HCC cell lines tested here, except HepG2, display p53 mutations.<sup>30</sup> The levels of total p53 did not change following TGF- $\beta$  exposure, despite p21<sup>Cip1</sup> accumulation (Fig. 3; Supporting Information Fig. 7B). Moreover, we observed no phosphorylation of wild-type p53 in HepG2 cells, following TGF- $\beta$  exposure (Supporting Information Fig. 7B). TGF- $\beta$  also did not affect p16<sup>Ink4a</sup> levels (Fig. 3). Indeed, the *CDKN2A* gene is frequently silenced in HCC.<sup>31</sup> Accordingly, p16<sup>Ink4a</sup> protein levels were extremely low in all tested cell lines, except in pRb-deficient Hep3B and Hep3B-TR cells (Supporting Information Fig. 7C). On the other hand, our

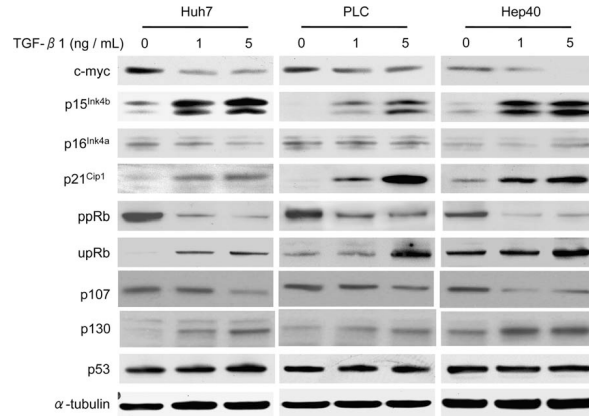


Fig. 3. TGF- $\beta$  treatment of HCC cell lines causes the induction of p15<sup>Ink4b</sup> and p21<sup>Cip1</sup> that is associated with c-myc down-regulation, pRb underphosphorylation, p107 decrease and p130 increase. The levels of p53 and p16<sup>Ink4a</sup> did not change. Untreated and TGF- $\beta$ 1-treated cells were tested for indicated proteins by western blotting on day 3. ppRb: phospho-Ser<sup>807</sup>/Ser<sup>811</sup>-pRb, upRb: underphosphorylated pRb. The  $\alpha$ -tubulin served as an internal control. p16<sup>Ink4a</sup> blots were overexposed to visualize weak expression.

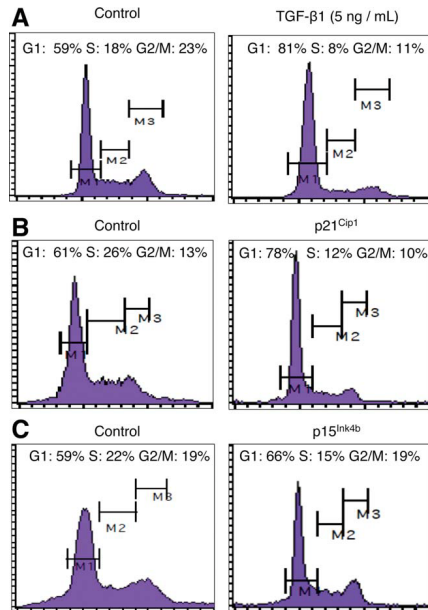


Fig. 4. G<sub>1</sub> arrest induced by TGF- $\beta$  treatment can be recapitulated by ectopic expression of p21<sup>Cip1</sup> and p15<sup>Ink4b</sup>. (A) Control and TGF- $\beta$ 1-treated Huh7 cells were subjected to cell cycle analysis after 3 days of culture. (B, C) Huh7 cells were transiently transfected with (B) p21<sup>Cip1</sup> and (C) p15<sup>Ink4b</sup> expression vectors, and subjected to cell cycle analysis after 8 days of culture. Control: cells transfected with empty plasmid vectors (B,C). [Color figure can be viewed in the online issue, which is available at [wileyonlinelibrary.com](http://www.wileyonlinelibrary.com).]

observation of senescence arrest in Hep3B cells suggests that pRb expression is also dispensable for TGF- $\beta$ -induced senescence in HCC cells. Taken together, these findings suggested that TGF- $\beta$  was able to induce senescence in HCC cells independent of p53, p16<sup>Ink4a</sup>, or pRb status.

**TGF- $\beta$  Induces a Permanent G<sub>1</sub> Arrest that Can Be Reproduced Either by p21<sup>Cip1</sup> or p15<sup>Ink4b</sup>.** Cellular senescence is defined as an irreversible arrest of mitotic cells at the G<sub>1</sub> phase, but some cancer cells enter senescence at the G<sub>2</sub> or S phases.<sup>1</sup> Initially, we used Huh7 cells for cell cycle studies. These cells accumulated at G<sub>1</sub> phase (from 59% to 81%) with a concomitant depletion of S phase cells (from 18% to 8%), after TGF- $\beta$ 1 exposure (Fig. 4A). Similar results were obtained with PLC/PRF/5 cells (Fig. 5) and other cell lines (data not shown). These observations suggested that p21<sup>Cip1</sup> and/or p15<sup>Ink4b</sup> are involved in TGF- $\beta$ -mediated G<sub>1</sub> arrest and senescence response.

Therefore, we tested respective contributions of p21<sup>Cip1</sup> and p15<sup>Ink4b</sup> in these responses, by transient transfection assays using Huh7 cells. The p21<sup>Cip1</sup>-transfected and p15<sup>Ink4b</sup>-transfected cells demonstrated highly increased p21<sup>Cip1</sup> protein (Supporting Information Fig. 8A) and moderately increased p15<sup>Ink4b</sup> expression (Supporting Information Fig. 8B), respectively. The p21<sup>Cip1</sup>-overexpressing cells accumulated at G<sub>1</sub> (from 61% to 78%), together with a depletion of S phase cells (from 26% to 13%; Fig. 4B). In association with these changes, SA- $\beta$ -Gal activity was increased (Supporting Information Fig. 9A) and BrdU

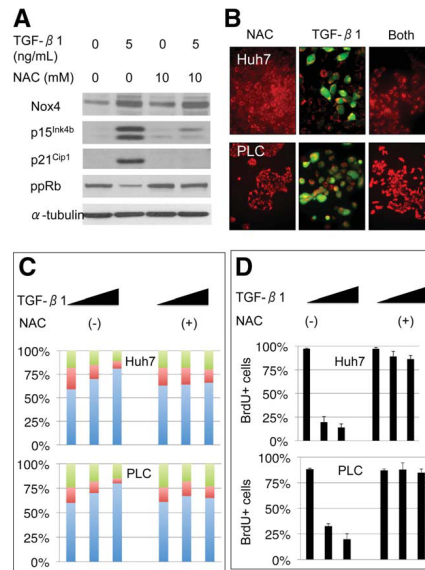


Fig. 5. Implication of Nox4 induction and ROS accumulation in TGF- $\beta$ -induced growth arrest. (A) TGF- $\beta$ 1 treatment induces the expression of Nox4, p15<sup>Ink4b</sup>, and p21<sup>Cip1</sup> together with ppRb down-regulation; ROS scavenger NAC inhibits p15<sup>Ink4b</sup> and p21<sup>Cip1</sup> induction, and ppRb down-regulation, but not Nox4 accumulation. Cell lysates were collected at day 3, following treatment with TGF- $\beta$ 1 and/or NAC, and tested by western blotting. (B-D) ROS accumulation observed in TGF- $\beta$ 1-treated cells is inhibited by NAC cotreatment (B), and this results in (C) inhibition of G<sub>1</sub> arrest, and (D) restoration of BrdU incorporation into cellular DNA. (A) PLC/PRF/5 cells were treated for 3 days with either 10 mM NAC or 5 ng/mL TGF- $\beta$ 1 alone, or in combination, and tested for Nox4, p15<sup>Ink4b</sup>, p21<sup>Cip1</sup>, and ppRb by western blotting. (B) Huh7 and PLC/PRF/5 (PLC) cells were treated with either 10 mM NAC or 5 ng/mL TGF- $\beta$ 1 alone, or in combination, and tested for ROS accumulation using a green fluorescent ROS indicator, and a red fluorescent mitochondrial marker as counterstain. The effects of 10 mM NAC cotreatment on growth inhibition by TGF- $\beta$ 1 (0, 1, or 5 ng/mL) were tested by (C) cell cycle analysis, and (D) BrdU incorporation assay. Blue, red, and green columns in (C) represent cells at G<sub>1</sub>, S, and G<sub>2</sub>/M, respectively.

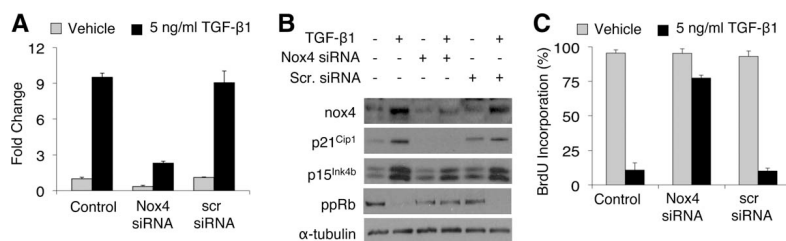


Fig. 6. Rescue of TGF- $\beta$ -induced p21<sup>Cip1</sup> and p15<sup>Ink4b</sup> accumulation and growth arrest by NOX4 gene silencing. (A) TGF- $\beta$ -induced accumulation of Nox4 transcripts was strongly inhibited by Nox4 siRNA, but not by control siRNA. Transcript analysis was performed by quantitative reverse transcription PCR. (B) NOX4 gene silencing rescued TGF- $\beta$ -induced Nox4, p21<sup>Cip1</sup>, and p15<sup>Ink4b</sup> protein accumulation, and the inhibition of pRb phosphorylation, as tested by western blotting. Compared to others, the inhibition of p15<sup>Ink4b</sup> accumulation was modest. (C) NOX4 gene silencing also rescued TGF- $\beta$ -induced inhibition of DNA synthesis, as tested by BrdU incorporation. Cells were labeled with BrdU for 24 hours prior to day 3, and percent BrdU-positive cells were counted manually.

incorporation into cellular DNA was inhibited ( $P < 0.001$ ; Supporting Information Fig. 9B). The p15<sup>Ink4b</sup> overexpression caused a moderate response (G<sub>1</sub> cells rising to 66% from 59%; S phase cells decreasing from 22% from 15%; Fig. 4C). However, p15<sup>Ink4b</sup> overexpression was also associated with increased SA- $\beta$ -Gal activity (Supporting Information Fig. 9C) and decreased BrdU incorporation ( $P < 0.001$ ; Supporting Information Fig. 9D).

**TGF- $\beta$ -Induced Senescence Depends on Nox4 Induction and Intracellular Accumulation of ROS.** TGF- $\beta$  induces Nox4 expression and ROS accumulation in hepatocytes.<sup>32-34</sup> Because ROS have been implicated in Ras-induced senescence,<sup>35</sup> we tested whether TGF- $\beta$ -induced senescence was associated with Nox4 induction and ROS accumulation. TGF- $\beta$ 1 induced Nox4 protein expression (Fig. 5A; Supporting Information Fig. 10A), as well as ROS accumulation (Fig. 5B). First, we used *N*-acetyl-L-cysteine (NAC) as a physiological ROS scavenger<sup>36</sup> to test the role of ROS in TGF- $\beta$ -induced senescence. The cotreatment of 5 ng/mL TGF- $\beta$ 1-treated cells with 10 mM NAC completely suppressed the accumulation of ROS (Fig. 5B) and TGF- $\beta$ 1 effects on p15<sup>Ink4b</sup>, p21<sup>Cip1</sup>, and pRb, but not Nox4 expression (Fig. 5A). More importantly, NAC cotreatment rescued cells from TGF- $\beta$ 1-induced senescence response (Supporting Information Fig. 10B) and growth arrest (Fig. 5C,D; Supporting Information Fig. 11). Next, we silenced NOX4 gene in Huh7 cells using a previously described NOX4-specific siRNA.<sup>14</sup> NOX4-specific siRNA inhibited the accumulation of Nox4 transcripts (~75%; Fig. 6A) and protein (Fig. 6B) under TGF- $\beta$ 1 treatment. This resulted in a strong inhibition of p21<sup>Cip1</sup> accumulation and a moderate inhibition of p15<sup>Ink4b</sup> accumulation in association with restoration of pRb phosphorylation (Fig. 6B). More importantly, Nox4 inhibition was sufficient to restore cell proliferation under TGF- $\beta$  treatment (Fig. 6C).

**TGF- $\beta$ -Induced Senescence and Antitumor Activity In Vivo.** We tested *in vivo* relevance of TGF- $\beta$ -induced senescence in human HCC tumors raised in

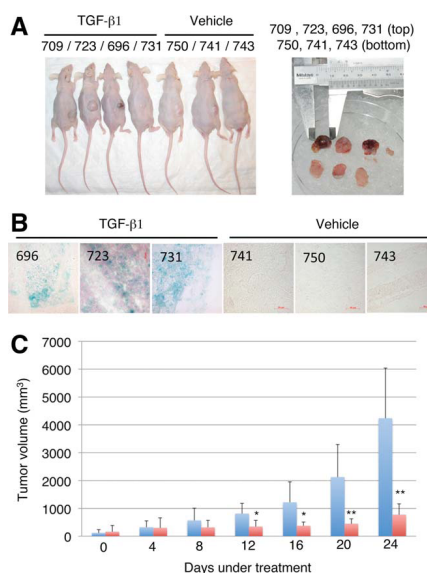


Fig. 7. TGF- $\beta$  induces senescence and inhibits the growth of Huh7 tumors in nude mice. (A,B) TGF- $\beta$ 1-induced SA- $\beta$ -Gal activity in Huh7 tumors. Huh7 tumors were obtained in nude mice and treated with TGF- $\beta$ 1 (~0.5 ng) or a vehicle only. (A) Animals were sacrificed 7 days later to collect tumor tissues. (B) Cryostat sections from freshly frozen tumors were subjected to SA- $\beta$ -Gal staining (blue). Counterstain: Fast Red. (C) Huh7 tumors were treated with 2 ng TGF- $\beta$  or vehicle only at 4-day intervals and tumor sizes were measured. TGF- $\beta$ -treated tumors were growth arrested, resulting in >75% inhibition of tumor growth. \* $P < 0.05$ ; \*\* $P < 0.01$ .



immunodeficient mice. TGF- $\beta$ 1 (~50  $\mu$ L of a 10 ng/mL solution)-injected Huh7 tumors were removed 1 week later (Fig. 7A) and subjected to SA- $\beta$ -Gal staining. TGF- $\beta$ 1 induced local but expanded SA- $\beta$ -Gal activity in three of four tumors tested; three tumors treated with vehicle only were negative (Fig. 7B).

To test antitumor effects of TGF- $\beta$ , early Huh7 tumors were treated with peritumoral injection of ~2 ng TGF- $\beta$  at 4 days of intervals. Vehicle-treated tumors displayed exponential growth to reach 4 cm<sup>3</sup> volume on average within 24 days. In contrast, TGF- $\beta$ -treated tumors were growth arrested throughout the experiment and remained <1 cm<sup>3</sup> on average at the same time period. Tumor inhibition was significant for at least 24 days ( $P < 0.01$  to  $P < 0.05$ ). The TGF- $\beta$  treatment was stopped at day 24 and animals were observed for an additional period of 4 weeks. All vehicle-treated and four TGF- $\beta$ -treated animals died, whereas complete remission was observed in two TGF- $\beta$ -treated animals (data not shown). We also compared *TGFBR2*-deleted Hep3B-TR cells<sup>21</sup> with parental Hep3B cells. Hep3B-TR cells formed palpable tumors 2 weeks after subcutaneous injection, and host animals died within 4-6 weeks. In contrast, Hep3B cells formed tumors with a latency of 6-7 weeks (Supporting Information Fig. 12).

## Discussion

Our findings provide strong evidence for senescence as a major response of HCC cells to TGF- $\beta$ . Senescence-associated changes included flattened morphology, p21<sup>Cip1</sup> and p15<sup>Ink4b</sup> accumulation, and positive SA- $\beta$ -Gal activity. This response has not been noticed previously, probably because of its late occurrence, at least 3 days after TGF- $\beta$  treatment. The primary findings of our mechanistic studies on TGF- $\beta$ -induced senescence in HCC cells are outlined in Fig. 8. TGF- $\beta$ -induced senescence response was associated with p21<sup>Cip1</sup>-mediated and p15<sup>Ink4b</sup>-mediated G<sub>1</sub> arrest, independent of p53 or p16<sup>Ink4a</sup>. This correlates with the earlier observations showing that TGF- $\beta$  uses p21<sup>Cip1</sup> and p15<sup>Ink4b</sup>, but not p16<sup>Ink4a</sup> nor p53 to induce G<sub>1</sub> arrest in other cell types.<sup>18</sup> Although TGF- $\beta$ -induced senescence had been described many years ago,<sup>37</sup> its mechanisms are poorly understood. Here, we show that the overexpression of p21<sup>Cip1</sup>, and p15<sup>Ink4b</sup> to a lesser degree, recapitulates TGF- $\beta$ -induced senescence response. Thus, p21<sup>Cip1</sup> and p15<sup>Ink4b</sup> are able to induce G<sub>1</sub> arrest and senescence response in HCC cells, as it occurs in other cell types.<sup>10</sup> Our most interesting finding was the implication of both Nox4 and ROS in the induction of p21<sup>Cip1</sup> and p15<sup>Ink4b</sup>, and

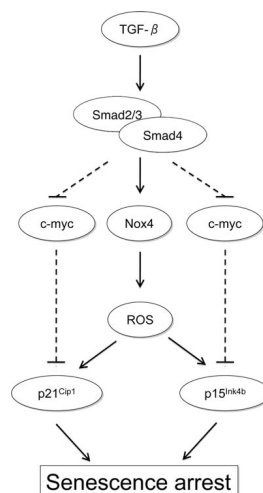


Fig. 8. A hypothetical model summarizing major components of TGF- $\beta$ -induced senescence in HCC cells.

G<sub>1</sub> arrest by TGF- $\beta$ . Either *NOX4* gene silencing or ROS scavenging was sufficient to interrupt the TGF- $\beta$  signaling toward growth arrest mediated by p21<sup>Cip1</sup> and p15<sup>Ink4b</sup> induction. Thus, the accumulation of both Nox4 protein and ROS is a critical step for p21<sup>Cip1</sup> and p15<sup>Ink4b</sup> accumulation in TGF- $\beta$ -exposed HCC cells (Fig. 8). Inhibition of p21<sup>Cip1</sup>-mediated ROS accumulation has been previously shown to rescue senescence,<sup>38</sup> and a feedback between p21<sup>Cip1</sup> and ROS production was necessary for stable growth arrest.<sup>39</sup>

Our findings also provided preliminary evidence for antitumor activity of TGF- $\beta$  against HCC. This effect was associated with *in vivo* induction of SA- $\beta$ -Gal activity in tumor cells. Thus, TGF- $\beta$ -induced senescence in human HCC cells, similar to p53-induced senescence in mouse HCC cells,<sup>12</sup> may be a potent tumor suppressor mechanism. The accelerated tumorigenesis of *TGFBR2*-deleted Hep3B-TR cells supports this hypothesis. Previous studies indicated that the disruption of TGF- $\beta$  signaling in mice through dominant-negative *Tgfr2* (transforming growth factor receptor 2) accelerates chemically induced hepatocarcinogenesis.<sup>40</sup> A similar disruption in  $\beta$ -spectrin embryonic liver fodrin knockout mice also leads to hepatocellular cancer.<sup>41,42</sup> However, our findings are limited to well-differentiated HCC cells that represent early forms of HCC.<sup>43</sup> Poorly differentiated HCC cell lines appear to

be resistant to TGF- $\beta$ -induced senescence (S. Senturk and M. Ozturk, unpublished data). Nevertheless, TGF- $\beta$  treatment might be an attractive therapeutic option for early HCCs.

**Acknowledgment:** We thank Edward B. Leof (United States) for providing pSBE4-luc and p3TP-lux reporter constructs, and Isabel Fabregat (Spain) for providing *NOX4*-specific siRNA sequence information prior to publication.

## References

- Campisi J, d'Adda di Fagnana F. Cellular senescence: when bad things happen to good cells. *Nat Rev Mol Cell Biol* 2007;8:729-740.
- Wiemann SU, Satyanarayana A, Tshuridu M, Tillmann HL, Zender L, Klempnauer J, et al. Hepatocyte telomere shortening and senescence are general markers of human liver cirrhosis. *FASEB J* 2002;16:935-942.
- Delhaye M, Louis H, Degraef C, Le Moine O, Deviere J, Peny MO, et al. Hepatocyte proliferative activity in human liver cirrhosis. *J Hepatol* 1999;30:461-471.
- Paradis V, Youssef N, Dargere D, Ba N, Bonvoust F, Deschatrete J, et al. Replicative senescence in normal liver, chronic hepatitis C, and hepatocellular carcinomas. *Hum Pathol* 2001;32:327-332.
- Ikeda H, Sasaki M, Sato Y, Harada K, Zen Y, Mitsui T, et al. Bile ductular cell reaction with senescent hepatocytes in chronic viral hepatitis is lost during hepatocarcinogenesis. *Pathol Int* 2009;59:471-478.
- Ikeda H, Sasaki M, Sato Y, Harada K, Zen Y, Mitsui T, et al. Large cell change of hepatocytes in chronic viral hepatitis represents a senescence-related lesion. *Hum Pathol* 2009;40:1774-1782.
- Kim H, Oh BK, Roncalli M, Park C, Yoon SM, Yoo JE, et al. Large liver cell change in hepatitis B virus-related liver cirrhosis. *HEPATOLOGY* 2009;50:752-762.
- Krizhanovsky V, Yon M, Dickins RA, Hearn S, Simon J, Miething C, et al. Senescence of activated stellate cells limits liver fibrosis. *Cell* 2008;134:657-667.
- Rudolph KL, Chang S, Millard M, Schreiber-Agus N, DePinho RA. Inhibition of experimental liver cirrhosis in mice by telomerase gene delivery. *Science* 2000;287:1253-1258.
- Ozturk M, Arslan-Ergul A, Bagislar S, Senturk S, Yuzugullu H. Senescence and immortality in hepatocellular carcinoma. *Cancer Lett* 2008;286:103-113.
- Ozturk N, Erdal E, Mumcuoglu M, Akcali KC, Yalcin O, Senturk S, et al. Reprogramming of replicative senescence in hepatocellular carcinoma-derived cells. *Proc Natl Acad Sci USA* 2006;103:2178-2183.
- Xue W, Zender L, Miething C, Dickins RA, Hernandez E, Krizhanovsky V, et al. Senescence and tumour clearance is triggered by p53 restoration in murine liver carcinomas. *Nature* 2007;445:656-660.
- Wu CH, van Riggelen J, Yetil A, Fan AC, Bachireddy P, Felsher DW. Cellular senescence is an important mechanism of tumor regression upon c-Myc inactivation. *Proc Natl Acad Sci USA* 2007;104:13028-13033.
- Carmona-Cuenca I, Roncero C, Sancho P, Caja L, Fausto N, Fernandez M, et al. Upregulation of the NADPH oxidase NOX4 by TGF- $\beta$  in hepatocytes is required for its pro-apoptotic activity. *J Hepatol* 2008;49:965-976.
- Sayan BS, Ince G, Sayan AE, Ozturk M. NAPO as a novel marker for apoptosis. *J Cell Biol* 2001;155:719-724.
- Wurmbach E, Chen YB, Khitrov G, Zhang W, Roayaie S, Schwartz M, et al. Genome-wide molecular profiles of HCV-induced dysplasia and hepatocellular carcinoma. *HEPATOLOGY* 2007;45:938-947.
- Gentleman RC, Carey VJ, Bates DM, Bolstad B, Dettling M, Dudoit S, et al. Bioconductor: open software development for computational biology and bioinformatics. *Genome Biol* 2004;5:R80.
- Siegel PM, Massague J. Cytostatic and apoptotic actions of TGF- $\beta$  in homeostasis and cancer. *Nat Rev Cancer* 2003;3:807-821.
- Yuzugullu H, Benhaj K, Ozturk N, Senturk S, Celik E, Toyu A, et al. Canonical Wnt signaling is antagonized by noncanonical Wnt5a in hepatocellular carcinoma cells. *Mol Cancer* 2009;8:90.
- Coulouarn C, Factor VM, Thorgerirsson SS. Transforming growth factor-beta gene expression signature in mouse hepatocytes predicts clinical outcome in human cancer. *HEPATOLOGY* 2008;47:2059-2067.
- Inagaki M, Moustakas A, Lin HY, Lodish HF, Carr BI. Growth inhibition by transforming growth factor beta (TGF-beta) type I is restored in TGF-beta-resistant hepatoma cells after expression of TGF-beta receptor type II cDNA. *Proc Natl Acad Sci USA* 1993;90:5359-5363.
- Zawel L, Dai JL, Buckhaults P, Zhou S, Kinzler KW, Vogelstein B, et al. Human Smad3 and Smad4 are sequence-specific transcription activators. *Mol Cell* 1998;1:611-617.
- Sandler MA, Zhang JN, Westerhausen DR Jr, Billadello JJ. A novel protein interacts with the major transforming growth factor-beta responsive element in the plasminogen activator inhibitor type-1 gene. *J Biol Chem* 1994;269:21500-21504.
- Herzer K, Ganten TM, Schulze-Bergkamen H, Grosse-Wilde A, Koschny R, Krammer PH, et al. Transforming growth factor beta can mediate apoptosis via the expression of TRAIL in human hepatoma cells. *HEPATOLOGY* 2005;42:183-192.
- Lin JK, Chou CK. In vitro apoptosis in the human hepatoma cell line induced by transforming growth factor beta 1. *Cancer Res* 1992;52:385-388.
- Ponchel F, Puisieux A, Tabone E, Michot JB, Froschl G, Morel AP, et al. Hepatocarcinoma-specific mutant p53-249ser induces mitotic activity but has no effect on transforming growth factor beta 1-mediated apoptosis. *Cancer Res* 1994;54:2064-2068.
- Oberhammer F, Bursch W, Parzefall W, Breit P, Erber E, Stadler M, et al. Effect of transforming growth factor beta on cell death of cultured rat hepatocytes. *Cancer Res* 1991;51:2478-2485.
- Gil J, Peters G. Regulation of the INK4b-ARF-INK4a tumour suppressor locus: all for one or one for all. *Nat Rev Mol Cell Biol* 2006;7:667-677.
- Classon M, Dyson N. p107 and p130: versatile proteins with interesting pockets. *Exp Cell Res* 2001;264:135-147.
- Erdal E, Ozturk N, Cagatay T, Eksioglu-Demiralp E, Ozturk M. Lithium-mediated downregulation of PKB/Akt and cyclin E with growth inhibition in hepatocellular carcinoma cells. *Int J Cancer* 2005;115:903-910.
- Roncalli M, Bianchi P, Bruni B, Laghi L, Destro A, Di Gioia S, et al. Methylation framework of cell cycle gene inhibitors in cirrhosis and associated hepatocellular carcinoma. *HEPATOLOGY* 2002;36:427-432.
- Sanchez A, Alvarez AM, Benito M, Fabregat I. Apoptosis induced by transforming growth factor-beta in fetal hepatocyte primary cultures: involvement of reactive oxygen intermediates. *J Biol Chem* 1996;271:7416-7422.
- Herrera B, Murillo MM, Alvarez-Barrientos A, Beltran J, Fernandez M, Fabregat I. Source of early reactive oxygen species in the apoptosis induced by transforming growth factor-beta in fetal rat hepatocytes. *Free Radic Biol Med* 2004;36:16-26.
- Carmona-Cuenca I, Herrera B, Ventura JJ, Roncero C, Fernandez M, Fabregat I. EGF blocks NADPH oxidase activation by TGF-beta in fetal rat hepatocytes, impairing oxidative stress, and cell death. *J Cell Physiol* 2006;207:322-330.
- Lee AC, Fenster BE, Ito H, Takeda K, Bae NS, Hirai T, et al. Ras proteins induce senescence by altering the intracellular levels of reactive oxygen species. *J Biol Chem* 1999;274:7936-7940.
- Droge W. Free radicals in the physiological control of cell function. *Physiol Rev* 2002;82:47-95.
- Lin HK, Bergmann S, Pandolfi PP. Cytoplasmic PML function in TGF-beta signalling. *Nature* 2004;431:205-211.

38. Macip S, Igarashi M, Fang L, Chen A, Pan ZQ, Lee SW, et al. Inhibition of p21-mediated ROS accumulation can rescue p21-induced senescence. *EMBO J* 2002;21:2180-2188.
39. Passos JF, Nelson G, Wang C, Richter T, Simillion C, Proctor CJ, et al. Feedback between p21 and reactive oxygen production is necessary for cell senescence. *Mol Syst Biol* 2010;6:347.
40. Kanzler S, Meyer E, Lohse AW, Schirmacher P, Henninger J, Galle PR, et al. Hepatocellular expression of a dominant-negative mutant TGF-beta type II receptor accelerates chemically induced hepatocarcinogenesis. *Oncogene* 2001;20:5015-5024.
41. Kitisin K, Ganesan N, Tang Y, Jogunoori W, Volpe EA, Kim SS, et al. Disruption of transforming growth factor-beta signaling through beta-spectrin ELF leads to hepatocellular cancer through cyclin D1 activation. *Oncogene* 2007;26:7103-7110.
42. Tang Y, Kitisin K, Jogunoori W, Li C, Deng CX, Mueller SC, et al. Progenitor/stem cells give rise to liver cancer due to aberrant TGF-beta and IL-6 signaling. *Proc Natl Acad Sci USA* 2008;105:2445-2450.
43. Kojiro M. Pathological evolution of early hepatocellular carcinoma. *Oncology* 2002;62(Suppl. 1):43-47.



## Subsequence-based feature map for protein function classification

Omer Sinan Sarac<sup>a</sup>, Özge Gürsoy-Yüzügüllü<sup>b</sup>,  
Rengul Cetin-Atalay<sup>b</sup>, Volkan Atalay<sup>a,\*</sup>

<sup>a</sup> Department of Computer Engineering, Middle East Technical University, 06531 Ankara, Turkey

<sup>b</sup> Department of Molecular Biology and Genetics, Faculty of Science, Bilkent University, 06533 Ankara, Turkey

Received 9 August 2007; accepted 30 November 2007

### Abstract

Automated classification of proteins is indispensable for further *in vivo* investigation of excessive number of unknown sequences generated by large scale molecular biology techniques. This study describes a discriminative system based on feature space mapping, called subsequence profile map (SPMap) for functional classification of protein sequences. SPMap takes into account the information coming from the subsequences of a protein. A group of protein sequences that belong to the same level of classification is decomposed into fixed-length subsequences and they are clustered to obtain a representative feature space mapping. Mapping is defined as the distribution of the subsequences of a protein sequence over these clusters. The resulting feature space representation is used to train discriminative classifiers for functional families. The aim of this approach is to incorporate information coming from important subregions that are conserved over a family of proteins while avoiding the difficult task of explicit motif identification. The performance of the method was assessed through tests on various protein classification tasks. Our results showed that SPMap is capable of high accuracy classification in most of these tasks. Furthermore SPMap is fast and scalable enough to handle large datasets.

© 2007 Elsevier Ltd. All rights reserved.

**Keywords:** Protein function prediction; Subsequence distribution; Function classification

### 1. Introduction

Along with the recent advances in genome sequencing technologies, the number of protein sequences with missing annotations increases rapidly. Thus, computational classification methods become valuable for providing a road map for the biologist for further investigation of the excessive number of unknown sequences *in vivo*. In general, *in silico* course of action for the classification of a new sequence is to find similar sequences whose functions are experimentally determined. This is usually performed by searching public databases using local alignment search tools such as BLAST or PSI-BLAST and annotations for the highest scoring hits are transferred onto the new sequence (Altschul et al., 1990, 1997). Although this simple method performs well in many cases, it has some important drawbacks such as excessive transfer of annotations, propagation of errors in the source database, threshold relativity and low

sensitivity/specificity (Devos and Valencia, 2000; Gilks et al., 2005; Sasson et al., 2006; Friedberg, 2006). It has been shown recently that although inferring homology through sequence similarity generally holds for the 3D structure, it is far less justified for the function. Additional information than just pairwise similarity is needed to find more accurate annotations (Devos and Valencia, 2000).

Existing approaches to the computational classification beyond simple homology-based transfer can be grouped into three classes: *improved homology-based methods*, *feature-based methods*, and *subsequence-based methods* (Pandey et al., 2006). Improved homology-based approach still uses sequence homology, however it incorporates additional information (Andrade et al., 1999; Riley et al., 2005; Martin et al., 2004), such as multiple sequence alignments or classifications of similarity results according to a hierarchical and structured organization of functions like in Gene Ontology (GO) database (Ashburner et al., 2000). On the other hand, both feature-based and subsequence-based approaches pursue discriminative methodology that explicitly models the differences between positive and negative examples. Two approaches differ in the way how they

\* Corresponding author. Tel.: +90 312 210 5576; fax: +90 312 210 5544.  
E-mail address: [volkan@ceng.metu.edu.tr](mailto:volkan@ceng.metu.edu.tr) (V. Atalay).

extract features from sequences. In the feature-based approach, biologically meaningful properties of a protein such as frequency of residues, molecular weight, secondary structure,  $n$ -gram frequencies, are extracted from the primary sequence. These properties are then arranged as feature vectors and used as input to classification techniques such as artificial neural networks (ANNs) or support vector machines (SVMs) (Duda et al., 2000; King et al., 2000; Pasquier et al., 2001; Jensen et al., 2002; Cai et al., 2003; Karchin et al., 2002; Cheng et al., 2005). On the other hand, conserved subsequences among a class of proteins are employed in subsequence-based methods. The main idea is that, conserved subsequences among different proteins are strong indicators of functional or structural similarity because functionally important regions (catalytic sites, binding sites, structural motifs) are conserved over much wider taxonomic distances than the sequences themselves. Thus, in subsequence-based approach feature vectors are constructed according to the existence of specific motifs or domains in the protein sequences. The critical step in this approach is the extraction and selection of motifs. One possibility is to use motif information from protein databases (Ben-hur and Brutlag, 2003; Wang et al., 2003) in which motifs are assumed to be already available for the family of proteins to be classified. Most of the methods of subsequence-based approach attempt to extract motifs explicitly for the given families (Hannenhalli and Russell, 2000; Wang et al., 2001; Liu and Califano, 2001; Kunik et al., 2005; Blekas et al., 2005). Although motifs are powerful discriminators even in low similarity (remote homology) situations, motif finding is a very difficult task, especially for protein sequences since there are 20 different amino acids and many plausible mutations. Multiple sequence alignments and other computational pattern extraction algorithms are often employed for motif finding. Unfortunately, algorithms that can find optimal solutions in all of these methods have exponential time complexities, hence approximation or heuristic algorithms are used instead. As a consequence, there is always the risk of missing some relatively implicit motifs. Furthermore, classical motif finding algorithms find a specified number of motifs even if there are not that many biological motifs in the family. These insignificant additional motifs might reduce the accuracy of the classification. One other issue is that, depending on the classification task, proteins to be classified might not have a common motif at all. As an example, in the problem of subcellular localization, when discriminating cytosolic proteins, it is not possible to find motifs specific to this class. Methods that consider overall sequence similarity may perform better in such cases.

In this study, we describe a feature space mapping, called subsequence profile map (SPMap), that takes into account the information coming from the subsequences of a protein. Our approach incorporates the information coming from important subregions that are conserved over a family of proteins as well as the overall sequence similarity. Instead of focusing on function specific motifs, SPMap considers all of the subsequences as a distribution over a quantized space by discretizing and reducing the dimension of an otherwise huge space of all possible subsequences.

## 2. Systems and Methods

The system described in this study is based on a discriminative method which requires positive and negative examples to classify and annotate proteins whose functions are not known. Instead of looking for the overall similarity of protein sequences, we make use of the distribution of short subsequences of a given protein over a subsequence profile map. We generated the profiles using all possible fixed-length subsequences of the protein sequences in the positive training set. Similar subsequences were clustered together and clusters were represented as probabilistic profiles. The major reasoning behind this approach is that, subsequences extracted from the conserved regions are more frequent than any other subsequence extracted from the positive training data. If the frequent subsequences are represented as dimensions of feature vectors, discriminative methods can make use of this information. If there is a conserved motif or a domain in the given sequences or there is an overall similarity between sequences, they would produce similar distributions on the profile map. Classifiers such as support vector machines (SVMs) may then identify these similar distributions and hence improve the classification accuracy.

In order to perform the classification, SVMs were used. We constructed fixed dimensional vectors that represent the subsequence distribution information. There are two critical steps in SPMap as shown in Fig. 1:

- A. subsequence profile map construction,
- B. feature vector generation and classification.

### 2.1. Subsequence Profile Map Construction

In SPMap, feature space representation of a protein sequence is the distribution of its subsequences over a map of generative models. General framework for finding this generative feature map is summarized as follows.

- Subsequence Extraction Module: Extract all possible subsequences of a given length from positive training sequences.
- Clustering Module: Cluster similar subsequences by an appropriate clustering method.
- Profile Construction Module: Build a model for each cluster.

The important step here is the clustering of subsequences. Note that the space of all possible subsequences of length  $l$  is of size  $20^l$ , since there are 20 possible amino acids. Instead of working in this very high dimensional space, we quantized this space using the clusters of subsequences that are actually existing in the positive training examples. One should note that, as we clustered the subsequences, we were not actually looking for underlying groupings. The aim here was to generate a meaningful quantization of the subsequence space that especially represent groups of frequent and similar subsequences in the positive training data. These subsequences might have been conserved because of their importance for the function of that

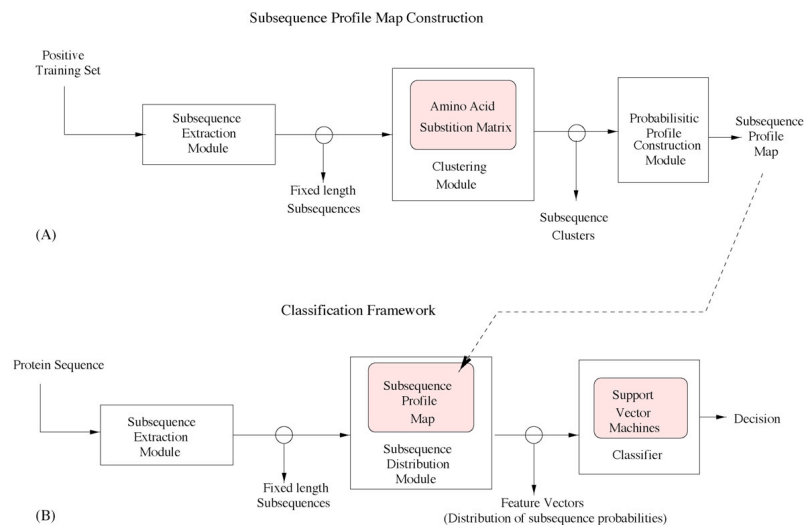


Fig. 1. SPMMap flow diagram. (A) Subsequence profile map construction: subsequences of the proteins in positive training set are clustered to construct subsequence profile map. (B) Classification: constructed profile map is utilized to find the feature space representation of the protein sequence to be classified.

class of proteins and we wanted our feature space to take them into account. Clustering algorithm is given in Algorithm 1. It is similar to the average link hierarchical clustering, however it can be implemented very efficiently without calculating all the pairwise distances. Initially the number of clusters is set to 0. Each subsequence is compared against all of the existing clusters and average similarity to the elements of each cluster is calculated. A subsequence is assigned to the cluster,  $C_{\max}$ , which gives the maximum average similarity value. If the similarity to  $C_{\max}$  is less than a threshold,  $\delta$ , a new cluster is created and the subsequence is assigned to the new cluster. Similarity between two subsequences  $x$  and  $y$  was calculated by the formula

$$s(x, y) = \sum_{i=1}^l M(x(i), y(i)) \quad (1)$$

where  $l$  is the length of the subsequences and  $M(x(i), y(i))$  is the value in the similarity matrix for the  $i$ th elements of  $x$  and  $y$ . For  $M$ , we used an amino acid similarity matrix, since it allows us to incorporate evolutionary information in finding and representing important conserved regions of a family of proteins. The final number of clusters depend on the threshold value  $\delta$ . If it is set to a high value, clusters will be smaller only allowing very similar subsequences and the total number of clusters will be high. If it is set to a low value, biologically unrelated subsequences might end up in the same cluster.

#### Algorithm 1. Clustering Algorithm.

---

**Algorithm 1** Clustering Algorithm

```

 $X \leftarrow$  all fixed length subsequences of the positive training set
 $C \leftarrow \{\}$ 
for all  $x_i \in X$  do
  for all Clusters  $C_k$  do
     $s_k = \frac{\sum_{x_j \in C_k} s(x_i, x_j)}{|C_k|}$ 
  end for
   $m = \text{argmax}_{k=1..|C|} s_k$ 
  if  $s_m > \delta$  then
    Add  $x_i$  to  $C_m$ 
  else
    Create a new cluster  $C_{|C|+1}$  and add  $x_i$  to  $C_{|C|+1}$ 
  end if
end for

```

---

After the clustering step, we generated a probabilistic profile for each cluster. A probabilistic profile  $PP_k$  for cluster  $k$ , is an  $l \times 20$  matrix, where  $l$  is the length of a subsequence. Entry  $PP_k(i, j)$  of this matrix represents the probability of amino acid  $j$  to occur at the  $i$ th position of the subsequence. Given a cluster  $C_k$ , the profile for this cluster is calculated by the following equation:

$$PP_k(i, j) = \log \frac{\phi_k(i, j) + \kappa}{|C_k|} \quad (2)$$

where  $\phi_k(i, j)$  represents the count of the amino acid  $j$  at position  $i$  of the subsequences in  $C_k$ . We added a pseudo-count  $\kappa$  for amino acids at each position to avoid over-fitting and zero probabilities. Actually, we took the log of the profiles and worked with log-probabilities in the conversion step.

## 2.2. Feature Vector Generation

Proteins were represented in the feature space as the distribution of their subsequences over the generated subsequence profile map. All the subsequences of a protein were extracted to construct a feature vector. Each subsequence  $x$  was compared with each probabilistic profile  $PP_k$  and a probability was calculated as

$$P(x|PP_k) = \sum_{i=0}^l PP_k(i, x(i)). \quad (3)$$

The value for the  $k$ th dimension of the feature vector  $V$  is set to

$$V(k) = \max_{x_i \in S} P(x_i|PP_k), \quad (4)$$

the probability of highest scoring subsequence of protein  $S$  on probabilistic profile  $PP_k$ . This algorithm is similar to the vector generation algorithm presented in Blekas et al. (2005) with the difference that we set  $V(k)$  to 0 if the probability is very small.

## 2.3. Classification

Once the protein sequences are mapped onto the feature space, any numerical machine learning tool can be employed. Our choice was to use SVMs since they are experimentally proven to be successful for various problems (Cristianini and Shawe-Taylor, 2000). Radial basis function (RBF) was chosen as the kernel for SVM. In all of the experiments, SVM parameter  $C$  and RBF kernel parameter  $\gamma$  were fixed to be 2 and 0.05, respectively. SVM-light software was used for learning and classification steps (Joachims, 1999).

## 2.4. Experimental Setup

In all of the experiments, BLOSUM62 matrix was employed to calculate the similarity between subsequences (Henikoff and Henikoff, 1992) although it is possible to use different similarity matrices depending on the sequence divergence or the taxonomic distance between the proteins to be classified (Atalay and Cetin-Atalay, 2005; Tomii and Kanehisa, 1996). BLOSUM62 is shown to be useful for a wide range of problems and is the default selection for most of the alignment tools (Altschul et al., 1990, 1997). Length of the subsequences was set to 5. Setting the subsequence length to 5 did not mean that we sought for motifs of 5 amino acid length. In SPMMap, motifs were the overall distribution of the subsequences over the profiles constructed from resulting 5 length subsequence clusters. Hence subsequence length 5 allowed us to capture longer motifs as a distribution over more than one profile. We tested the performance of SPMMap by changing the subsequence length in the interval [5,12] on selected sample sets of data. We observed that although there were differences in the performance with respect to the change in the subsequence length, 5 was the optimal in the sense of performance versus computational complexity. Threshold similarity score  $\delta$  in Algorithm 1 was fixed to 8 where the expected similarity score of two random subsequences of

Table 1  
Average ROC scores and standard deviations for subcellular localization predictions

Localization	Data size	Mean ROC	S.D.
ER targeted	3115	0.97	0.006
Cytoplasmic	1789	0.95	0.005
Mitochondrial	1148	0.96	0.006
Nuclear	2225	0.96	0.005

length 5 using BLOSUM62 matrix is  $-5.325$ . Compared to the expected value, 8 is high enough to disallow random similarities. Extensive tests with different threshold values showed that 8 performed better in most of the test cases and it was set as default in all of the experiments.

## 3. Results

### 3.1. Subcellular Localization

The idea of subsequence distribution was first proposed in P2SL (Atalay and Cetin-Atalay, 2005). However, we developed more robust, reliable and efficient method for this idea. In order to be able to show the improvement, we first performed tests on the subcellular localization dataset on which P2SL was trained and tested. Dataset was composed of four different classes, namely ER targeted (ER), cytoplasmic (C), mitochondrial (M) and nuclear (N) (Atalay and Cetin-Atalay, 2005). ER targeted and mitochondrial proteins have signal peptides of length 25 and 35 amino acids, respectively, at the N-terminal of the proteins. While extracting subsequences for feature map construction we used first 30 amino acids for ER targeted proteins and first 40 amino acids for mitochondrial proteins. Two types of tests were performed. First, in a one-versus-all setting, ROC scores were calculated for each localization and results are given in Table 1.

In the second test case, classifiers for each localization were combined using the winner-take-all principle. Each test sample was assigned to the location whose classifier produced the highest SVM score. The confusion matrix obtained by averaging fourfold cross-validation tests and their comparison with P2SL results are given in Table 2 (Atalay and Cetin-Atalay, 2005).

### 3.2. G-protein-Coupled Receptor Subfamily Classification

Tests are subsequently carried on G-protein-coupled receptor (GPCR) subfamily classification problem that was extensively studied in the literature. Consequently, GPCR subfamily classification constitutes a good benchmark dataset for comparing with other methods. For GPCR subfamily classification, we used the dataset presented in Karchin et al. (2002) to compare with the results of various classifiers presented in Karchin et al. (2002) and Cheng et al. (2005). Same train and test splits were used for twofold cross validation for fairness of comparison. SPMMap was tested on level I and level II subfamily classification of GPCR proteins. In level I subfamily classification, there

Table 2  
Confusion matrix representing average percentage results of fourfold prediction tests compared with P2SL results

Actual	Predicted label			
	N (%)	C (%)	M (%)	ER (%)
N				
SPMap	<b>89.83</b>	7.5	1.1	1.58
P2SL	<b>75.34</b>	19.94	3.29	1.43
C				
SPMap	7.14	<b>89.05</b>	1.8	2.02
P2SL	14.66	<b>79.33</b>	3.65	2.36
M				
SPMap	2.09	5.4	<b>89.29</b>	3.22
P2SL	3.31	7.23	<b>83.80</b>	5.66
ER				
SPMap	2.07	2.5	1.41	<b>94.03</b>
P2SL	4.89	6.19	3.29	<b>85.63</b>

were 1269 sequences from 19 subfamilies within classes A and C in addition to 149 non-GPCR sequences. In level II subfamily classification, there were 1170 GPCR sequences from 70 different level II subfamilies. Some of the sequences in level I subfamily classification have no level II subfamily classification and some of the level II subfamilies only have one protein so they are grouped as other sequences with non-GPCR sequences. Datasets and train and test splits are available at [http://www.soe.ucsc.edu/research/compbio/gpcr/subfamily\\_seqs](http://www.soe.ucsc.edu/research/compbio/gpcr/subfamily_seqs).

The comparison of accuracy of various classifiers and SPMap is presented in Table 3. Fisher-SVM, BLAST, SAM-T2K HMM, and kernNN methods were presented in Karchin et al. (2002) and Decision Tree and Naïve Bayes methods were presented in Cheng et al. (2005).

### 3.3. Enzyme Class Classification

Finally we evaluated the performance of SPMap on enzyme class classification. Enzymes play a central role in many of the biological functions in a cell. They are indispensable for understanding the molecular systems in a cell and are important drug targets. Hence accurate classification is very important in enzyme research.

Dataset for enzyme classification is extracted from BRENDA database (Schomburg et al., 2002). International Union of Biochemistry and Molecular Biology defines the numerical clas-

Table 3  
Comparison of accuracy of various classifiers at GPCR levels I and II subfamily classification

Classifier	Level I accuracy	Level II accuracy
BLAST	83.3	74.5
Decision Tree	77.3	70.8
Fisher-SVM	88.4	86.3
kernNN	64.0	51.0
Naïve Bayes	93.0	92.4
SAM-T2K HMM	69.9	70.0
SPMap	<b>95.4</b>	<b>93.8</b>

Table 4  
Comparison of success rates of various classifiers on six major enzyme classes calculated with leave-one-out cross-validation

Classes	Total	Success (%)				
		Lu et al.	Blast	Psi-Blast	SVM-Prot	SPMap
Oxidoreductase	436	<b>93.53</b>	89.68	91.06	73.62	80.73
Transferase	832	<b>93.63</b>	88.46	87.98	82.45	66.23
Hydrolase	741	<b>94.20</b>	86.10	86.77	77.33	71.93
Lyase	170	75.29	75.29	70.59	68.82	<b>94.12</b>
Isomerase	114	74.56	73.68	73.68	68.42	<b>96.49</b>
Ligase	150	89.33	<b>90.00</b>	88.67	37.33	88.00

sification scheme for enzymes based on the chemical reactions they catalyze. Each enzyme is described by a sequence of four numbers (EC numbers) resulting from a four-level hierarchy where first number specifies the most general class and the last one specifies the most specific. At the highest level there are six major classes of enzymes. Automated prediction methods are successfully applied to enzyme classification according to the first (Lu et al., 2007) and second level of EC numbers (Cai et al., 2003). We also performed tests according to the first and second EC numbers. On the first level there are six major classes of enzymes. Dataset used for this level is presented in Lu et al. (2007). Each class is filtered so that there are no pair of proteins with more than 25% sequence identity. The success rates for various methods and SPMap for six classes with leave-one-out cross-validation is presented in Table 4.

We also classified proteins according to their first two EC numbers, resulting in 56 classes. We omitted classes with very few members. Sensitivity and specificity values calculated over fourfold cross validation are presented in Table 5. This classifier for 56 enzyme classes is available as an online service at <http://gen.ceng.metu.edu.tr/spmap/cgi-bin/enzyme.cgi>.

## 4. Discussion

### 4.1. Computational Complexity

SPMap is composed of two main parts. First part is the sub-sequence profile map construction. It is only performed once for a new classifier to be trained. Hence, its efficiency does not affect the performance during the classification of new sequences. The most expensive part of the map construction is the clustering of subsequences. Most of the standard clustering algorithms require numerical vectors to work on. More specifically, they require a metric to calculate the distance between the cluster representations and data points and a method to update these cluster representations throughout the course of the algorithm. These methods usually perform  $O(nk)$  distance calculations where  $n$  is the number of data points and  $k$  is the number of clusters. They require the number of clusters  $k$  to be given at the start. There are also clustering algorithms that use only pairwise distances between data points. They do not require the number of clusters  $k$  as a parameter but they have



Table 5  
Sensitivity ( $TP/(TP + FN)$ ) and specificity ( $TN/(TN + FP)$ ) values for 56 enzyme class classifiers calculated over fourfold cross validation

Enzyme class	Data size	Sensitivity	Specificity
EC 1.1 Acting on the CH–OH group of donors	8878	95.33	85.05
EC 1.2 Acting on the aldehyde or oxo group of donors	4099	91.63	97.17
EC 1.3 Acting on the CH–CH group of donors	2455	85.75	98.09
EC 1.4 Acting on the CH–NH <sub>2</sub> group of donors	1573	88.64	99.74
EC 1.5 Acting on the CH–NH group of donors	1244	81.35	99.72
EC 1.6 Acting on NADH or NADPH	5572	94.54	95.85
EC 1.7 Acting on other nitrogenous compounds as donors	802	83.67	99.93
EC 1.8 Acting on a sulfur group of donors	1699	89.94	99.82
EC 1.9 Acting on a heme group of donors	1620	93.99	98.51
EC 1.10 Acting on diphenols and related substances as donors	813	86.86	99.98
EC 1.11 Acting on a peroxide as acceptor	1267	91.56	99.97
EC 1.12 Acting on hydrogen as donor	243	68.89	99.97
EC 1.13 Acting on single donors/with incorporation of molecular oxygen (oxygenases)	1048	87.66	99.97
EC 1.14 Acting on paired donors, with incorporation/or reduction of molecular oxygen	1909	83.3	98.42
EC 1.15 Acting on superoxide radicals as acceptor	935	93.56	99.99
EC 1.16 Oxidising metal ions	142	65.71	99.96
EC 1.17 Acting on CH or CH <sub>2</sub> groups	1063	90.31	99.92
EC 1.18 Acting on iron–sulfur proteins as donors	745	91.94	99.97
EC 1.20 Acting on phosphorus or arsenic in donors	66	66.67	99.99
EC 1.21 Acting on X–H and Y–H to form an X–Y bond	60	88.89	100
EC 1.97 Other oxidoreductases	169	80.95	99.99
EC 2.1 Transferring one-carbon groups	6061	92.28	90.97
EC 2.2 Transferring aldehyde or ketonic groups	1058	94.32	99.94
EC 2.3 Acyltransferases	6149	92.52	91.55
EC 2.4 Glycosyltransferases	6004	92.65	89.54
EC 2.5 Transferring alkyl or aryl groups, other than methyl groups	5188	93.94	96.73
EC 2.6 Transferring nitrogenous groups	2011	95.22	99.85
EC 2.7 Transferring phosphorus-containing groups	23424	89.78	91.08
EC 2.8 Transferring sulfur-containing groups	982	87.35	99.91
EC 2.9 Transferring selenium-containing groups	72	88.89	100
EC 3.1 Acting on ester bonds	9879	74.79	96.05
EC 3.2 Glycosylases	4789	93.76	91.98
EC 3.3 Acting on peptide bonds (peptidases)	5945	93.4	87.48
EC 3.5 Acting on carbon–nitrogen bonds, other than peptide bonds	5942	90.28	88.25
EC 3.6 Acting on acid anhydrides	7430	96.23	88.22
EC 3.7 Acting on carbon–carbon bonds	66	81.25	100
EC 3.8 Acting on halide bonds	101	49.33	99.98
EC 4.1 Carbon–carbon lyases	7606	93.77	87.95
EC 4.2 Carbon–oxygen lyases	7211	93.23	87.46
EC 4.3 Carbon–nitrogen lyases	1264	91.14	99.89
EC 4.4 Carbon–sulfur lyases	626	82.91	99.8
EC 4.6 Phosphorus–oxygen lyases	614	91.28	99.9
EC 4.99 Other lyases	297	90.99	99.98
EC 5.1 Racemases and epimerases	2030	92.18	99.66
EC 5.2 <i>cis</i> – <i>trans</i> –Isomerases	1232	92.86	99.92
EC 5.3 Intramolecular isomerases	2910	90.65	99.18
EC 5.4 Intramolecular transferases (mutases)	2195	88.57	99.37
EC 5.5 Intramolecular lyases	135	71.72	99.98
EC 5.99 Other isomerases	1418	95.57	99.96
EC 6.1 Forming carbon–oxygen bonds	6285	97.05	98.39
EC 6.2 Forming carbon–sulfur bonds	1112	93.17	99.91
EC 6.3 Forming carbon–nitrogen bonds	6784	94.53	95.25
EC 6.4 Forming carbon–carbon bonds	785	94.9	99.87
EC 6.5 Forming phosphoric ester bonds	433	89.2	99.97
EC 6.6 Forming nitrogen–metal bonds	118	90.81	99.97

to perform  $O(n^2)$  pairwise distance calculations and that might be very inefficient in terms of time and memory for large  $n$ . Note that  $n$  in this case is the total number of subsequences extracted from all of the positive training examples, which is

roughly the number of amino acids in the positive training examples. However, Algorithm 1 can be implemented in  $O(nk)$ . The critical step is the calculation of the average distance of subsequence  $x_i$  to the cluster  $u$  given in the following equa-

tion:

$$s_u = \frac{\sum_{x_j \in C_u} s(x_i, x_j)}{|C_u|} \quad (5)$$

With this definition, Algorithm 1 requires  $n^2$  pairwise subsequence similarity calculations. Combining Eqs. (1) and (5) and rearranging the formula,  $s_u$  can be written as given in the following equation:

$$s_u = \sum_{t=1}^l \sum_{j=1}^{20} f_u^t(a_j) M(x_i(t), a_j) \quad (6)$$

where  $x_i(t)$  denotes the amino acid appearing at the  $t$ th position of the subsequence  $x_i$  and  $M(x_i(t), a_j)$  is the entry of similarity matrix for amino acids  $x_i(t)$  and  $a_j$ .  $f_u^t(a_j)$  represents the frequency of amino acid  $a_j$  at the  $t$ th position of subsequences in cluster  $u$ . The complexity of Algorithm 1 becomes  $O(nkl)$  where  $l$  is the length of the subsequences,  $k$  is the number of clusters, and  $n$  is the total length of all of the proteins in positive training set. Since  $l$  is an arbitrary but fixed parameter, it can be said that it is  $O(nk)$  with respect to the size of the input sequences.  $k$  is dependent on the threshold value  $\delta$  given in Algorithm 1; but it is around 1800 for the default  $\delta$  value, 8. It is almost constant or varying very slowly with the data size. The second part of the presented method is construction of the feature vectors. Since the probability of each subsequence of the protein against all of the subsequence profiles must be calculated, it again can be implemented in  $O(nk)$  time. In this case,  $n$  represents the length of the given protein to be mapped and  $k$  is the number of subsequence profiles. SPMMap is linear in the size of the input data. It is very efficient and scalable to handle large datasets.

#### 4.2. Performance Test Results

SPMap has a significant improvement over P2SL for subcellular localization classification. The improvement is both in terms of accuracy and computational efficiency. In order to discretize the subsequence space, P2SL uses self-organizing maps (SOMs) which are hard to train because of the necessity of large training data and convergence problems. As a result different runs on SOM might result in different feature spaces. P2SL is prone to missing some important subsequences since it does not consider all possible subsequences. Since SOM requires numerical vectors, P2SL encodes amino acids as 20 dimensional vectors which causes a 5 length subsequence to be represented as a 100 dimensional vector further complicating the SOM training. SPMMap uses clusters of all possible subsequences for discretization of subsequence space instead of SOM in P2SL. Similarity between subsequences are calculated using an amino acid similarity matrix and standard string similarity calculation methods, avoiding high dimensional encoding of subsequences. One of the advantages of SPMMap is that it works well on wide range of different classification tasks with the default parameter values. This makes it easier to use without expertise and optimization. Furthermore, our feature space mapping algorithm have only one

parameter, the threshold value  $\delta$ , which has a well performing default value in general.

We also investigated the performance of SPMMap on functional classification tasks other than subcellular localization. In order to assess and compare the capabilities of SPMMap, we performed tests on G-protein-coupled receptor subfamily level classification. GPCRs are very important targets in drug design but known to be hard to classify, because they have highly diverse family at the sequence level (Moriyama and Kim, 2006). It can be seen that SPMMap outperformed other classifiers in both level I and level II GPCR subfamily classification. To our knowledge, at the time of writing this paper, Naïve Bayes approach of Cheng et al. (2005) was the best performing method on the benchmark dataset presented in Karchin et al. (2002).

The application of SPMMap on enzyme class classification demonstrated that our method too generates comparable or better results to those obtained by previous studies. The dataset used for the test on 6 major enzyme classes was filtered so that there are no pair of proteins with more than 25% sequence identity. This makes the classification task more difficult especially for the methods that only use sequence or subsequence similarity. Furthermore, SPMMap depends solely on the available training data to generate the subsequence feature map, where the method presented in Lu et al. (2007) uses domains that are already available in the databases. Nevertheless, results were interestingly complementary. SPMMap achieved very high accuracy when the other methods performed poorly and vice versa. For the second level of enzyme hierarchy SPMMap achieved high sensitivity in most of the classes. We used all the available data in fourfold cross validation. As a result, a few classes with comparably large data sizes were biased towards false positives, hence relatively low specificity. Selecting a representative training subset for large classes might enhance the specificity of the classifier.

#### 4.3. Perspectives

Since supervised discriminative methods model the differences between families of positive and negative examples explicitly, they provide better solutions for most of the problems of function classification. Most widely used discriminative method is the support vector machines (SVMs) combined with an appropriate kernel or feature space mapping (Cristianini and Shawe-Taylor, 2000). The main issue in classification of proteins according to their primary sequences is to find a kernel or a feature mapping that captures the information hidden in the important discriminative regions of the given sequences. Since, functionally important regions (catalytic sites, binding sites, structural motifs) are conserved over much wider taxonomic distances than the sequences themselves, conserved subsequences among different proteins are strong indicators of functional or structural similarity. Hence, SPMMap pursued a new approach based on distribution of subsequences over a map constructed using the actual protein sequences in the positive training set.

The idea of constructing similarity graphs of subsequences and extracting motifs from the clusters of these graphs was already exploited for DNA sequences (Fratkin et al., 2006). In

SPMap, we did not try to identify the motifs explicitly. We just let the classification algorithm learn which subsequence distributions are in fact discriminative. One advantage of SPMap is that it allows further investigation of these constructed profiles to identify motifs of positive training family. As a feature study, constructed profiles can be investigated to see how similar or different they are, compared to the aligned regions resulting from a multiple sequence alignment of that family of proteins.

One further step may be identifying disordered regions and extracting subsequences from these regions. Most of the active sites, catalytic sites, etc. lies along disordered regions (Dunker et al., 2002; Wright and Dyson, 1999). This would reduce the number of unrelated subsequences hence the noise during the feature map construction.

One reason the discriminative methods do not receive as much attention among the biologists compared to the standard sequence alignment methods is the requirement of handling large number of functional classes. It is almost prohibitive if one wants to perform the classification in a one-versus-one scheme. In this study we preferred to use one-versus-all classification. If the number of classes is large, it would be infeasible to use all of the proteins in the negative classes. One-class classifiers might provide a good solution for this problem.

The use of discriminative classifiers is confined to selecting the correct function among a small set of functional classes. In order to develop a general annotation system with a discriminative approach, one might define a hierarchical classification system over a function ontology structure. Examples of two such annotation systems are Gene Ontology (GO) and Mips Functional Catalogue (FunCat) (Ashburner et al., 2000; Ruepp et al., 2004). Although GO is an intensively used annotation system, implementing such a discriminative framework over GO hierarchy might pose (present) some problems. First, GO describes gene products with fine granularity resulting in thousands of terms. As a result many terms have none or very few gene products. One should carefully filter and generate relevant classes for the classification system. Secondly, GO allows directed acyclic graphs in its hierarchy, further complicating the selection of terms to generate classes for the discriminative system. Being a tree hierarchy with especially relevant terms, FunCat might provide an easier framework to develop a general discriminative annotation framework. Once such a framework is established, each classifier might be extended to incorporate useful information other than the primary sequence, such as structural motifs or structural alignments (Can and Wang, 2004; Sacan et al., 2007).

## 5. Conclusion

We described a discriminative system for functional classification of protein sequences. It uses a subsequence similarity based feature space mapping, SPMap, to convert protein sequences into vector representations. The main idea was to consider the distribution of the subsequences of a given protein over a set of subsequence profiles as its feature representation. SPMap outperformed P2SL tool in subcellular localization and various well known methods in GPCR subfamily classification. In enzyme class classification SPMap produced better

or at least comparable results to some of the existing methods.

Our results showed that using subsequence distributions over a quantized space as a feature space for classification of proteins is an effective method in wide range of different classification problems. Furthermore, the proposed method is computationally efficient and capable of handling large datasets.

## Acknowledgement

This study is partially supported by TUBITAK under EEEAG-105E035.

## References

- Altschul, S.F., Gish, W., Miller, W., Myers, E.W., Lipman, D.J., 1990. A basic local alignment search tool. *J. Mol. Biol.* 215, 403–410.
- Altschul, S.F., Madden, T.L., Schaffer, A.A., Zhang, J., Zhang, Z., Miller, W., Lipman, D.J., 1997. Gapped BLAST and PSI-BLAST: a new generation of protein database search programs. *Nucleic Acids Res.* 25, 3389–3402.
- Andrade, M.A., Brown, N.P., Leroy, C., Hoersch, S., De Daruvar, A., Reich, C., Franchini, A., Tamames, J., Valencia, A., Ouzounis, C., Sander, C., 1999. Automated genome sequence analysis and classification. *Bioinformatics* 15 (5), 391–412.
- Ashburner, M., Ball, C., Blake, J., Botstein, D., Butler, H., Cherry, J., Davis, A., Dolinski, K., Dwight, S., Eppig, J., et al., 2000. Gene Ontology: tool for the unification of biology. *Nat. Genet.* 25, 25–29.
- Atalay, V., Cetin-Atalay, R., 2005. Implicit motif distribution based hybrid computational kernel for sequence classification. *Bioinformatics* 21 (8), 1429–1436.
- Ben-hur, A., Brutlag, D., 2003. Remote homology detection: a motif based approach. *Bioinformatics* 19, 26–33.
- Blekas, K., Fotiadis, D.I., Likas, A., 2005. Motif-based protein sequence classification using neural networks. *J. Comput. Biol.* 12 (1), 64–82.
- Cai, C., Han, L., Ji, Z., Chen, X., Chen, Y., 2003. SVM-Prot: Web-based support vector machine software for functional classification of a protein from its primary sequence. *Nucleic Acids Res.* 31 (13), 3692–3697.
- Can, T., Wang, Y.-F., 2004. Protein structure alignment and fast similarity search using local shape signatures. *J. Bioinformatics Comp. Biol.* 2, 215–239.
- Cheng, B.Y.M., Carbonell, J.G., Klein-Seetharaman, J., 2005. Protein classification based on text document classification techniques. *Proteins* 58 (4), 955–970.
- Cristianini, N., Shawe-Taylor, J., 2000. An Introduction to Support Vector Machines and Other Kernel-based Learning Methods. Cambridge University Press.
- Devos, D., Valencia, A., 2000. Practical limits of function prediction. *PROTEINS: Struct. Function Genet.* 41, 98–107.
- Duda, R.O., Hart, P.E., Stork, D.G., 2000. *Pattern Classification*, 2nd ed. Wiley-Interscience.
- Dunker, A.K., Brown, C.J., Lawson, J.D., Iakoucheva, L.M., Obradovic, Z., 2002. Intrinsic disorder and protein function. *Biochemistry* 41, 6573–6582.
- Fratkin, E., Naughton, B.T., Brutlag, D.L., Batzoglou, S., 2006. MotifCut: regulatory motifs finding with maximum density subgraphs. *Bioinformatics* 22 (14), e150–e157.
- Friedberg, I., 2006. Automated protein function prediction—the genomic challenge. *Briefings Bioinformatics* 7, 225–242.
- Gilks, W.R., Audit, B., de Angelis, D., Tsoka, S., Ouzounis, C.A., 2005. Percolation of classification errors through hierarchically structured protein sequence databases. *Math Biosci.* 193, 223–234.
- Hannenhalli, S.S., Russell, R.B., 2000. Analysis and prediction of functional sub-types from protein sequence alignments. *J. Mol. Biol.* 303 (1), 61–76.
- Henikoff, S., Henikoff, J.G., 1992. Amino acid substitution matrices from protein blocks. *Proc. Natl. Acad. Sci. U.S.A.* 89, 10915–10919.
- Jensen, L.J., Gupta, R., Blom, N., Devos, D., Tamames, J., Kesmir, C., Nielsen, H., Staerfeldt, H.H., Rapacki, K., Workman, C., Andersen, C.A.F., Knudsen,

- S., Krogh, A., Valencia, A., Brunak, S., 2002. Prediction of human protein function from post-translational modifications and localization features. *J. Mol. Biol.* 319 (5), 1257–1265.
- Joachims, T., 1999. Making large-Scale SVM Learning Practical (Book Chapter). *Advances in Kernel Methods—Support Vector Learning*, MIT Press.
- King, R.D., Karwath, A., Clare, A., Dehaspe, L., 2000. Accurate prediction of protein functional class from sequence in the *Mycobacterium tuberculosis* and *Escherichia coli* genomes using data mining. *Yeast* 17 (4), 283–293.
- Karchin, R., Karplus, K., Haussler, D., 2002. Classifying G-protein coupled receptors with support vector machines. *Bioinformatics* 18 (1), 147–159.
- Kunik, V., Solan, Z., Edelman, S., Rupp, E., Horn, D., 2005. Motif extraction and protein classification. In: *Proceedings of the Computational Systems Bioinformatics (CSB)*, pp. 80–85.
- Liu, A.H., Califano, A., 2001. Functional classification of proteins by pattern discovery and top-down clustering of primary sequences. *IBM Syst. J.* 40 (2), 379–393.
- Lu, L., Qian, Z., Cai, Y., Li, Y., 2007. ECS: an automatic enzyme classifier based on functional domain composition. *Comput. Biol. Chem.* 31, 226–232.
- Martin, D.M.A., Berriman, M., Barton, G.J., 2004. GOTcha: a new method for prediction of protein function assessed by the classification of seven genomes. *BMC Bioinformatics* 5, 178.
- Moriyama, E.N., Kim, J., 2006. Protein family classification with discriminant function analysis. In: Gustafson, J.P. (Ed.), *Genome Exploitation: Data Mining the Genome*. Springer.
- Pandey, G., Kumar, V., Steinbach, M., 2006. *Computational Approaches for Protein Function Prediction*. TR 06–028, Department of Computer Science and Engineering, University of Minnesota, Twin Cities.
- Pasquier, C., Promponas, V.J., Hamodrakas, S.J., 2001. PRED-CLASS: cascading neural networks for generalized protein classification and genome-wide applications. *Proteins* 44 (3), 361–369.
- Riley, M.L., Schmidt, T., Wagner, C., Mewes, H.W., Frishman, D., 2005. The PEDANT genome database in 2005. *Nucleic Acids Res., Database issue* 33, D308–D310.
- Ruepp, A., Zollner, A., Maier, D., Albermann, K., Hani, J., Mokrejs, M., Tetko, I., Guldener, U., Mannhaupt, G., Munsterkötter, M., Mewes, H.W., 2004. The FunCat, a functional annotation scheme for systematic classification of proteins from whole genomes. *Nucleic Acids Res.* 32 (18), 5539–5545.
- Sacan, A., Ozturk, O., Ferhatosmanoglu, H., Wang, Y., 2007. LFM-Pro: a tool for detecting significant local structural sites in proteins. *Bioinformatics* 23 (6), 709–716.
- Sasson, O., Kaplan, N., Linial, M., 2006. Functional classification prediction: All for one and one for all. *Protein Sci.* 15, 1–16.
- Schomburg, I., Chang, A., Schomburg, D., 2002. BRENDA, enzyme data and metabolic information. *Nucleic Acids Res.* 30 (1), 47–49.
- Tomii, K., Kanehisa, M., 1996. Analysis of amino acid indices and mutation matrices for sequence comparison and structure prediction of proteins. *Protein Eng.* 9, 27–36.
- Wang, J.T.L., Ma, Q., Shasha, D., Wu, C.H., 2001. New techniques for extracting features from protein sequences. *IBM Syst. J.* 40 (2), 426–441.
- Wang, X., Schroeder, D., Dobbs, D., Honavar, V.G., 2003. Automated data-driven discovery of motif-based protein function classifiers. *Inf. Sci.* 155 (1–2), 1–18.
- Wright, P.E., Dyson, H.J., 1999. Intrinsically unstructured proteins: re-assessing the protein structure–function paradigm. *J. Mol. Biol.* 293, 321–331.

**ELSEVIER LICENSE  
TERMS AND CONDITIONS**

Jan 23, 2011

---

---

This is a License Agreement between Ozge Gursoy Yuzugullu ("You") and Elsevier ("Elsevier") provided by Copyright Clearance Center ("CCC"). The license consists of your order details, the terms and conditions provided by Elsevier, and the payment terms and conditions.

**All payments must be made in full to CCC. For payment instructions, please see information listed at the bottom of this form.**

Supplier	Elsevier Limited The Boulevard, Langford Lane Kidlington, Oxford, OX5 1GB, UK
Registered Company Number	1982084
Customer name	Ozge Gursoy Yuzugullu
Customer address	Bilkent university ankara, other 06800
License number	2594950761848
License date	Jan 23, 2011
Licensed content publisher	Elsevier
Licensed content publication	Cancer Letters
Licensed content title	The aflatoxin-induced <i>TP53</i> mutation at codon 249 ( <i>R249S</i> ): Biomarker of exposure, early detection and target for therapy
Licensed content author	Doriane Gouas, Hong Shi, Pierre Hainaut
Licensed content date	1 December 2009
Licensed content volume number	286
Licensed content issue number	1
Number of pages	9
Start Page	29
End Page	37
Type of Use	reuse in a thesis/dissertation
Portion	figures/tables/illustrations
Number of figures/tables /illustrations	1
Format	both print and electronic
Are you the author of this Elsevier article?	No

Will you be translating?	No
Order reference number	
Title of your thesis/dissertation	Role of dietary etiological factors involved in the molecular pathogenesis of liver cancer
Expected completion date	Feb 2011
Estimated size (number of pages)	180
Elsevier VAT number	GB 494 6272 12
Permissions price	0.00 USD
Value added tax 0.0%	0.0 USD / 0.0 GBP
Total	0.00 USD
Terms and Conditions	

### INTRODUCTION

1. The publisher for this copyrighted material is Elsevier. By clicking "accept" in connection with completing this licensing transaction, you agree that the following terms and conditions apply to this transaction (along with the Billing and Payment terms and conditions established by Copyright Clearance Center, Inc. ("CCC"), at the time that you opened your Rightslink account and that are available at any time at <http://myaccount.copyright.com>).

### GENERAL TERMS

2. Elsevier hereby grants you permission to reproduce the aforementioned material subject to the terms and conditions indicated.

3. Acknowledgement: If any part of the material to be used (for example, figures) has appeared in our publication with credit or acknowledgement to another source, permission must also be sought from that source. If such permission is not obtained then that material may not be included in your publication/copies. Suitable acknowledgement to the source must be made, either as a footnote or in a reference list at the end of your publication, as follows:

“Reprinted from Publication title, Vol /edition number, Author(s), Title of article / title of chapter, Pages No., Copyright (Year), with permission from Elsevier [OR APPLICABLE SOCIETY COPYRIGHT OWNER].” Also Lancet special credit - “Reprinted from The Lancet, Vol. number, Author(s), Title of article, Pages No., Copyright (Year), with permission from Elsevier.”

4. Reproduction of this material is confined to the purpose and/or media for which permission is hereby given.

5. Altering/Modifying Material: Not Permitted. However figures and illustrations may be altered/adapted minimally to serve your work. Any other abbreviations, additions, deletions and/or any other alterations shall be made only with prior written authorization of Elsevier Ltd. (Please contact Elsevier at [permissions@elsevier.com](mailto:permissions@elsevier.com))

**ELSEVIER LICENSE  
TERMS AND CONDITIONS**

Jan 23, 2011

---

---

This is a License Agreement between Ozge Gursoy Yuzugullu ("You") and Elsevier ("Elsevier") provided by Copyright Clearance Center ("CCC"). The license consists of your order details, the terms and conditions provided by Elsevier, and the payment terms and conditions.

**All payments must be made in full to CCC. For payment instructions, please see information listed at the bottom of this form.**

Supplier	Elsevier Limited The Boulevard, Langford Lane Kidlington, Oxford, OX5 1GB, UK
Registered Company Number	1982084
Customer name	Ozge Gursoy Yuzugullu
Customer address	Bilkent university ankara, other 06800
License number	2594960572362
License date	Jan 23, 2011
Licensed content publisher	Elsevier
Licensed content publication	Science of The Total Environment
Licensed content title	Selenium in food and the human body: A review
Licensed content author	Miguel Navarro-Alarcon, Carmen Cabrera-Vique
Licensed content date	1 August 2008
Licensed content volume number	400
Licensed content issue number	1-3
Number of pages	27
Start Page	115
End Page	141
Type of Use	reuse in a thesis/dissertation
Intended publisher of new work	other
Portion	figures/tables/illustrations
Number of figures/tables /illustrations	2
Format	both print and electronic

**ELSEVIER LICENSE  
TERMS AND CONDITIONS**

Jan 23, 2011

---

---

This is a License Agreement between Ozge Gursoy Yuzugullu ("You") and Elsevier ("Elsevier") provided by Copyright Clearance Center ("CCC"). The license consists of your order details, the terms and conditions provided by Elsevier, and the payment terms and conditions.

**All payments must be made in full to CCC. For payment instructions, please see information listed at the bottom of this form.**

Supplier	Elsevier Limited The Boulevard, Langford Lane Kidlington, Oxford, OX5 1GB, UK
Registered Company Number	1982084
Customer name	Ozge Gursoy Yuzugullu
Customer address	Bilkent university ankara, other 06800
License number	2594960572362
License date	Jan 23, 2011
Licensed content publisher	Elsevier
Licensed content publication	Science of The Total Environment
Licensed content title	Selenium in food and the human body: A review
Licensed content author	Miguel Navarro-Alarcon, Carmen Cabrera-Vique
Licensed content date	1 August 2008
Licensed content volume number	400
Licensed content issue number	1-3
Number of pages	27
Start Page	115
End Page	141
Type of Use	reuse in a thesis/dissertation
Intended publisher of new work	other
Portion	figures/tables/illustrations
Number of figures/tables /illustrations	2
Format	both print and electronic



Ref: PPL-EX-2011-00004

Ozge Gursoy Yuzugullu  
Bilkent University  
Bilkent University Molecular Biology Department

24 January 2011

Dear Ozge Gursoy Yuzugullu

RE: Your request to reproduce Table 1 from:  
Frederick P. BELLINGER, Arjun V. RAMAN, Mariclaire A. REEVES, and Marla J. BERRY  
(2009) Regulation and function of selenoproteins in human disease *Biochem J.*, **422** 11–22.

We hereby grant you permission to reprint the aforementioned material, in your Dissertation entitled Role of dietary etiological factors involved in the molecular pathogenesis of liver cancer, at no charge subject to the following conditions:

1. If any part of the material to be used is credited to another source, permission must be sought from that source.
2. The following credit line is to be placed on the page where the material appears: Reproduced with permission, from Author(s), (year of publication), (*Journal title*), (**Volume number**), (page range). © the Biochemical Society.
3. This permission is granted for one-time use only and is for non-exclusive world rights in volume form in both print and electronic format.

Yours sincerely,



Paula Butler  
**Projects Manager**  
[editorial@portlandpress.com](mailto:editorial@portlandpress.com)



**The Publishing Division**  
*of the Massachusetts Medical Society*

**Publishers of**  
*The New England Journal of Medicine, Journal Watch Newsletters, &  
AIDS Clinical Care*

### **Grant of Permission**

January 26, 2011

Bilkent University  
Ms. Ozge Gursoy Yuzugullu  
06800 Bilkent  
Ankara,  
TURKEY

Customer Reference #: Role of dietary etiological factors...  
NEJM Invoice #: 858

Dear Ms. Gursoy Yuzugullu,

Permission is granted for limited, one-time, non-exclusive educational use of the material requested, subject to the terms and conditions outlined within this document. This permission gives distribution rights throughout the world.

This is not a "blanket" permission allowing unrestricted use of this material in future reproductions, editions, revisions, ancillary products, or other derivative works. This permission is contingent upon payment of the invoice.

### **Terms & Conditions**

This permission applies only to copyrighted content that the Massachusetts Medical Society ("MMS") owns, and not to copyrighted content from other sources. If material appears in our work with credit to another source, you must also obtain permission from the original source cited in our work. All content reproduced from copyrighted material owned by the MMS remains the sole and exclusive property of the MMS. The right to grant permission to a third party is reserved solely by the MMS.

MMS' copyrighted content may not be used in any manner that implies endorsement, sponsorship, or promotion of any entity, product or service by the MMS or its publications. MMS cannot and does not authorize the use of any author's name on promotional materials; such approval must be obtained directly from the author.

This grant of permission is issued for the content to be used as originally published by MMS. MMS does not approve adaptations or modifications. Formatting, stylistic changes, and any explanatory material or figure legends used by the requester must accurately reflect the material as originally published by MMS.

**CREDIT LINE:** This permission requires a full credit link either in close proximity to where the MMS content appears or on the copyright page of any publication that incorporates MMS content. This credit line must include reference to the original article, together with a notice of copyright ownership.

**Intended Use of NEJM Content:**

Content Type: Figures/Tables

Permission Type: thesis/dissertation

Target Audience: thesis jury

Sponsor: n/a

Anticipated Duration of Use: n/a

Number of Users or Copies: N/A

Translation Rights Required: Y

Format: Print, Online

**Licensed Content**

<b>The New England Journal of Medicine Article Title:</b>	Epigenetics in Cancer
<b>The New England Journal of Medicine Authors:</b>	Esteller
<b>Year of Publication:</b>	2008
<b>Article DOI:</b>	10.1056/NEJMra072067

**Total Number of Figures/Tables: 1**

**Total USD: \$0.00**